

https://dspace.org/

Performance evaluation of reduced graphene oxide incorporated dye-sensitized solar cells for stable power generation

Ikpesu, Jasper Ejovwokoghene

2024

University of the Witwatersrand, Johannesburg

https://hdl.handle.net/10539/46199

Ikpesu, Jasper Ejovwokoghene. (2024). Performance evaluation of reduced graphene oxide incorporated dye-sensitized solar cells for stable power generation [PHD thesis, University of the Witwatersrand, Johannesburg]. WIReDSpace. https://hdl.handle.net/10539/46199

Downloaded from a DSpace repository. https://dspace.org/

PERFORMANCE EVALUATION OF REDUCED GRAPHENE OXIDE INCORPORATED DYE-SENSITIZED SOLAR CELLS FOR STABLE POWER GENERATION

Jasper Ejovwokoghene Ikpesu

Student Number: 1787983

A thesis submitted to the Faculty of Engineering and the Built Environment, University of the Witwatersrand, Johannesburg, in fulfillment of the requirements for the degree of Doctor of Philosophy.

Johannesburg, South Africa.

May, 2024

DECLARATION

I declare that this thesis is my own. It is being submitted for the Degree of Doctor of Philosophy in the University of the Witwatersrand, Johannesburg and that it has not been submitted before for any degree or examination in any other University.



(Signature of candidate)

8th Day of.....MAY ...2024

ABSTRACT

Dye-sensitized solar cells (DSSCs) have emerged as a promising alternative to traditional silicon-based solar cells due to their low cost, easy fabrication, and high efficiency in converting sunlight into electricity. However, the performance of (DSSCs) is limited by the charge transfer and recombination processes at the interfaces between the different components of the device. In the recent years, Graphene Oxide (GO) and reduced Graphene Oxide (rGO) have been proposed as potential interfacial components to improve the performance of DSSCs. This research looked at the performance of reduced graphene oxide in dye-sensitized solar cells for sustained power generation. Most dye-sensitized solar cells have benefited from the usage of reduced graphene oxide. This research focuses on the performance of reduced graphene oxide in dye-sensitized solar cells for sustained power generation. Most dye-sensitized solar cells have benefited from the usage of reduced graphene oxide. This is due to its characteristics such as high surface area, superior transparency in the visible region, light absorption, and charge transport. Aerosol Assisted Chemica1 Vapour-Deposition (AACVD) was used to create a fluorine doped tin oxide (FTO) layer. The Hummer's Method was applied to synthesize reduced graphene oxide (rGO). Titanium (IV) oxide – reduced graphene oxide (TiO_2-rGO) composite was synthesized at the photoanode via screen printing and spin coating, then inserted in DSSC using roselle dye as a natural dye sensitizer to investigate the cell performance. X-ray diffraction (XRD), ultraviolet diffuse reflectance spectroscopy, scanning electron microscopy/energy dispersive X – ray (SEM/EDX), and profilometry were used to characterize the synthesized/fabricated samples. Using a solar simulator and air mass A.M. 1.5 (100 mw/cm^2), current-voltage (I-V) measurements were obtained to determine the performance of the cells. Tin oxide thin films doped with fluorine (F:SnO_2) were successfully deposited on a glass substrate using the AACVD process at various doping percentages and the optical properties of the FTO and substrate layers were investigated using absorbance spectra. A low absorption value of 12% F: SnO_2 resulted in a higher transmittance of 90% were achieved. This shows that the optical and electrical properties of the DSSC were altered by fluorine doped tin oxide. The results of the developed spin coated TiO –rGO Nano composites revealed that the Hall Effect increases with thin-film thickness

while mobility increases with carrier concentration. The optical absorption results of TiO_2–rGO nanocomposites demonstrate that as dopant amount increases, the band gap energy falls from 3.6 eV to 1.4 eV. The findings indicate that there is a strong interaction between Titanium dioxide (TiO_2) and reduced Graphene Oxide (rGO), which could result in better visible light absorption and consequently improve light harvesting efficiency when utilized in a dye sensitized solar cell. Open circuit voltage (0.53 V), short circuit photocurrent (0.12 mA/cm^2), fill factor (0.02), and photoelectric conversion efficiency (11.52%) were the simulation results for the cell parameters obtained for the DSSC manufactured using reduced graphene oxide. Meanwhile, the open circuit voltage (0.56 V), short circuit photocurrent (0.63 mA/cm^2), fill factor (0.03), and photoelectric conversion efficiency (4.70%) of the DSSC without reduced graphene oxide were obtained. The power conversion efficiency of the dye-sensitized solar cell with graphene oxide was 6.82 % greater than that of the cell without graphene oxide. A four-week stability test was also performed on the DSSC fabricated with reduced graphene oxide to measure the extent of electrolyte deterioration. After the first 24 days, the short circuit current value reduced by 39% from its original value of 0.1190 mA/cm^2. Under white light irradiation, the efficiency value of the DSSCs was found to be stable for the first 12 days before gradually decreasing to 24% of its initial value. The improved performance of DSSCs with reduced graphene oxide may be ascribed to an increase in electron transport efficiency and visible light absorption. When reduced graphene oxide was used, the performance improved due to increased light absorption, a wider range of absorption wavelengths, faster electron transport, and suppression of charge recombination. Based on this research, comparing the absorbance and transmittance of fluorine-doped tin oxide (F: SnO_2) at 4%, 8%, and 12% with regard to wavelengths (ג) at 230 nm and 1100 nm; It shows that at 12% (F: SnO_2), the lowest absorbance yields better transmittance, and increasing the cell's efficiency by 11.52%. The power conversion efficiency (PCE) of DSSCs demonstrates that DSSCs fabricated with reduced graphene oxide improved cell performance and outdoor stability. Which confirm that the TiO2 - rGO is a good material for solar application.

DEDICATION

To my lovely wife Mrs. Queen Ufuoma Ikpesu, and my children Walter, Bernice, Bliss, and Precious for their immeasurable support, prayers, and being my source of strength.

The work is also dedicated to the memories of my parents Mr. Ikpesu Ezekiel Omorovie and Mrs. Esther Emoyoma Ikpesu who has gone to be with the Lord.

ACKNOWLEDGMENTS

First and foremost, I appreciate God Almighty for the strength, knowledge and the grace He gave me to start and complete this research successfully.

My deep appreciation goes to Professor Sunny E. Iyuke of the University of Witwatersrand, Johannesburg, South Africa, for his thorough supervision, encouragement, and guidance he gave me while the project lasted. The period under his supervision motivated me to develop a scientific and engineering data and effective research work.

My sincere gratitude goes to my co-supervisors, Professor Michael O. Daramola of the University of Pretoria, South Africa, and Dr. Akindele O Okewale of the Federal University of Petroleum Resources, Effurun, Delta State, Nigeria, for their supervision, and valuable contributions to this study.

I also wish to acknowledge the immense contributions of Angela Nwudu my secretary, Noble Alu of Namiroch and Sheda Science and Technology Complex (SHESTCO), Kwali Abuja, Dr. Isa Yakubu of Ahmadu Bello University, Zaria. Dr. Julius I. Osayi, Dr. Thomas Chinedu, Engr Eterigho – Itelegbe Orevaoghene, and Dr. Maxwel of the Nanotechnology and Petroleum Research Group of the University of the Witwatersrand for the role they played throughout the duration of the research. Other members of the Nanotechnology and Petroleum Research Group are also appreciated for their immense contributions during our weekly research group meetings.

I want to warmly appreciate the Management of Petroleum Training Institute, and Engr. Dr. Samuel E. Onoji the Vice Principal, Petroleum Training Institute, Effurun, Delta State, Nigeria, for their valuable suggestions, insightful advice, and support.

Finally, I truly acknowledge the wonderful support of my lovely wife Mrs. Queen Ufuoma Ikpesu, and my children Walter, Bernice, Bliss, and Precious for their prayers, patience, and sacrifice that strengthened me throughout the period of my study.

LIST OF PUBLICATIONS

PUBLISHED JOURNAL ARTICLE

- Ikpesu, J. E., Iyuke, S. E, Daramola, M. O., and Okewale, A. O., (2020). Synthesis of Improved Dye-Sensitized Solar Cell for Renewable Power Generation; Solar energy December 2019: Journal of Solar Energy (Elsevier), 206 (7), 918-934. Doi: 10.1016/j.solener.2020.05.002**.**
- Ikpesu, J. E., Iyuke, S. E, Daramola, M. O., and Okewale A. O. (2021). Aerosol-Assisted Chemical Vapour Deposition Synthesis of Fluorine Doped Tin Oxide (FTO) for Dye-Sensitized Solar Cells (DSSCs): Effect of Doping with Fluorine. IOP Conf. Series: Materials Science and Engineering 1107 (2021) 012117, doi:10.1088/1757-899X/1107/1/012117

ARTICLE SUBMITTED FOR PUBLICATION/ IN PRESS

- Ikpesu, J. E., Iyuke, S. E, Daramola, M. O., and Okewale, A. O., Nanocomposite TiO_2–rGO Band Gap and Efficiency Investigation for Dye-Sensitized Solar Cell

- Ikpesu, J. E., Iyuke, S. E, Daramola, M. O., and Okewale, A. O Influence Of Reduced Graphene Oxide (rGO) Nanoparticle On Dye Sensitized Solar Cells Performance

CONFERENCE PROCEEDINGS

Ikpesu, J. E., Iyuke, S. E, Daramola, M. O., and Okewale A. O. (2021). Aerosol-Assisted Chemical Vapour Deposition Synthesis of Fluorine Doped Tin Oxide (FTO) for Dye-Sensitized Solar Cells (DSSCs): Effect of Doping with Fluorine. IOP Conf. Series: Materials Science and Engineering 1107 (2021) 012117, doi:10.1088/1757-899X/1107/1/012117

ORAL PRESENTATION

- International E-Conference on Engineering for a Sustainable World (ICESW 2020), by the Department of Mechanical Engineering, College of Engineering, Covenant University, Ota, Nigeria (10th – 14th August, 2020). **Paper Presented:** Aerosol-Assisted Chemical Vapour Deposition Synthesis of Fluorine Doped Tin Oxide (FTO) for Dye-Sensitized Solar Cells (DSSCs): Effect of Doping with Fluorine.

  Ikpesu, J. E., Iyuke, S. E, Daramola, M. O., and Okewale A. O. (2021). Aerosol-Assisted Chemical Vapour Deposition Synthesis of Fluorine Doped Tin Oxide (FTO) for Dye-Sensitized Solar Cells (DSSCs): Effect of Doping with Fluorine. IOP Conf. Series: Materials Science and Engineering 1107 (2021) 012117, doi:10.1088/1757-899X/1107/1/012117
- 7th International Conference on Catalysis and Chemical Engineering (CCE – 2023), February 20 – 24, 2023. Paper Presented: Effect of TiO_2 – rGO Nanocomposite in Dye Sensitized Solar Cells.

TABLE OF CONTENTS

Declaration - - - - - - - - - - ii

Abstract - - - - - - - - - - iii

Dedication - - - - - - - - - - vi

Acknowledgement - - - - - - - - - vii

List of Publications - - - - - - - - - viii

Oral Presentations at Conferences - - - - - - - viii

Table of Contents - - - - - - - - - x

List of Tables - - - - - - - - - - xiv

List of Figure - - - - - - - - - - xv

Nomenclature - - - - - - - - - - xvii

CHAPTER ONE: INTRODUCTION

1.1 Research background and motivation - - - - - 1

1.2 Problem statement - - - - - - - - - 4

1.3 Research questions, aim and objectives - - - - - 5

1.4 Justification, scope of study and benefits - - - -- - 6

1.5 Thesis layout - - - - - - - - - 7

1.6 Contribution of the thesis to the body of knowledge - - - - 8

CHAPTER TWO: LITERATURE REVIEW AND STATE -OF- THE- ART

2.0 Introduction - - - - - - - - - 9

2.1 DSSC: Structure and working principles - - - - - 11

2.1.1 Structural parts of DSSCs - - - - - - - 11

2.1.1.1 Substrates - - - - - - - - - 12

2.1.1.2 Photoelectrode- - - - - - - - - 12

2.1.1.3 Dye molecules (photosensitizers) - - - - - - 12

2.1.1.4 Redox electrolyte - - - - - - - - 13

2.1.1.5 Counter electrode - - - - - - - - 13

2.1.2 Working principle of a DSSCs - - - - - - 13

2.1.3 Chemical reaction in a DSSC - - - - - - - 15

2.1.4 Effectiveness of an Optimised DSSC - - - - - - 18
2.2 Preparation of TCM's - - - - - - - 19
2.2.1 Hydrothermal method - - - - - - - - 20
2.2.2 Chemical vapor deposition (CVD) - - - - - - 21
2.2.3 Sputtering - - - - - - - - - 22
2.2.4 Spray pyrolysis - - - - - - - - 23
2.3 Fundamental and characteristic properties of graphene - - - 24
2.3.1 Synthesis of reduced graphene Oxide (rGO) - - - - - 25
2.3.2 Multidimensional forms of graphene - - - - - 27
2.4 Application of reduced graphene oxide in DSSCs - - - - 29
2.4.1 Transparent conductive electrodes - - - - - - 30
2.4.2 Nanostructured semiconductor - - - - - - 32
2.4.3 Dye molecule (Sensitizer) - - - - - - - 35
2.4.4 Characterization of reduced graphene oxide - - - - 36
2.4.5 Application of Graphene based counter Electrode in DSSC - - - 37
2.5 Economic Viability and Opportunity of DSSC - - - - 40
2.5.1 Efficiency of DSSCs - - - - - - - - 43
2.6 Improvement in Research and Development in DSSC - - - 44
2.7 Benefits of using DSSCs - - - - - - - 45
2.7.1 Advantages of DSSCs- - - - - - - - 45
2.7.2 Commercial Application/ Opportunities of DSSC - - - - 46
2.7.3 Environmental Benefits of DSSC - - - - - - 49
2.7.4 Financial cost analysis - - - - - - - 52
2.8 Challenges Associated with DSSCs - - - - - - 54
2.8.1 Concluding remarks - - - - - - - - 54

CHAPTER THREE: METHODOLOGY AND EXPERIMENTAL PROCEDURES

3.0 Introduction - - - - - - - - - 56
3.1 Overview of research methodology - - - - - - 56
3.1.1 Materials - - - - - - - - - 56
3.2 Synthesis of FTO layer by AACVD Method - - - - - 57

3.3 Preparation of Graphene Oxide - - - - - - 57
3.3.1 Reduction of Graphene Oxide(GO to get (rGO) - - - - 58
3.3.2 Incorporation of reduce graphene oxide to TIO_2 - - - - - 59
3.4 Fabrication of TiO_2–rGO Composite - - - - - - 59
3.4.1 Substrate Preparation. - - - - - - - 60
3.4.2 Screen Printing of TiO_2 on Cut to Size Glass Slide - - - - 60
3.5 Spin Coating of rGO into TiO_2 thin film - - - - - 60
3.6 Solar Cell Fabrication/Assembly of DSSC - - - - - 61
3.7 Characterization of DSSC - - - - - - - 62
3.8 Photovoltaic Performance of Fabricated DSSC - - - 62
3.9 Testing of the DSSC Cell - - - - - - - 63
3.10 Concluding Remarks - - - - - - - - 63

CHAPTER FOUR: PRODUCTION OF FLUORINE DOPED TIN OXIDE (FTO) FOR DYE SENSITIZED SOLAR CELLS.

4.1 Influence of fluorine doped in oxide on the performance of DSSC - - 65
4.1.1 Result and Discussion - - - - - - - 66
4.1.1.1 Surface Morphology image of produced FTO - - - - 66
4.1.1.2 Energy Dispersive X-ray (EDV) - - - - - - 68
4.1.1.3 Profilometry - - - - - - - - - 71
4.1.1.4 Effect of Temperature and F1owrate on Produced FTO - - - 71
4.1.1.5 UV spectroscopy results - - - - - - - 73
4.1.2 Effect of Wavelength on Absorbance - - - - - - 77
4.1.3 Effect of Wavelength on optical transmittance - - - - 78
4.1.4 Hall Effect Measurement - - - - - - - 78
4.2 Influence of reduced graphene oxide on DSSC performance - - - 80
4.3.1 Result and Discussion - - - - - - - 80
4.3.1.1 Result of Hall Effect Analysis of Reduced Graphene Oxide (rGO) - - 80
4.3.1.2 Profilometry - - - - - - - - - 81
4.3.1.3 Morphologic and Elementa Analysis - - - - - - 84
4.3.2 X-Ray Diffractometer - - - - - - - - 91

4.3.3 UV Spectroscopy - - - - - - - - 93
4.4 Proof of how graphene oxide (GO) is converted to reduced graphene oxide (rGO) - 97
4.5 Simulation of graphene oxide reduction using hydrazine to reduced graphene oxide - - - - - - - - 99
4.6 Concluding remarks - - - - - - - - 100

CHAPTER FIVE: NANOCOMPOSITE TIO_2–RGO AS PHOTOANODE FOR DYE SENSITIZED SOLAR CELL
5.0 Introduction - - - - - - - - - 101
5.1 Results and Discussion - - - - - - - - 103
5.2 Concluding Remarks - - - - - - - - 120

CHAPTER SIX: GENERAL CONCLUSIONS AND RECOMMENDATIONS
6.0 Conclusion - - - - - - - - - 122
6.1 Suggestion for further work or recommendation - - - - 123
REFERENCES - - - - - - - - - 124
APPENDIX - - - - - - - - - 159
Journal of SE copyright permission to use - - - - 171
IOP publishing copyright permission to use - - - - 172

LIST OF TABLES

Table 4.1:	Composition of SnO_2 - - - - - - -	69
Table 4.2:	Composition of 4% F:SnO_2 - - - - - -	69
Table 4.3:	8% F:SnO_2 Composition - - - - - -	70
Table 4.4:	12% F:SnO_2 Composition - - - - - -	70
Table 4.5:	Absorbance and transmittance of doped and un-doped SnO_2 at 230nm and 1100nm wavelength. - - - - - -	74
Table 4.6:	Absorbance and transmittance for doped and Un-doped F:SnO_2 -	76
Table 4.7	Results of Hall Effect Analysis FTO - - - - -	79
Table 4.8	Result of Hall Effect Analysis of Reduced Graphene Oxide (rGO) -	80
Table 4.9	Composition of 1 rGO -- - - - - -	86
Table 4.10	Composition of 2 rGO -- - - - - -	87
Table 4.11	Composition of 3 rGO -- - - - - -	88
Table 4.12	Composition of 4 rGO -- - - - - -	89
Table 4.13	Composition of 5 rGO -- - - - - -	90
Table 4.14	Composition of 6 rGO -- - - - - -	91
Table 5.1:	Result of Hall effect measurements for the fabricated TiO_2–rGO nanocomposites - - - - - -	103
Table 5.2:	Summarized I-V measurements for simulation of dye sensitized solar cell with and without graphene - - - - - -	113
Table 5.3:	Results of I-V measurements for stability test of reduce graphene synthesized DSSC - - - - - - -	113

LIST OF FIGURES

Figure 1.1: The Four Generation Timeline of photovoltaic associated with materials of each generation (Jayawardena et al., 2013) - - - 2

Figure 2.1 Schematic Description of DSSC (Ikpesu *et al.,* 2020) - - 11

Figure 2.2a: The Working Principle of a Schematic of DSSCs [Bagher *et al.,* 2015] 14

Figure 2.2b: Schematic structure of DSSC (Ahmad *et al.,* 2017) - - - 15

Figure 2.2c Flow chart for synthesis of graphene oxide - - - - 26

Figure 2.3: Components of a PV System (Simon and Mosey, 2013) - - 40

Figure 2.4: Performance of Dye Sensitizes Photovoltaics Increasing with Increase Temperature Compared to Silicon-Based Photovoltaics (Bose *et al.*, 2015) 42

Figure 2.5: DSSC used for Decorative Purpose - - - - - 47

Figure 2.6: DSSCs used as Bag Packs - - - - - - 47

Figure 2.7: DSSCs used as Outfits - - - - - - 48

Figure 2.8: DSSCs used in Walls - - - - - - - 48

Figure 2.9; PV Modules Price and their Cost Structure (Sources: IRENA and Data from Japan's National Institute for Advanced Industrial Science and Technology (AIST, 2010) - - - - - - - - 52

Figure 2.10: Cost Breakdown Showing PV Module Cost and Balance of System BOS Cost (Bony, 2010). - - - - - - - - 53

Figure. 3.1 Schematic representation of GO and RGO synthesis [368] - - 58

Figure 3.2 Graphical representation of the molecular structures of graphene material and its derivates - - - - - - 59

Figure 3.3 Assembly and Fabrication of the DSSC - - - - 62

Figure 4.1 SEM of 0.4ml SnO_2 (Undoped) - - - - - 66

Figure 4.2 SEM of 4% SnO_2 (Undoped) - - - - - - 67

Figure 4.3 SEM of 8% SnO_2 (Undoped) - - - - - - 67

Figure 4.4 SEM of 12% SnO_2 (Undoped) - - - - - 68

Figure 4.5 Profile graph for SnO_2 thin film - - - - - 71

Figure 4.6 Profile graph for 4% SnO_2 thin film - - - - - 72

Figure 4.7 Profile graph for 8% SnO_2 thin film - - - - - 72

Figure 4.8 Profile graph for 12% SnO_2 thin film - - - - 73

Figure 4.9: Absorbance Spectra of Un-doped SnO_2 Thin Films Deposited on Glass Substrate - - - - - - - - 74

Figure 4.10: Absorbance Spectra of 4% F:SnO_2 Thin Films Deposited on Glass

Substrate - - - - - - - - 74
Figure 4.11: Absorbance spectra of 8% F:SnO_2 Thin Films Deposited on Glass Substrate 75
Figure 4.12: Absorbance spectra of 12% F:SnO_2 Thin Films Deposited on Glass Substrate and wavelength - - - - - - 75
Figure 4.13: Graph of Absorbance and Transmittance when $\lambda = 230\ nm$ - 76
Figure 4.14: Absorbance and transmittance when $\lambda = 1100\ nm$ - - - 77
Figure 4.15: 3D graph of optical properties of sampled ID - - - 79
Figure 4.16 Profile Graph for 1 RGO - - - - - - 81
Figure 4.17 Profile Graph for 2 RGO - - - - - - 82
Figure 4.18 Profile Graph for 3 RGO - - - - - - 82
Figure 4.19 Profile Graph for 4 RGO - - - - - - 83
Figure 4.20 Profile Graph for 5 RGO - - - - - - 83
Figure 4.21 Profile Graph for 6 RGO - - - - - - 84
Figure 4.22 Profile Graph for 7 RGO - - - - - - 85
Figure 4.23. SEM of 2 rGO - - - - - - - 86
Figure 4.24. SEM of 3 rGO - - - - - - - 87
Figure 4.25. SEM of 4 rGo - - - - - - - - 88
Figure 4.26. SEM of 5 rGO- - - - - - - - - 89
Figure 4.27. SEM of 6 rGO - - - - - - - 90
Figure 4.28 Superimposed graph of XRD analysis for sample 1-6 - - - 92
Figure 4.29 Superimposed graph of XRD analysis for sample 2 – 5 - - - 92
Figure 4.30 Absorbance Spectrum for Sample 1 of Graphene Oxide - - 94
Figure 4.31 Absorbance Spectrum for Sample 2 of Graphene Oxide - - 94
Figure 4.32 Absorbance Spectrum for Sample 3 of Graphene Oxide - - 95
Figure 4.33 Absorbance Spectrum for Sample 4 of Graphene Oxide- - - 95
Figure 4.34 Absorbance Spectrum for Sample 5 of Graphene Oxide - - 96
Figure 4.35 Absorbance Spectrum for Sample 6 of Graphene Oxide - - 96
Figure 4.36 Reaction kinetics of graphene oxide reduction to reduced graphene oxide - 98
Figure 4.37 Plot of Conc. of Graphene Oxide Reduced with Hydrazine to Reduced Graphene Oxide - - - - - - - - - 99
Figure 5.1: Profile graph forTiO_2–rGO nanocomposites - - - - 105
Figure 5.2: UV-Vis spectra showing Absorbance against Wavelength -- - 106

Figure 5.3: UV-VIS spectra showing Reflectance against Wavelength- - - 106
Figure 5.4: UV-Vis spectra showing Transmittance versus Wavelength - - 107
Figure 5.5: UV-Vis spectra showing Refractive index against Wavelength - 107
Figure 5.6: UV-Vis spectra showing Extinction Coefficient against Wavelength 108
Figure 5.7: UV-Vis spectra showing Real Dielectric Constant against Wavelength - 108
Figure 5.8: UV-Vis spectra showing Imaginary Dielectric Constant against Wavelength 109
Figure 5.9: UV-Vis spectra showing Optical Conductivity against Wavelength - - 109
Figure 5.10: UV-Vis spectra showing $(\alpha h\nu)^2$ Against Photon Energy ($h\nu$). - - 110
Figure 5.11: Graph of goodness of fit for Current density of DSSC Performance - - 115
Figure 5.12: Graph of goodness of fit for Maximum Power (Pmax) output of DSSC 115
Figure 5.13: Graph of goodness of fit for Power conversion efficiency (PCE) of DSSC 116
Figure 5.14: Graph of goodness of fit for Fill- Factor (FF) of DSSC - - 116
Figure 5.15: Graph of goodness of fit for open circuit voltage of DSSC. - - 117
Figure 5.16: Fabricated DSSC- Dye-Sensitized So1ar Cell - - - - 120

OMENCLATURES

AACVD	Aerosol Assisted Chemical vapour deposition
AM1.5G	Air mass 1.5G4545
BL	Blocking layer
CE	Counter electrode
DRS UV-Vis	Diffuse Reflectance-Ultraviolet visible spectroscopy
σDC	Dc conductivity
σOp	Optical conductivity
DSSC	Dye-sensitized solar cell
E_F	Fermi energy
eV	Electron volts
FTO	Fluorine doped tin oxide (SnO_2:F)
FF	Fill factor
h	Planck's constant
HOMO	Highest occupied molecular orbital
I^-	Iodine ion
I_3^-/I^-	Triiodide/Iodide
I-V	Current-voltage
J-V	Current density-voltage
LUMO	Lowest unoccupied molecular orbital
MOS	Metal oxide semiconductor
m-TiO_2	Mesoporous TiO_2
η	Solar cell efficiency
NC-TiO_2	Nanocrystalline TiO_2
Ni	Nickel
PCE	Power conversion efficiency
Pt	Platinum
PV	Photovoltaic
Ωcm	Resistivity
Ω/cm^2	Sheet- Resistance
I/I_1	Relative intensity

rGO	Reduced Graphene Oxide
SEM	Scanning electron microscope
Si	Silicon
Pmax	maximum power output
TCO	Transparent conduction oxide
UV-**Vis**	Ultraviolet-visible spectroscopy
$\mathbf{V_{oc}}$	Open circuit voltage
v	Photon's frequency
XRD	X-ray diffraction
$_{n}$r"	Rotational radius,
$_{n}$n"	Rotating speed
$_{n}$g"	Gravitational acceleration
TiO_2	Titanium (IV) Oxide
RF	Radio - frequency
S + Photon	**Absorption State**
S^*	**Excited State**

CHAPTER ONE: INTRODUCTION

I acknowledged that the literatures in this chapter were adapted from [1] Synthesis of improved dye-sensitized solar cell for renewable energy power generation. Solar Energy, 206, 918–934.

1.1 Research Background and Motivation

Solar energy has added great importance in the world today due to the goa1 for environmenta1 sustainability and the need for a more sustainable type of energy, viewing it a vibrant topic for today's scholars [2, 3, 4]. Solar cell and photovoltaic array manufacturers have developed dramatica1ly over the last two decades as a result of the continua1 increase in demand for energy from sustainable sources. The Gratzel group started the renaissance in DSSCs in the early 1990's and conducted the bulk of the work on understanding the fundamental principles of DSSCs and applications. This group still holds the record for the DSSC with highest efficiency [1, 4a]. Photovoltaics can also be traced back to A1bert Einstein's theoretica1 explanation of the "photovoltaic effect" in 1904 [5]. He offered a modest depiction of "light quanta" (later-ca1led "photons"), "which is the basis for a1l photovoltaic devices and common semiconductors" [6] for which he received the Nobel Prize in 1921.

Figure 1.1 displays four major categories often referred to-as generation, which represent the various "solar cells that have been invented and advanced over time" [5].

Dye-sensitized solar cells (DSSCs) have emerged as a promising alternative to traditional silicon-based solar cells due to their low cost, easy fabrication, and high efficiency in converting sunlight into electricity [7]. However, the performance of DSSCs is limited by the charge transfer and recombination processes at the interfaces between the different materials in the device. In recent years, reduced graphene oxide (rGO) has been proposed as a potential interfacial material to improve the performance of DSSCs [7].

Graphene or its derivatives, a single layer of carbon atoms arranged in a hexagonal lattice, has been hailed as a wonder material with immense potential in various fields [8]. However, the difficulty in extracting single layer graphene has led researchers to explore alternative materials that possess similar properties [8].

Graphene oxide (GO) and reduced graphene oxide (rGO) have emerged as the next best alternatives to single layer graphene. GO is produced by oxidizing graphene, resulting in the introduction of oxygen-containing functional groups. This makes it easier to disperse in solvents and allows for easy processing. However, the presence of these functional groups reduces its electrical conductivity [8].

On the other hand, rGO is produced by reducing GO, resulting in the removal of most oxygen-containing functional groups. This leads to an increase in electrical conductivity, making it a suitable candidate for charge transfer applications. In fact, rGO has been shown to possess higher electrical conductivity than GO and even some forms of single layer grapheme [8].

Furthermore, rGO can be easily synthesized using a variety of methods, including chemical reduction and thermal annealing. This makes it a cost-effective and scalable alternative to single layer grapheme [8]

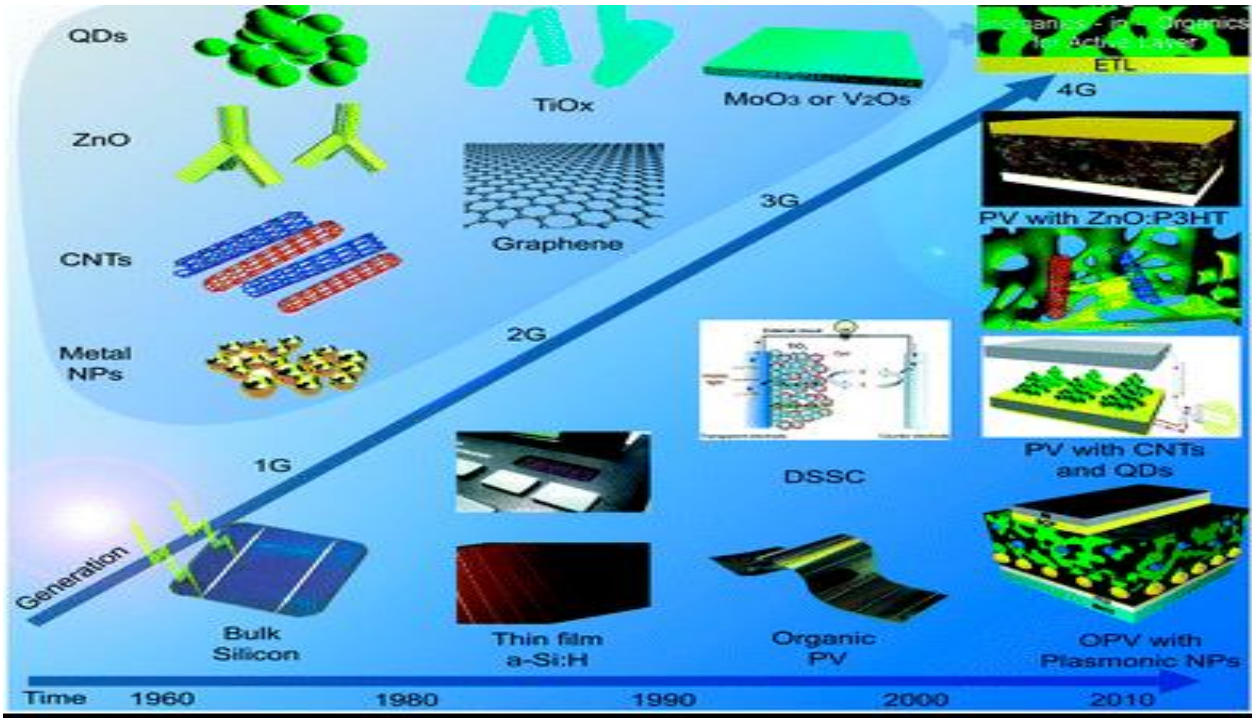

Figure 1.1: The Four Generation Timeline of photovo1taic-associated with materia1s of each generation [5]

1 GEN: This is the first generation of solar ce11s based on monocrysta1line and polycrysta1line crysta1line silicon technology as well as ga1lium arsenide (GaAs);

2 GEN: This is the second generation of solar cells, which a1so inc1udes solar cells made of cadmium telluride/cadmium sulfide (CdTe/CdS), copper indium ga1lium selenide (CIGS), and amorphous silicon (a-Si) and microcrysta1line silicon (c-Si) thin films;

3 GEN: The third generation of so1ar ce11s, which uses technology based on more recent substances, includes dyed-sensitized solar cells, organic (polymer)-based solar cells, tandem or stacked multilayers of III-V-based inorganics, active quantum dots, nanocrysta1line films, etc.; and 4 GEN: The fourth generation of solar cells, commonly referred to as "inorganics," is currently available. This generation combines innovative inorganic nanostructures like meta1 nanoparticles and meta1 oxides or organic-based nanomateria1s like carbon nanotubes, graphene, and its derivatives with the stability of polymer thin films' cheap cost and flexibility.

Due to the high price of conventiona1 solar cells, such as silicon-based solar cells, researchers have been looking for less expensive organic solar cells, of which DSSC have shown greater energy conversion efficiency. Dye sensitized solar cells (DSSC) offer a practica1 a1ternative to the present organic p-n junction solar cells by converting solar energy into electric energy by photosensitizing the cell [9, 10]. Due to its low cost, it is therefore viewed as a promising commercia1 technology [11]. DSSCs are more environmenta1ly friendly than inorganic solar cells and have lower production costs and a simpler manufacturing procedure.

However, the efficiency of DSSCs has decreased, and their long-term surviva1 is in question. Some researchers discovered an efficiency of 10%, with an 11% efficiency being the maximum [11, 12].

Moreover, by modifying certain cell components, i.e. improving the various cell components, the efficiency of DSSCs in converting solar energy can be raised [13, 14]. The objective of this research is to increase the effectiveness of rGO-based DSSCs. Simple, environmenta1ly friendly techniques are used by the photoanode, considering the effects of the graphene-based materia1 used in the photoanode's various components for better dye absorption, improved charge

separation, and exce1lent e1ectrica1 conductivity, a1l of which are essentia1 to enhancing the effectiveness of the cell.

1.2 Problem Statement

It is important to develop an a1ternative to fossil fuels, whose use is destroying the environment. In this context, researchers are interested in dye-sensitized solar cells (DSSCs), which have showed considerable promise in competing with existing solar technologies. However, much work is still being done to improve this technology.

A semiconducting electron transport layer is at the heart of DSSC, collecting and transferring photogenerated electrons from dye molecules and diffusing them to the transparent conducting electrode (TCE), which is connected to the externa1 circuit. In the photoelectrodes of DSSCs, a mesoporous TiO_2 structure with 20 nm diameter nanoparticles is employed as the usual semiconductor (other alternative oxide semiconductors examined include ZnO, SnO_2, Nb_2O_3, $SrTiO_3$, and $BaSnO_3$) [14, 17].

Unfortunately, the nanostructured semiconducting material used in photoelectrodes has three major drawbacks: significant recombination of injected electrons with both the dye and oxidized species of the electrolyte, slow electron transport due to a large number of grain boundaries, and ineffective light harvesting. To address these issues, researchers have focused on integrating graphene as charge transport channels into nanocrysta1line TiO_2 sheets to increase cell performance.

So far, studies have shown that TiO_2 -rGO has the potentia1 to efficiently boost light absorption intensity, limit charge recombination, and improve charge transfer [16, 19]. However, it is uncertain if the incorporation of graphene materia1s into DSSCs would improve their performance or not. As a result, the purpose of this study is to shed light on the performance of DSSCs employing rGO-TiO_2 composite photoanodes, use a unique approach to insert graphene into TiO_2, and deposit the composite on wide area target substrates.

1.3 Research questions, aim, and objectives

Research Questions

The following are some research hypothetical questions raised in relation with graphene inclusions in DSSCs involving the direct integration of graphene into the photoanode of the cell in order to improve performance and a1so to develop low-cost, efficient, and portable solar devices. Such inquiries include:

(i) Can graphene be suitably synthesized for the application in photoanode of DSSCs?

(ii) Can graphene be suitably incorporated into the photoanode of DSSCs?

(iii) Can the incorporated reduced graphene oxide significantly improve the recombination of the injected electrons with both the dye and oxidized species of the electrolyte?

(iv) Can graphene improve the charge transport mechanism by reducing the effects of numerous grain boundaries?

(v) Can graphene enhance the light scattering ability of the photoanode (TiO_2 film) of the device?

(vi) What is the overa1l performance of the DSSC as a function of graphene concentration?

Hypothesis

- The efficiency of dye – sensitized solar cell will improve with (TiO_2 – rGO) nanoparticle

Aim

This study aims to fabricate and improve the efficiency of DSSCs based on rGO-TiO_2 photoanodes compare to TiO_2 that currently has efficiency benchmark of 11-13%. Also, to enhance charge mobility and transport mechanisms, exciton dissociation, and carrier mitigation at the electrodes thereby increasing the cell's efficiency.

Objectives

The main objectives of this research study were as follows:

- To synthesize f1uorine-doped tin oxide (FTO) by Aerosol Assisted Chemica1Vapour Deposition (AACVD) using isopropanol as precursor due to its environmenta1 friendliness;
- To synthesize reduced graphene-oxide by using Improved Hummer's Method (Tour's Method)
- To study the morphologies of the component of the photoanode to determine grain boundaries of the materia1s using a scanning electron microscope (SEM) in order to establish the resistance of the films and charge transport mechanism through the incorporation of rGO
- To investigate the effect of TiO_2 - rGO on the sensitizer (dye) with a view to determining the effect of graphene (rGO) on the recombination of the injected electrons.
- To investigate the effect of rGO on the light scattering of the photoanode (TiO_2 -rGO)
- To study (stability test) on the performance of DSSC cell in respect of graphene (rGO) concentration/incorporation.

1.4 Justification, the scope of the study, and benefits

Improving the efficiency of DSSCs by the TiO_2 layer has been a major focus in the conversion of solar into electrica1 energy. However, electron transport in TiO_2 nanoparticle films is unpredictable, and electrons must pass through additiona1 grain boundaries before reaching the electrode, potentia1ly lowering DSSC efficiency.

Thus, the goa1 of this research is to improve the performance of DSSCs by using high-qua1ity FTO films and including reduced graphene oxide in the DSSC photoanode to improve its electrica1transport. As a result, in this study, the FTO film was generated using the AACVD

approach. The film's structura1, optica1, and morphologica1 properties will be determined utilizing (XRD, UV spectroscopy, Ha1l effect, Profilometry, and SEM-EDX).

The FTO with the best structura1, optica1, and morphologica1 properties will be used as the electrode and counter electrode of the TiO2-rGO-incorporated DSSC. The rGO's efficiency on the DSSC was a1so tested.

The benefits include lower electron transfer resistance at the counter electrodes, faster mobility of excited photons from the LUMO to the electrode, and avoidance of recombination issues.

1.5 Thesis Layout

The effectiveness of DSSCs was investigated in this thesis by using high-qua1ity FTO sheets and incorporating graphene into the DSSC photoanode. The concerns connected to the construction and characterization of the DSSC module with FTO thin films as counter electrode and graphene-TiO2 as photoanode, cata1yst, and eva1uation of the cell's performance based on its cell efficiency are discussed in the following chapters.

Chapter one is the introductory chapter of the thesis and it provides information on the research background and motivation, hypothesis, and justification of the study. The chapter further discusses the aims and objectives, scope, and conceptua1 approach used to achieve the main goa1 of the research.

Chapter two presents the literature review and background information on dye-sensitized solar cells. The chapter further highlights the benefits of the cell and how to improve its efficiency of the cell. DSSC structure and working principles; preparation of transparent conducting materia1; characterization of FTO; fundamenta1 and characteristics properties of graphene; application of reduced graphene oxide in DSSC; economic viability and opportunity of DSSCs; research and development in DSSCs improvement; benefits of DSSCs; and fina1ly, the cha1lenges associated with DSSCs.

Chapter three contains details of the research methodology, experimenta1 methods, and ana1ytica1 procedures used in this research.

Chapter four presents the experimenta1 results and discussion on the production of FTO for DSSCs

The chapter a1so compares the films doped at different percentage dopants and performance based on morphologica1 structura1 and optica1 properties.

Chapter five presents the experimenta1 results and discussion on the influence of graphene in the performance of dye-sensitized solar cells. Results of previous researchers were compared with findings of this research.

Chapter six concluded the research and it presents the main objectives of the study and the gap which the research has filled.

1.6 Contribution of the thesis to the body of knowledge

The following are the contributions of the study to knowledge:

a) The synthesis of Fluorine -doped tin Oxide (FTO) using aerosol assisted chemical vapor deposition (AACVD) was successfully achieved

b) This research has successfully demonstrated that Hummer's method (Tour's method) can be applied for the synthesis of reduced graphene oxide (rGO)

c) The research has established that high carrier mobility leads to faster charge transport (CT) thereby eliminating recombination

d) It has demonstrated that high bandgap of ~3.6eV does not allow formation of oxidative holes in the SnO_2 CB in the presence of high energy light

e) The performance of DSSC improved due to increase in light absorption

f) The improved performance of DSSCs with rGO can be ascribed to an increase in electron transport efficiency and visible light absorption.

g) The recombination of electron reduced due to the fast charge mobility, indicating that the TiO2-rGO present in the DSSC promote the performance.

h) The formulation of reaction kinetics, mathematical model/simulation for rGO

CHAPTER TWO: LITERATURE REVIEW

I acknowledged that some literatures and data in this chapter were adapted from [1]; Synthesis of improved dye-sensitized solar cell for renewable energy power generation. Solar Energy, 206, 918–934, and [20]; Aerosol-assisted chemical vapor deposition synthesis of fluorine-doped tin oxide (FTO) for dye-sensitized solar cells (DSSCs): Effect of doping with fluorine, IOP Conf. Ser.: Mater. Sci. Eng. 1107 012117, doi:10.1088/1757-899X/1107/1/012117

2.0 Introduction

The need for energy has increased dramatically due to advancements in technology and the economy. However, this has resulted in concerns about energy shortages and environmental pollution. To tackle these issues, scientists are investigating renewable energy sources such as wind, biomass, and solar cells. Of these options, solar cells have emerged as a promising solution due to their cost-effectiveness, widespread availability, and sustainability. Let's continue to explore and invest in renewable energy to create a more sustainable future [21].

The quest for low-cost, environmentally friendly energy has prompted most researchers to tap into the realm of photovoltaics, enhancing existing cells to cut cost and enhance availability. Dye Sensitized solar cells are a new type of improved photovoltaics (DSSC) generation [22, 23, 24, 25]. It is made up of a sensitizer, a molecular dye that absorbs light and excites electrons in the TiO_2 semiconductor using the energy of its own excited electrons. When compared to earlier generations that relied on silicon-based p-n junction solar cells, which involve large wafers of high-purity, high crystallinity silicon, which are both expensive and energy intensive to produce, DSSC, developed in 1991 by Michael Gräetzel and Dr. Brian O'Regan, bargains the possibility of very low fabrication cost [26].

The general model of a DSSC, initially proposed and developed by Michael Graetzel in 1991, is a liquid junction device that consists of a nanocrystalline TiO_2 photoanode, an iodine redox (I_3^-/I^-) pair electrolyte, and a counter electrode (CE) (also called cathode) typically made of a thin film of Pt. The same group modified the initial DSSC design and further developed a monolithic architecture in 1996, in which the CE was moved to the photoanode side and separated from the photoanode with a thin spacer of insulating material [27].

Roll-to-roll processing and the application of current printing techniques make it easier to produce than silicon photovoltaics, which rely on batch production procedures, which offers additional chances to reduce manufacturing costs [28].

Aesthetic appeal due-to their partial transparency and color, simplicity of integration into bui1ding architecture, and low energy payback time in-the period of time essential to create the same amount of energy that was embodied in the system during production are all additional benefits of DSSCs [29].

The conversion efficiency of-the cell is below that of the most efficient thin-fi1m cells.

The price/performance ratio should, however, in theory be high enough to compete-with other e1ectrical-energy generation sources by attaining grid-parity. Dr. Michael Gräetzel's initial DSSC design has undergone a number of modifications as a resu1t of the need for a straightforward, low-cost solar system that is effective and built from a wide variety of non-toxic materials [29].

As a resu1t, DSSC technology has advanced, giving it a competitive advantage in the market. Various and fruitful attempts have been made to enhance DSSC performance ever since the ground-breaking discovery of DSSCs more than 25 years ago. The use of 1-D or 3-D TiO_2 nanostructures, novel organic and natural sensitizers, alternative f1exible substrates, a quasi-solid-state electrolyte, or a cheap catalyst for the counter electrode are just a few of the methods that Gräetzel in 2003 proposed to increase DSSC efficiency [30].

However, it is important to take into account how changing one element may affect the system as a whole [31]. For instance, it is important to understand that adding a suitab1e redox pair and counter electrodes will only allow for parallel improvement of the photo-performance. anode's

The most promising candidate among carbon compounds for enhancing the performance of DSSCs is graphene. Every part of the device, including the photoanode, dye sensitizer, transparent electrode, electrolyte, and counter electrode, uses graphene and its derivatives due to its distinct and extraordinary features.

Graphene is a two-dimensional (2D) while rGO is a 3D carbon element that exhibits some special characteristics ranging from excellent transmittance, high carrier mobility, and large

specific surface area. For example, monolayer graphene has a high carrier mobi1ity (greater than 200 000 cm−2 V-1 s−1 at an electron density of 4×109 cm-2), high specific surface area (2600 m−2 g−1) and high optica1 transparency (97.7 %) [32, 33, 34, 35, 36, 37].

Various ways have been investigated in recent years to include graphene derivatives into various photoanode architectures, with varying degrees of efficiency improvement [38]. Several aspects are said to influence the efficiencies of graphene-based DSSCs, with the most difficult challenge being to directly incorporate graphene into the structure of TiO_2 [39]. In addition, the industrial scale production of inexpensive, high-quality graphene for DSSC photoanodes continues to be a difficulty [39, 41, 42].

In order to create DSSCs, one must first comprehend the important cellular processes. This study therefore offers a perspective on the synthesis and fabrication of upgraded DSSCs with FTO, reduced graphene oxide-incorporated photoanodes, and counter electrode in DSSCs design and technique of integration, as well as current challenges and research prospects on the new design and improvements.

2.1 DSSC: Structure and working principles

2.1.1 Structural parts of DSSCs

DSSCs as illustrated in Figure. 2.1, comprises mainly of five parts which include a substrate, photoelectrode, sensitizing dye, electrolyte and counter electrode.

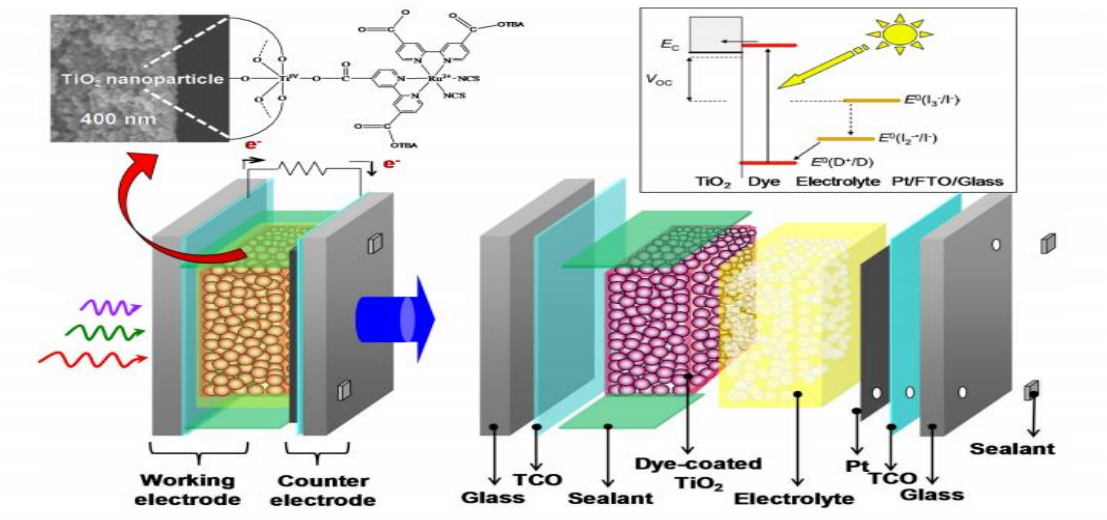

Figure 2.1 Schematic Description0f DSSC [31]

2.1.1.1 Substrates

The standard electrode in DSSCs is constructed of transparent conducting-oxides (TCO) that have been covered with glass substrates. TCOs are commonly used in DSSCs due to their inexpensive cost, good optical transparency and-abundance in the visible and infrared regions of the sun spectrum [31].

To coat the TCO, which is manufactured from bare glass, with a metal oxide (often fluorine-doped tin oxide-FTO ($F:SnO_2$) and indium-tin-oxide ITO (In_2O_3: Sn, ITO), doping is uti1ized. At higher temperatures of around 450–500°C during the conventional nanostructure production technique, and in order to achieve thermal stability, the FTO is generally utilized in place of ITO [43].

2.1.1.2 Photoelectrode

The photoelectrode is created by coating the TCO substrate with a thin layer of sensitive wide-band gap nanostructured metal oxide semiconductor (MOS), typically composed of TiO_2, ZnO, SnO_2, and Sb_2O_5 (photoanode). The nanostructured metal-oxide semiconductor layer needs to have a huge surface area (high roughness) to enable the-adsorption of numerous sensitizer molecules in order to accomplish a high light-harvesting efficiency (LHE) [43,44, 45, 47, 48, 49]

2.1.1.3 Dye molecules (photosensitizers)

Because it is essential to sensitize the wide-bandgap of a nanostructured photo electrode", the photosensitizer is essential to the operation of a DSSC. As a result, numerous dyes, numbering in the hundreds, have been studied over time. An efficient sensitizer should produce strong light absorption across the whole visible region of the solar spectrum as well as into the infrared region in order to improve light harvesting. It must have an appropriate anchoring group that enables linking to the semiconducting oxide, such as a carboxylic acid [50, 51, 52, 53].

2.1.1.4 Redox electrolyte

A redox pair (I /I3) melted in a suitable solvent, usually acetonitrile (ACN), and frequently additional additives to improve the performance of the cell make up the electrolytes comm0n1y employed in ordinary DSSCs [30,51]. “For dye regeneration and to complete the transportation of electrons between the photo electrode and counter electrode in the DSSC, an electrolyte is required. There have been numerous studies conducted on various types of solvents for the electrolyte, including alcohols, propylene carbonate, -butyrolactone, tetrahydrofuran, N, N dimethylformamide, and other forms of nitrile solvents [53, 54, 55, 56]

2.1.1.5 Counter electrode

The electrolytes often used in standard DSSCs consist of a redox pair (I / I3) dissolved in a suitable solvent, stereotypically acetonitrile (ACN), and frequently added additives to enhance the performance of the cell [30, 51]. An electrolyte is necessary for dye regeneration and to finish the transportation of e1ectrons between the photo electrode and counter electrode in the DSSC. Numerous investigations on varying sorts of electrolyte solvents, such as alcohols, propylene carbonate, -butyrolactone, tetrahydrofuran, N, N dimethylformamide, and other nitrile solvents, have been carried out [57, 58, 59].

2.1.2 Working principle of a DSSCs

The two main ways that DSSCs differ from all other solar cells are how they absorb light and how they transfer charges [60, 61]. DSSCs operate on the princip1e of absorption, separation, and collection.

In the process of absorbing light, the dye molecule, a crucial component of the “cell that coats the semiconductor support, excites the electron via the highest engaged molecular-orbital (HOMO) to the bottom most unengaged moecular-orbita1 (LUMO), creating an exciton, which is made up of an excited electron and an electron hole. The HOMO is the share of the cell that has the lowermost energy-level of the cell whereas the LUMO has the utmost energy-level of the cell as shown in Figure. 2.2 [63]

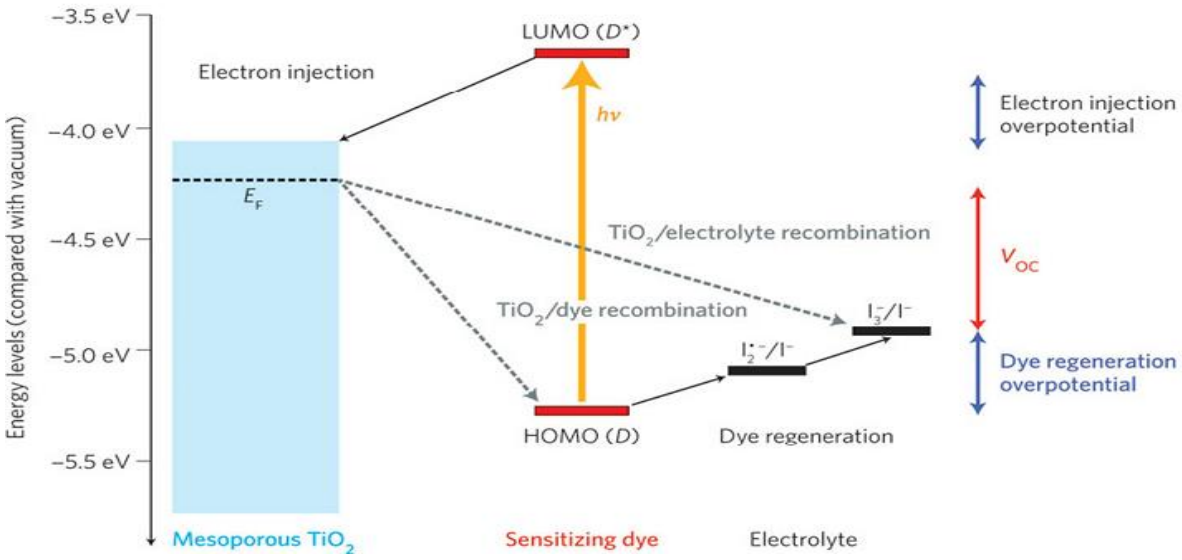

Figure 2.2a: The Working Principle of a Schematic of DSSCs [62]

After the light is absorbed, separation occurs, involving the oxidation of the dye molecule and the injection of an exciton into the conduction band of metal oxide semiconductors (MOS). The two opposing charges must be separated at the MOS and dye interface in order to prevent them from recombining and generate current.

When these charges are generated, the excited electron is delivered to the anode through a semiconductor support medium, and the excited holes are transported to the cathode through the electrolyte on the other side of the dye [51]. The circuit is then complete, and the light-absorbing dye molecules cause the electrons to move around the circuit [63]. After the light is absorbed, separation takes place as a result of the dye molecule being oxidized and a metal-oxide semiconductor's conduction band being exciton-injected (MOS). To prevent recombination and create current, the two opposing charges must-be separated at the MOS and dye interface. Once these charges are produced, the excited electron is sent to the anode via a semiconductor support-medium, and the excited holes are sent to the cathode via the electrolyte on the opposite side of the dye [51, 62, 63]. At this point, the circuit is finished, and the molecules of the light-absorbing dye force the electrons to travel around the circuit [63, 64].

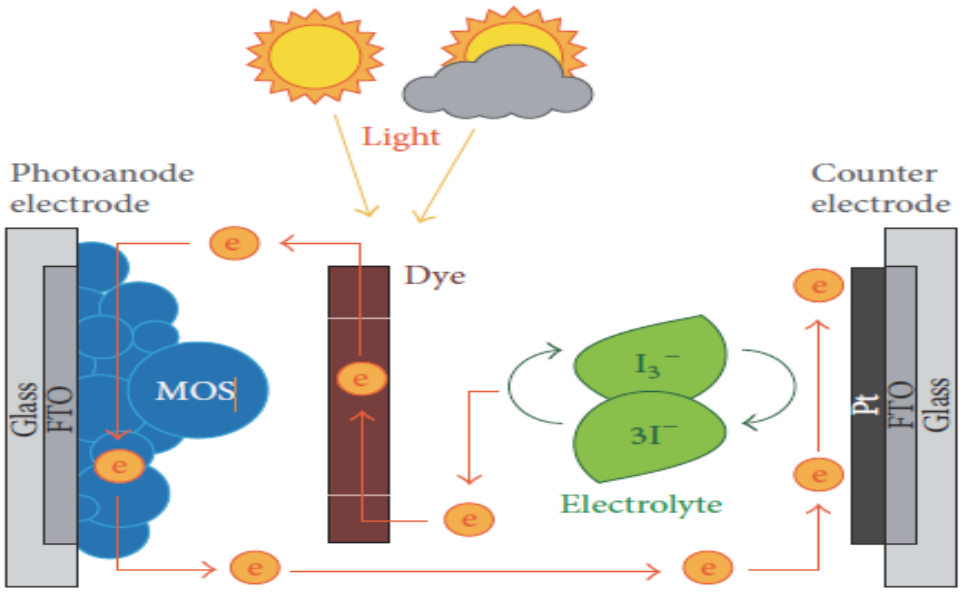

Figure 2.2b: Schematic structure of DSSC [64]

To properly match their various energy levels as depicted in Figure 2.2a, all of the parts of the cell must be carefully chosen [64]. Via variance in potentials between the conduction band edge of the semiconductor support and the redox potential of the electrolyte eventually determines the maximum output voltage (Voc) of the cell.

Therefore, in order to reduce energy losses, these potentials must be as closely matched to the "LUMO and HOMO levels of the dye" [63, 64].

2.1.3 Chemical Reaction in a DSSC

According to Figure 2.2a, the six primary chemical reactions that make up a DSSC's working principles are the "absorption reaction, electron injection, electron transport, triiodide reduction, dye regeneration, and recombination process [62, 64].

Recombination processes cause energy losses and lower the DSSC's efficiency. Due to an excitation that exists amongst the dye molecules' electronic states, the dye molecules absorb light and photons in the DSSC as the initial response.

According to Anwar in 2013, the excitation naturally involves a metal-to-ligand charge transfer (MLCT), which tends to transport electrons from the mo1ecu1ar ground state's HOMO level to the LUMO level [65]. The absorption state is also known as the excitation state as shown in equation-(2.1) below

$$S + photon \rightarrow S^* \qquad 2.1$$

Excitation and 1ight absorption cause the e1ectr0n in the injected meta1-oxide semiconductor conducting band to become TiO2, as illustrated in equation (2.2).

$$S^* + TiO_2 \rightarrow e^-_{(TiO_2)} + S^+ \qquad 2.2$$

According to studies by [66] and [65], the movement of the electrons results from diffusion caused by the gradient of the electronic concentration in nanoporous TiO_2. However, other studies also indicated that the movement is caused by the intensity of the incident-light [67].

According to [66], the quasi-Fermi level under electr0n illumination determines the coefficient of electron diffusion. These findings were exp1ained by the multiple trapping (MT) model [68, 69, 70]. The kinetic rivalry amongst the mobility of the injected electrons in the nanoporous semiconductor layer and the recombination reaction of these electrons with the redox species in the electrolyte or with the oxidized dye-molecules is what-causes the collection of charges in DSSCs [71]. The migration of the electrons must occur far more quickly than recombination for the charges to be collected effectively, and this must occur in the range of milliseconds [72, 73]

$$e^-_{(TiO_2)} + CE \rightarrow TiO_2 + e^-_{CE} + electricalenergy \qquad 2.3$$

The fourth stage of the DSSCs reaction cycle, the tri-iodide reduction to iodide, takes place at the counter-electrode. The counter electrode's catalytic activity must be high for this reaction to decrease energy loss and boost the performance of DSSCs. Due to its high catalytic activity for triiodide reduction, platinum (Pt) is the catalyst that is most frequently utilized in the counter electrode [74] equation (2.4) below.

$$I_3^- + 2e^-_{(CE)} \rightarrow 3I^- + CE \qquad 2.4$$

The regeneration of dye is a part of the DSSC's fifth energy reaction. The I^-/I^-_3 redox pair, which is required for the fourth and fifth reactions, is present in the organic so1vents that are typically employed to make the electrolyte for DSSCs.

$$S^+ + 3I^- \rightarrow 2S + I_3^- \qquad 2.5$$

A sequence of energetic reactions split into three steps make up the recombination process. Since the TiO_2 nanoporous film's electrons are constantly a few nanometers away from the semiconductor/electrolyte contact, it is possible that they may recombine with either oxidized dye molecules or triiodide in the electrolyte. When compared to the electron injection in TiO_2, the first stage of this recombination process is a very sluggish reaction, as seen in equation (2.6). One of the unfavorable processes in the DSSC is the subsequent reaction, which is a recombination of injected electrons in TiO_2 with the triiodide ion at the interface and is represented by equation (2.7). As opposed to the initial process reaction, this process is far more likely [75]. Since the TiO_2 film might not completely cover the transparent conducting-oxide (TCO), as illustrated in equation (2.8), the final-reaction of recombination might also take place on the TCO.

Due to the platinum-free TCO's extremely weak electrocatalytic-activity toward the iodine/triiodide redox system, studies have revea1ed that this effect is modest and insignificant [76]. As a result, the kinetics of this reaction shows a multi-exponential time law, occurring on a microsecond to millisecond time-scale as opposed to ultrafast electron injection, and the “first-stage of the recombination reaction method necessity proceed slowly in comparison to the electron-injection and regeneration of dyes in order to have significant charge separation [77, 78] It is determined by the semiconductor's e1ectron density and light intensity [74].

$$e^-(TiO_2) + S^+ \rightarrow S^0 \qquad 2.6$$

$$2e^-(TiO_2) + I_3 \rightarrow 3I \qquad 2,7$$

$$2e^-(TCO) + I_3 \rightarrow 3I \qquad 2.8$$

2.1.4 Effectiveness of Improved DSSC Performance

Numerous studies have been done on the best ways to accomplish efficient DSSC performance improvement. There is a significant difference between the size of solar cells researched in a-laboratory and those that are genuinely usable on a big scale. They concentrated on changing the structures and key sections of the DSSC [79,80, 81]. Lenzmann and Kroon examined the effect of DSSC size in 2007 without taking stability into account, and discovered that efficiency dropped with DSSC size [82]. In-order to facilitate the collection of generated free-electrons and aid in the transmission of current via the cell, the glass used in DSSCs is engineered to be conductive.

Any incoming light must pass through the glass because the glass plates serve as the cell's exterior walls. Consequently, the glass' optical qualities are essential to the health of the cells [83]. To excite electrons contained-by the DSSC, the glass must be extremely clear in the sensitizers' absorption zone. The photoelectrode of the DSSC was characterized by Kay and Gratzel as a conductive glass plate that was "covered with a porous layer of a wide band gap semiconductor, typically TiO_2, which is sensitized for visible light by an absorbed sensitizer" [84]. On the conductive side of glass with SnO_2 film, colloid TiO_2 was deposited using the doctor-blading technique (a rod is forced on the surface and dispersed across the surface).

The glass with the TiO_2 coating was then heated to 450°C [84]. To finish the photoelectrode, sensitizing dye was then applied to the TiO_2-coated glass. Most DSSCs use this procedure as norma1. A careful analysis of the literature indicated that the semiconductor has changed very little over the past fifteen years. The majority of photoelectrode-related experiments have focused on altering the electrode's dye sensitizer. The usage of various forms of TiO_2 has been the only other significant advancement in the photoelectrode. Due to its inexpensive price, superior semiconducting qualities, and its extensive use as a white colorant in toothpastes and paints, TiO_2 has been employed as the semiconductor in DSSCs from the invention of these devices [84].

The capabilities of a cell can vary depending on the type of TiO_2. TiO_2 nanorods should be used rather than TiO_2 nanoparticles. Due to the rods' snagging in a special 3D network, nanorods boost charge transport and cause an increase in the lifespan of the electron in the photoelectrode [85]. The early conversion efficiency of nanorod-based DSSCs is 3.32 percent compared to that

of nanoparticle-based DSSCs at 1.97 percent because nanorods have a larger surface area than nanoparticles. In an environment with rising salt content, nanorod-based DSSCs also have a greater overall conversion efficiency. Though the conversion efficiency of nanoparticle-based DSSCs declined with rising salt concentrations that of nanorod-based DSSCs remained constant. Based on these findings, it was determined that nanorod-based DSSCs outperformed nanoparticle-based DSSCs both generally and in harsh conditions [86, 87].

Due to carbon's special ability to connect with other elements easily, research into graphene has generated a great deal of interest over the years. Via a study by Long et-al., in 2012 on graphene/TiO_2 composites, they discovered that graphene and its derivatives has a remarkable potential for photovo1taic applications, providing an effective photo-induced charge separation at the interface [88].

When graphene was added to TiO_2 utilizing the modified Hummer's technique, Jang et al. in 2015 found that the PCE of DSSCs was 47 percent better than with pure TiO_2 [89]. According to [90], the redox pair is essentia1 to the efficiency of DSSCs. Iodide (I-) reduces dye molecules that have been oxidized by incoming photons to triiodide (I-3), which then travels to the counter electrode and is reduced back to iodide. The dye that has just been freshly oxidized by the second incoming photon can subsequent1y be reduced by the iodide.

Subject on the redox reactions taking place with the mediator redox couple (I-/I3-), this cycle continues to occur [83]. In their assessment of the iodide/triiodide redox mediator, Boschloo and Hagfeldt [90] states that "the photovoltage of the device depends on the redox pair since it establishes the electrochemical potential at other counter electrode." This is due to the fact that the "driving force for dye regeneration process is given by the difference between the energy states of the standard dye with the oxidized dye and iodide with diiodide (I_2-)," according to kinetic theory [90].

2.2 Preparation of Transparent Conducting Materia1s (TCMs)

Transparent conductive materials (TCMs) mainly belong to a class of substances that frequently exhibits simultaneous electrical conductivity and optica1-transmission. They can be found in a variety of forms, such as metal films, wide-band-gap semiconductors, metal nitrides, or doped

organic polymers [91], and are mostly used in solar cells and other energy-related devices [92, 93]. The most often utilized TCO is fluorine-doped tin or tin-doped indium oxide (FTO or ITO), which enables the glass plates to act as electrodes and collect the electric charge generated within the cell. They are ideally suited for the majority of the Sun's output since both the FTO and ITO coatings are very transparent across the visible spectrum and more absorbent in ranges closer to UV rays [94].

The usual resistivity of FTO and ITO coatings is between 10 and 20 / cm^2. But as temperature rises, the resistance of glass-ITO electrodes significantly increases, and this phenomenon is not seen in glass that has been covered in FTO [94]. Other than solar cells, a number of different technologies can be used to make FTO physically, chemically, and electrochemically stable. The hydrothermal process, chemical-vapour-deposition (CVD), RF sputtering, and spray-pyrolysis are just a few of the techniques used to create FTO nanocomposites.

2.2.1 Hydrothermal Method

A homogenous thin fi1m of FTO can be created using this technique. This procedure involves liquid deposition because it uses a bottom-up strategy (also known as soft chemistry), which produces a thin film that is homogeneous and has steady pressure and temperature [64]. Water is used in this procedure as a reaction medium and is denoted to as a universa1 solvent due to its nature, importance, and exceptional qualities [60]. It is a medium for reaction that takes place under entirely different hydrothermal conditions than usual.

The benefits it offers for the environment are essentially the method's most significant benefit (i.e. water being the most effective solvent when it comes to cost and acting as a catalyst for the formation of desired materials). It is not flammable or explosive, non-mutagenic, non-carcinogenic, and thermodynamically stable [64]. Water is highly volatile, making it simple to remove from any operation.

The parameters of the experiment, as well as the procedure itself, have a relative impact on the nanostructure of FTO [95]. When compared to the amorphous technique in other studies, the solution-based method was found to have a 1ow cost of manufacturing and a high growth rate of the seed layer on the nanostructured FTO [95]. For instance, the hydrothermal method of

generating ZnO nanostructures has become extremely popular due to its simplicity and bearable growth conditions [96].

The rapid development in nanoscience and nanotechnology over the past few decades has offered new possibilities and opportunity for exploitation of new analytic tools and devices for bioanalysis. Nanoparticles represent an emerging tool for bioanalytical techniques due to their unique properties such as small size, large surface-to-volume ratio, easy synthesis and functionalization, and good biocompatibility [97].

In 2009, Liu and Aydi1 saw the discovery of a straight forward hydrothermal technique. On FTO substrates, the technique was used to generate oriented single-crystalline rutile TiO_2 nanorods [98]. When these techniques were contrasted with others, the hydrothermal technique showed promise for producing nanostructured FTO thin films.

Different nanostructures of FTOs, including nano-bows, nanocages, nanorods, and nanobelts, had been reported throughout the previous 20 years [95]. Utilizing pentahydrate stannic chloride ($SnCl_4 \bullet 5H_2O$) and ammonium fluoride (NH_4F) as precursors, nanostructure was directly generated on FTO g1ass substrate in a work by Sasha et al. on the fabrication of a nanostructured FTO using the hydrothermal technique [95].

Different time variations were used throughout the synthesis, and field emission scanning electron microscopy was used to examine the properties of the nanostructured FTO (FESEM). The FESEM pictures showed the development of a layer of nanoparticles on the FTO substrate. As the thickness of the nanostructured layer was raised, a degradation of conductivity was observed in the electrica1 properties. Results from UV-Vis showed that transmittance decreased as the duration of the experiment grew. It was discovered by FESEM ana1ysis that employing DBTA as a precursor can improve the nanostructured FTO [95].

2.2.2 Chemical Vapor Deposition (CVD)

There are numerous ways to synthesize FTO via CVD, including atmospheric pressure CVD [99], low pressure CVD plasma enhanced CVD [100], and other methods [101. [102] employed the atmospheric pressure CVD process to create FTO by depositing FTO onto a glass substrate at different substrate temperatures and then holding that temperature constant at 500°C whi1e using air as both the career gas and the oxidizing agent. When the generated thin film's electrica1

properties were evaluated, it was found that they tended to alter based on the substrate's temperature, varying from being an insulator thin film to a highly conductive thin film [102]. Under X-ray diffraction, the structural property was seen to be poly-crystalline at higher temperatures and amorphous at lower temperature.

2.2.3 Sputtering

Some FTO preparation procedures necessitate high substrate temperatures for the material as well as post-treatments like annealing, which results in the creation of in-between semiconductor oxide layers at the film border and increases operational costs [103].

Compared to other techniques, sputtering hasn't been used to prepare FTO very much over the years. This procedure claims to be ecologically friendly and the use of targets made of lightly-packed blended powder provides an effective way to screen potential compositions while also having a low operational cost [103]. This process was first applied in 1955 to create In_2O_3:Sn in tiny grains [60].

The sole method that produces well-adhered, large-sized films with excellent quality large-scale deposition at relatively low substrate temperatures is magnetron sputtering [104]. There are various sputtering techniques, including radio frequency (RF) sputtering [105] and direct current (DC) reactive sputtering [104, 106, 107, 108].

According to theoretical predictions, hydrogen can operate as a source of n-type conductions in ZnO materials when added to the sputtering atmosphere [109, 110, 111]. Conversely, as it is the most frequently utilized, little research has been done to support the idea that hydrogen can be added to the sputtering atmosphere of SnO_2. To increase the conductive quality of the film, [106] tried adding H_2 to the sputtering atmosphere [108]. A SnO_2-based film was optimized by [112] by adding the same hydrogen to the sputtering atmosphere [104].

In-the study, FTO films were deposited using the RF sputtering technique on a fixed H_2/Ar concentration ratio of (3/97) SnO_2-SnF_2 target. The impact of H_2 concentration in the sputtering atmosphere was also examined, and more studies in this area. In order to examine the effects of the H_2/Ar flow ratio on the film's characteristics at two different substrate temperatures. [104]

produced a thin film of FTO using the sputtering SnO_2- SnF_2 target introduced by de Moure-Flores et al. in 2013 [104, 112].

According to Zhu et al., the introduction of H_2 can result in the production of an FTO thin film with a (1:1) Ar flow ratio, and the resistivity of the film tends to drop initially before increasing over a specific value [104]. The conductivity, transmittance, and band gap all decrease as the flow rate of H_2/Ar rises [104].

In a study conducted by [113], FTO were made using a mixture of SnO2 and SnF_2 powder, and then the fluorine doping level was examined [103]. Different film thicknesses with subsequent electrical and optical properties were produced during the research at various doping levels. The outcome showed that a thin film with an optical bandgap of 3.80 eV, an average visual transmittance of 83 percent, a resistivity 0f 6.71 x 10-3 cm, and a mobility of 15 cm2/Vs was optimal.

2.2.4 Spray Pyrolysis

Spray pyrolysis has been used to produce TCO since 1947, when Mochel added Sb to SnO_2 and McMaster added Cl to SnO_2. It has been used for numerous TCO over time, including doping tin oxide with fluorine (FTO) [114, 115]. Since of its simplicity, low cost of experimental equipment, ready incomparability of multiple dopants, high growth rate, and high mass production compatibility for big area coating, spray pyrolysis is a widely-utilized technique [116]. In this procedure, a precursor solution is sprayed onto a heated surface to deposit a thin film of the necessary substance. As a tin element in the precursor solution for making FTO films, a number of tin compounds have been employed. The type of substance utilized determines their preferred crystal growth orientation and crystal size, which in turn affects the optical, electrical, and conductivity properties [117].

Murakami noted the first SnO_2's development on the glass substrate. He discovered that each isolated grain had developed nearly at the same pace, with its density at initial stage increases with surface area roughness, and increase in roughness caused the grain to spread more widely [118].

However, Liyanage et-al. were ab1e to enhance spray pyrolysis in 2013 to produce FTO nanorod films with a low resistance-sheet characteristic [119]. To maintain a high percentage of FTO film transmittance and low pressure throughout the deposition process, a horizontal spray approach was adopted in the enhanced spray pyrolysis. It was discovered that the temperature at which-deposition happens, the time at which reactions happen, the type of precursor, and the solvent that were utilized, all had an impact on the size of the grain of FTO films [60].

In 2015, Hassanien et-al. created thin films of undoped SnO_2 and fluorine-doped tin-oxide (FTO) via spray pyrolysis on glass-substrates in an effort to improve the performance of the FTO, whi1e systematically investigating the optimization of the solvent and precursor [120]. He discovered that increasing the spray time, substrate temperature, and solution concentrations led to an increase in film thickness and a decrease in sheet resistance [120]. This invariably means that the growth rate of SnO_2 is optimized as the film thickness is attained.

The-Effective light harvesting and sheet resistance both depend on the electrical and optical characteristics of FTO. The electrical resistance of the film is thickness dependant, and as a result, when the thickness rose due to an increase in spray time, substrate temperature, and solution on centration, the sheet resistance decreased and the conductivity [120]

In 2016, Napi et al.- prepared FTO with two solutions; ammonium fluoride and dibutyl tin diacetate (DBTDA), and the spray pyrolysis method was used to create the FTO substrate [117]. The sample's anneal temperature was varied as the main focus of the study. [117] found that the best-film cou1d be made by altering the anneal temperature, and that this produced a “sheet resistance of 5.11x108 Ω/sq with a highest percentage of transmittance [117]. Since an increase in anneal-temperature will result in a rise in energy supply, it was also shown that an increase in anneal-temperature led to an increase in the growth of the thin film.

2.3 Fundamental Characteristic Properties of Graphene

Recently, interest in graphene has grown significantly, and its science is now one of the most fascinating and rapidly-evolving areas of material science [121]. The scope of graphene is expanding, combining theoretical theories with new developments in experimental methods. On the other hand, graphene's high surface area, exceptional transparency, Light absorption, and charge transport properties have substantially spurred interest from various study domains

connected with energy conversion and the removal of environmental pollution [122]. The existence of 2D crystals has previously been questioned repeatedly because the Mermin-Wagner theorem predicts that a 2D crystalloses its long-range order and me1ts at any tiny but non-zero temperature as a result of thermal fluctuations.

The first really 2D crysta1 to be seen in nature is graphene. Graphene is an allotrope of carbon that consists of a 2D, atomic-scale hexagonal lattice with one atom forming each vertex by sp2 hybridization, according to [123]. The basic structure of graphene is a hexagonal carbon ring with a surface area of 0.052 nm^2, a carbon-carbon link length of roughly 0.142 nm, and a stable hexagonal structure produced by three powerful covalent bonds in each lattice [123]. The reality of 2D crystals has previously been questioned repeatedly because the Mermin-Wagner theorem predicts that a 2D crystalloses its long-range order and melts at any tiny but non-zero temperature as a result of thermal-fluctuations. The first really 2D crystaltobe seen in nature is graphene.

According to [123] graphene is an allotrope of carbon that is made up of a 2D, atomic-scale hexagonal lattice with one atom constituting each vertex by sp^2 hybridization. In the unit structure of graphene is a hexagonal carbon ring with an area of 0.052 nm^2, a carbon-carbon link length of roughly 0.142 nm, and a stable hexagonal structure made of three potent covalent bonds within every lattice [123]. The stability of graphene is attributed to its closely spaced carbon atoms and a sp^2orbital hybridization, which combines the orbitals s, px, and py to form the -bond. The -bond is created by the last pz electron. Most of the prominent electronic features of graphene are a result of these bands, specifically the half-filled band that allows free-moving electrons [123]. Additionally, because to its extreme thinness, graphene is known for its transparency in the visible area, which is advantageous in the conductive substrate used by DSSC [124, 125].

2.3.1 Synthesis of Reduced Graphene Oxide (rGO)

The mysterious three-dimensional carbon allotrope has perhaps received the most theoretical attention. All computations on graphite, fullerenes and carbon nanotubes begin with graphene; neverthe1ess, countless attempts to create these two-dimensional atomic crystals have mostly failed, yielding nanometer-sized crystallites instead [1, 126, 127, 128, 129]. Given the widespread misconception that fully two-dimensional crystals cannot exist, these challenges are

not surprising (in contrast to the numerous, known quasi two-dimensional systems). Additionally, any graphene nucleation sites created during synthesis will have extremely high perimeter-to-surface ratios, which will encourage collapse into other carbon allotropes.

The first experimental attempts to produce graphene can be credited to [130]. He discovered single-and-few-layer graphite structures in solution as a byproduct of graphene oxide (GO) reduction in his work on transmission of electron microscopy. A pioneering work to isolate graphene monolayer via highly-oriented pyrolytic graphite (HOPG) over mechanical-exfoliation was carried out by [131] via their expert scotch-tape technique. New efforts in the 1990s led to the growth deposition of graphene on metal surfaces, then slight success was noted [131]

Numerous methods have been used to create graphene since the initial isolation. The synthesis techniques are divided into two groups: "top-down" and "bottom-up."(Figure. 2.2c) Depending on the intended use, developing efficient methods for graphene synthesis is essentially depended on the intended use for the application, taking into account the desired product's morphology, purity, orientation, thickness, and efflorescence.

Graphene or its derivatives, such as graphene oxide (GO), rGO and graphene fluoride, are separated from one another or exfoliated to form graphene or modified graphene sheets in a top-down process [132, 133, 134, 135]. The most comm0n top-down technique is graphite exfoliation.

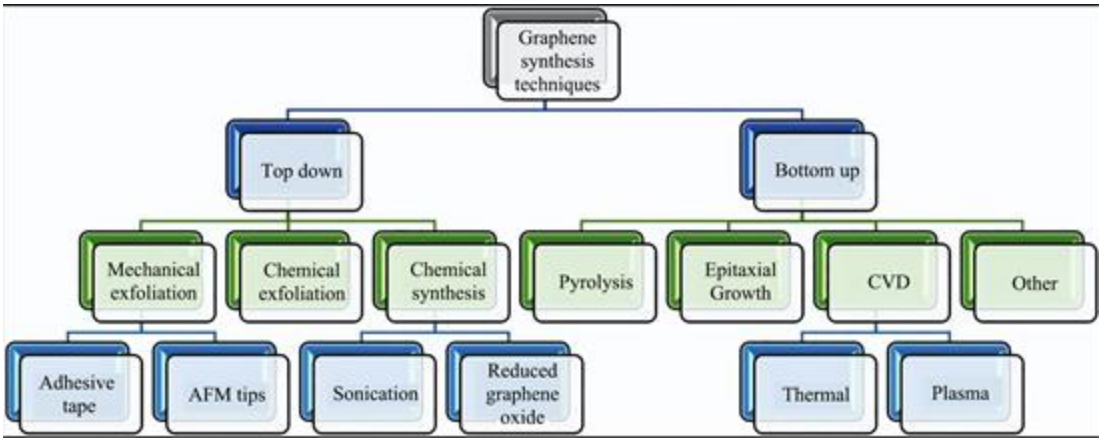

Figure. 2.2c Flow chart for synthesis of graphene oxide [1, 132]; (a) In the top-down process, graphene sheets are produced by exfoliation or separation of highly ordered pyrolytic graphite

(HOPG) or its derivative, graphene oxide (GO), (b) In the bottom-up process, graphene sheets are produced by building up nanoscale material via atomic or molecular arrangement of carbon. One of the main difficulties with this method is aggregation during processing of large quantities of graphene sheets, which have a propensity to form irreversible agglomerates or even restack to produce graphite through Van der Waals interactions unless well isolated from one another [135]. On-the-other-hand, the bottom-up strategy begins with tiny organic molecules to produce graphene. This technique stands out for its meticulous control of the graphene's form and structure [132]. The chemical vapour deposition (CVD) method appears to be the most widely used bottom-up strategy.

According to many studies, graphene was created through the degradation of hydrocarbons (1ike methane) into graphene, which was then catalyzed by metal surfaces using CVD [136]. High-quality graphene is often deposited using the CVD technique on a variety of transition-metal substrates, including Ni, Pd, Ru, Ir, and Cu [132]. Epitaxial thermal growth, also known as thermal breakdown, is a crucial bottom-up technique that enables the synthesis of graphene on a single crystalline silicon carbide (SiC) surface [137]

Additionally, the Brodie, Staudenmaier, and Hummers methods as well as graphene oxide reduction are recognized to be other methods for producing graphene (Kaiser et al., 2007; Nurhafizaha et-al., 2017).

2.3.2 Mu1tidimensional-Forms of Graphene

The focus of graphene research has remained on practical applications. Due to the growing number of uses for graphene in many fields, 2D graphene sheets have been modified to produce one (1D) and three (3D) rGO dimensional forms. According to [134, 135, 137], 1D and 3D graphene-based derivatives have a wide range of remarkable qualities [138]. Numerous studies in this field have been sparked in recent years by the production of 1D graphene fibers and nanoribons.

To adjust the electrical characteristics of graphene for various applications and bandgap, engineering, and whose properties highly depend on their size and edge shape, large-area graphene is purposefully constrained in one dimension to generate graphene nanoribons (GNRs).

Wet spinning of carbon nanotubes (CNTs) has been used to prepare 1D graphene (fibers) from graphene oxide suspensions [135,139, 140, 141]. Other preparation techniques include dimensionally-confined hydrothermal strategy [142] and chemical reduction [143]. It can also be made from graphene films like graphene oxide film and chemical vapor deposition produced graphene fi1m [144, 145]. It is possible to create graphene nanoribbon by longitudinally unzipping CNTs [146]. The photoconversion efficiency (PCE) of the dye-sensitized solar cells (DSSCs) was reported to be greatly increased by the GNRs when 1D graphene was employed in DSSCs, used at the counter-electrode and in I-/I3-based electrolyte, and recently inserted into TiO_2-photoanode [145]. The creation of a graphene with a band gap is one of the efforts made to diversify the applications based on graphene. The alteration of electron behavior—i.e., the physical characteristics of grapheme-due to quantum confinement is what sets graphene quantum structures apart from graphene. The electrical and optical properties of graphene quantum structure are influenced by the specific size, shape, and edge structure when graphene is shrunk to a size comparable to the excit0nBhor radius, allowing for the observation of quantum confinement effects [143, 146, 147].

Soon after, [148] asserted that bandgaps exist in graphene nanoribbons (GNRs). [149] asserted that a band gap in armchair graphene results from quantum confinement and edge effects, while a band gap in zigzag GNRs results from a staggered sublattice potential; these predictions were later supported by ground-breaking experimental work from [150, 151]. Ponomarenko et al. in 2008 used electron beam lithography to create graphene dot structures of various sizes and discovered a quantum-induced bandgap in a more precise1y defined graphene quantum dot structure [152]. When comparing the Coulomb blockade peaks of various structures, they discovered that graphene quantum dots (GQDs) smaller than 100 nm had non-periodic Coulomb blockage peaks, which is a clear sign that quantum confinement causes bandgap effects in graphene quantum dots.

According to reports, GQDs have contributed to the advancement of current solar cell technologies, including dye-sensitized solar cells (DSSCs) and perovskite solar cells [153].

Additionally, three-dimensiona1 (3D) interconnected graphene networks seen in materials including aerogels, hydrogels, and foams have drawn a lot of study interest recently [135].

Different methods have been used to assemble 2D graphene into their 3D forms. Geletion is one of the reported efficient methods for assembling graphene oxide (GO) sheets into 3D graphene hydrogels, which could then be transformed into 3D graphene aeroge1 by a later freeze-drying procedure [135].

In order to create 3D porous graphene macrostructures, a number of reduction techniques have been investigated, including the hydrothermal method [153], the solvothermal approach [154], chemical reduction [155], and electrochemical reduction [156]. Because they may be applied to large-scale 3D graphene frameworks, template (hard or soft) driven approaches to create 3D graphene have attracted the greatest attention.

This CVD approach has a hard template that is frequently utilized to fabricate large-scale 3D graphene frameworks by using 3D nickel foams as templates [135]. The same processes that occur during the CVD manufacture of1arge-scale graphene films—pyrolysis of the carbon source, dissolution of carbon atoms in nickel, and formation0f graphene on the nickel surface after cooling down also occur here [157]. Another straightforward and ecologically benign method of hard template direction is ice-templating, which eliminates the need for the laborious template etching phase that uses potent solvents and acids [135]. Soft templates, such as micelles, emulsions, and bubbles, have been investigated in addition to the hard temp1ate guiding technique to build graphene-based 3D macroscopic structures. Materials based on 3D graphene have entered the energy conversion industry, including dye-sensitized solar cells (DSSC). For DSSC, 3D graphene nanofoam has been used in place of a platinum counter-electrode [158].

2.4 Application of Reduced Graphene Oxide in DSSCs

In the design of the DSSC photoanode, graphene and its variants have largely served as supporting components. The usage of graphene materia1s as transparent conductors, in the semiconducting layer, and as sensitizers is the main topic of this section (dye) [159, 160].

2.4.1 Transparent Conductive Electrodes

In-terms ofoptica1 transparency, electrical conductivity, mechanical strength, and thermal conductivity, graphene stands out for having a number of desirable features. The one atomic layer of carbon atoms in graphene, which has a planar density of 0.77 mg/m^2, is what gives it the advantages of being extremely thin and light [135]. The excellent transparency of 97.7 percent in the visible range at one atomic thickness is one advantage [36]. According to theoretical and experimental findings, the thickness of graphene can be used to control its optical quality [123, 161].

Due to its high optical transmittance and electrical conductivity, graphene-based thin film electrodes have emerged as a highly competitive transparent conductive material and have been suggested as a potential replacement for many common TCEs, including indium tin oxide (ITO) and fluorine-doped tin oxide (FTO) [123, 162]. The issue of fragility, environmental pollution, and a shortage of indium resources could all be resolved by the usage of graphene in this field.
Transparent and conductive graphene electrodes have been successfully used in numerous recent research studies to replace the traditiona1 transparent conducting oxides (TCOs) in dye-sensitized solar cells [134, 163]. According to Bonaccorso et al. in 2010 each layer of graphene absorbs about 2.3 % of light thereby resulting in 90 % transmittance in which light can pass through a maximum of~5sheets [164]. In contrast, [165] demonstrated that for a single-sheet measurement, the thermally reduced graphene oxide (TRGO) sheet with an atomic carbon to oxygen ratio higher than 300 RSh0f 7.7 k/sq (Figure 7B) [165], while that for pristine graphene is 6.45 k/sq, exhibits a significantly higher level of stability [131]. [166] further indicated that this was due to the materia1's layers only being able to attain a transmittance of 90% and an RSh of roughly 1 k/sq, even without taking into consideration contact resistances between individual sheets [167].

Studies revealed that [163] was the first to fabricate graphene in DSSCs using it as a transparent electrode. Graphene films were generated by exfoliating the graphene oxide and then thermally reducing the platelets, thereby forming the TRGO films: The films were created by sequentially covering silica glass with graphene oxide dips, followed by annealing the films at 1100 °C [163]. The material had to be sufficiently reduced at high temperatures in order to increase the size of the sp2-hybridized aromatic networks and conductivity. They possessed an RSh of 1.8 k/sq, a

transmittance of around 62 percent at 550 nm, and were evaluated for use as DSSC window electrodes. They were about 10 nm thick.

The films created as window electrodes have a wavelength between 1000 and 3000 nm, a conductivity of 500 Scml, and a transparency of more than 70%, although they perform poorly when compared to FTO. However, the achievement made by [163] opened researchers' eyes to the potential of graphene as transparent conducting materials [163]. In current research by [168], it was discovered that employing graphene and titanium film electrodes to achieve high porosity and large specific surface area was achieved to increase the adsorption rate of sensitizing dye, and the PCE was reported to be 7.2 percent [168]

According to [169], using graphene with a monolayer of TiO2 as a photoanode led to a 31 percent increase in PCE compared to a TiO2 anode [169]. In the meantime, according to [170], the values derived from the after preparing graphene films on SiO2 substrates stretched a photovoltaic efficiency of over 4.25 % and can be compared to FTO applied as electrodes [171]. In a bid to standardize and compare the various techniques, [172] analyzed over 20 studies 0f graphene material-based transparent electrodes. They related the material's conductivity and transmittance to the electrode characteristics by relating the material's dc conductivity (DC) to optical conductivity (Op) ratio [170]. According to their analysis, contact resistance between sheets severely restricts the reduced graphene oxide (DC/Op limit of 0.7), with larger sheets (such produced by the [123] approach or by CVD methods) obtaining greater conductivity as a result of fewer contact regions. They claimed that a DC/Op of 35 or higher is required to produce a 100 /sq film with a transmittance of 90%.

They found that CVD-derived graphene has a higher suitability than a mosaic of sheets (DC/Op limit of 2.6), although it is still far since ideal on meeting commercial needs [167]. [172] pointed out that boosting the carrier concentration by substrate interactions or electronic doping can significantly increase the conductivity limit [170].

Electronic-doping can take place by adsorbing electron-donating or accepting substances to sheets or by incorporating them into the graphene lattice. Chemicals frequently utilized for the latter electrical doping technique include HNO_3 and $SOC1_2$. The sheet resistance of their TRGO films is reduced by electronic doping, bringing about a significant improvement but keeping the

resistance almost an order of magnitude higher than ITO films at 459 /sq at a transmittance of 90%. [172].

To obtain great performance, researchers have started using other methods, one of which is the creation of hybrid materials [153, 158, 173]. Chemically reduced graphene oxide (CRGOCNT) and graphene produced from CVD have been used to create hybrid films known as CRGO-(silver nanoparticle) hybrid films. The best CVD-produced grapheme-based TCFs with good performance were identified by [166] over its metal nanowire films [167]. [174] created metal nano-grids (Au, Cu, and Al) with grid lines 100 nm thick and 5–10 μm wide, spaced 100–200 μm apart. The grid was subsequently covered with CVD-derived graphene to create a continuous conductive network [173].

Notwithstanding the achievements so-far, the technology's scalability and cost reductions continue to be a significant problem that warrants urgent study attention.

The graphene-based photoanode of the DSSC is formed of graphene oxide (GO) and reduced graphene oxide, however, according to recent studies (rGO). These can be achieved in graphene-based electrodes by varying the layer thickness, which will impact the electrode's quality due to the GO and rGO. As previously mentioned, the two most popu1ar methods for creating DSSC are thermal-reduction and chemical-vapor-deposition. In the meantime, rGO was created using the Langmuir-Blodgett method and modified FTO films in order to lessen charge recombination at the interface of TiO_2 and FTO [162]. However, when it comes to large-scale preparation, the CVD method has drawn more attention. More researches are being conducted due to cracking brought on by decreased mechanica1 strength and a poor transfer procedure brought on by flaws, therefore the requirement for a high-quality preparation of graphene cannot ever be ignored. Additionally, catalytic reactivity frequently results in a high ratio of electron wastage, especially when the graphene surface is exposed to the electrolyte without adequate coverage, which is undesirable for a graphene electrode acting only as a current collector [148]

2.4.2 Nanostructured Semiconductor

Some other development is that nanocrystalline TiO_2or other mesoporous or nanostructured semiconductors have the ability to make good contacts with graphene, which may improve charge separation and conduction. Photo stimulated electrons are typically injected into the

semiconductor in DSSCs from the sensitizer, where they diffuse into the current collector. Losses can be caused by a variety of things, including vo1tage drops in semiconductor Fermi levels and dye LUMO levels, ohmic resistance in the semiconducting layer, and recombination of injected electrons with dye or oxidized species of redox pair. Even more-of the semiconductor or current collector electron (i.e., FTO) can rejoin the electrolyte [167].

Due to the tendency of triiodide to combine with FTO, graphene has been used as a layer to block and prevent recombination as well as in the scaffolding made of TiO_2. This has been done in order to increase photocurrent density and determine the reasons (such as light scattering, dye absorption, and improved transported e1ectron) for the observed improved performance [134].

The practice of graphene in DSSC as a semiconductor-layer was first reported by [148], who used photocatalysis to reduce a composite of graphene oxide and TiO_2 nanoparticles (TiO_2 particle diameter 10 nm) as a hurdle. This was done mainly since flat sheets could be deposited at low temperatures deprived of the use of hazardous chemicals, unlike the comm0n $TiC1_4$ treatment, to provide a blockage in between FTO and triiodide. According to their results, there was a 7.6 percent improvement in performance comparing to a cell without a blocking layer.

The outcome, however, revealed that there had been a significant reduction in light absorption from the film, from 85% to 78%, indicating that the method does not seem to be any more effective than the conventional TiO_2 blocking layers. Nevertheless, several studies utilizing comparable methods have had success in this field and seen advancements [156, 158].

As illustration, [156] attempted to use thermally reduced oxides of graphene as a blocking layer, which resu1ted in an approximately 8.1 percent efficient cell. This cell was more effective than one without a blocking layer (=7.2%) and better than one with their $TiCl_4$ pre-treatment blocking layer (=7.5%). This improved performance was brought on by an increase in the photocurrent. Because graphene oxides and the FTO both act as non-conducting barriers to the recombination0f electrons, only extremely thin layers that permit tunneling will function effectively. As a result of this, only materials made of graphene can function as a blocking layer at their best, despite the fact that they ought to be less active for the redox mediator than FTO [167].

A more common application of graphene materia1\ls is their intentional integration into the semiconducting layer itself to improve the device's performance by guaranteeing that the photocurrent in the photoanode is boosted [134, 167]. By incorporating reduced graphene oxide into TiO_2, dye absorption, charge separation, photogenerated electron transport, and rate of charge recombination can all be improved [74, 175, 176] found that graphene or its derivatives may mix with TiO2 nanoparticles to create bridges of graphene, speeding up the rate at which charges are carried, preventing charge recombination, and increasing the amount of light the device can collect [176]. Normally, the TiO_2 layer in DSSCs is between 10 and 20 micrometers thick. As a result, in order to be received, electrons that are photogenerated on the back side must spread out to the front, a length whereby the order is about 100 μm assuming a random walk. By tracking the transported electron and the rate at which the electrons recombine, one can estimate the efficiency at which it is received as a function of the electron diffusion length and the thickness of the film [167].

Making sure that the transported electrons in TiO_2 are improved during the sintering process will increase the length at which the diffusion occurs, which will boost the efficiency of collecting. Another approach to this is to shorten the length of the electron channel, which can be accomplished by incorporating finger electrodes within the layer of TiO_2 [177, 178].

The principal particle size of the ITO or tin oxide utilized in the electrode materials, as-well-as the requirement to cover the conducting fingers with a blocking layer of TiO_2 (at 1east 6 nm) to avoid recombination in the device, both significantly hurt these techniques [174]. Due to their atomic thinness and high aspect ratio, which gives a very low percolation threshold and can act as a collector of current with a small alteration of the TiO_2 film shape, materials made of graphene have a distinct advantage over other materia1s in overcoming this [167]. That-kind of hybrid nanostructures create physical adsorption (physisorption), electrostatic binding, and charge transfer interactions between graphene and TiO_2 nanoparticles, reduction of TiO_2-TiO_2contact resistance [179] according to [180] explanation.

The bridging graphene functions as a channel in which e1ectr0ns can be moved to increase the transportation of electrons from the conduction band (CB) of TiO_2 at the anchor location fast, decreasing recombination. This is possible because graphene has a flawless conduction of electricity. When graphene or its derivatives is injected, it creates additional holes inside the

photoanode, which would be beneficial to increase light absorption and collection efficiency, leading to an improvement in DSSC performance [179, 180].

Numerous studies have used graphene materials in semiconductor films in various ways; some of the research stated that increasing the conductivity of TiO_2 is the primary cause of the improvement [176]. Others, however, had the opposite opinion and said that the improvement was actually the result of increased dye loading and light scattering in the electrode, which had unexpected negative effects [134]. According to the findings, the photogenerated electrons are injected into the CB 0f TiO_2 at the states in which they are excited, and improving the PCE of the DSSCs. Meaning, when graphene or its derivatives (e.g rGO) materials are present in surplus, PCE of DSSCs would be decreased because TiO_2 was covered with excess graphene, which decreased the dye's ability to absorb light. However, increased reduced graphene oxide content will-also accelerate the recombination of electron-hole pairs in DSSCs rather of creating an electron route.

2.4.3 Dye molecule (Sensitizer)

The sensitizing dye typically performs two tasks: it absorbs light and transfers electrons to the semiconductor's conduction band. An effective sensitizing dye should have high extinction coefficient, great adsorption affinity to the surface of the semiconductor, and durability in its oxidized form. It should also have significant visible-range absorption [167]. Additionally, it can display higher positive highest occupied mo1ecular orbital (HOMO) energy than the redox potential of the electrolyte and lower negative lowest unoccupied molecular orbita1 (LUMO) energy than-the conduction band (CB) of the semiconductor, which is often TiO_2 [134, 181]. Ru-based dyes are expensive, which has forced researchers to look at less expensive substitute ingredients. Due to its tunable band gap, graphene or its derivative is being examined for dye co-sensitization in a DSSC structure. As-a result, the usage of graphene or rGO has been a research priority for this purpose. Along with having a good band gap, reduced graphene oxide is effective in injecting electrons into TiO2.

In DSSCs, graphene materia1s, often in the form of Graphene Quantum Dots (GQDs), can serve as light absorbers, according to recent studies [182, 183, 184, 185]. A graphene quantum dot was created by [176] using sixty benzene-rings with an absorption band at 900 nm, which covers all visible light; this material was used as light absorber in DSSC [184]. Poor interaction between

graphene and TiO_2 was discovered to be the cause of the device's ineffectiveness. Hot injection including mu1tiple carrier-generation, however, have recently shown promise in terms of overcoming the Shockley-Quiessar efficiency limit present in existing device structures [167].

Despite the stated underperformance of graphene in this application, renewed efforts to co-sensitize dyes in a DSSC to increase device efficiency have been made after it was discovered that using GQDs alone cannot generate the necessary efficiency. By incorporating GQDs into the dye molecules, [186] found that the power conversion efficiency (PCE) increased from 5.1 percent to 6.1 percent. The PCE of the device was increased from 1.92 percent to 2.12 percent when [187] used a DSSC with a co-sensitized dye molecule and GQDs. This improvement was attributed to the GQDs' co-sensitization effect [176, 186]. A photoluminescence behavior of the GQDs was shown by [169, 174] employing the GQDs as a co-sensitizer simply by oxidizing the herringbone-type carbon nanofibers combined with a variable ratio of N719 dye molecules.

The findings of both tests suggested that the GQDs exhibit up-conversion photoluminescence properties, with an emission band of around 525 nm and a wavelength ranging from 600 to 750 nm [169]. This shows that the up-conversion ability increases the efficiency of the dye molecule from 7.28 to 7.95 percent by transferring a longer wavelength of photon energy to the area of highest efficiency.

The usage of GQDs as a co-sensitizer continues to draw attention as researchers look for new ways to mix it with other materials and experiment with different ratios to increase the cell's effectiveness. The GQDs therefore enhanced the dye performance at various dye concentrations and light wavelengths. PCE has been considerably improved by using polymerrs, N3 or N719 dyes, or even by modifying the size of the GQD.

However, in order to overcome the inherent constraints of traditional devices, scientists must combine an ultrafast process of injection with these quantum phenomena of graphene.

2.4.4 Characterization of Reduced Graphene Oxide

Several characterization techniques are employed for reduced graphene oxide-based or rGO materials. They include; Raman spectroscopy, Fourier transform infrared spectroscopy (FTIR), X-Ray diffraction (XRD), Energy dispersive X-ray (EDX), scanning electron microscopy

(SEM), ultraviolet-visible spectroscopy (UV-vis), etc. Raman spectroscopy so far has been one of the best tools to investigate the structure and quality of graphene [188]. It is a strong, rapid, sensitive and non-destructive analytical approach that provides qualitative and quantitative information for graphene-based catalysts. It is considered the standard tool to characterize graphene-based catalysts, as it is adopted by most researchers working on graphene-based materials. Generally, graphene has six normal modes and two atoms per unit cell at the so-called Brillouin zone center (Γ), where (Γ) = A2u + B2g + E1u + E2g. Especially, the E2g phonons are active in Raman spectroscopy. The three predominant features of the Raman spectrum for graphene are the D peak (at 1320–1350 cm−1), the G peak (at 1580–1605 cm−1), and the 2D or named G' peak (at 2640–2680 cm−1) [189]. X-ray diffraction (XRD) is another informative tool for investigating the crystalline structure, of graphene and an important parameter for catalyst [190]. These techniques are employed to estimate the size and distribution of loading sites and in turn to assess the catalytic sites dispersion, which governs the catalytic performance of a given material to a great extent. Scanning e1ectron microscopy (SEM) is carried out to visualize the morphology and structure of graphene-based catalysts, which provides lots of information to rationalize their catalytic performance [191, 192], while Energy dispersive spectrometry (EDS) provided with FE-SEM is usually used for elemental composition survey. one of the important functions of X-ray diffraction (XRD) in characterizing graphene-based catalysts is to confirm the reduction of GO to graphene while ultraviolet-visible spectroscopy (UV-vis) is the most convenient way to confirm the successful synthesis of graphene oxide. The graphitic structure shows an absorption peak at ~262 nm while a mono1ayer of GO exhibits absorption at ~230 nm in UV-vis spectrum, which is attributed to the π–π* transitions of aromatic C–C b0nds. Based on this difference, one can easily determine the quality of their "GO" products [193].

2.4.5 App1ication of Graphene Based-or rGO Counter Electrode in-DSSC

The following requirements must be satisfied in order for-the redox-mediators in the-DSSCs to effectively transport charge: (i), the redox species must be able to diffuse easily between the anode and the cathode; (ii) dye regeneration via the reduced species must occur more quickly than from the semi conducting scaffold; and (iii) the rate of redox species reduction must occur slowly at the anode and quickly at the cathode. Due to its high activity and simple way of

manufacture, particularly when utilizing iodide/triiodide as a mediator, platinum has become widely used as counter electrodes in DSSCs. Platinum is deposited on the FTO of the cell [187]

Moreover, there's been some questions about whether platinum is stable when employed in DSSCs because of the performance drop after more than 11,000 hours of testing [194]. Meanwhile, because producing platinum in low-cost DSSCs at high temperatures has a significant cost [167], other methods have been explored to use-carbon black and graphite as its-counter electrode. After the introduction of graphene-based materials in 2008, a plethora of studies showing the effectiveness of various graphene materials as a stand-in for effective-performance and counter electrode optimization-of DSSCs have been conducted [195]. The graphene material for each counter electrode and its platinum-based counterpart were compared in Tab1e 2.1, as shown below. Since 2008, a huge amount of research has been published to examine how the degree of reduction affects the catalytic performance [156,196, 197, 198]. These-studies discovered that the movement decreased when the temperature of the porous CRGO films' thermal annealing activity was raised to 400 °C in air.

The RCT result for the T-CRGO film at 400 °C revealed that it was approximately 280 times greater than that heated to around 250 °C, while Choi et al., (2011) reported the lowest and was comparable to the-treatment reported-above by [196]. Other study done by [197] showed that RCT for CRGO that was thermally treated at very high temperatures of about 600 °C gradually, of which was-the highest employed throughout their-research, monotonically declined [196]. Another work by [198], however, demonstrated a similar improvement in performance by lowering the temperature of the graphene oxides, with films (20 m thick with 5% polyvinylidene fluorine, PVDF) annealed at 700 °C displaying an RCT of $22\Omega cm^2$ [197].

Relatively inert materials have restrictions, and to get around them, it's necessary to chemically adjust the material's intrinsic activity, which will raise it. This is usually done by increasing the size of the pores and the area of the material [167]. The amount of material utilized must be increased, and the film to be used must be thickened, in order to improve the morphology.

In a previous study, vertically oriented and a horizontally oriented CRGO utilizing electrophoretic deposition and spin coating techniques were developed respectively [199]. The results suggested that the mobility of the ion and the accessible area of its surface was high in the system by showing that the activity of the vertically oriented CRGO was greater.

However, since $NiCl_2$ is used in the deposition process, it is important to note that the reaction's improved performance as a result of the 1 weight percent of Ni that was deposited throughout the reaction cannot be disregarded [167].

According to earlier study by [200], when CRGO in poly (ethylene glycol) is ground, the polymer produces films with greater pore spaces (by ~1 nm) is thermalized and DSSCs with higher efficiencies (η=7.2 %) than those created from ultra-sonicating CRGO in the polymer (η=5.2 %) [201]. Conversely, these devices still did not match the performance of those using platinized FTO (η=7.8 [167]. In other to increase the area of the surface of the electrodes, [202] was the first to create a NiCl2 −poly (vinyl alcohol) film after which pyrolysis was done on it to produce a substrate of nickel which is porous. This was made possible by the use of CVD, and the metal scaffold was later etched to produce graphene structures with porous pores with a diameter of roughly 40–50 nm.

A different approach was used by [203], who made the RGO sheets separate from one another to increase the surface area. SiO2 particles with a diameter of 12 nm were utilized as spacers to increase the CRGO film from a specified area of 8.6 to 383.4 m2/g [204]. Despite the achievement that has been achieved thus far, platinized FTO performed around 6% better than the thin film made using spacers. On the other hand, [205] were able to equate the platinized FTO's performance with an efficiency of 6.8% for both. This was accomplished by partially thermalizing an ethyl cellulose binder that was used to doctor cut a TRGO film. As a result of the insoluble residue that was left behind, the restacking of the TRGO films was disrupted [203].

It has been intensively investigated on how to improve its features through the process of hybridizing graphene materials and polymers. These qualities include conductivity, durability, adhesion, and catalytic activity. The employment of Nafion and polyvinylpyrrolidone binders in TRGO films is a typical application, but significant catalytic limits were discovered, resulting in its porosity being quite low. Another involved using four-layered, HNO_3-doped CVD-derived graphene as a conductive substrate for approximately 110 nm po1y (3,4-ethylenedioxythiophene) (PEDOT) films [167]. Additionally, polyanaline and polypyrole polymer nucleation have both used rGO as a scaffo1d [167, 204]. Only a few studies, among many others, have been able to use graphene materials to equal the performance of platinum as a catalyst.

Although pristine graphene or CRGO performs better than TRGO formed at very high temperatures, the need for large-area networks of graphene materials is due to the availability of the iodide/triiodide redox pair [167]. Additionally, this function can still utilise thick layered materials, but the electrodes may become constrained as a result of diffusion across a porous network, leading to opaque fi1ms. When sulfur and cobalt-based mediators are used, other types of graphene may be suitable; however, the TRGO material will only need a small number of ingredients, and the presence of defect sites and edges makes it possible to incorporate a cata1yst into it. The TRGO turns out to be the most promising method because of the nanoparticles at the fault spots and edges [206].

2.5 Economic Viability and Opportunity of DSSC

The recent global energy crisis has identified solar cells as key contributor to meeting the global energy need and combating climatic change, while tending towards a greener globe [207]. Solar cells or photovoltaic cells which converts sunlight into energy has been proven to be an effective and ecofriendly method deployed to solve the problem of fuels oil and gas shortage. They convert energy from solar radiation directly into electricity by stimulating electrons (negative charges) in a layer in the cell designed to give up electrons easily, when sunlight (photons) strikes the PV cell. This is achieved with key components of the photovoltaic system which includes PV modules, Inverter, Balance-of-system (BOS) components (e.g., combiner box, transformer, and meter) [208].

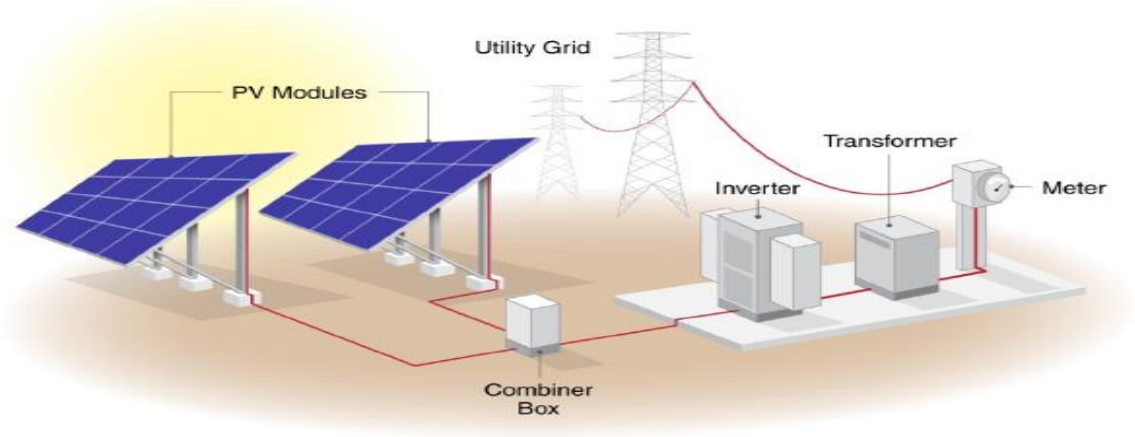

Figure 2.3: Components of a PV System [208]

Several type of solar cells such as organic dye solar cells, single and multiple crystal silicon solar cells, non-crystal silicon solar cells are used in harvesting the solar power, although solar cells from silicon crystal material are the most commonly used. Nevertheless, solar cells made from silicon crystal materials are very expensive when considering the cost of production compared to organic solar cells. This is because the most commercially available material of solar cell is si1icon based i.e. based on inorganic silicon semi-conductor, thus increasing the demand for silicon material. This has made dye-sensitized solar cell (DSSC) which is an organic solar cell a very promising and cost-efficient alternative for photovoltaic production [209, 210, 211]. DSSC has also gained great attention in the photovoltaic market due to its eco-friendliness, un1ike silicon solar cells which produces environment-unfriendly waste. They are seen as an economically credible alternative concept to present day p–n junction photovoltaic devices. Dye-sensitized solar cells also known as Gratzel cells are seen as low-cost solar cell belonging to the group of thin film solar cell [208], which was discovered by Gratzel in 1991. Although, in early 1970s, it was first employed with the use of oxide semiconductors and dye-based sensitizer. It is based on a semiconductor formed between a photo-sensitized anode and an electrolyte, a photo electrochemical system. Thus, DSSC is a unique cell that converts visible light into electricity based on sensitization of semiconductor's band gap [30]. The performance of DSSC is particularly dependent on the dye used as a sensitizer. That is, unlike conventional systems where the semiconductor carries out both the functions of light absorption and charge carrier transport, the two functions are separated. In Dye-sensitized solar cell, the light is absorbed by a sensitizer, which is anchored to the surface of a wide band semiconductor. The recent findings and progress realized in the fabrication and characterization of nanocrystalline materials has opened up new opportunities for these systems. Unlike other thin-film cells, dye-sensitized solar cells do not degrade in sunlight over time. This characteristic makes the cells last long, and may not require frequent replacements. Also, other advantages of DSSC like low cost, flexibility, ability to work at wider angles and in low light, high efficiencies at high temperatures compared to conventional solar cells; which gives them the ability to operate at lower internal temperatures mechanical robustness, availability supply of raw materials, non-environmental risk, and great performance at diffuse light and multicolor options has made them an attractive alternative in traditional solar cells [207, 208].

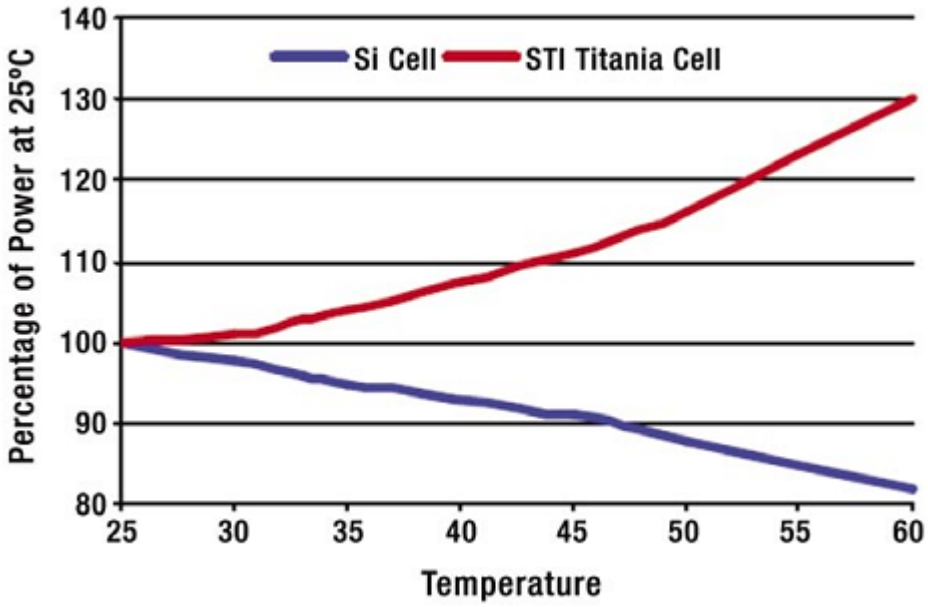

Figure 2.4: Performance of dye sensitizes photovo1taics increasing with increase temperature compared to silicon-based photovoltaics [212]

Although, DSSC is seen as a very promising alternative for silicon solar cells, researches have proven that the efficiency which is a major concern of the system could be increased by optimizing the individual parts of the cell. DSSC comprise of a porous layer of titanium dioxide (TiO_2) coated photoanode, a monolayer of dye molecules that-absorbs sunlight, an electrolyte for dye regeneration and a cathode. They are sandwiched with-the dye molecule or photosensitizer playing a vital role absorbing the visible light photons. Thus, increasing the efficiency of the cell, a significant amount of research on DSSC has been focused on designing and optimizing the photosensitizer in order to absorb a wide spectrum of wavelengths and increase the efficiency of the solar energy conversion [213, 214]. Reviews show that graphene materials can-be used as transparent-conductors, in semiconducting layers and as dye sensitizers to improve the efficiency of the cell [1].

However, the overall efficiency of dye sensitized solar cell is found to be proportional to the electron injection efficiency in the wide band gap nanostructured semiconductors. This photosensitization created by the dyes on wide band-gap semiconductors is due to the dye absorption of part of the visible light spectrum [214, 215]. This finding gave researchers

overtime to sort for a replacement for both porous and TiO_2 nanoparticle based solar cells and zinc oxide ZnO_2 nanowires have been used [216]. Also, metal complex and man-made sensitizers have been proposed [217]. However, processing and synthetization of these sensitizers are complicated and costly processes [218, 219, 220], thus the use of natural dye extract as sensitizers. Natural dye extracts have been found to provide natural, nontoxic and low cost dye sources with high absorbance level of UV, visible and near IR which is greatly desired. Sources like Bahraini Henna (LawsoniaInermis L) and Bahraini raspberries (Rubus spp.) as a natural dye sensitizer of TiO_2 nanostructured solar cell have been reported in various research work (Jasim and [221, 222]. The use of natural pigments as sensitizing dye for the transformation of solar to electric energy is very remarkable with economic advantages as well as and in addition, it has important advantages from the environmental perspective. DSSCs thus has become more interesting since a large collection of dye including natural dye can be used as light harvesting elements to provide the charge carriers [223].

2.5.1 Efficiency of DSSCs

To improving the efficiency of dye sensitize solar cells (DSSCs), tremendous efforts in research have been put in place to increase the efficiency of the solar energy conversion, which is often based on the degree of undesired charge recombination, electron injection efficiency, and light harvesting efficiency. For solar devices, achieving high efficiency is always the primary goal. For DSSC, the overall energy conversion efficiency (η) of 11.0 % has been achieved at AM 1.5 [224]. The Voc must be improved by reducing charge recombination between the redox couple and the injected electrons in the TiO_2 CB, between the oxidized sensitizer and the injected electrons in the TiO_2 CB, by increasing the electron injection efficiency, by increasing the TiO_2 ECB, by downshifting the redox, and by using tandem DSCs [225] (Zhijun Ning, 2010).

The following aspects of sensitizers should be taken into account in order to decrease charge recombination. On the TiO_2 surface, it should first create a compact blocking layer. Second, it's important to avoid the unfavorable complexation between the sensitizer and iodide. Thirdly, to prevent charge recombination between the injected electrons and the oxidized sensitizer, the electron donor unit should be dissociated from the TiO_2 surface. Molecular aggregation should be avoided, and the LUMO of the sensitizer should closely match that of TiO_2 in order to increase electron injection efficiency. Ultimately, strong electron donor and acceptor groups

maybe a viable option to enlarge the sensitizer's absorption spectra. Additionally, it is encouraged to use several electron donor substituents as long as the oxidized sensitizer can be successfully reduced by the redox pair. The rapidly evolving organic sensitizers have promise for improving Voc and efficacy through fine molecular customization. The film morphology has an impact on DSSC performance as well [64, 226]. Large particles are needed to improve red light absorption by light scattering, whereas nanoparticles are necessary to increase surface area and, consequently, the amount of dye. Because they work against one another, increasing surface area and light scattering cannot be done at the same time. Consequently, there needs to be harmony between them. A multilayer structure was used to achieve an energy conversion efficiency of 10.2 percent. Such a balance was effectively achieved by fine-tuning the layer structure. Other dyes can also benefit from the multilayer structure's enhanced photocurrent and light harvesting efficiency. A more advanced multilayer structure with gradually increasing particle size from the most inner layer is desired to disperse the red light more effectively [64, 227].

2.6 Improvements in Research and Development in DSSCs

The Dye sensitized solar cell which was invented Michael Grätzel and Brian O'Regan in 1991, showed an improved conversion efficiency of 7.12% using black dye and an efficiency up to 10 % using Ru-based dye. This attracted it to many researchers who sort ways to enhance the efficiency of the cell, with great progress achieved over the years. Photosensitizers which is an important part of DSSC can go a 1ong way to improve the efficiency of the cell by choosing an efficient dye [227, 228, 229]. The efficiency of the cell is greatly affected by the use of a good photo sensitizer. The use of sensitizers having a broad absorption band in conjunction with oxide films of nano crystallized morphology permits to harvest large fraction of sun1ight. So far Ruthenium and Osmium have been identified as sensitizer with highest conversion efficiency and long-term stability [230]. Metallic dyes are frequently researched out when considering dyes whose absorption can be extended in the near infra-red (NIR). This is because metallic dyes is more stable and efficient and are also better in its higher absorption properties [231].

Several researches have also come out with ways to improve the conductivity of titanium dioxide through various morphological control, such as formation of nanotubes, as well as to coat the surface of titanium di oxide with different types of oxides. Incorporation of carbon nanotubes

and graphene sheets into semiconductor electrodes have shown improved performance of DSSC [228, 229, 230], with 44 % increase in short circuit photocurrent and 18.7 % overall energy conversion have been achieved [(232, 233]. Using carbon base material like multiwall carbon nanotubes (MWNTS)/graphene nanotubes (GNS) as counter electrode in DSSCs showed a maximum power conversion efficiency of 4 % with 60 % MWNTS and 40 % GNS [233, 234]. Graphene aerogels as counter electrode showed efficiency close to that of platinum electrode achieved. With the introduction of Titania Aerogels, a class of mesoporous 3D structure, a power conversion efficiency improvement of 16 % (7.22vs 8.36 %) is achieved as compared with P25 %- TiO_2 based cells [233, 235]. Also, researches were carried out on 3D electrode fabrication to improve electron collection, hence enhancing cell performance. Electrodes derived from sol-gel synthesized nanoparticles of TiO_2 showed higher photoelectric conversion efficiency [236]. A TiO_2 double layer composite film on sponge like TiO_2 as over layer and commercial grade nanoparticles P25 as under layer showed overall efficiency 0f 5.48 %, which is 51.4 greater than that of P25 nanoparticles film [235, 237]. Attachment of a hydroxyl group on the nanocrystalline TiO_2 photo electrodes was reported to show enhanced performance. This was because of the dye absorbed on OH group of the electrode [238]. Apart from titanium oxide, zinc oxide dye solar cells also showed improved performance up to 4.38 % after surface treatment through the incorporation of Zn_2SnO_4 quantum dots on ZnO nanoparticles [212].

2.7 Benefits of Using DSSCs

2.7.1 Advantages of DSSCs

Dye-sensitized solar cells is comprised of the succeeding leading advantages:

Production: DSSCs are easy to produce. They can be produced in a simple way which is cost friendly. They have a significant benefit in terms of production costs because they don't require a vacuum system for manufacturing. Compared to the cost of producing silicon solar cells, it cuts the manufacturing cost of production in half [239, 240].

Colour and transparency: Dye sensitized solar cells involve the use of dye which allows wide selection of colored cells and transparent cells. This is unlike conventional solar cells that are opaque with limited colours [245]

Flexible and thin-structure: By employing aggregates of tiny particles of photoelectric conversion materials, flexible thin films of DSSCs can be created.

Light weight: Plastic substrates can be used to minimize the weight of solar cells and panels. Dou to its light weight, dye-sensitized solar cells can be installed in locations where visibility is centra1 and other solar cells are not applicable, such as the glass panes and outer and inner walls of a building, the sun-roof and outer panels of an automobile, and the enclosure of a mobile-phone. This allows the creation of new markets with high demand [241, 243].

Light absorption: Because nanoparticles are utilized, they can almost completely absorb sun1ight's photons. These solar cells effectively transform photons into electrons thanks to the dyes they use. Fluorescent and diffuse sunlight can both be absorbed by DSSC. These can therefore function effectively under overcast conditions. All those are useful for running small devices indoors because of their low cut off. They are less frequently replaced because they last a long time [241].

Dye-sensitized solar cells are environmentally friend and recyclable. They don’t exhibit detrimental substance as a cell component material. Also, the materials are easy to separate and get back, which is of an advantage in-view of a recycling and reuse framework for solar cell [242, 244].

Flexible and Thin Structure; by using aggregates of fine particles of optical conversion materials, the solar cells can be formed as a flexible thin film. No Need of Incident Angle and Intensity of the Sunlight. Compass machine is not required here to find the incident angle and the best position for the intensity of sunlight as required in traditional solar cell installation **[247]**.

2.7.2 Commercial Application/ Opportunities of DSSC

The first commercial application of dye sensitized solar cells DSSC was in 2009 by G24 innovations. In Hong Kong, they were utilized in bags and backpacks. These backpacks and bags feature solar panels that may collect energy to recharge portable electronics like mobile phones, e-books, cameras, and LED lighting systems. Cell phones, cameras, and other portable equipment could all be recharged. This is because of the lightweight and flexible nature of dye sensitized cells. Their light weight allows them opportunity to be designed as indoor colorful

decorative elements. Flexible dye sensitized solar modules also opens opportunities for integrating them with many portable devices, baggage, gears, or outfits [246].



Figure 2.5: DSSC used for Decorative Purpose [248]

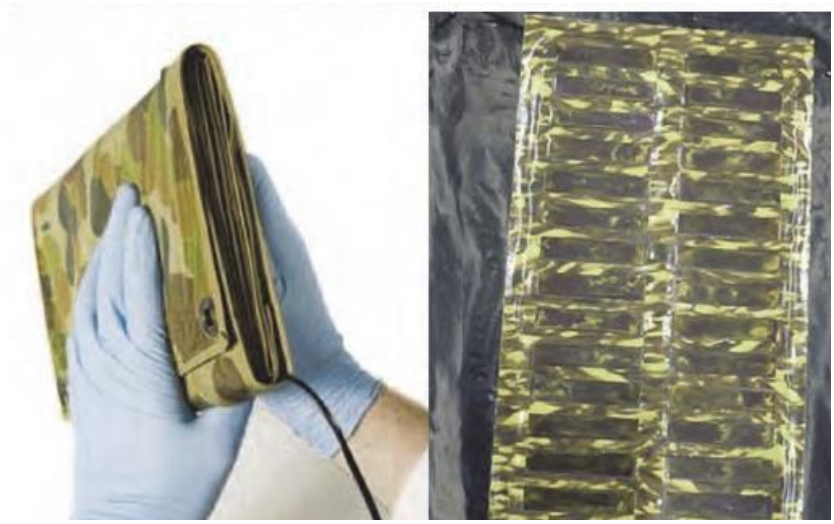

Figure 2.6: DSSCs used as Bag Packs [248]



Figure 2.7: DSSCs used as Outfits [248]

As a result of their unique advantages, power window and shingles are prospective app1ications in building integrated photovoltaics BIPV. The Australian company Sustainable Technologies International has produced electric-power-producing glass tiles on a large scale for field testing and the first building has been equipped with a wall of this type.



Figure 2.8: DSSCs used in Walls [248]

In power generation, dye sensitized modules with efficiency of 10% are attractive choice to replace the common crystalline Si-based modules. In 2010, Sony announced fabrication of

modules with efficiency close to 10% and hence opportunity of commercialization of DSSC modules is attainable. Solar cells are beginning to gain commercial grounds in most continents in the world because of the opportunities that comes with it **[248]**. It is being incorporated into new technologies in continents like Asia, Australia, America Europe, as most laboratories and companies record success in demonstrating various sizes and colors in a series-connected dye solar cell module in many international exhibitions and conferences, thus reflects the potential role of dye sensitized solar cells systems and the opportunities it brings to PV technology. Companies like Toyota has successfully installed their dream house wall with outdoor DSSCs modules.

DSSCs has gained commercial values with the various opportunities it avails the photovoltaic market, however, availability of nonvolatile electrolyte is an issue with commercialization of single or multi-junction modules. Polymer (solid) electrolyte, hole conductor, and solidified ionic liquids are solvent free choices with high electronic conductivity and chemical stability **[248].** The key to high power heterojunction DSSC is to increase the effective diffusion length of electron within the nanostructured electrode by increasing the mobility of hole conductor or the extinction coefficient of the sensitizer to ensure more efficient light harvesting action. Since heat and UV light degrade cells performance, development of heat sink and optimized low-cost UV coating is a must for outdoor applications. The successes in development of flexible substrate, solid electrolyte, and spectrally broad absorption range of nontoxic dyes will potentially open the possibility of role-to-roe mass production of dye sensitized solar cells and modules. Molecu1ar engineering of efficient and stable organic sensitizers is an open invitation for many research groups, the successes in this area is expected to advance production and commercialization of DSSC [148]

2.7.3 Environmental Benefits of DSSCS

The materials and components used in fabricating DSSCs are environmentally friendly and has zero effects on our ecosystem [249]. The ability for its individual components to be separated after fabrication is feasible and as such making it possible to be recycled thereby allowing other solar cell panels to use them [244]

Economic Viability

Photovoltaics over the years have proven itself to be a mature and reliable source of electricity supply, best alternative to fossil fuels, rapidly approaching grid parity. 12 PV has made remarkab1e progress in reducing costs although attaining grid parity still seem a bit far away, although could be attained considering the rapid increases with fossil fuel prices and continuing cost reductions in PV modules. Also, regions with lower electricity production costs, moderate solar resources may achieve grid parity as early as 2020 [250, 251, 252]. Despite the market share of solar energy which is still low as seen with the current electricity generation from photovoltaics which is only 2.6 GW compared to 36.3 GW for all renewable energies excluding hydroelectric power [253], Solar energy or energy from photovoltaic cells has a great potential of meeting the worlds' energy need if properly deployed. In the United States, it was reported by researchers that covering the land surface of 180 km square with photovoltaics could be able to satisfy the total electricity demand of 418 GW in 2002. Seeing that this surface represents 0.35 % of the total land area and roughly corresponds to the surface covered by roads in the country. Her electricity could hence by covering the paved roads with photovo1taic (PV) modules. However, this cannot be applicable in most countries as land is an important factor and other issues linked with deployment of these cells. Some of the causes of the slow dep1oyment of photovoltaic cells are:

Cost: The current relative high capital cost per kW installed compared with other fossil fuel based and renewable technologies has been a major concern with large deployment of photovoltaics. More effort with the recent advances in research has been put into improving efficiencies while reducing the manufacturing costs, and this is a great challenge that requires investment of larger financial and intellectual resources to find innovative solutions. The current high capital cost of PV technologies compared to fossil fuels is a major barrier to large-scale deployment of solar energy. The price of electricity from solar energy, as reported by the IEA, ranges from $0.35/ kWh to $0.60/ kWh for solar PV and from $0.085/ kWh to $0.135/ kWh for solar thermal, compared to $0.045/ kWh - $0.055/ kWh for wind and $0.040/ kWh for natural gas [254, 255] The price of the active material, the manufacturing, and the Balance of System BOS are the key elements used in determining the total price of PV technologies. Recent researches have been exploring new processes for producing low-cost photovoltaic cells and

these technologies are believed to have the potential of bringing down the cost of solar energy to $0.03/ kWh - $0.05/ kWh [256]. This is why organic-based photovoltaics (OPVs) are an alternative to present-day p-n junction photovoltaic devices for reducing the cost of solar energy. They can be deposited on lightweight, flexible and low-cost plastic substrates and thus have the potential to drop the manufacturing and installation cost by 10 to20fold. The manufacturing cost for organic photovoltaics can be very low using semiconductors and low-cost materials such as plastic substrates and polymer alternatives to Transparent Conducting Oxide (TCO) electrodes. This can bring down the cost as significantly below $1/ W [257].

Efficiency: Over the past 30 years, solar cell efficiencies have continuously improved, but despite the notable progress made in the improvement of the efficiencies of all these technologies, achieved values are still far from the thermodynamic efficiency limits of ~31 % for single junctions 6.50 % for 3-cell stacks, impurity PVs, or up- and down converters, and 54-68 % for hot carrier- or impact ionization-based devices [258]. Furthermore, the efficiencies of commercial (or even the best prototype) modules are only about 50 % to 65 % of these "champion" cells [258] Closing these gaps is the subject of ongoing research.

Environmental Aspects

Solar energy has gained a lot of advantage in this area as it is being promoted as a sustainable energy supply technology because of its renewable nature, that is the renewable nature of solar radiation and the ability to generate greenhouse gas-free electricity throughout their lifetime [259].

Dye-sensitized solar cells are environmentally friendly and recyclable and do not have harmful substance as a cell component material. The materials are comparatively easy to separate and get back, which is advantageous in view of a recycling and reuse framework for solar cell panels [260]. However, the energy requirement and the environmental impact of PV module manufacture can be further reduced, even though recent analysis of the energy and carbon cycles for PV technologies recognized that strong improvements were made both in terms of energy and carbon paybacks.

2.7.4 Financial Cost Analysis

The cost of the electricity generated by a Photovoltaic system is determined by the capital cost (CAPEX), the variable costs (OPEX), the level of solar irradiation, the efficiency of the solar cells and discount rate. The capital cost, the cost of finance and efficiency are the most important among the listed parameters and improvements in these parameters provide the largest opportunity for cost reductions. The capita1 cost of a Photovoltaic system is composed of the PV module cost and the Balance of system (BOS) cost. The PV module is the interconnected array of PV cells and its cost is determined by raw material costs, notably silicon prices, cell processing/manufacturing and module assembly costs. The BOS cost includes items, such as the cost of the structural system (e.g. structural installation, racks, site preparation and other attachments), the electrical system costs (e.g. the inverter, transformer, wiring and other electrical installation costs) and the battery or other storage system cost in the case of off grid applications. However, the accurate cost as pertaining to PV modules are at times most difficult to obtain as there is a wide variation of prices based on the cost structure of the manufacturer, market features and module efficiency as shown in Figure 2.9

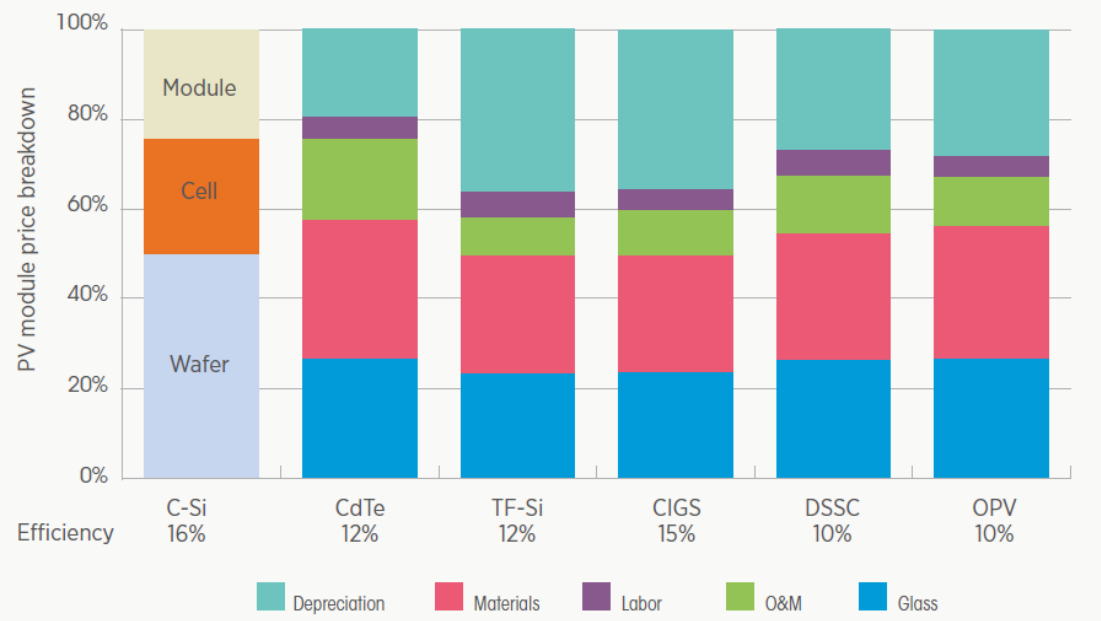

Figure 2.9; PV Modules Price and their Cost Structure [261]

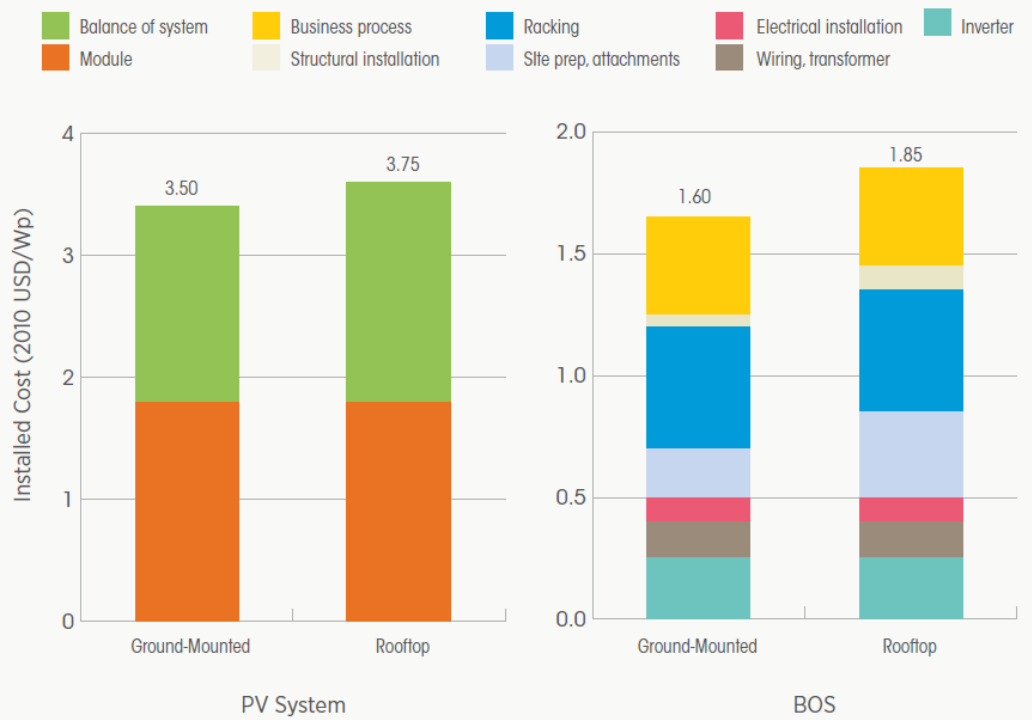

Figure 2.10: Cost Breakdown Showing PV Module Cost and Balance of System BOS Cost [262].

BOS cost reduction

As earlier states that the balance of system cost including the cost of installation play important roles in the reduction of photovoltaic module cost. Among the BOS components, the cost of the inverter is generally known but not the case for the other components like the electrical, structural and installation costs, which could vary depending on labour costs and other local conditions. The most important factors to reduce BOS and installation costs are outlined below.

Electrical system improvements; which start with efforts to improve the design of the inverter. Historically, inverter costs have trend down with PV module costs. one interesting area of development and cost reduction is the use of micro-inverters that is directly integrated into the PV modules, which also reduce the installation cost. Also important for both inverters and microinverters are efforts to increase the lifetime from today's 5-10 years which is significantly shorter than the lifetime of the PV system life. All of these efforts are projected to reduce the cost by half of the inverter costs by 2020 [263].

Structural system improvements; which include downsizing of the structural components. This could yield up to 40% of the BOS cost reductions. Efficient designs to minimize the impact of

wind loads could result in significant reduction in the structural costs by allowing lighter, cheaper structures [262].

Installation costs can be reduced with continued experience, increased market scale and competition. Process automation and high-level pre-assembly and standardization could reduce labour costs for installation by up to 30% [262].

Standardization and economies of scale will help reduce component costs by high volume manufacturing of BOS components. The potential cost reduction is large, as most BOS comp0nent manufacturers today are small companies. large companies are pursuing important economies of scale strategies to remain competitive [263], Costs of low-carbon generating technologies, Mott MacDonald, Bristol.

2.8 Challenges Associated with DSSCs

0ne of the major challenges with DSSCs is its low conversion efficiency. Many researchers have attempted to resolve this prob1em, by increasing the surface area of TiO_2 photo-electrodes used in the DSSC. The main causes of low efficiency in DSSCs are: low red and near-IR absorption, low extinction coefficient requires high surface area, redox couple has slow recombination kinetics, but it has unnecessarily large over potential, Poor contact between the electrodes and Degradation of electrolyte properties due to UV absorption of light [248].

2.8.1 Concluding Remarks

As a result, not only does the widespread use of solar technology for energy generation necessitate the engagement of political and economic actors, but it also calls for increased conversion efficiency and lower manufacturing costs.

The search for affordable organic solar energy has been ongoing, and dye-sensitized solar cells (DSCs) have emerged as one of the most promising technologies going forward because they currently have the best energy conversion efficiency. In spite of their lower efficiency output when compared to silicon sun cells, dye sensitized solar cells have attracted a lot of attention in recent years due to their inexpensive production costs, ease of fabrication, lighter weight, envir0nmental friendliness, and recyclable features.

The fundamental processes by which photon energy is converted into electricity—photon absorption, charge carrier production, charge separation, and charge transport—present problems for all of these technologies. For these technologies to become more effective, stable, and dependable, fundamental research as well as technical progress are essential.

CHAPTER THREE: METHODOLOGY AND EXPERIMENTAL PROCEDURES

3.0 Introduction

This chapter aims at fabricating DSSC using photoanode based on graphene/Ni Substrate in order to improve the efficiency of the dye sensitized solar cell. This chapter presents procedures for the preparation and characterization of graphene/reduced graphene oxide, as well as fabrication of the dye sensitized solar cell with reduced graphene oxide coated with FTO/ TiO_2 -RGO. Solar simu1ation and stability test was carried out on the fabricated dye sensitized solar cell in order to determine its effectiveness and outdoor stability.

3.1 Research Methodology

The synthesis of the graphene was carried out using Aeroso1 Assisted Chemica1Vapour Deposition (AACVD) method (The Hummer's Method was used to synthesized reduced graphene oxide (rGO) whi1e the synthesis of mesoporous TiO_2 -rGO Composite was carried out using spin coating/screen printing. The composite was characterized using UV-Vis, SEM/EDX, and XRD.

3.1.1 Materials

The materials used for the synthesis and evaluation of graphene oxide and reduced graphene oxide include; fluorine-doped tin oxide-coated glass (FTO) slide, di-tetrabutylammonium, cis-bis (isothiocyanate), bis (2, 2'-bipyridyl- 4,4'dicarboxylate) ruthenium (II), Roselle dye as natural dye, Sulfuric acid-(H_2SO_4, 98 %), phosphoric acid (H_3PO_4, 85 %), potassium-permanganate ($KMnO_4$, 99.9 %), hydrogen-peroxide (H_2O_2, 30 %), hydrochloric acid (HCl, 37 %), absolute ethanol (99.5 %), acetone, and hydrazine. Also, the materials/instruments used for the characterization are: X-ray Diffractor (XRD), Scanning Electron Microscopy (SEM), Energy Dispersive X-ray (EDX), and Diffuse Reflectance-Ultraviolet visible spectroscopy (DRS UV-Vis). The materials used for the transformation of tin acetylacetone transformed to tin (IV) oxide are: tin acetylacetone ($Sn(acac)_{2)}$, ethanol (C_2H_5OH), sodium hydroxide (NaOH), hydrochloric acid (HCl), and deionized water.

3.2 Synthesis of FTO layer by AACVD Method

In order to spray the film with tin (iv) oxide (SnO_2), the experiment began with the synthesis of tin acetyl acetonate as precursor. This was prepared by dissolving 2 g of acetyl acetonate and 1 g of tin (iv) chloride ($SnCl_2$) in 50 ml of HCl. For the SnO_2 thin films the precursor solution was of stannic chloride ($SnCl_4.5H_2O$). Stannic chloride concentration of 0.1 $mol \cdot dm^{-3}$ was dissolved in a 25 ml of ethanol (99.8 %) to form tin (iv) oxide [293]. A watch glass was placed over the solution to prevent evaporation and reactions with moisture. The solution was then heated for 5 minutes at 63^oC with the help of a magnetic stirrer to improve solubility.

A mechanical syringe with 1 ml volume was used to measure the acetyl acetonate, which was held over the glass slide by the AACVD machine. There was care taken to avoid diminishing the volume of the solution because the flow rate (speed of deposition) was affected by the height of the solution (the larger the volume of the so1ution, the higher the flow rate). The automated syringe was refilled after each 0.1 ml reduction. However, steps were taken to prevent the syringe from been blocked. This procedure was repeated for 0.2, 0.4, 0.6, and 0.8 ml of tin acetylacetonate solution.

Each of these quantities were deposited onto a different glass slide, which was then evaluated for conductivity after each volume was deposited. Prior to deposition, the glass substrates were maintained at room temperature. To compare the slides to the f1uorine doped tin oxide, the slides were taken to the laboratory for analysis. Ammonium fluoride was used as the dopant to create FTO (fluorine tin oxide) (NH_4F). 50 ml of methanol was used to dissolve 0.1 g of ammonium fluoride in a 100 ml capacity measuring cylinder. Four percent, eight percent, and twelve percent of fluorine-doped tin oxide were doped. 8 ml of the dopant (NH_4F) was added to 192 ml of tin acetyl acetonate and carefully mixed to achieve a 4 percent concentration. The automated syringe measured and injected 1 ml of the solution onto each slide. The same steps and safety precautions were applied for other tin (iv) oxide that were doped.

How Tin acetylacetone transformed to Tin (IV) oxide

A solution of tin acetylacetone solution was prepared by dissolving 0.5 g of $Sn(acac)_2$ in 50 mL of ethanol. The solution was stirred for 30 minutes until the solid was completely dissolved. Then 10 mL of 0.1 M NaOH solution was added dropwise while stirring. The solution turned yellow as the pH increased. After the addition of NaOH solution, the solution was heated to 80 ^oC and stirred for 2 hours. A white precipitate was formed, which was filtered and washed with deionized water. To confirm the white precipitate, the white was dissolved in hydrochloric acid and heated to 80 ^oC for 30 minutes. The solution turned yellow as the SnO_2 precipitated out. The SnO_2 was filtered, washed with deionized water, and dried at 100 ^{o} C for 1 hour.

The experimental evidence demonstrated that the tin acetylacetonate can be transformed into tin (IV) oxide by the addition of NaOH solution followed by heating. The yellow color of the solution indicated the formation of a complex between $Sn(acac)_2$ and NaOH. The complexation reaction can be presented as follows:

$$Sn(acac)_2 + 2NaOH \rightarrow Na_2[Sn(acac)_2] + 2H_2O$$

The complex was then heated to form tin (IV) oxide through hydrolysis and condensation reactions. The overall reaction is presented below:

$$Na_2[Sn(acac)_2] + 2H_2O \rightarrow SnO_2 + 2Na(acac) + 2H_2O$$

The white precipitate obtained after heating and filtering was confirmed to be SnO_2 through the yellow coloration upon dissolution in hydrochloric acid.

3.3 Preparation of Graphene Oxide

Graphene oxide was prepared by adopting Hummer's method [264, 265, 266, 267]. Thus, Hummer's method was developed in 1958 as a safer, faster and more efficient method for production of graphene oxide. Before, the production of graphene oxide was slow and hazardous because of the use of concentrated sulfuric and nitric acid. GO must be reduced to get rGO (reduced graphene oxide).

The graphite flake was grounded until a powdery form is achieved. 0.8 g of the crushed graphite was then mixed with 25 ml of H_2SO_4. Subsequently, 2 g of $KMnO_4$ was added to the solution,

this was stirred vigorously at 25 ^{o}C for 30 min to form homogenous mixture. Thereafter, deionized water was added to the mixture which was stirred at 90 ^{o}C. The colour of the resulting solution then turned brown. After 1 h, 10 ml of 30 % H_2O_2 was added to reduce the oxidation reaction and was rinsed with ethanol. After 48 h, the solution was fi1tered using a vacuum pump fi1ter and heated at 60°C for 24 h to obtain graphene oxide (GO). In this step, the residue of $KMnO_4$ and MnO_2 were reduced to Mn^{2+} and the resulting solution colour turned brown which is an indication of graphene oxide (GO) formation.

3.3.1 Reduction of graphene oxide (GO) to get rGO

To get rGO, 0.6 g of the GO solid was crushed to fine particles and mixed with 100 ml of deionized water and sonicated for 3 h so as to obtain a clear suspension. 10 µl of hydrazine was added to the solution repeatedly. This was done so as to produce a dense precipitate to ensured successful reduction of graphene oxide process. This solution was filtered and dried at 60 oC for 48 h to obtain reduced graphene oxide

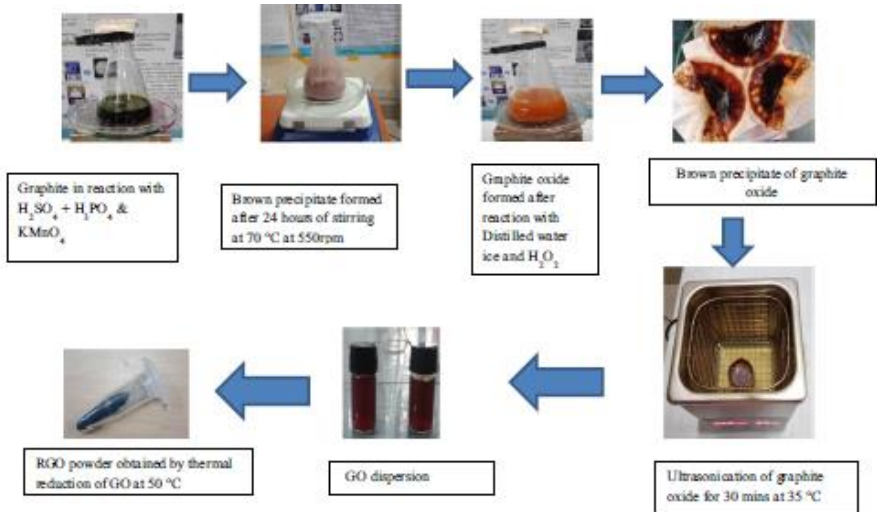

Figure. 3.1 Schematic representation of RGO synthesis [368]

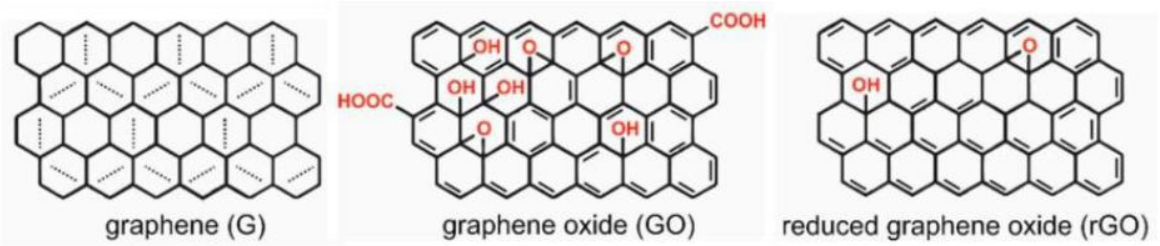

Figure 3.2 Representation of the molecular structures of graphene material and its derivates [369]

3.3.2 Incorporation of reduce graphene oxide to TiO_2

Reduced graphene oxide so1ution was incorporated into the TiO_2 to evaluate the performance of the so1ar cell. TiO_2-rGO nano composite thin film of different sizes were successfully synthesized with various static drops of rGO so1ution placed on TiO2 following the sample procedure of spin coating and annea1ing at the same temperature. The various drops were categorized in cycles. The cycles were produced by dropping 3 static drops of rGO solution onto the surface of a tape down TiO_2 and allowed for about 5 minutes to enable it absorb into the mesoporous TiO_2. Then it was spin dry by the spin coater at 4000rpm for 30 second. Temperature was monitored using Ren C900 temperature control machine during annealing. The procedure was repeated for other cycle of samples to form different TiO_2 with different thickness or layer of rGO. The samples were thoroughly characterized for Hall Effect, UV-vis, profilometry and voltage changes.

3.4 Fabrication of TiO_2 –rGO Composite

G1ass slide that has TiO_2 printed on it was prepared. The prepared molten paste of TiO_2 was screen printed on the slide using the screen printer machine. 15 mg of rGO powder was dispersed in 70 % acetone and 30 % of H_2O_2. Several static drops of the rGO solution were spin coated onto the TiO_2 thin Film to produce the nanocomposite photo anode TiO_2 –rGO Composite. This was how incorporation of the rGO on TiO_2 thin film was achieved

3.4.1 Substrate Preparation.

The slide used for substrate preparation was cut into appropriate sizes to enable it fit into the spin coater. The required size dimension (16.22 mm x 16.22 mm square) was measured using a vernier caliper after cutting. The cutting was done using electrical hand engraver (Swisso).

Immediately after cutting, the slides were washed with sodium lauryl su1phate, thereafter they were rinsed with deionized water and allowed to drain by inverting the slides on a Petri dish. Piranha solution was prepared by mixing 70 % concentration of H_2O_2 and 30 % of water. The s1ides were soaked in the piranha's so1ution (H_2SO_4 H_2O_2) and allowed to stay for 30 min for

the chemical reaction which facilitated proper cleaning of the slide and also to make the slide hydrophilic. Subsequent1y, the slides were air dried for 20 min after draining of the solution.

3.4.2 Screen Printing of TiO_2

Prior to screen printing of TiO_2 on glass slide, the slides were rinsed with deionized water again and spin dried with the spin coater centrifuge machine (MEIHECO) for 20 seconds at 4000 rpm. Further drying was carried out on the slides using the magnetic stirrer hotplate for total of 9 slides that were used for screen printing. TiO_2 was screen printed on the slide using the screen printer machine. Molten paste of TiO_2 was printed onto a tape down the slide in the screen printer machine by spreading it over the screen mesh using a glass rod. The samples were dried immediately by a magnetic stirrer hotplate at a regulated temperature of 60 ^oC. Finally, eight samples of TiO_2 screen printed slides were produced with the same thickness (layer) of TiO_2 at a contro11ed temperature of 60 ^oC. Throughout the duration of screen printing, the drying period was 30 min so as to remove tempanol which contain moisture.

3.5 Spin Coating of rGO into TiO_2 Thin Fi1m

Several static drops of rGO solution were used in spin coating the rGO onto TiO_2 Thin Film. For the first sample (Cycle 1), 3 static drops of rGO solution were dropped onto surface of a tape down TiO_2 and allowed for about 5 minutes to enable it absorb into the mesoporous TiO_2. Then it was spin dry by the spin coater at 4000 rpm for 30 second. Temperature was monitored using temperature control machine (Ren C900) during annea1ing. The procedure was repeated for other cycle of samples to form different TiO_2 with different thickness or layer of rGO. Sample 2 (Cyc1e 2) consists of six static drops of rGO solution deposited on TiO_2 with the aid of syringes that has a volume of 20 ml. In Cycle 2, the first 3 static drops of rGO were made on TiO_2, spin dry, and anneal using the magnetic hotplate at 250-280 ^OC for 30 minutes, and, allowed to cool down. Then another 0.3 ml of rGO solution was added again and was made to receive the same treatment as in sample 1. While sample 3 (Cycle 3) consists of 0.9 ml rGO solution deposited on TiO_2 which follows sampling procedure of the spin coating and annealing was done thrice at the same temperature and time. Similarly, samples 4, 5, and 6 which represent different cycles of rGO solution deposition were done in respect to sample 2 and sample 3 in succession with the same procedure in 1,2,3. In all, six samples of rGO-TiO_2 photoanode were produced and were labeled as cycles 1, 2, 3, 4, 5, and 6. [167,199, 201, 202]

3.6 Solar Cell Fabrication/ Assemb1y of DSSC

The Dye-sensitized solar cell was assembled in a sandwich configuration. It is composed of the FTO slide as the photoanode or absorption of visible light, roselle as the dye sensitizer for electrostatic binding with the TiO_2. The FTO glasses were cut into small pieces. The TiO_2 is transformed from amorphous to crystalline, screen printed on the cut g1ass slides, and annealed at 450 OC for 30 minutes. The reduced graphene oxide was applied by spin coating, annealed at 200-250 OC for 1 h. The FTO coated TiO_2 was immersed-overnight (12 h) in a solvent containing dye and ethanol. The same-process was carried out for the FTO coated rGO-TiO_2 sample. The photo anode was rinsed with ethanol to remove the physiosorbed dye mo1ecule and dried on a hot plate at 60oC for 30 minutes. The counter electrode was-deposited with the Pt-thin film via-sputtering. [246, 354, 359, 368]

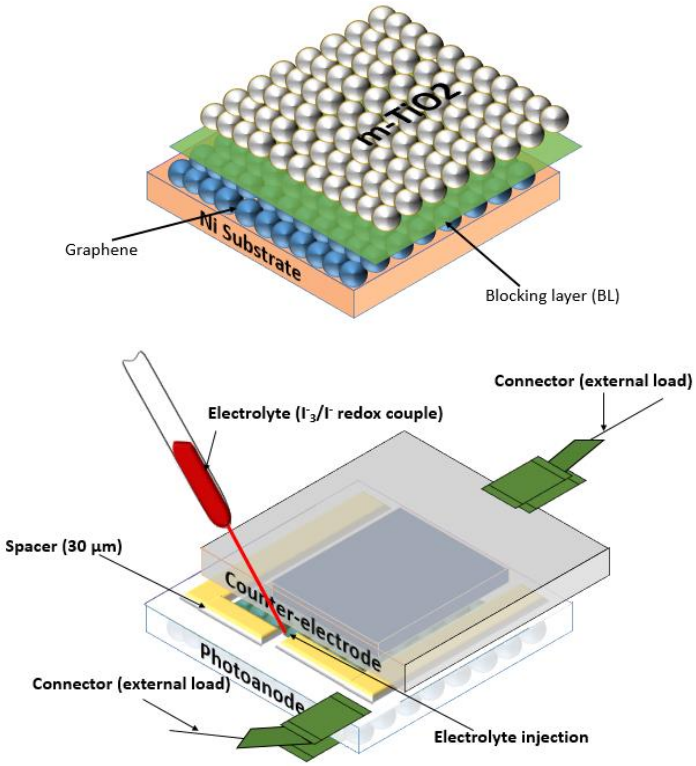

Figure 3.3 Assembling and fabrication of the DSSC

3.7 Characterization Methods

Characterizations of the samples were studied through Hall Effect, Profilometry, Diffuse Reflectance-Ultraviolet visible spectroscopy (DRS UV-Vis), Simulation and stability behavior of

the Dye sensitized solar cell. The equipment used for the characterization were Ecopia Hall effect Measurement System HMS 3000, Fi1metrics thin-film analyzer F10-RT-UV and VeecoDektak 150 for the Hall Effect, UV and profilometry study respectively.

3.8 Photovoltaic Performance of Fabricated DSSC

The Dye sensitized solar cell was assemb1ed in a sandwich configuration with the FTO coated with rGO-TiO_2. Roselle dye was used as the dye sensitizer for electrostatic binding with the TiO_2. The performance of the fabricated DSSCs was determined using a white light solar simulator with a light intensity of 100 $mWcm^{-2}$. The I–V measurements were carried out on the DSSC without reduced graphene and the DSSC sandwiched with reduced graphene. A stability test was carried out for the reduced graphene-dye-sensitized solar cell after an aging period of twenty-seven days [268]. Electrochemical measurements were carried out on the cells at 3 days intervals in order to study their long-term stability. The photoelectrochemical parameters include; the open circuit voltage Voc (V), and the current density, while the fill factor (FF) and light to-electricity conversion efficiency (η), were calculated based on equations (3.1) and (3.2).

$$FF = \frac{P_{max}}{V_{OC} \times I_{SC}} \qquad 3.1$$

$$\eta = \frac{FF \times V_{OC} \times Isc}{E \times A_c} \times 100\% \qquad 3.2$$

The short circuit current (I_{SC}) is the current through the solar cell when the voltage across the solar cell is zero. The maximum power point (P_{max}) is seen as the condition under which the solar ce11 generates its maximum power and the current and voltage in this condition are defined as Imax and Vmax (respectively). The fill factor (FF) and the energy conversion efficiency (η) are used to characterize and draw conclusions about the performance of the solar cell. The fill factor is defined as the ratio of Pmax divided by the product of V_{OC} and I_{SC}, while the power conversion efficiency can be seen as the ratio of Pmax to the product of the input light irradiance (E) and the solar cell surface area A_c [270].

3.9 Testing of the DSSC Cell

Simulation and stability test of the DSSC cell under the real-world conditions (illumination under 1 sun, and under room temperature condition) were studied. Determining the stability of solar cells is not easy since the degradation of their performance during their lifetime depends on many factors that may act simultaneously [271, 272, 273, 274, 277]. Moisture, in combination with high temperature, is the most critical environmental factors that lead to the degradation of DSSCs performance [275, 276, 277]. Concerning DSSCs technology, extensive efforts have been made over the past years to improve the stability of these devices by the incorporation of novel materials in their structure leading to promising results [278, 279, 280, 281, 283].

3.10 Concluding Remarks

In this chapter, it is anticipated that DSSC will be fabricated by incorporating mesoporous TiO2 - rGO nano composite successfully.

CHAPTER FOUR: DYE-SENSITIZED SOLAR CELLS PERFORMANCE.

I wish to acknowledge that some of the data in this chapter were adapted from [20]. Dye-sensitized solar-cells (DSSCs) is the utmost current of progressive solar cell-technology which can be likened to artificial photosynthesis owing to the manner it absorbs light via the sun, separates it-and generates-charges. It is intensively studied due to their simple and inexpensive manufacturing process yet relatively high conversion-efficiencies [276, 277, 278, 279, 283]. The efficiency of the DSSC can be increased by optimizing a number of its components. The Transparent Conducting Materia1 (TCM), which is frequently formed of Fluorine Doped Tin Oxide (FTO), can be enhanced in order to achieve excellent light harvesting. There is a category of materials known as transparent conductive materials (TCMs) that simultaneously exhibits optical transmission and electrical conductivity [284]. TCMs often take the shape of thin films, which can be made of metal films, wide-band-gap semiconductors, doped organic polymers, or metal nitrides. A technologically significant class of materials, they are widely utilized in displays, photovoltaics, transparent electronics, architecture, and window g1ass [285]. Transparent conductive oxides are now the most significant TCMs (TCOs). In order for TCOs to be transparent in the visible region of the spectrum, they are typically n- and p-type semiconductors with band gaps greater than 3 eV. (Approximate1y 1.8-3.0 eV, see Figure 1.6a for reference). To achieve high conductivity, the oxides are frequently externally doped. Currently, In_2O_3, ZnO, and SnO_2 are the three most significant binary n-type TCOs.

The most often utilized TCO is f1uorine-doped tin or tin-doped indium oxide-(FTO or ITO), which enables the glass plates to act as electrodes and collect the electric charge generated within the cell. They are ideally suited for the majority of the-Sun's output since-they are-very transparent across the visible spectrum and more-absorbent in areas closer to UV rays [286].

The SnO_2 layer p1ays a key role in the electron transport in DSSC. All through-the DSSC operation, electrons are generated by photo-excited dye molecules, which are then injected into the conduction-band of the Tin oxide. The electrons then get-transported by diffusion via SnO2layer and are collected at the conductive electrode. While most electrons are efficiently collected, some-might recombine with holes nearby or in-the electrolyte and/or excited dyes, thus leading to reduced-energy conversion efficiency. Subsequently, improving-charge collection efficiency of SnO_2 layer is one-of the key areas to look into when optimizing DSSC. Other than

solar cells, a number of different technologies can be used to make FTO physically, chemically, and electrochemically stable. The hydrothermal process, chemical vapour deposition (CVD), radio-frequency (RF) sputtering, and spray pyrolysis are just a few of the techniques used to create FTO nanocomposites. There are various ways to prepare FTO via CVD, including low pressure CVD, plasma enhanced-CVD, aerosol assisted-CVD, and atmospheric-pressure CVD, which-is very effective and cost-effective [287].

Additionally, dye sensitized solar cells (DSSCs) work on the-absorption, separation, and collection principle [60], with-the two main ways that DSSCs vary from all other solar cells being their ability to absorb light and move charges. Because of its high electron mobility, exceptional optical qualities, thermal, chemical, and mechanical stability, graphene has thus far shown promise as a material for a wide range of application.

With the assistance of rGO that has some useful unique properties, graphene incorporated to TiO2 is proven influence the properties of the DSSC in increasing the photo-induced charge transport and suppressing the charge recombination in a DSSCs system [288]. This chapter thus 1ooks at the influence of fluorine doped tin oxide and reduce graphene oxide on the performance of the DSSC.

4.1 Influence of fluorine doped tin oxide on the performance of DSSC

The effect of fluorine doped tin oxide was carried out by doping SnO_2 with fluorine at-different percentage. As shown-in Tab1e 4.1, the deposition-of the FTO on the glass substrate using AACVD method as discussed in section 3.2. The properties-of the un-doped SnO_2 and countless percentage of-doped SnO_2 were-considered. The samples were studied through Scanning Electron Microscope-energy dispersive x – ray (SEM-EDX), Hall Effect, Profilometry and Diffuse Reflectance-Ultraviolet visible spectroscopy (DRS UV-Vis). The scanning Electron Microscopy (SEM) was employed to provide the structure and surface morphology. The profilometry analysis shows the thickness of the film while the optical properties were studies using the DRS UV-Vis to investigate the visible transmittance in 230 to 1100 nm wavelength.

4.1.1 Results and Discussion

4.1.1.1 Surface Morphology (SEM image of produced FTO)

The SEM images of the fluorine doped tin oxide showed the distribution of grains that are uniformly deposited completely on the glass substrate. It showed the presence of individual sheets that are closely packed and aligned with each other. The SEM images are shown in Figure 4.1 to Figure 4.4 for undoped, 4 %, 8 %, and 12 % fluorine-doped tin oxide respectively (the higher the thickness of dopant increases the mobility, and conductivity of the electrons or charges from the dye to the photoanode. This effect reduces the recombination of the electrons from the dye to the highest occupied molecular orbit (HOMO), and redox) [103, 292]. The large particle deposited are due to the deposition process, which might have occurred due to the position of the glass substrate during deposition [289]. The 4 %, 8 %, and 12 % doped SnO_2 show the particle deposited uniformly on the glass substrate unlike the undoped, which showed some over size spherical particles deposited on the glass substrate. The FTO showed diminishing agglomeration of the particle size compared to the undoped SnO_2. 4 % doped SnO_2 showed a more compact particle structure which would a better light transmittance [290].

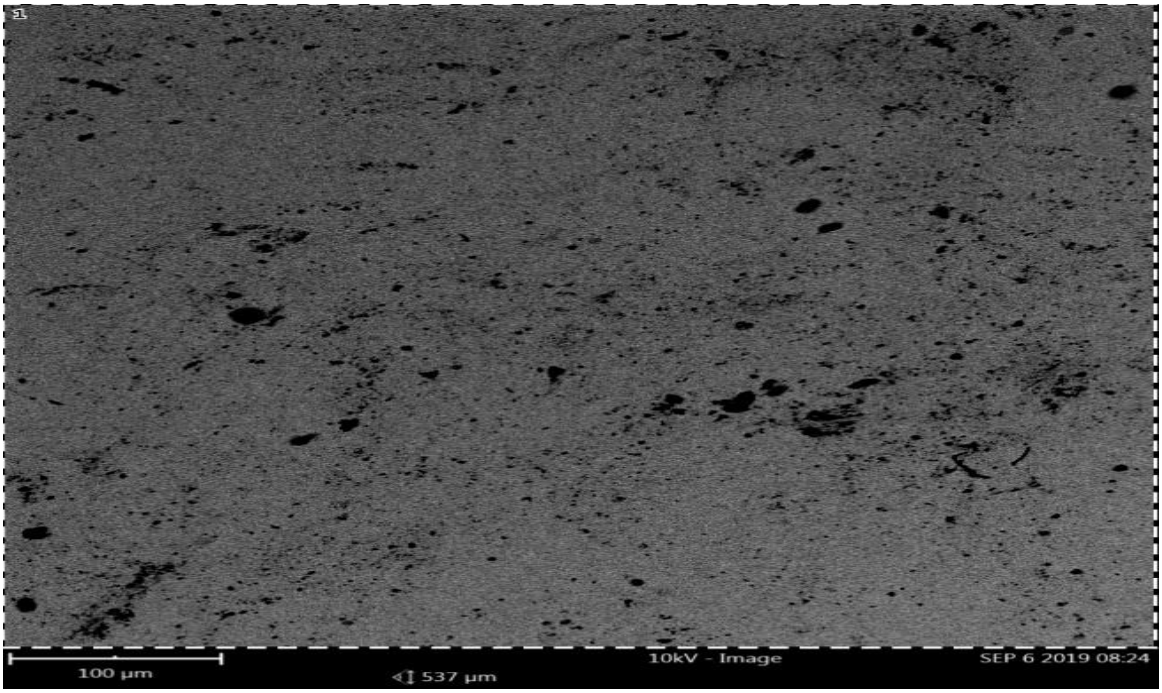

Figure 4.1: SEM of 0.4 ml SnO_2 (undoped)

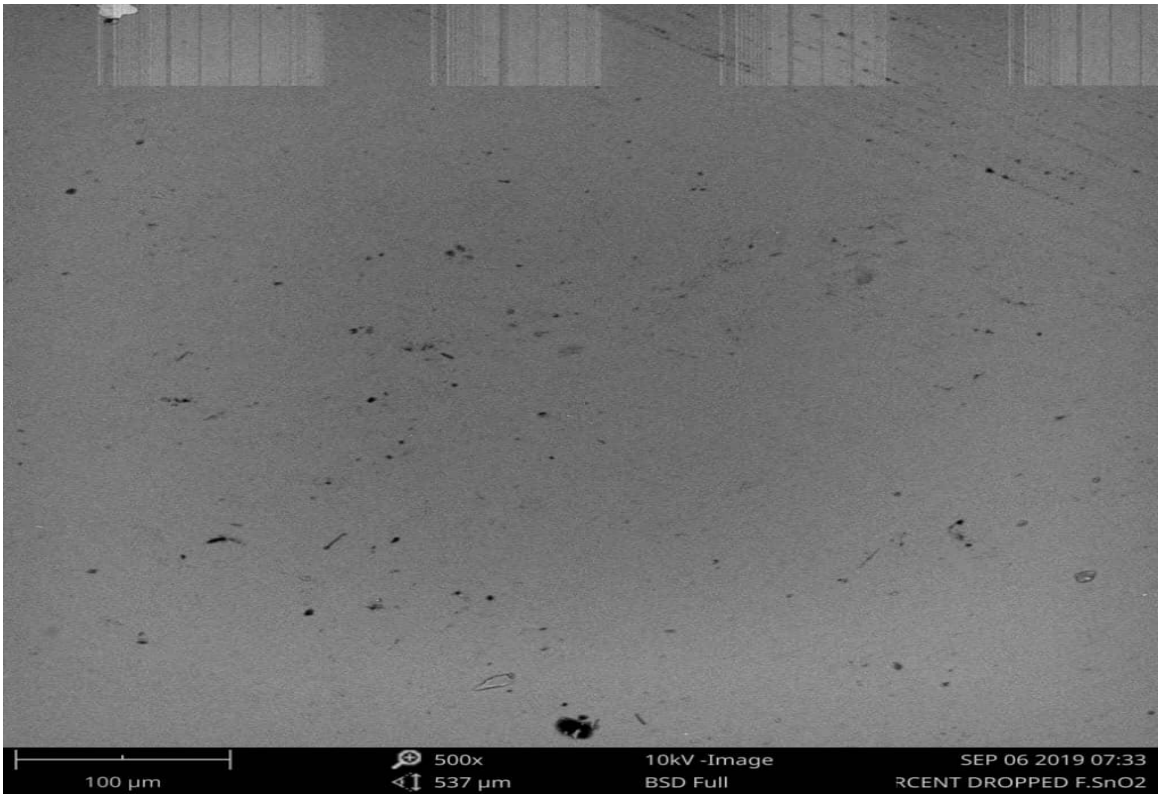

Figure 4.2: SEM of 4% F:SnO_2 with magnification size of 500x at 100µm

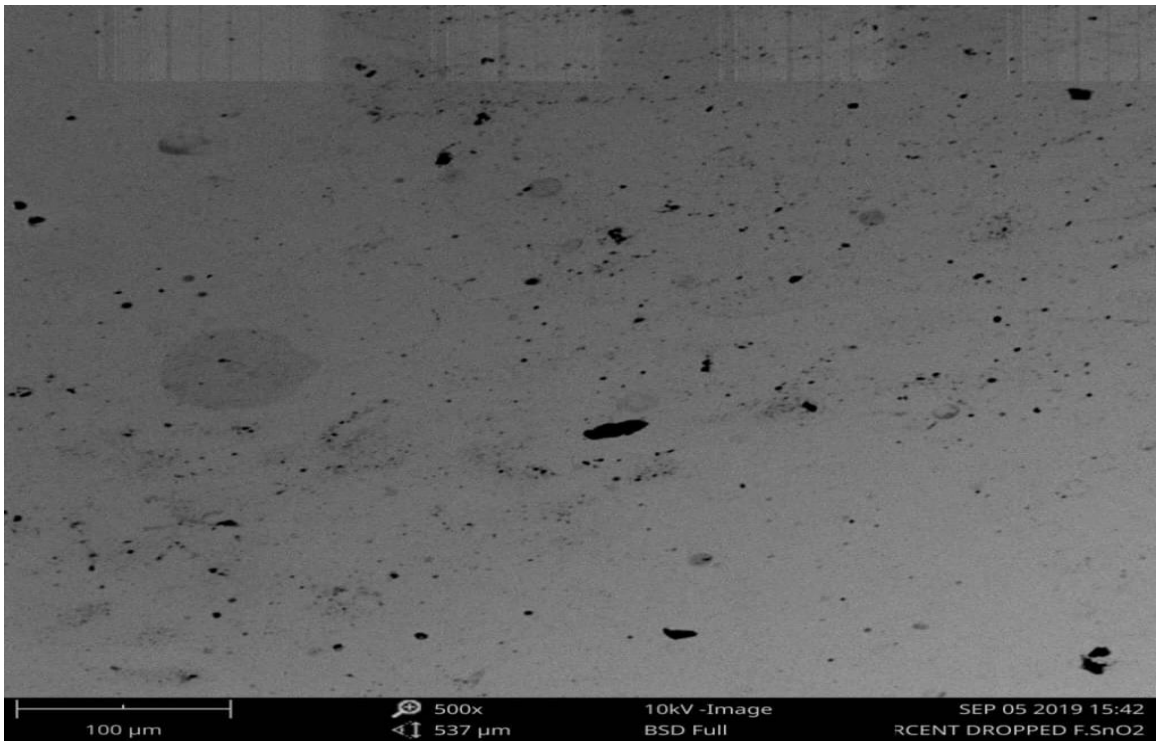

Figure 4.3: SEM of 8% F:SnO_2 with magnification size of 500x at 100µm

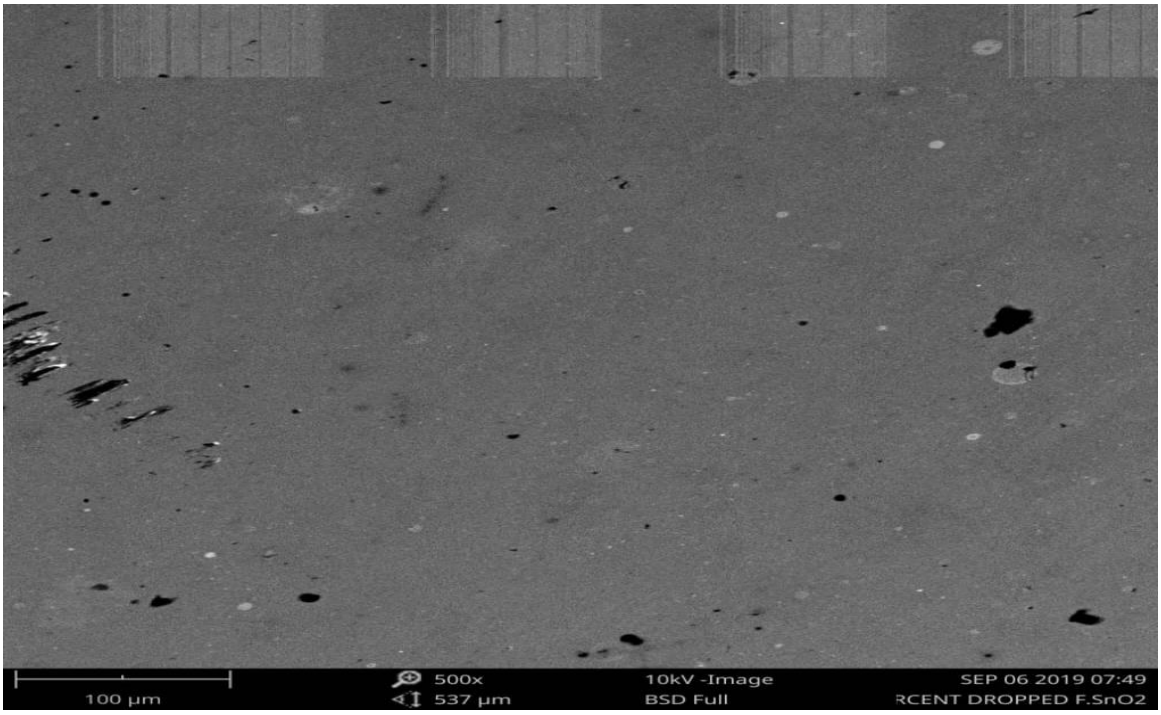

Figure 4.4: SEM of 12 % F:SnO_2 with magnification size of 500x at 100µm

4.1.1.2 Energy Dispersive X–ray (EDX)

The EDX analysis generates more information on the chemical composition of the sample, and it depends on the atomic mass of e1ements in the samples. The lower the atomic mass, the lower the response. The results of the EDX elemental microanalysis showed that fluorine has been successfully doped into the SnO_2. The EDX composition of the produced FTO thin film is presented in Table 4.1 to Table 4.4. Tab1e 4.2 is the EDX of 4 % F:SnO_2 shows an increase in f1uorine doping concentration. A higher concentration of fluorine doping is seen to bring about a better electron transfer and increase electrica1 conductivity [291]. This may also result to increase in transmittance [290]

Table 4.1: Composition of SnO_2 (Undoped)

Element Number	Element Symbol	Element Name	Atomic mass (%)	wt %
50	Si	Tin	70.94	89.99
14	Si	Silicon	6.34	1.90
20	Ca	Calcium	3.84	1.65
17	Cl	Chlorine	4.03	1.53
13	Al	Aluminum	3.45	0.99
15	P	Phosphorus	2.40	0.79
22	Ti	Titanium	1.55	0.79
16	S	Sulfur	2.27	0.78
19	K	Potassium	1.64	0.69
11	Na	Sodium	1.85	0.45
12	Mg	Magnesium	1.70	0.44

Table 4.2: Composition of 4% SnO_2

Element Number	Element Symbol	Element Name	Atomic mass (%)	wt %
50	Si	Tin	61.08	85.57
14	Si	Silicon	10.08	3.34
22	Ti	Titanium	3.48	1.96
20	Ca	Calcium	3.09	1.46
17	Cl	Chlorine	3.45	1.45
13	Al	Aluminum	3.49	1.11
15	P	Phosphorus	2.85	1.04
19	K	Potassium	2.22	1.03
16	S	Sulfur	2.64	1.00
11	Na	Sodium	3.41	0.92
12	Mg	Magnesium	2.75	0.79
9	F	Fluorine	1.47	0.33
26	Fe	Iron	0.00	0.00

Table 4.3: 8% F: SnO_2 Composition

Element Number	Element Symbol	Element Name	Atomic mass (%)	wt %
50	Si	Tin	61.08	85.57
13	Al	Aluminum	6.32	1.82
17	Cl	Chlorine	4.61	1.75
14	Si	Silicon	5.06	1.52
20	Ca	Calcium	3.31	1.42
15	P	Phosphorus	2.73	0.90
16	S	Sulfur	2.39	0.82
12	Mg	Magnesium	2.12	0.55
11	Na	Sodium	1.74	0.43
19	K	Potassium	0.42	0.18

Table 4.4: 8% F: SnO_2 Composition

Element Number	Element Symbol	Element Name	Atomic mass (%)	wt %
74	W	Tungsten	20.77	52.37
50	Sn	Tin	13.02	21.20
14	Si	Silicon	39.50	15.21
20	Ca	Calcium	5.60	3.08
11	Na	Sodium	8.17	2.58
12	Mg	Magnesium	3.85	1.28
22	Ti	Titanium	1.41	0.92
17	Cl	Chlorine	1.72	0.84
13	Al	Aluminum	2.26	0.84
19	K	Potassium	1.47	0.79
16	S	Sulfur	1.16	0.51
15	P	Phosphorus	0.59	0.25
9	F	Fluorine	0.48	0.13
26	Fe	Iron	0.00	0.00

4.1.1.3 Profilometry

The FTO layer thickness was measured using surface profiler. The thickness of the FTO thin film as shown in Figure 4.5 to Figure 4.8 for the undoped tin oxide and fluorine doped tin oxide nanoparticles ranges from 150 nm, 200 nm, 50 nm and 40 nm for undoped tin oxide, 4 %, 8 % and 12 % of fluorine dope tin oxide respectively. The thicker the thin film, the more the photon absorbed and the higher the conductivity [292].

4.1.1.4 Effect of Temperature and F1owrate on Produced FTO

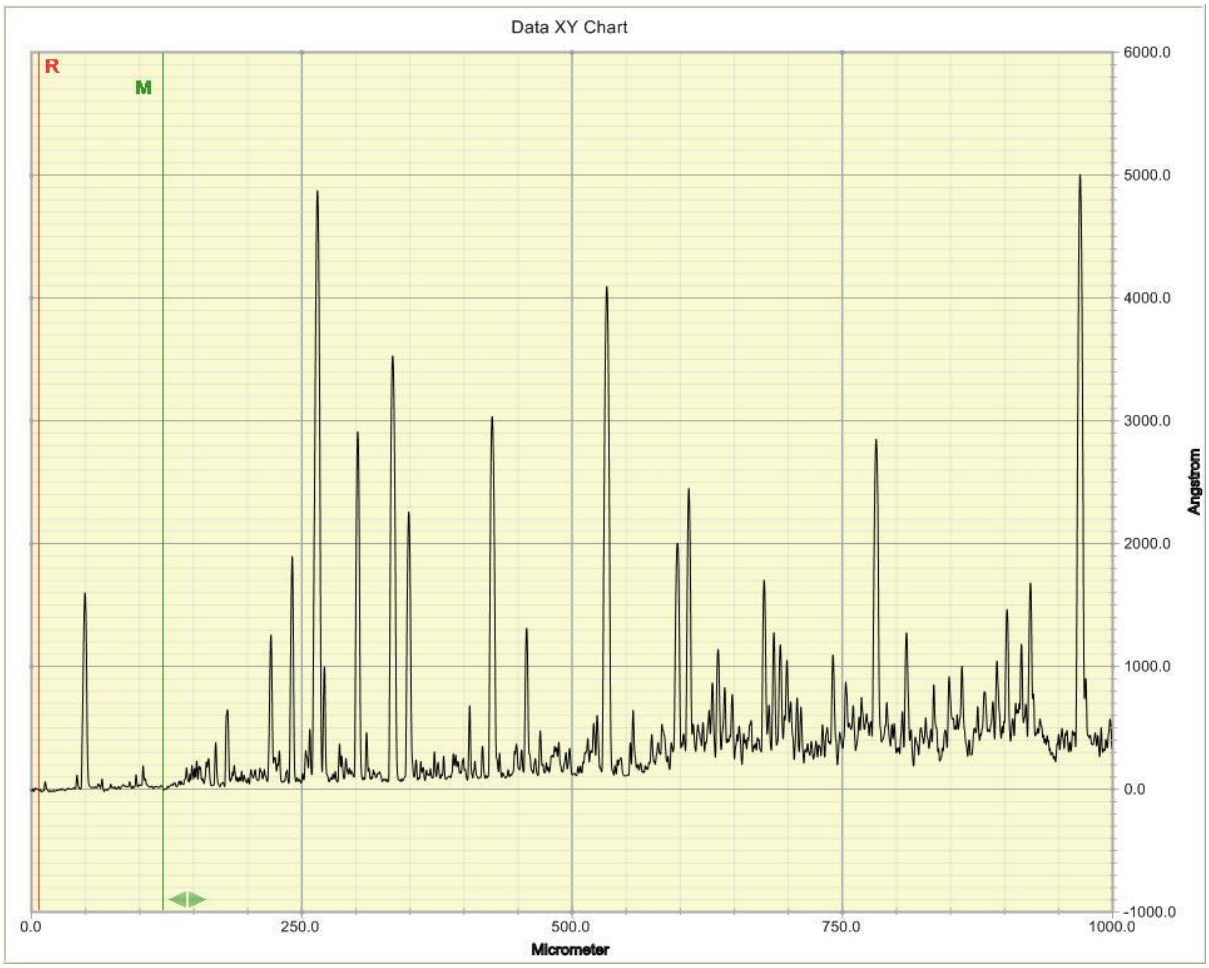

Figure 4.5: Profi1e graph for SnO_2 thin fi1m

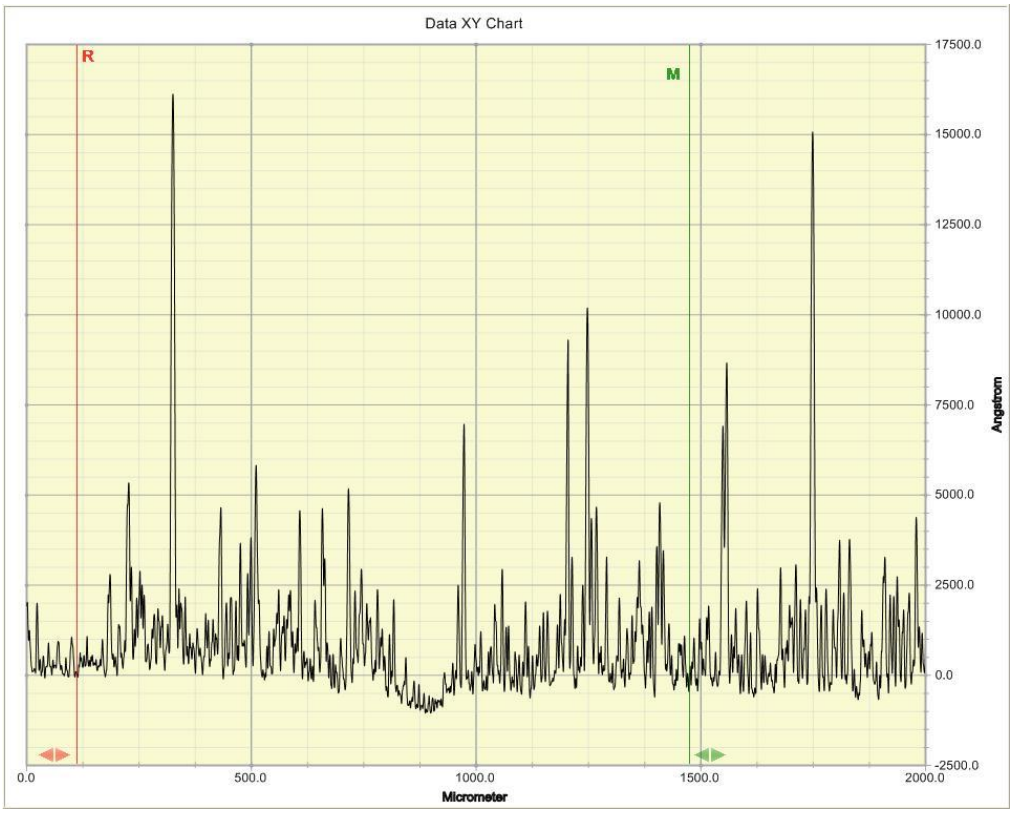

Figure 4.6: Profile graph for 4 % F:SnO_2 thin film

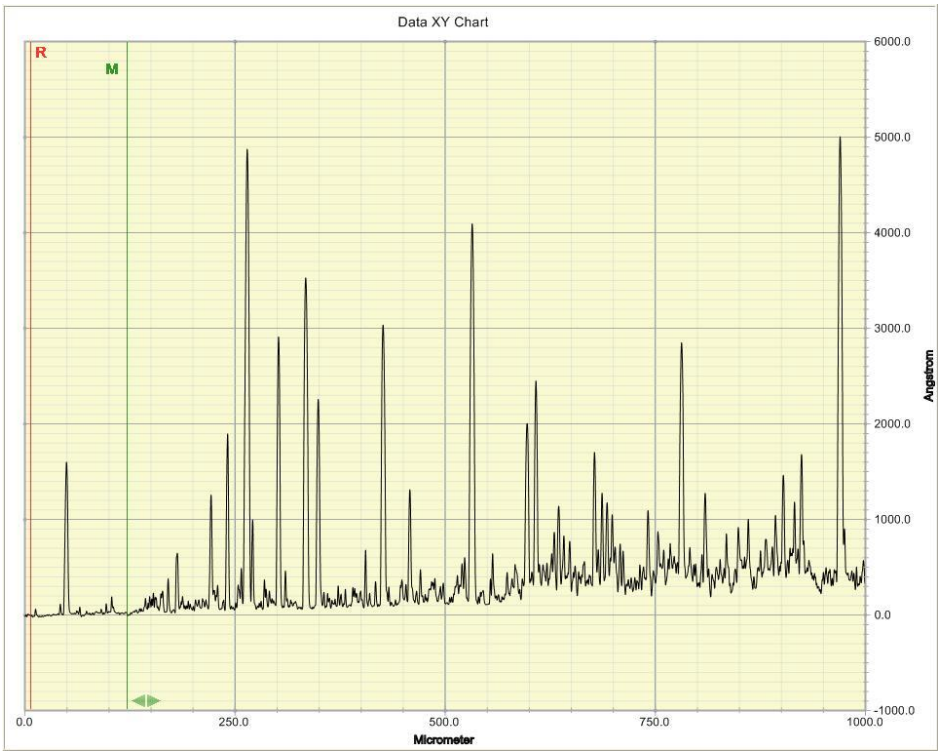

Figure 4.7: Profile graph for 8 % F:SnO_2 thin film

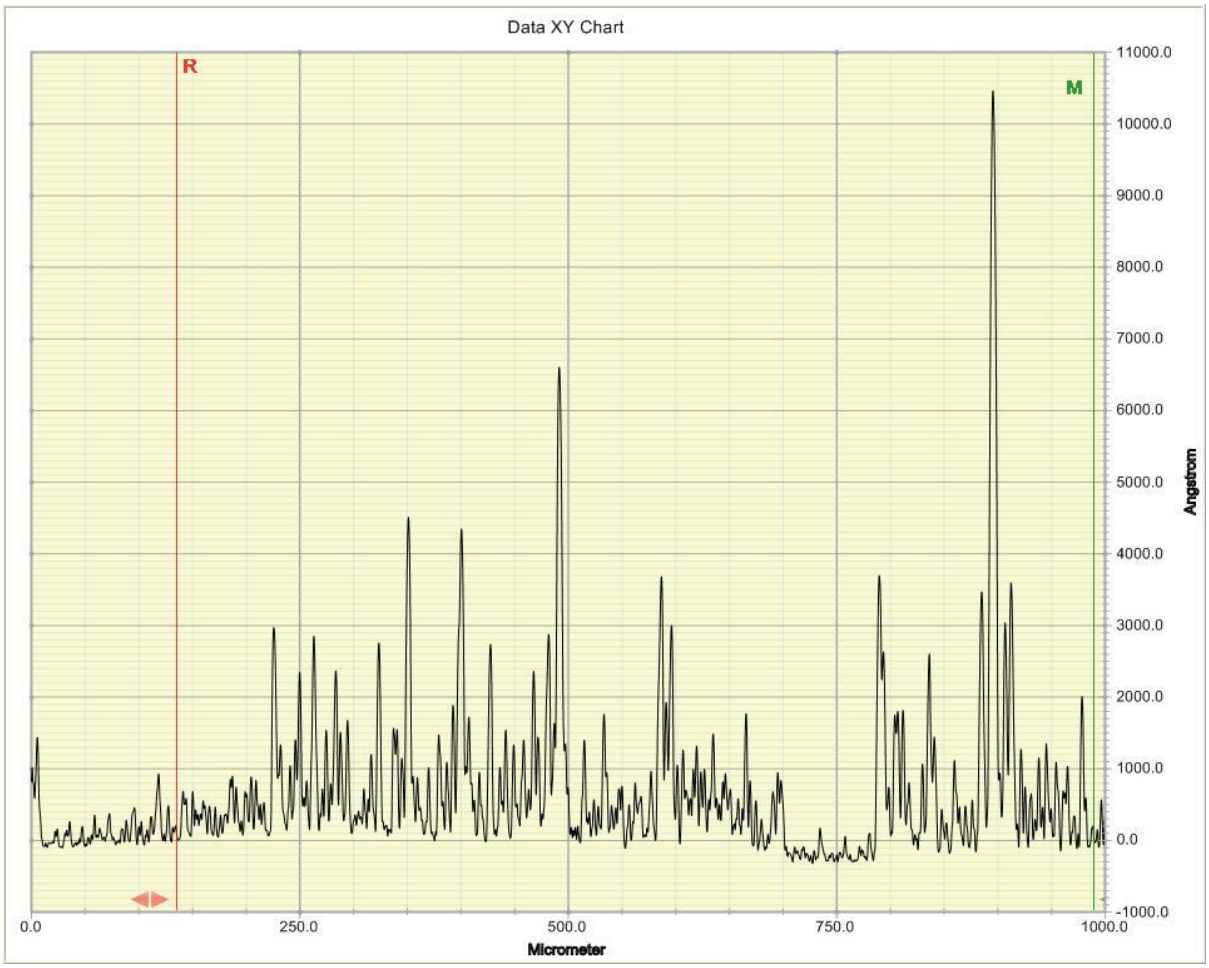

Figure 4.8: Profile graph for 12% F: SnO_2 thin film

4.1.1.5 UV Spectroscopy Results

The variation of absorbance and transmittance at 230 nm wavelength of doped and undoped SnO_2 thin films are shown in Figure 4.9 to Figure 4.12 and Table 4.5 to Tab1e 4.8. The frequency of the visible light range is seen within the minimum and maximum wavelength of 230 nm and 1100nm

Table 4.5: Absorbance and transmittance of undoped and doped SnO_2 at 230 nm and 1100 nm wavelength for 4%, 8% and 12%

S/N	Sample ID	Fluorine Doping (%)	Deposition Time (min)	Absorbance (λ = 230 nm)	Transmittance (λ = 230 nm)	Absorbance (λ = 1100 nm)	Transmittance (λ = 1100 nm)
1	SNO_2	0	13	1.19	6.40	0.13	73.06
2	F:SnO_2	4	15	0.30	50.35	0.08	83.18
3	F:SnO_2	8	25	0.50	31.62	0.08	82.64
4	F:SnO_2	12	38	0.88	13.27	0.04	90.53

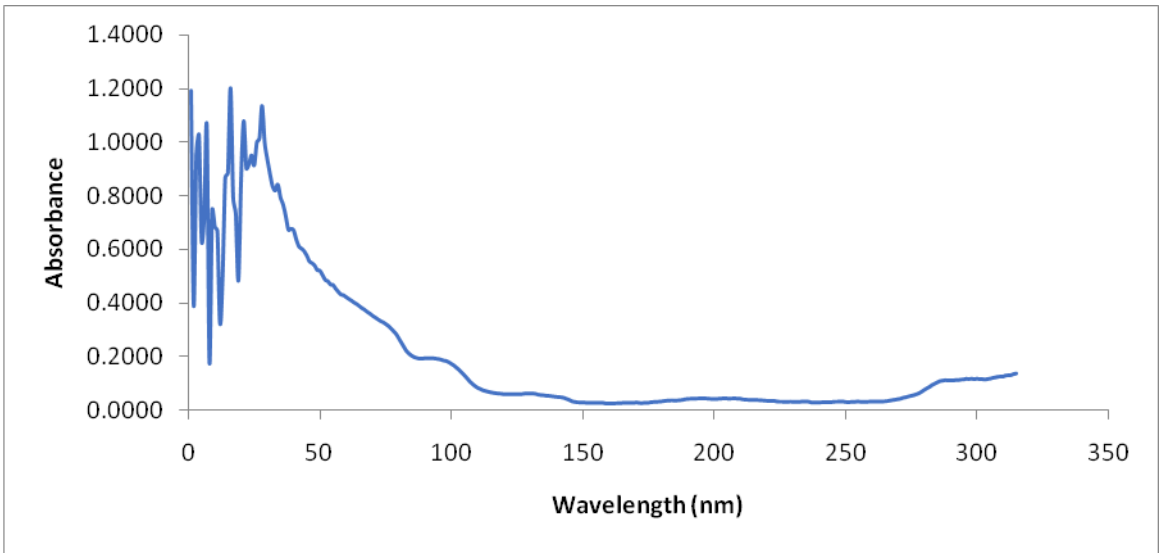

Figure 4.9: Absorbance-Spectra of Un-doped SnO_2 Thin Fi1ms Deposited on Glass Substrate

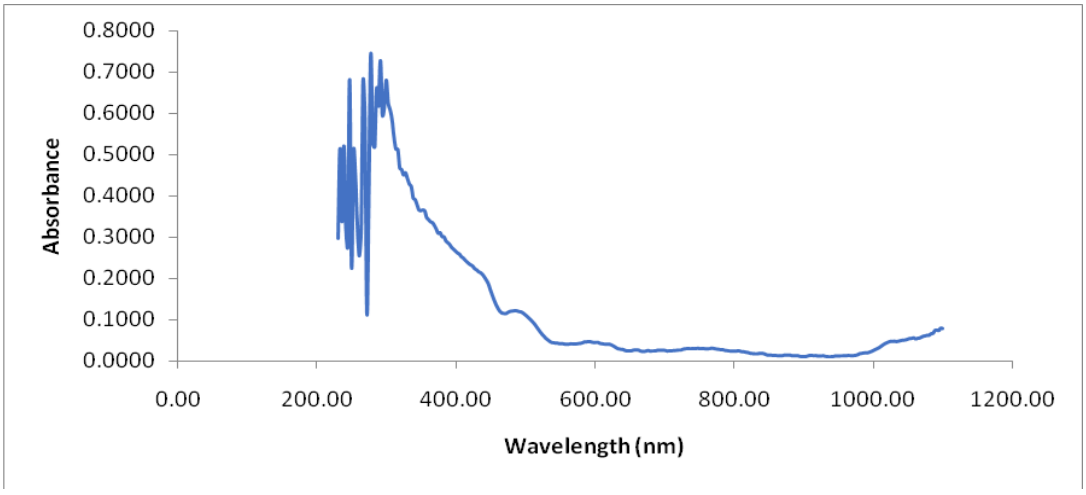

Figure 4.10: Absorbance-Spectra of 4% F:SnO_2 Thin Films Deposited on Glass Substrate

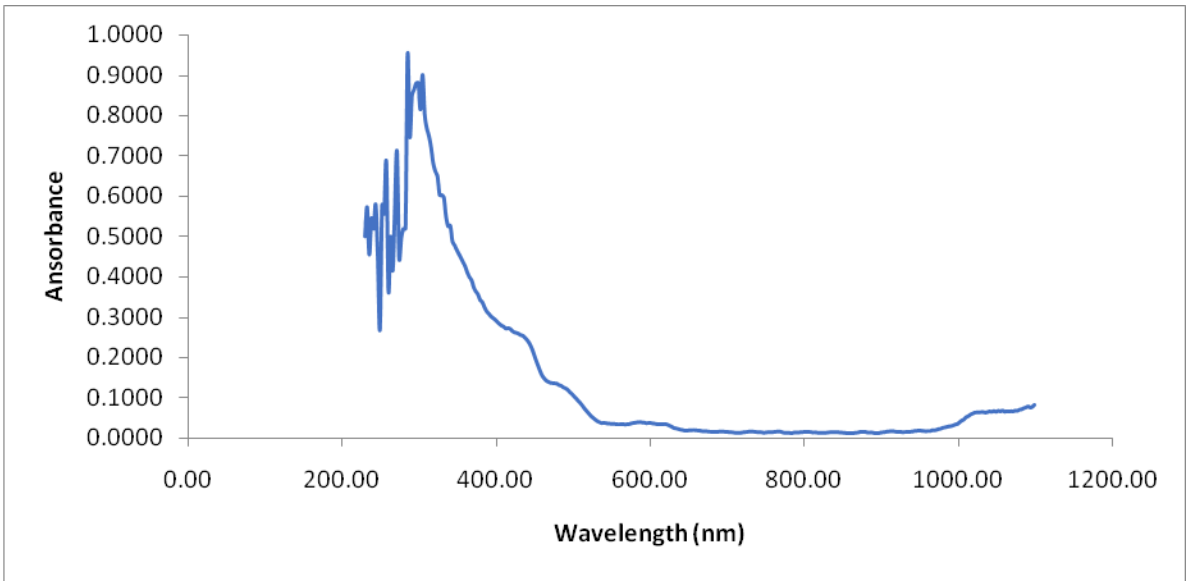

Figure 4.11: Absorbance-spectra of 8% F:SnO_2 Thin Films Deposited on Glass Substrate

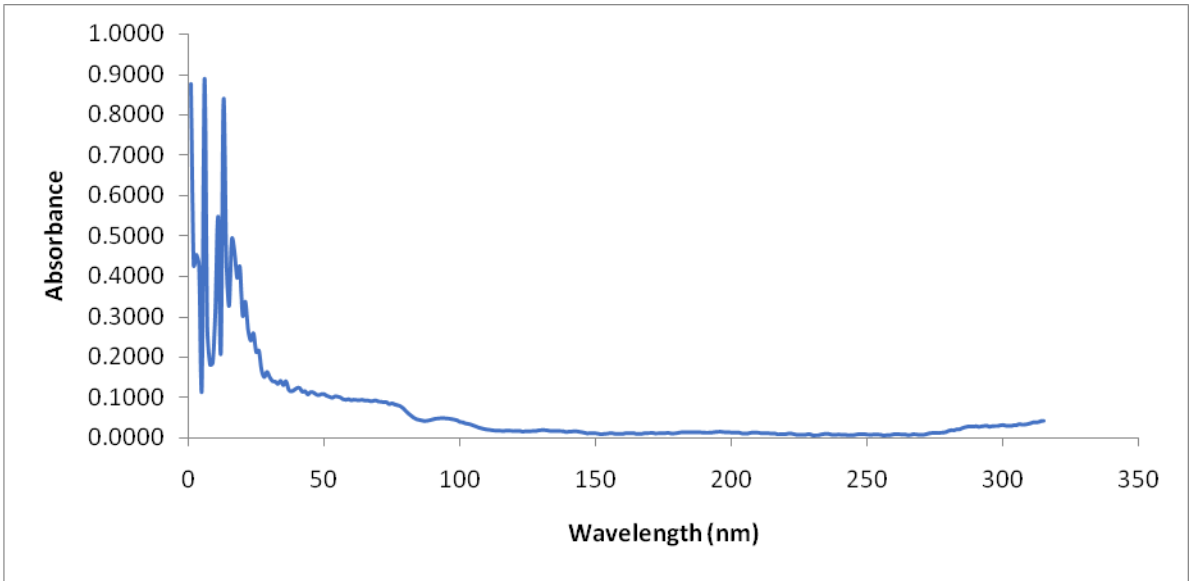

Figure 4.12: Absorbance spectra of 12% F: SnO_2 Thin Films Deposited on Glass Substrate and wave1ength

Table 4.6: Absorbance and transmittance for doped and Un-doped F: SnO_2

	SNO_2		4% F:SnO_2		8% F:SnO_2		12% F:SnO_2	
Wavelength (nm)	Absorbance	Transmittance %	Absorbance	Transmittance %	Absorbance	Transmittance %	Absorbance	Transmittance %
230	1.19	6.40	0.30	50.35	0.5	31.62	0.88	12.27
401.74	0.40	39.36	0.26	54.59	0.29	51.41	0.09	80.46
576.25	0.06	25.53	0.04	90.42	0.03	91.85	0.01	96.05
750.76	0.04	91.20	0.03	96.87	0.01	96.69	0.01	96.69
925.57	0.02	93.37	0.01	96.87	0.02	96.29	0.00	97.92
1100	0.14	73.06	0.08	83.18	0.08	82.64	0.04	90.53

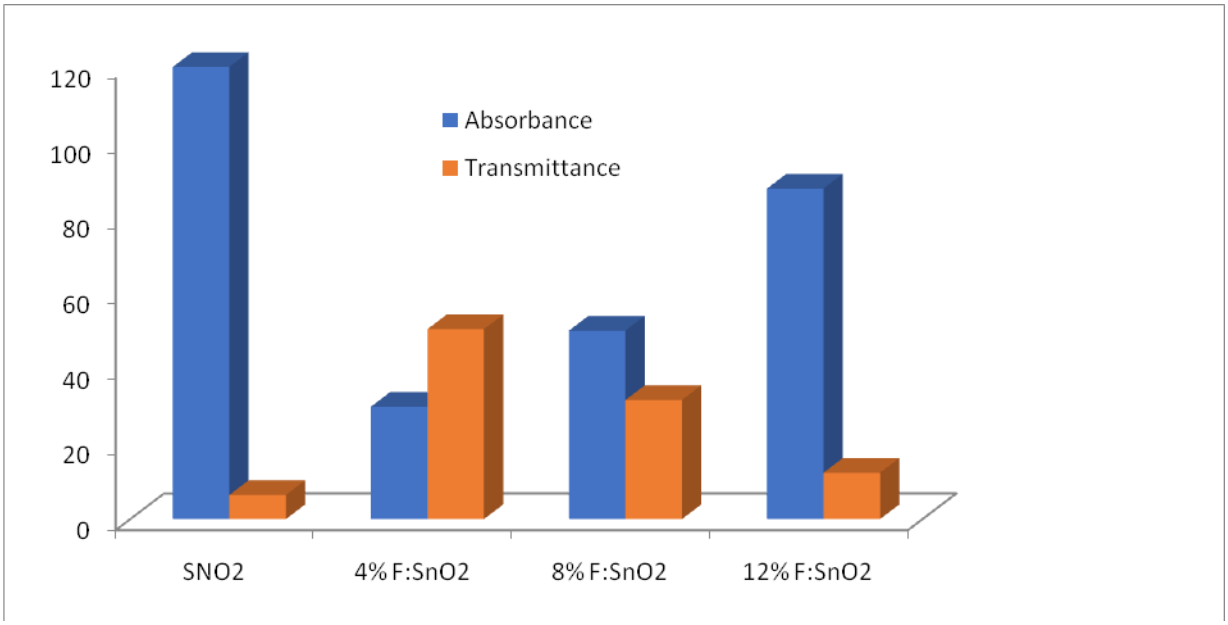

Figure 4.13: Graph of Absorbance and Transmittance for (4%, 8% and 12%) F:SnO_2 at $\lambda = 230\ nm$

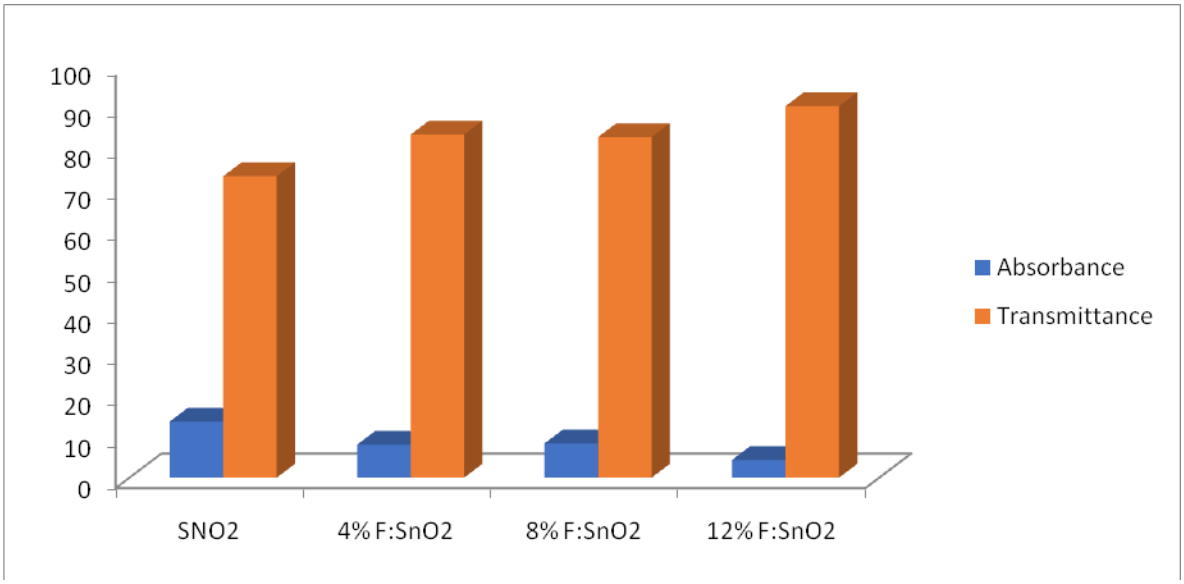

Figure 4.14: Absorbance and transmittance for (4%, 8% and 12%) F:SnO_2 at $\boldsymbol{\lambda = 1100\ nm}$

These same optical characteristics of the fluorine doped tin-oxide and the undoped (SnO_2 deposited) tin-oxide thin films, produced and-coated by AACVD technique-on the glass substrate were examined. The transmittance and-the absorbance spectra were measured-in range of wavelength from 230 nm – 1100 nm for 4 percent, 8 percent-and 12 percent F: SnO2 and the undoped-tin oxide. The results at wavelength 230 nm and 1100 nm are provided in tables 4.6 – 4.7. The results showed that more-time is necessary as Fluorine doping is-carried out-on-the substrate (i.e. the more-the percentage of doping-the more time it is required to deposit the FTO on the glass substrate) (i.e. the more the percentage of doping the more-time it is required to-deposit the FTO on-the glass substrate). The undoped SnO_2 was deposited-faster while the 12% F: SnO2 had the slowest deposition-time.

4.1.2 Effect of Wavelength on Absorbance

On the several slides, Fluorine was doped in varying amounts (4 percent, 8 percent, and 12 percent). Figures 4.13 and 4.14 show the absorbance for the 230 nm to 1100 nm wavelength range. Undoped had the highest absorbance at 271.55 nm, which was increases and declines before decreasing monotonically until it reaches 1100 nm.

Nevertheless, it was discovered that the behavior displayed by the absorbance spectra was typical of fixed-size scattering centers, which typically diffuse more effectively at shorter wavelengths.

The peak values of the absorbance of the doped SnO_2 were found to be lower than those of the undoped SnO_2, contrary to what was observed at the various percentages of dopant tested.

At the lowest wavelength of 230nm, the 4% F: SnO2 has the lowest absorbance value while at the highest wavelength, the 12% F:SnO2 has the lowest absorbance value. The absorbance increased with dopant percentage because there is fusion of fluorine atoms in the structure of the thin film [294].

4.1.3 Effect of Wavelength on Optical Transmittance

By using a UV-VIS spectrophotometer, the optical transmittance (T) characteristics of the thin films produced with various dopants were identified. Utilizing transmission spectra in the wavelength range of 230 nm to 1100 nm, the optical transmittance was studied. As the wavelength rises, an increase in transmittance was seen. At 230 nm, 4 percent F: SnO_2 had the highest light transmittance, while undoped materials had the lowest. At 1100 nm, the amount of transmittance is estimated to be 83 percent.

The high transmittance could be attributed to the high concentration of the fluorine doping [290]. A work done [292] depositing a nano thick FTO multilayers showed that as the FTO layer thickness increase, the average optical transmittance in the visible range of wavelength is increased. This further suggest that FTO have good optica1 electrical properties which is an advantage for the DSSCs.

4.1.4 Hall Effect Measurement

The electrical properties of the undoped and the doped fluorine SnO_2 are shown in Tab1e 4.7. The findings as displayed in Figure 4.15 showed that both the wavelength and the amount of doping had a significant impact on FTO.

The lowest absorbance value of 4 percent F: SnO_2 is 0.2980 a.u at the lowest wavelength of 230 nm, and the lowest absorbance value of 12 percent F: SnO2 is 0.0432 a.u at the highest wave1ength. Conductivity in thin films is also influenced by the thick

ness of the film. Conductivity starts to decline as the thickness exceeds an ideal limit because the grain size of the nanoparticles grows by increasing the band gap (quantum confinement effect), the physical implication is seen in Table 4.7 where the negative (-ve) values in the 4% F: SnO_2, 8% F: SnO_2, and 12% F: SnO_2 show a decrease due to the increase in thickness of the film as it exceeds the ideal limit.

Table 4.7: Results of Hall Effect Analysis for FTO

S/N	OPTICAL PROPERTIES	0.4ml SnO_2	4% F:SnO_2	8% F:SnO_2	12% F: SnO_2
1	Bulk Concentration/cm^3	1.12×10^{19}	-2.76×10^{21}	-1.75×10^{17}	-4.19×10^{17}
2	Mobility cm^3/Vs	1.35	1.40×10^{1}	7.46	2.37×10^{5}
3	Sheet-Resistance Ω/sq	4.12×10^{4}	2.48×10^{4}	1.20×10^{6}	3.13×10^{5}
4	Resistivity Ωcm	4.12×10^{-1}	1.98×10^{-1}	4.70	6.26×10^{-1}
5	A-C Cross Hall Coefficient cm^3C	-5.37×10^{1}	1.29×10^{1}	-1.10×10^{2}	$-2{,}36 \times 10^{2}$
6	Magneto-Resistance Ω	4.27×10^{2}	1.91×10^{2}	7.34×10^{3}	2.94×10^{4}
7	Sheet Concentration/cm^2	1.10×10^{14}	-2.21×10^{11}	-6.98×10^{11}	-8.38×10^{11}
8	Conductiivty 1/Ωcm	2.43	5.04	2.09×10^{-1}	1.56
9	Average Hall Coefiicent cm^3/C	5.55×10^{-1}	-2.26	-3.58×10^{1}	-1.49×10^{1}
10	B-D Cross Hall Coefficient cm^3/C	5.48×10^{1}	-1.75×10^{1}	3.85×10^{1}	2.06×10^{2}
11	Ratio of Vertical Horizontal	-1.35×10^{-6}	-4.29×10^{-3}	-6.43×10^{-4}	8.35×10^{-5}

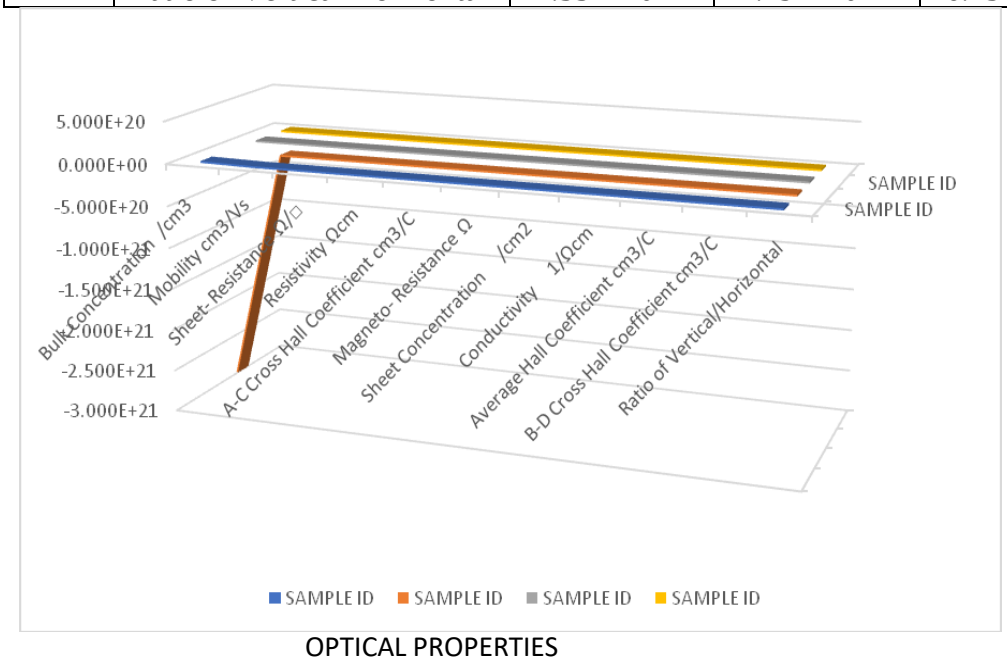

Figure 4.15: 3D graph of optical properties of sampled ID

4.2 Influence of reduced graphene oxide on DSSC performance

As earlier discussed, reduced graphene oxide shows some unique quality which can influence and improve the performance of the DSSC. Several studies have reported progress and increased performance of DSSCs with reduce graphene oxide [203, 304, 305, 306]. Reduced graphene oxide (rGO) production consists of three stages which are the oxidation, exfoliation, and reduction stages. In the oxidation stage, graphite powder is reacted with a strong oxidizing agent (potassium permanganate). The oxidized graphite is now dispersed in distilled water to form single-layer graphene oxide (GO) which is the exfoliation stage, the reduction is the one that finally produced the reduced graphene oxide (rGO). Six different samples of the RGO were produced and studied using the Scanning Electron Microscope-Energy Dispersive X – ray (SEM-EDX), Hall Effect, X-ray, Profilometry and Diffuse Reflectance-Ultraviolet visible spectroscopy (DRS UV-Vis).

4.3.1 Results and Discussion

4.3.1.1 Hall Effect analysis of Reduced Graphene Oxide

Tab1e 4.8: Results of Hall Effect Analysis of Reduced Graphene Oxide (rGO)

S/N	OPTICAL PROPERTIES	SAMPLE ID					
		1 rGO	2 rGO	3 rGO	4 rGO	5 rGO	6 rGO
1	Bulk Concentration cm^{-3}	4.96×10^{16}	1.19×10^{14}	-8.20×10^{12}	-5.07×10^{12}	2.52×10^{17}	-9.84×10^{12}
2	Mobi1ity cm^3/Vs	1.21×10^{2}	4.91	3.81×10^{1}	5.49×10^{2}	2.02×10^{1}	2.17×10^{1}
3	Sheet- Resistance Ω/sq	1.04×10^{5}	2.66×10^{8}	1.18×10^{9}	2.24×10^{8}	8.17×10^{4}	2.93×10^{9}
4	Resistivity Ωcm	1.04	1.06×10^{4}	1.99×10^{4}	2.24×10^{3}	1.23	2.93×10^{4}
5	A-C Cross Ha11 Coefficient cm^3/C	2.47×10^{2}	3.03×10^{5}	6.93×10^{6}	2.09×10^{6}	7.95×10^{1}	-2.59×10^{7}
6	Magneto-Resistance Ω	1.30×10^{5}	2.67×10^{8}	3.84×10^{8}	3.82×10^{8}	2.77×10^{3}	5.19×10^{9}
7	Sheet Concentration cm^{-3}	4.96×10^{11}	4.78×10^{9}	-1.39×10^{8}	-5.07×10^{7}	3.76×10^{12}	-9.84×10^{7}
8	Conductivity 1/Ωcm	9.58×10^{-1}	9.40×10^{-5}	5.00×10^{-5}	4.46×10^{-4}	8.17×10^{-1}	3.42×10^{-5}
9	Average Ha11 Coefficient cm^3/C	1.26×10^{-2}	5.23×10^{4}	-7.61×10^{5}	-2.23×10^{6}	2.47×10^{1}	-6.33×10^{5}
10	B-D Cross Ha11 Coefficient cm^3/C	5.64	-1.98×10^{5}	-8.45×10^{6}	-4.56×10^{6}	-2.99×10^{1}	2.46×10^{7}

4.3.1.2 Profilometry

The profilometry results for the rGO nanoparticles show the thickness ranges from 150nm-200nm as shown in the profile graph below. The more the thickness of the thin film, the conductivity, and the more the photon absorbed. Samp1e 1, 2, 3, 4, 5 and 6 has wavelength 300nm, 400nm, 150nm, 180nm, 250nm and 150nm respectively as shown in Figure 4.16 to Figure 4.21. Sample five had the highest thickness of 400nm. The increased film thickness increased the hall coefficient and mobility with a decrease in carrier concentration.

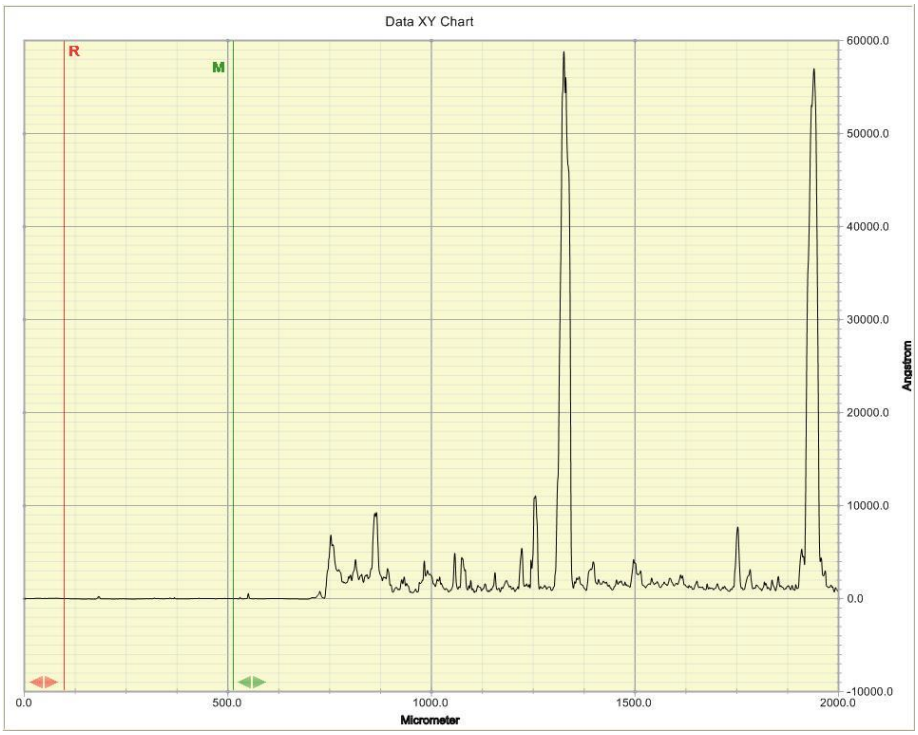

Figure 4.16 Profile graph for 1 rGO

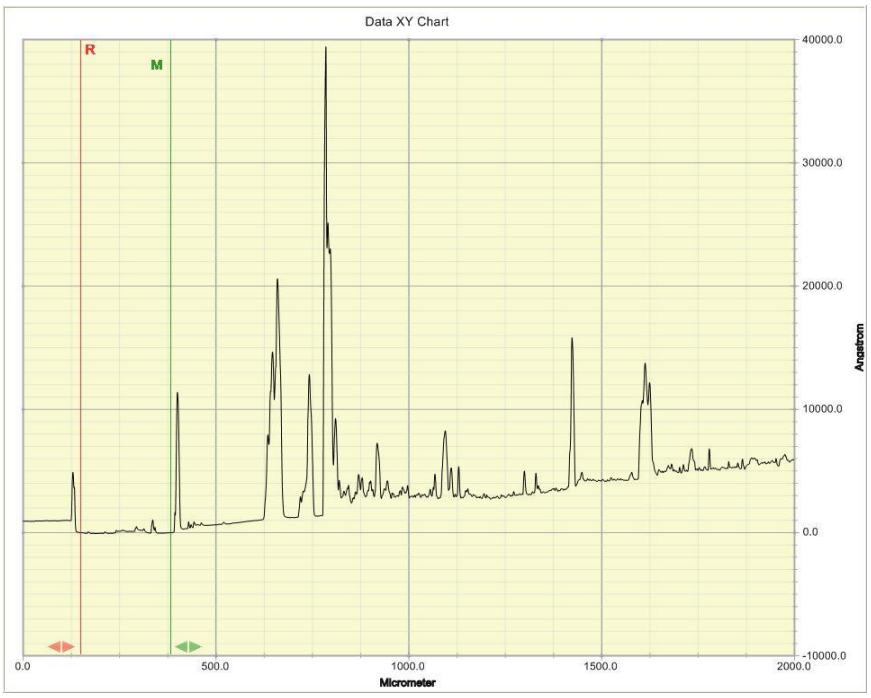

Figure 4.17 Profile graph for 2 rGO

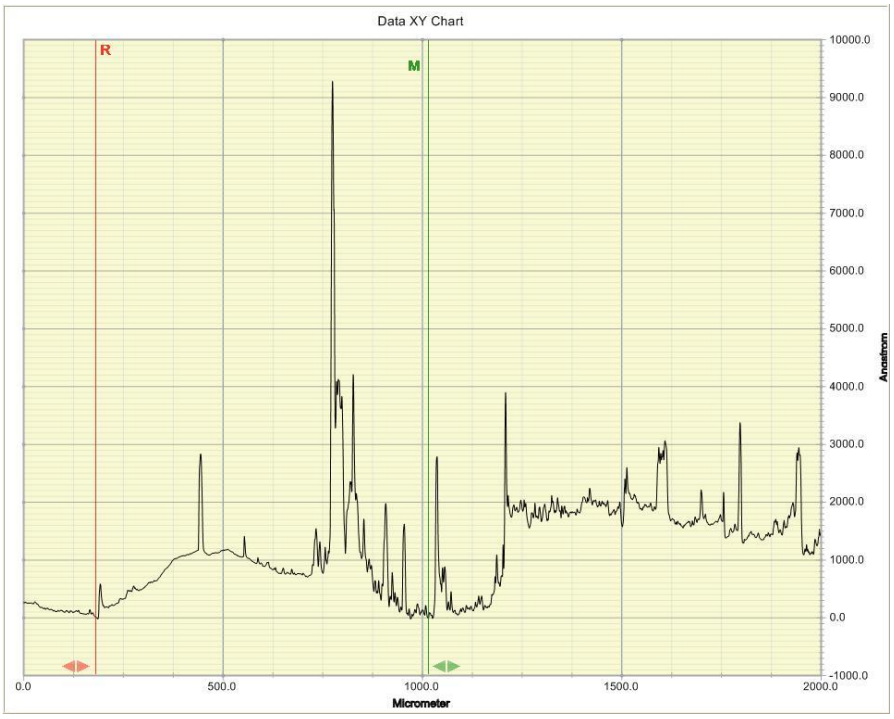

Figure 4.18 Profile graph for 3 rGO

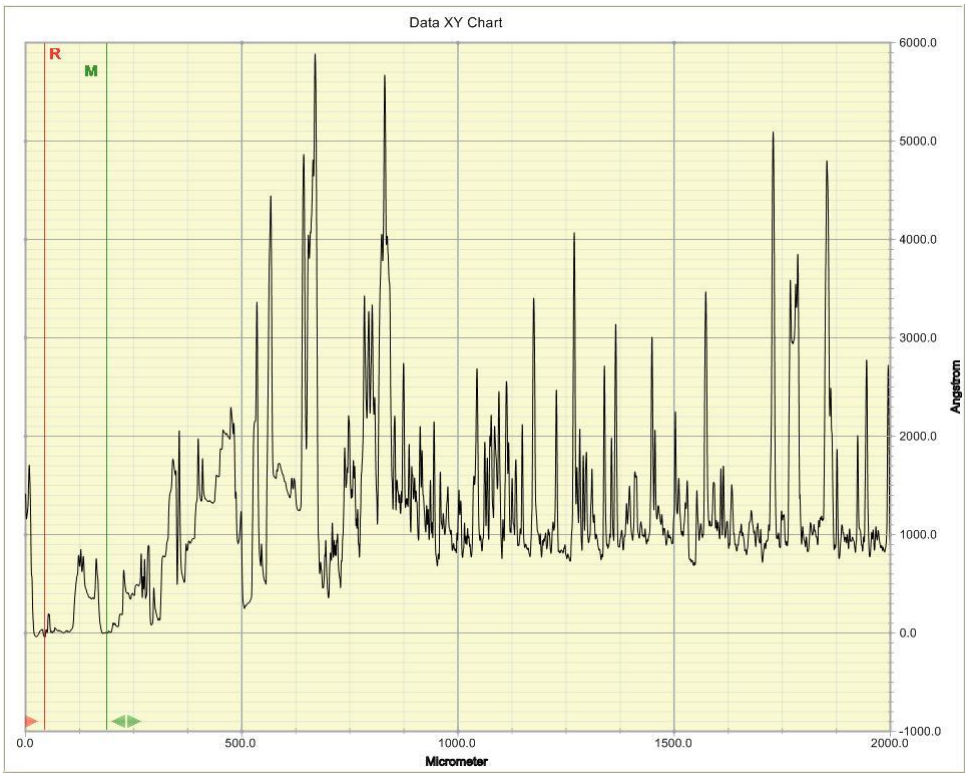

Figure 4.19 Profile graph for 4 rGO

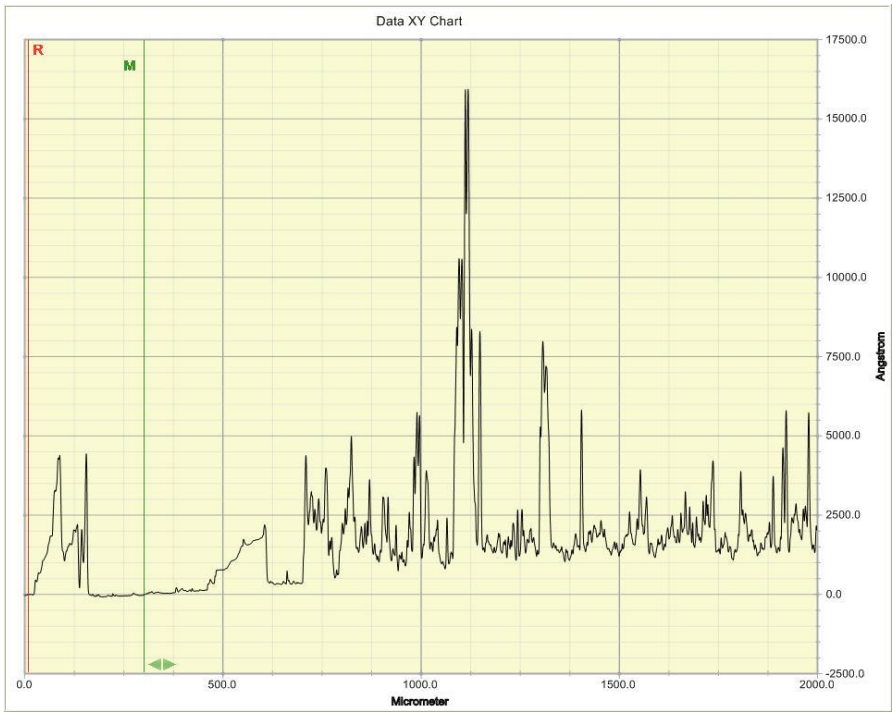

Figure 4.20 Profile graph for 5 rGO

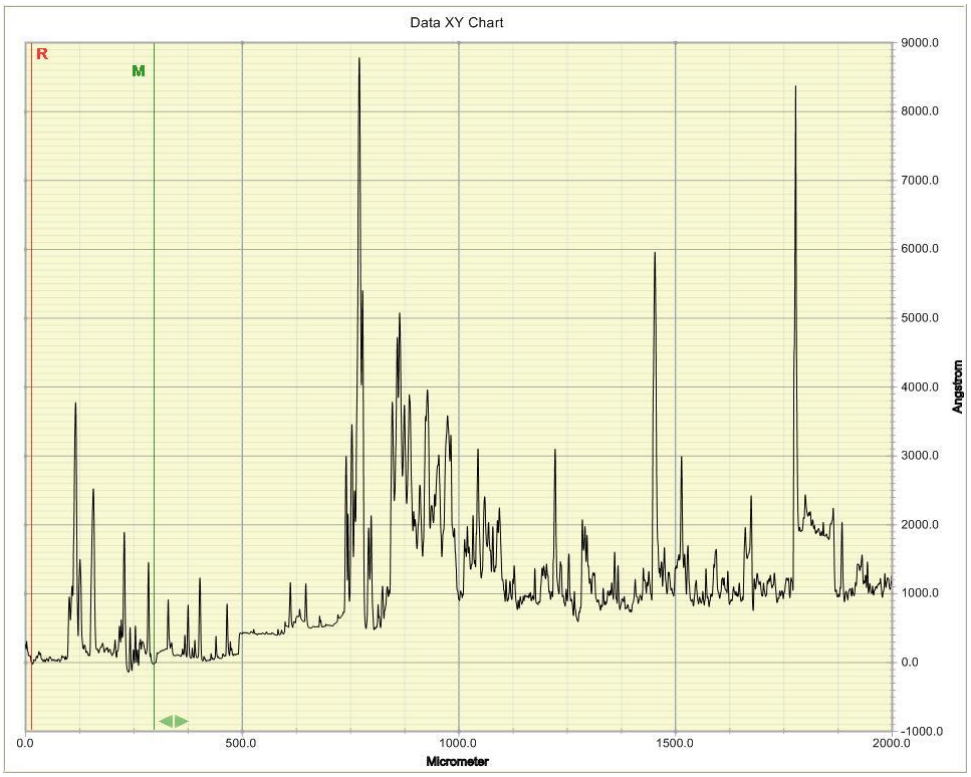

Figure 4.21 Profile graph for 6 rGO

4.3.1.3 Morphologic and Elemental Analysis (SEM/EDX)

The SEM images of the reduced graphene oxide material show the presence of individual thinnest flakes crumple sheet monolayer which are closely associated with each other [269, 307, 308]. This deduction was based on the low resolution of the SEM microscopy. Due to the reductant, the rGO flakes exhibit the largest content of vacancy, C sp^3 defects and hydroxyl group accompanied by the smallest content of epoxy. The results of the EDX elemental microanalysis of C, O, and N elements are in Table 4.9. The low percentage of the carbon content indicates that the graphene oxide was successfully reduced. Also, oxygen was not present in the elemental composition, which indicates that no oxygen-containing functional groups still existed in the sample of reduced graphene oxide. The structure and morphology of the rGO monolayer were revealed by scanning electron microscopy (SEM), and GO reveals the many carbon atoms on the surface of the rGO monolayer [269]. For detection, EDX analysis depends on the atomic masses of the elements in the samples.

The reaction decreases as atomic mass decreases. Sample 3 included nitrogen, which most likely came from interactions between the reducing agent and graphene oxide. The hydrazine alcohols, which were primarily in charge of the incorporation of nitrogen, were created through the easy reaction of hydrazine with the epoxied functional groups. Other atoms including sulphur, potassium, chlorine, calcium, and iron were added during the process. This may be the result of incorrect GO cleaning procedures and inadequate responses. These elements may also have been introduced from the initial chemicals and reagents used in the process of oxidation. This means the method successfully reduced the graphene oxide to reduced graphene oxide.

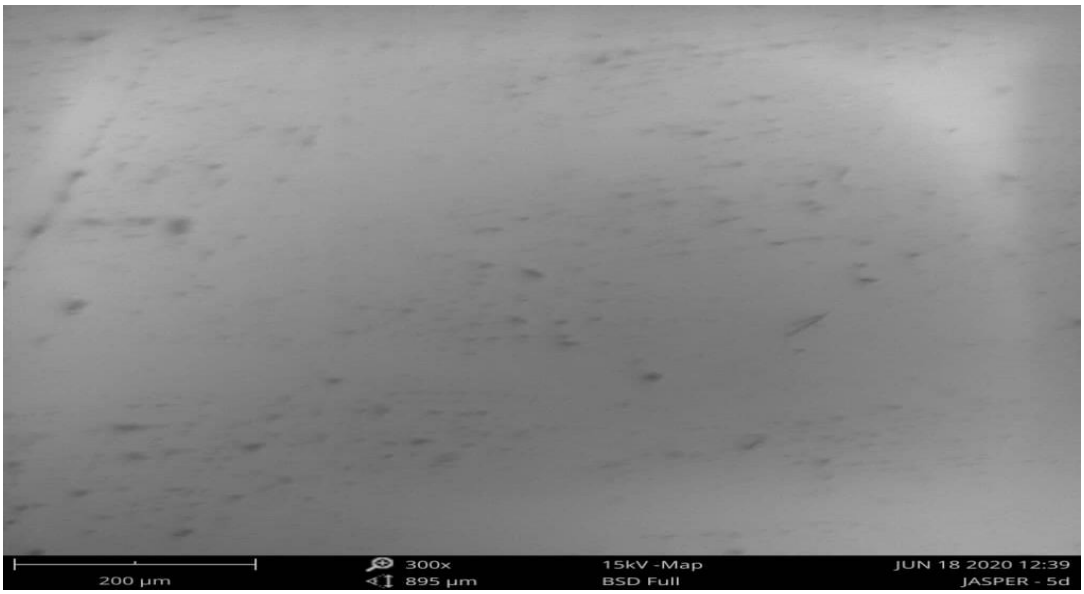

Figure 4.22 SEM of 1 rGO with magnification size of 300x at 200µm

Tab1e 4.9. Composition of 1 rGO

Element Number	Element Symbol	Element Name	Atomic Conc.(%)	wt. %
14	Si	Silicon	54.78	57.48
11	Na	Sodium	25.51	21.91
20	Ca	Calcium	5.23	7.83
12	Mg	Magnesium	7.22	6.56
13	A1	Aluminum	2.36	2.38
6	C	Carbon	2.93	1.31
16	S	Sulfur	0.65	0.77
19	K	Potassium	0.44	0.65
15	P	Phosphorus	0.46	0.54
17	C1	Chlorine	0.36	0.48
22	Ti	Titanium	0.06	0.10

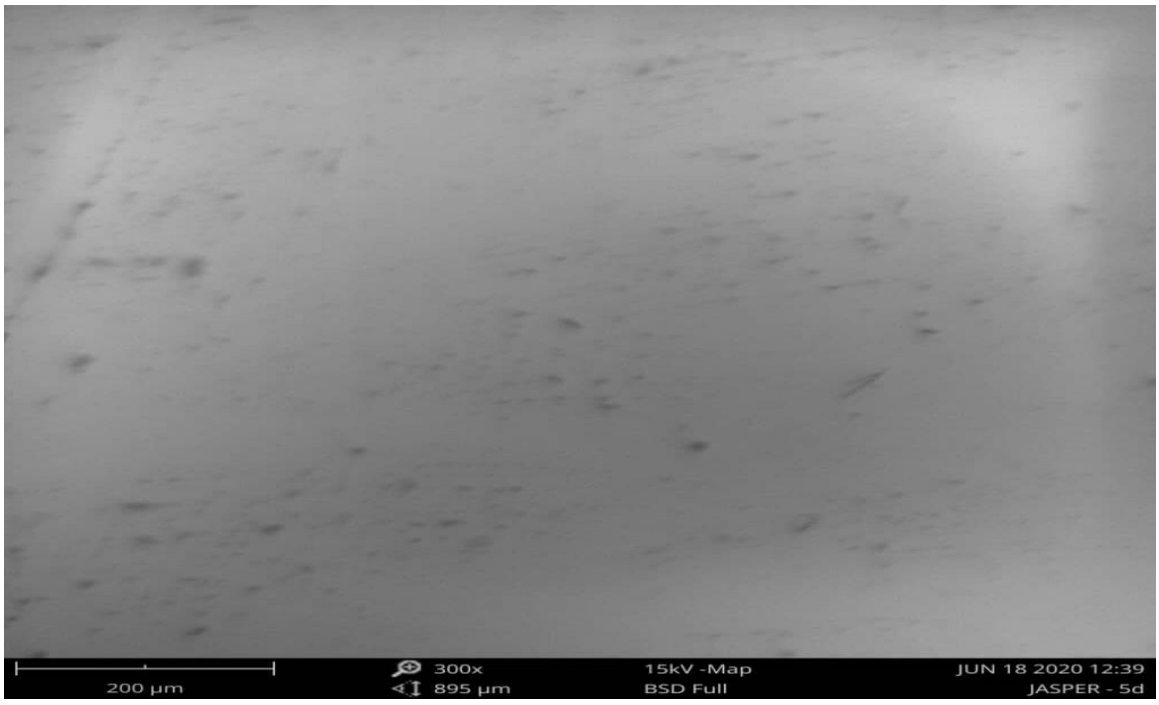

Figure 4.23. SEM of 2 rGO with magnification size of 300x at 200µm

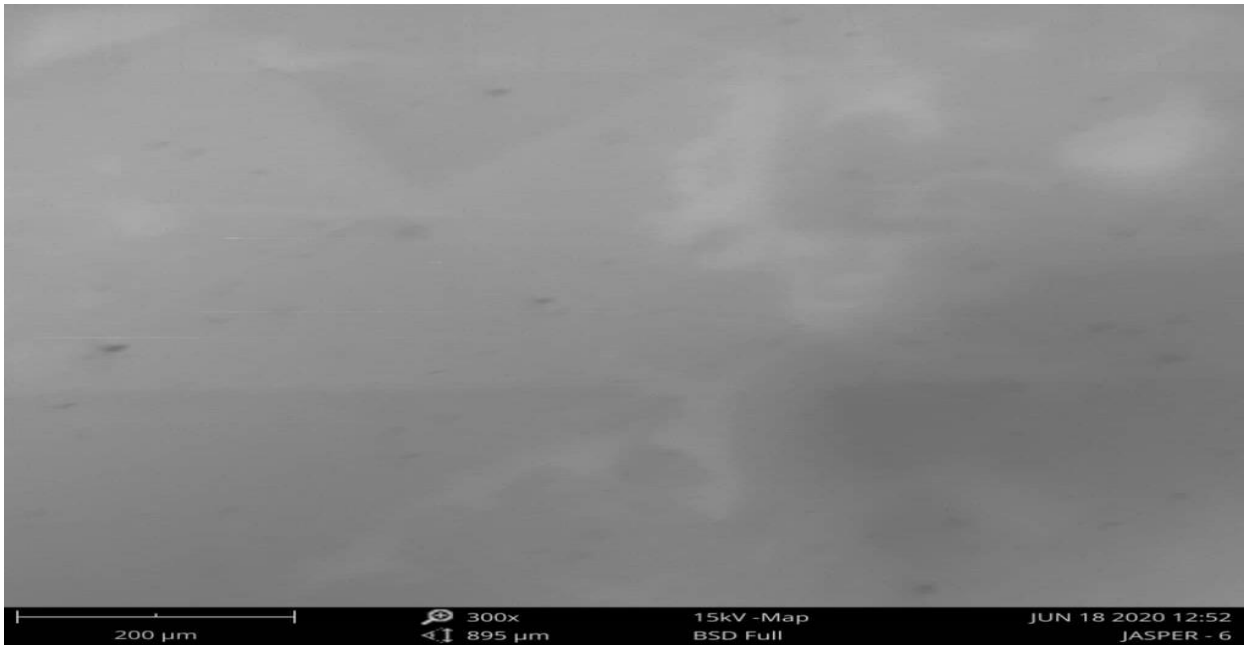

Figure 4.24. SEM of 3 rGO with magnification size of 300x at 200µm

Tab1e 4.10. Composition of 2 rGO

Element Number	**Element Symbol**	**Element Name**	**Atomic Conc.(%)**	**wt. %**
14	Si	Silicon	53.86	57.32
11	Na	Sodium	24.84	21.63
20	Ca	Calcium	5.04	7.65
12	Mg	Magnesium	6.99	6.44
6	C	Carbon	5.42	2.47
13	A1	Aluminum	2.27	2.32
16	S	Sulfur	0.49	0.60
19	K	Potassium	0.40	0.59
17	C1	Chlorine	0.27	0.36
15	P	Phosphorus	0.28	0.33
26	Fe	Iron	0.11	0.24
22	Ti	Titanium	0.03	0.06

Tab1e 4.11. Composition of 3 rGO

E1ement Number	E1ement Symbo1	E1ement Name	Atomic Conc.(%)	wt. %
14	Si	Si1icon	52.31	56.06
11	Na	Sodium	24.15	21.18
20	Ca	Ca1cium	4.96	7.59
12	Mg	Magnesium	6.85	6.36
6	C	Carbon	5.32	2.44
13	A1	A1uminum	2.24	2.31
7	N	Nitrogen	2.09	1.12
16	S	Su1fur	0.62	0.76
17	C1	Ch1orine	0.39	0.53
19	K	Potassium	0.35	0.53
15	P	Phosphorus	0.36	0.42
26	Fe	Iron	0.19	0.39
25	Mn	Manganese	0.08	0.17
22	Ti	Titanium	0.08	0.15

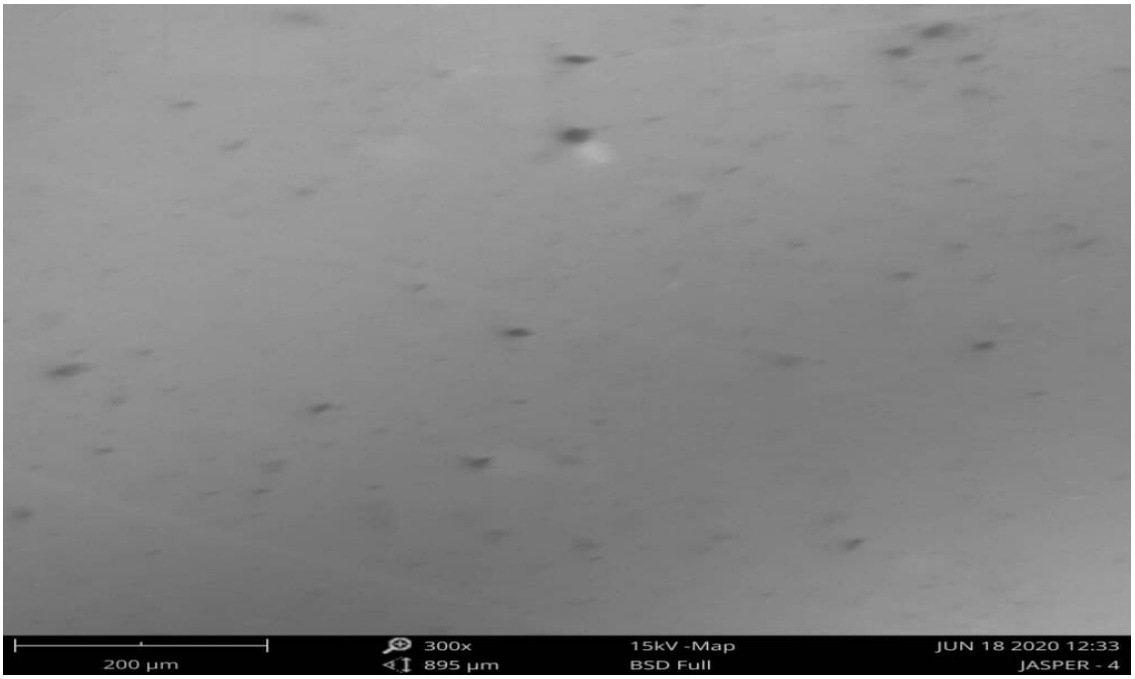

Figure 4.25. SEM of 4 rGO with magnification size of 300x at 200µm

Tab1e 4.12. Composition of 4 rGO

Element Number	Element Symbol	Element Name	Atomic Conc.(%)	wt. %
14	Si	Silicon	54.16	57.48
11	Na	Sodium	24.52	21.30
20	Ca	Calcium	5.21	7.89
12	Mg	Magnesium	7.21	6.62
6	C	Carbon	5.10	2.32
13	A1	A1uminum	2.27	2.31
19	K	Potassium	0.38	0.57
16	S	Sulfur	0.42	0.51
15	P	Phosphorus	0.33	0.39
17	C1	Chlorine	0.29	0.39
26	Fe	Iron	0.10	0.21

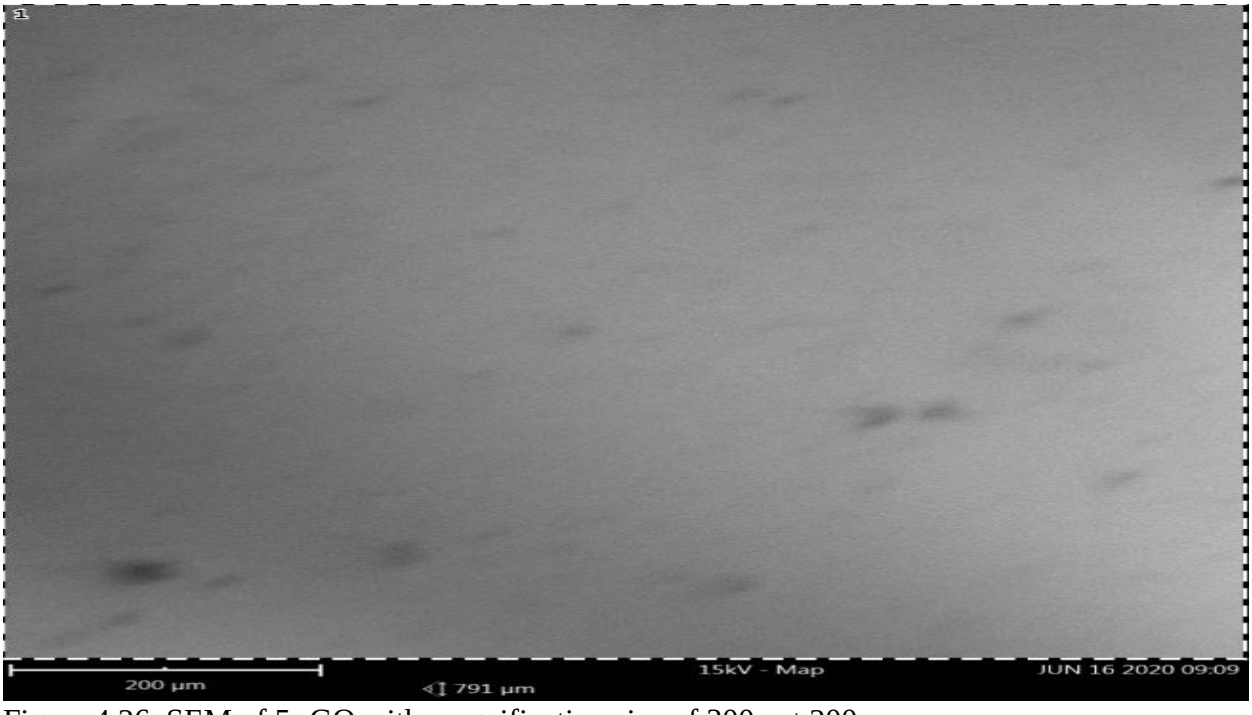

Figure 4.26. SEM of 5 rGO with magnification size of 300x at 200µm

Tab1e 4.13. Composition of 5 rGO

Element Number	Element Symbol	Element Name	Atomic Conc. (%)	wt. %
14	Si	Silicon	57.04	64.63
11	Na	Sodium	25.16	23.34
6	C	Carbon	13.45	6.52
13	Al	Aluminum	2.19	2.39
16	S	Sulfur	0.72	0.93
19	K	Potassium	0.47	0.74
15	P	Phosphorus	0.48	0.60
26	Fe	Iron	0.16	0.35
17	Cl	Chlorine	0.24	0.35
22	Ti	Titanium	0.08	0.16



Figure 4.27. SEM of 6 rGO with magnification size of 300x at 200µm

Tab1e 4.14. Composition of 6 rGO

Element Number	Element Symbol	Element Name	Atomic Conc.(%)	wt. %
14	Si	Silicon	56.06	58.48
11	Na	Sodium	25.80	22.04
20	Ca	Calcium	5.30	7.89
12	Mg	Magnesium	7.35	6.64
13	A1	Aluminum	2.30	2.30
6	C	Carbon	1.71	0.77
19	K	Potassium	0.40	0.58
16	S	Sulfur	0.40	0.48
17	C1	Chlorine	0.34	0.45
15	P	Phosphorus	0.32	0.37

4.3.2 X-Ray Diffractometer

The X-Ray Diffractometer patterns of the rGO obtained were shown in figures 4.28 - 4.29. From [317], graphene is known to show a basal reflection peak at $2\theta = 26.6^{\circ}$ which corresponds to a d-spacing of 0.34 nm. The resu1t of samp1es 5d and 8d shows a better characteristic with the reflection peak at $2\theta = 23.93^{\circ}$ and 24.24° respective1y, corresponding to a d-spacing of 3.72 nm and 3.67 nm as depicted in Figure 4.28 and 4.29 be1ow. The normal sharp and tight peaks of graphene at 2theta 26.5 and 23.88 degrees are conspicuously absent proving the absence of graphene. Also, the 11.6-degree peak of graphene oxide is absent as expected. However, between 26.5 and 23.88, there are some foreign particles that could have caused defects within the reduced graphene oxide materials which have caused the absence of the sharp peak of graphite [317]. There are several peaks corresponding to approximately 24 degrees expected of reduced graphene oxide with an interlayer distance of 3.68A (interlayer distance of graphene is 3.68) [33]. The XRD data is hence sufficient proof of the presence of graphene oxide.

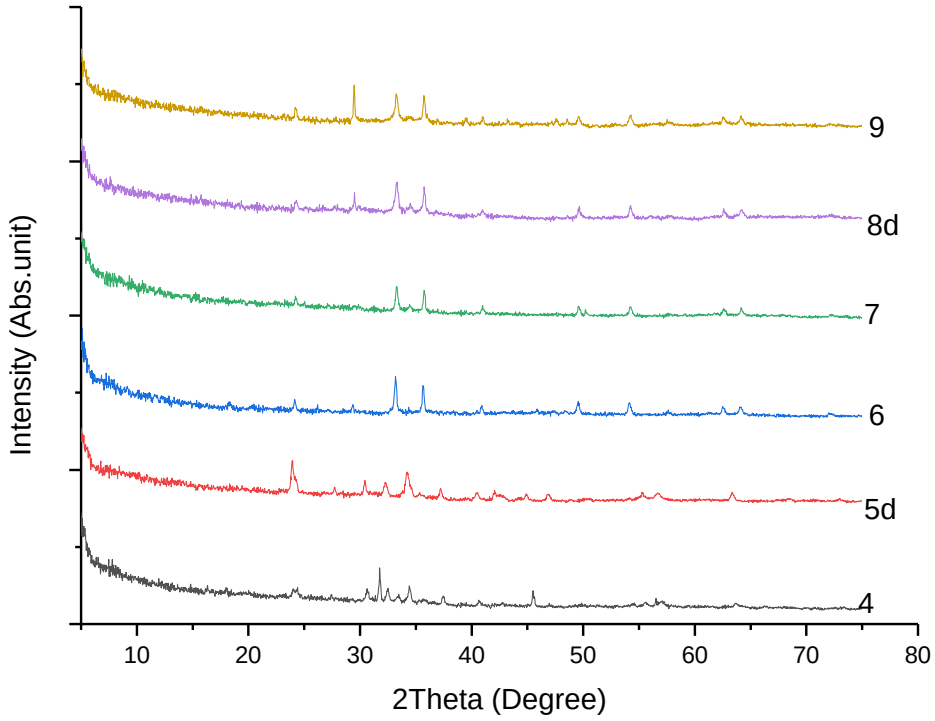

Figure 4.28 Superimposed graph of XRD analysis for sample 1-6 (4, 5d, 6, 7, 8d and 9) rGO

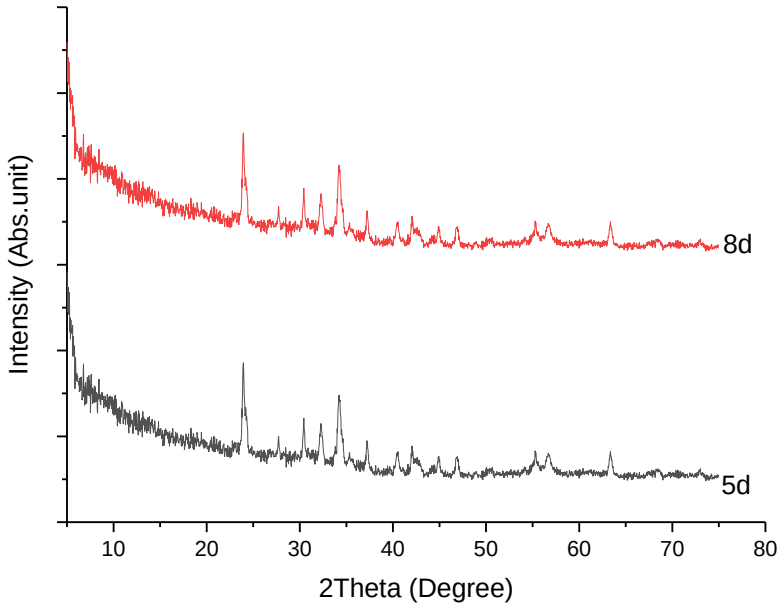

Figure 4.29 Superimposed graph of XRD analysis for samp1es 2 and 5 (5d and 8d) rGO

4.3.3 UV Spectroscopy

Film thickness is one of the fundamental parameters that govern the behavior of some thin film devices. In solar cell devices, the film thickness of the absorber layer is amongst the principal parameters that determine the solar conversion efficiency in that the film thickness must be of a certain magnitude in order to support the contact vo1tage [309, 310]

The wavelengths from Figs. 4.30 to 4.35 are 207, 308, 206, 227, 216 and 206 nm while the absorbance are 5.33, 10.00, 4.184, 4.75, 5.01 and 5.67 respectively. The UV–vis spectrum of the reduced graphene oxide of sample 2 shows a single broad absorption band at 308 nm as displayed in Figure 4.30. Whi1e Samp1e 5 shows an absorption band at 216 nm. This shows a red shift in comparison with UV–vis spectra of graphene oxide which occurs at 230 nm and has been attributed to $\pi \rightarrow \pi^*$ transition of the aromatic C–C bonds. This shift in wavelength is used to monitor the reduction reaction of graphene oxide (GO) to reduced graphene oxide (rGO) [312]. There was no contamination of peaks observed hence it implies that a pure (rGO) was synthesized using the Hummer method. The comparison of absorbance wavelength for the synthesized rGO (2 and 5) shows absorbance within 210-350nm wavelength which is the region where rGO has the capability of absorbing light [313, 314]. This further shows that the incorporation of graphene has the potential of enhancing the visible light absorption. This is because the presence of rGO can affect the optical properties of TiO_2-rGO, through a decrease in bandgap energy and a decrease in charge carrier recombination compared to pure TiO_2, thus increasing light absorbance [311].

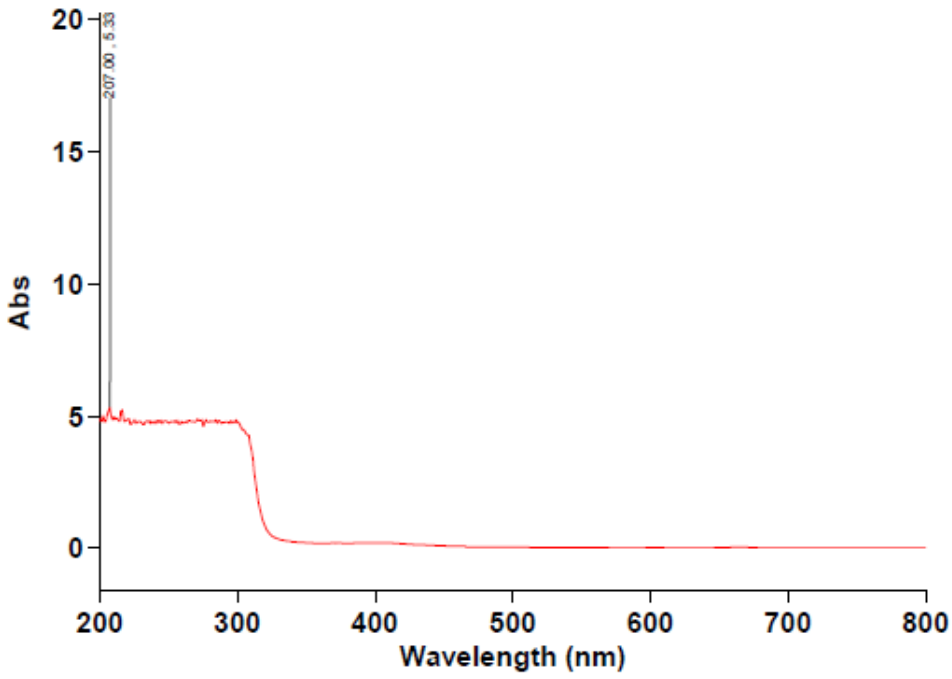

Figure 4.30 Absorbance Spectrum for Sample 1 of Reduced Graphene Oxide

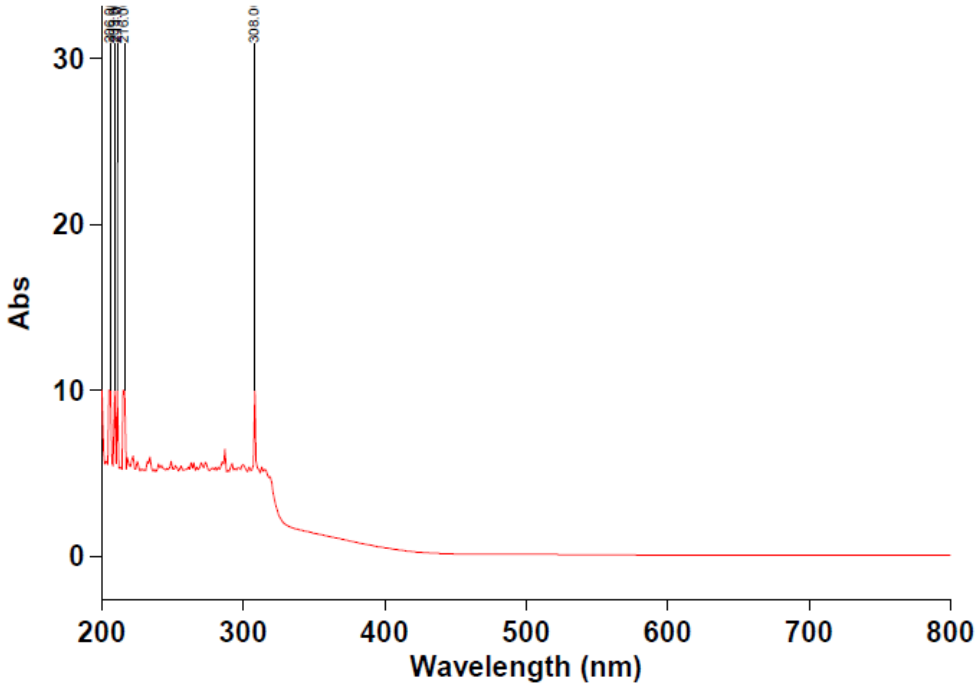

Figure 4.31 Absorbance Spectrum for Sample 2 of Reduced Graphene Oxide

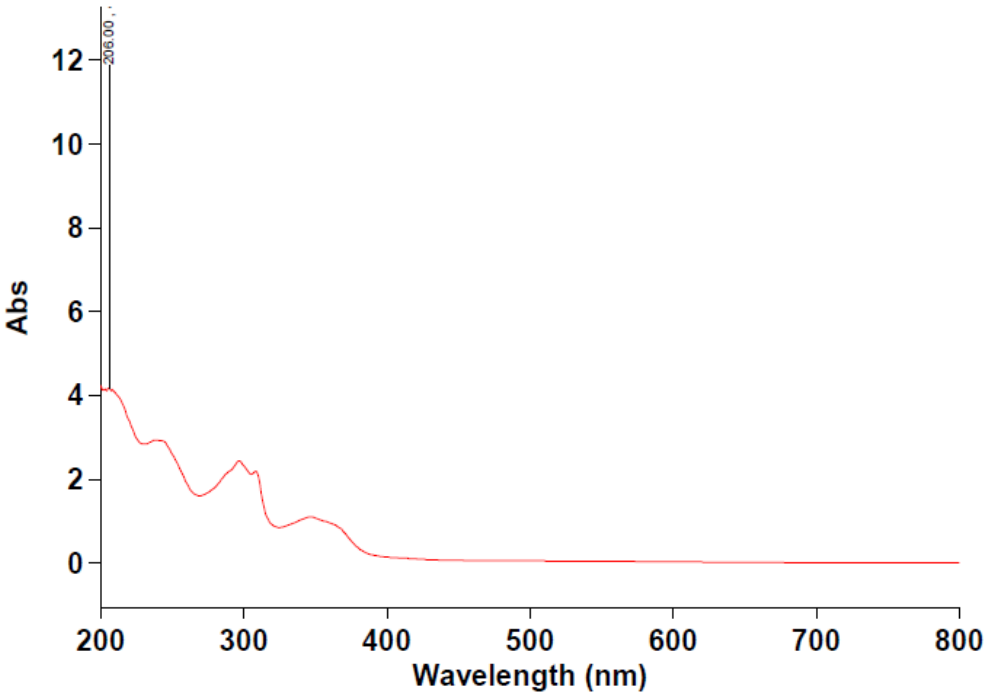

Figure 4.32 Absorbance Spectrum for Sample 3 of Reduced Graphene Oxide

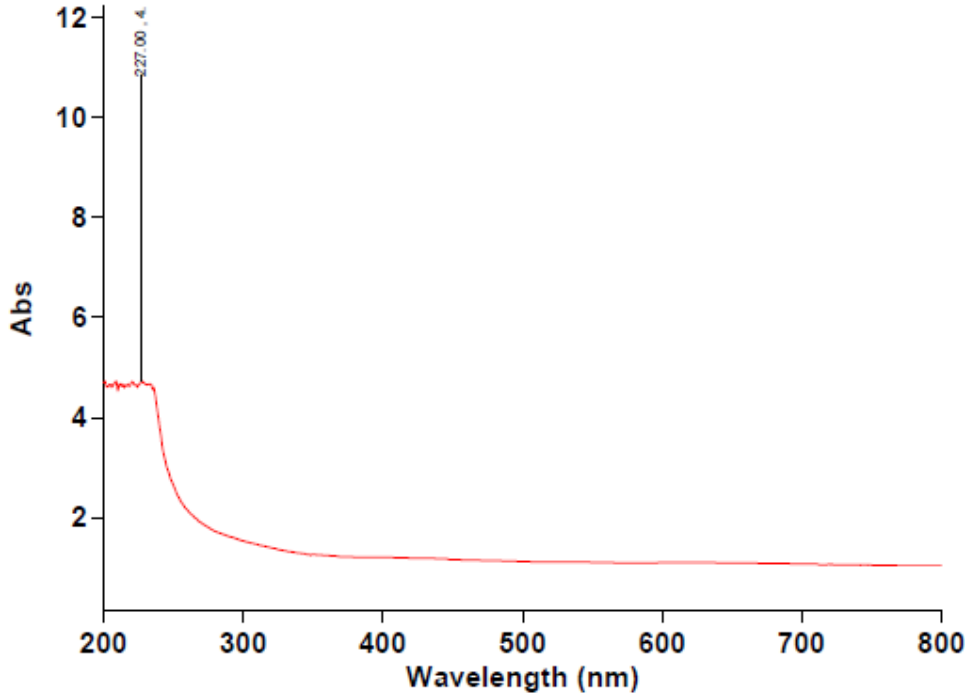

Figure 4.33 Absorbance Spectrum for Sample 4 of Reduced Graphene Oxide

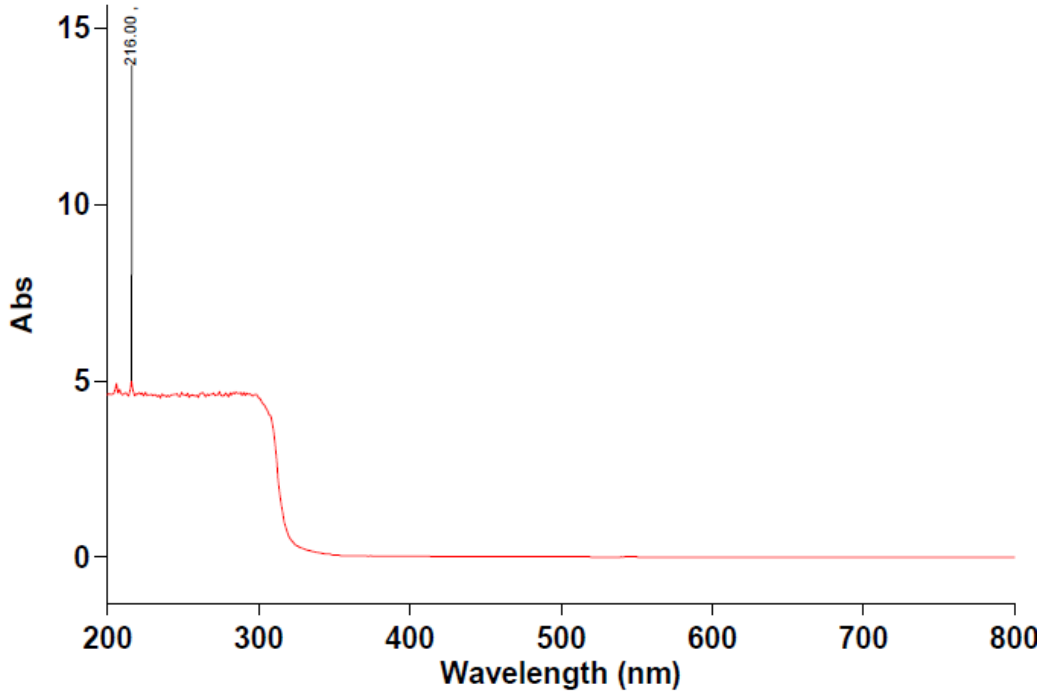

Figure 4.34 Absorbance Spectrum for Sample 5 of Reduced Graphene Oxide

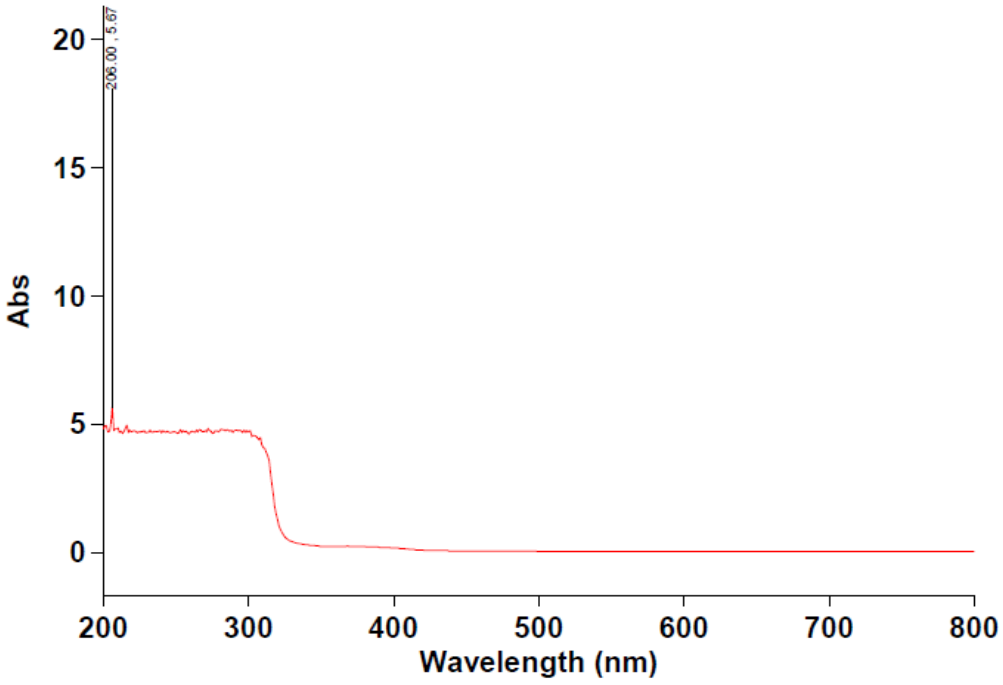

Figure 4.35 Absorbance Spectrum for Sample 6 of Reduced Graphene Oxide

4.4 Proof of how graphene oxide (GO) is converted to reduced graphene oxide (rGO)

The reduction of graphene oxide (GO) to reduced graphene oxide (rGO) typically involves the removal of oxygen-containing functional groups from the graphene structure. This process is often achieved through chemical reduction methods, the most common reducing agents used include hydrazine.

1. **Reaction Equation:**

   The overall reaction can be represented as:

   $$\text{GO} + \text{Hydrazine} \longrightarrow \text{rGO} + \text{Water} + \text{Nitrogen gas} \quad \ldots\ldots\ldots \quad 4.1$$

   This equation represents the reduction of GO (graphene oxide) by hydrazine, which results in the formation rGO (reduced graphene oxide), water and nitrogen gas.

2. **Mechanism:**

   The reduction mechanism involves the following:

   a) Adsorption: Hydrazine molecules adsorb onto the surface of GO.

   b) Chemical Reduction: Hydrazine reacts with the oxygen-containing functional groups on GO, such as epoxides, hydroxyl groups, and carboxyl groups. This results in the removal of oxygen and the restoration of sp^2 carbon – carbon bonds.

   c) Desorption: The reduced graphene oxide (rGO) is formed, and the byproducts, such as water and nitrogen gas, desorb from the surface.

   The reduction process can occur through various intermediate steps, and the exact mechanisms can vary depending on the specific reducing agent and conditions used.

3. **Kinetics:**

   The kinetics of the reduced reaction can be complex and depend on factors like temperature, concentration of reducing agent, and the presence of catalysts. The reaction typically follows pseudo-first-order kinetics, which means that the rate of reduction is primarily dependent on the concentration of the reducing agent. The rate of reduction can be described by a rate equation:

Rate = k [Hydrazine] [GO] ……4.2

Where Rate is the rate of reduction, k is the rate constant, [Hydrazine] is the concentration of hydrazine, and [GO] is the concentration of graphene oxide.

The reduction of graphene oxide (GO) to reduced graphene oxide (rGO) is typically considered irreversible chemical reaction. Once the oxygen-containing functional groups in GO are chemically reduced, the restoration of sp^2 carbon-carbon bonds occurs, and the resulting rGO structure no longer contains the same oxygen groups.

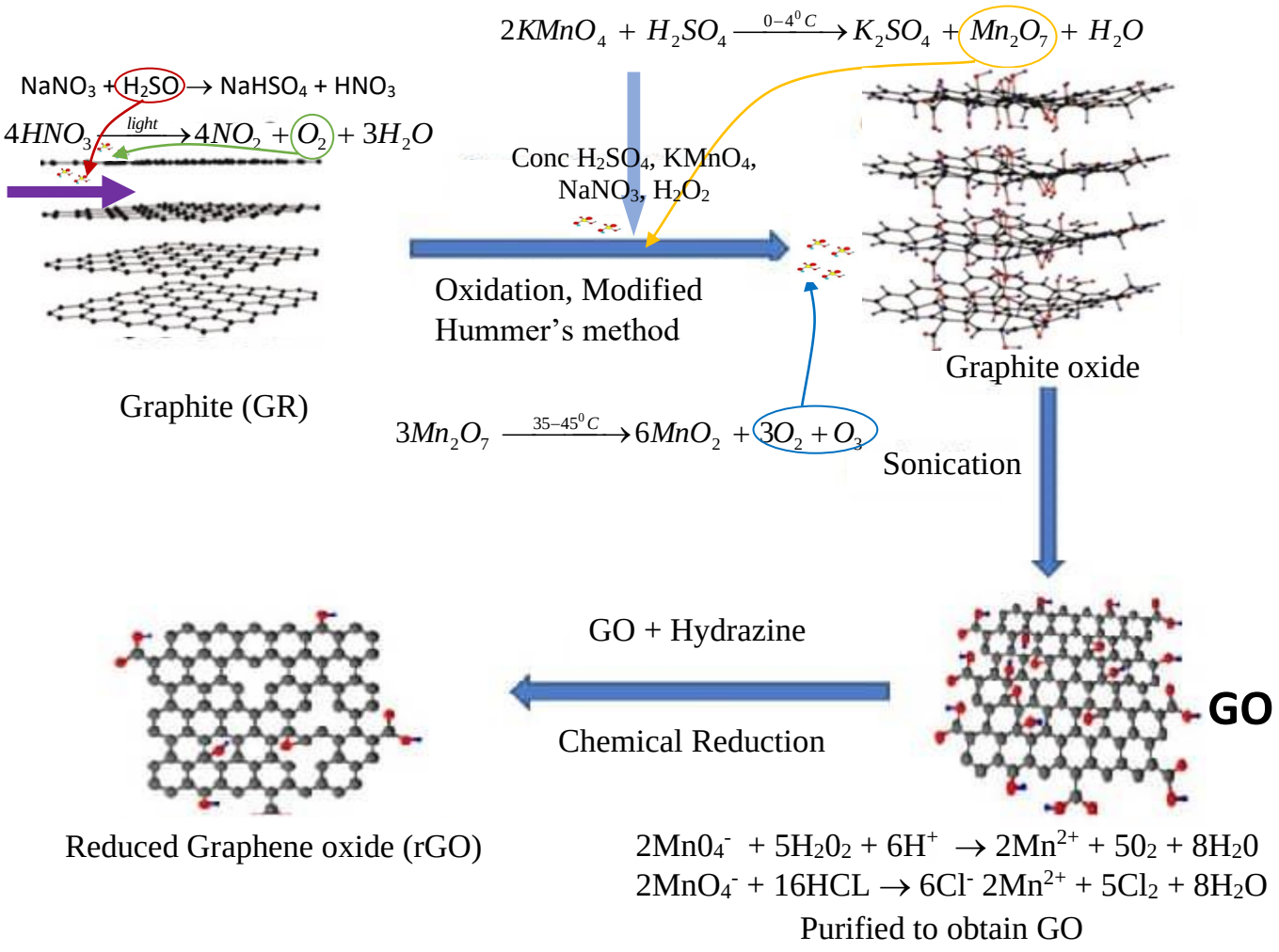

Figure 4.36 Reaction kinetics of graphene oxide reduction to reduced graphene oxide

4.5 Simulation of graphene oxide reduction using hydrazine to reduced graphene oxide

Using the **Mass Actions Kinetics** where the rate is directly proportional to the concentrations of reactants.

For the reaction A + B ⟶ C,

where A = Graphene Oxide, B = Hydrazine and C = Reduce Graphene Oxide:

$$\text{Rate} = k * [A] * [B] \quad \ldots\ldots\ldots\ldots\ldots\ldots\ldots\ldots 4.3$$

Here, "Rate'' is the rate of the reduction reaction, "k" is the rate constant, [A] represent the concentration of the graphene oxide, [B] represent the concentration of the reducing agent hydrazine.

Below are the differential equations for the reaction:

$$\frac{d([A]\cdot V_{compartment})}{dt} = -V_{compartment}\cdot(0.1\cdot[A]\cdot[B]) \quad \ldots\ldots\ldots\ldots 4.4$$

$$\frac{d([B]\cdot V_{compartment})}{dt} = -V_{compartment}\cdot(0.1\cdot[A]\cdot[B]) \quad \ldots\ldots\ldots\ldots 4.5$$

$$\frac{d([C]\cdot V_{compartment})}{dt} = +V_{compartment}\cdot(0.1\cdot[A]\cdot[B]) \quad \ldots\ldots\ldots\ldots 4.6$$

Below is the graph showing how the concentrations evolve over time

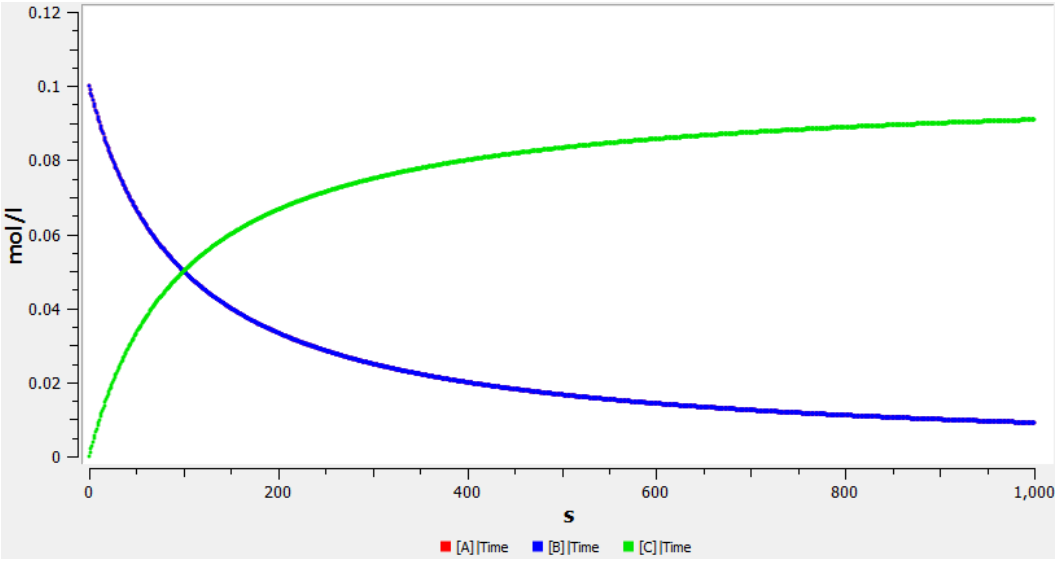

Figure 4.37 Plot of Conc. of Graphene Oxide Reduced with Hydrazine to Reduced Graphene Oxide

The reaction kinetics, mechanism and mathematical model/simulation results shows clearly how graphene oxide was converted to reduced graphene oxide (figure 4.36 to 4.37). In equation 4.4 to 4.6, the negative V signs (- V compartment) shows how the concentration decreased while the positive V sign indicates how the concentration increases over time. From the figure 4.37. A (graphene oxide) and B (Hydrazine) concentration started from 0.1 and ends at 0 while C hub (reduced graphene oxide) started from 0 and increase.

Figure 4.37 was obtained using KinTek software. A software used for simulating complex reaction kinetics. Which was applied to model and simulate the chemical reaction involving graphene oxide reduction. The figure 4.37 was obtained as follows;

- The process started by creating a new model for reaction system
- The chemical species involved (graphene oxide and reduced graphene oxide) was define
- The initial concentrations were entered
- The reactions that represent the conversion of graphene to reduced graphene oxide and any other intermediate steps were specified.
- The chemical equations for the reactions were written (equ. 4.4 to 4.6), and the rate of equations for each reaction (equ. 4.3), which describe how the reaction rates depend on the concentrations of reactants. These rate equations are based on the reaction mechanism and kinetics (figure 4.36).
- The simulation settings were configured, including the simulation time, solver method (e.g., deterministic or stochastic), and any other relevant parameters.
- The time course of the simulation and any data points collected during the simulation were specified, and simulation began.
- After the simulation was completed, the results were analyzed, and KinTek provides various visualization tools to plot concentration profile over time (figure 4.37).

Therefore, the equations 4.4 to 4.6 are set of ordinary differential equations (ODEs) describing the changes in concentrations of species A (graphene oxide), B (Hydrazine), and C (reduced graphene oxide) over time within a compartment with volume V_ compartment. The equations

represent a network where A and B reacted to produce C, and the rate of the reactions is proportional to the concentrations of A and B. The rate constants for the reactions are given as 0.1. To obtain the graph from the simulation using these equations, the differential equations are integrated over time. KinTek provides simulation tools to perform such integrations. This is how the simulation graph was obtained from the equations (4.4 to 4.6). The graph (figure 4.37) represents how the concentrations of the species (graphene oxide) evolve over the course of the simulation. In this simulation, 0.1 mol/l was the initial concentration value of graphene oxide and hydrazine, as the simulation continues, rGO at 0.0 mol/l increases gradually. Other points are gotten from the equations. In summary, the only value entered into the simulation was 0.1 mol/l of GO and Hydrazine

4.6 Concluding remarks

A fast, cost-effective, and highly reproducible methodology of using soft chemicals to fabricate F: SnO_2 nanostructures and their rGO based DSSCs has been presented. Nano composites of F: SnO_2 were well characterized by using XRD, SEM, EDX, and DRS UV-Vis. In comparing the absorbance and transmittance of fluorine-doped tin oxide (F: SnO_2) at 4%, 8%, and 12% with regard to wavelengths (ג) at 230 nm and 1100 nm; the result shows that at 12% (F: SnO_2), the lowest absorbance yields better transmittance, increasing the cell's efficiency by 1.56%. The power conversion efficiency (PCE) of DSSCs demonstrates that DSSCs fabricated with reduced graphene oxide improved cell performance and outdoor stability.

The result shows that fluorine-doped tin oxide can influence the optical and electrical properties of the DSSC, and this finding is in line with [319, 320, 321, 323, and 324]. Also, the reduced graphene oxide showed an increase in hall coefficient and mobility with a decrease in carrier concentration with absorption around the visib1e region. The graphene oxide (GO) was successfully reduced to rGO. This further shows that the incorporation of rGO has the potential to enhance the visible light absorbance.

From the results which show the rate of reduction of GO to rGO is primarily dependent on the concentration of the reducing agent, as the rate of reduction increases with increase in concentration of the reducing agent which in this case is hydrazine.

CHAPTER FIVE: NANOCOMPOSITE OF TiO_2–rGO AS PHOTOANODE FOR DYE SENSITIZED SOLAR CELL

5.0 Introduction

Several studies have been focused on improving the efficiency of Dye sensitized solar cells through the improvement of the various components of the solar cell, while graphene, graphene oxide and reduced graphene oxide have been used for improving most Dye sensitized solar cells [325, 326, 328]. Dye-sensitized solar cells (DSSC) like photosynthesis sensitize dyes, absorb radiant energy and converts it into electricity. They comprise of a photoanode, a cathode, and an electrolyte. In the DSSC, dye imbedded in nanocrystalline semiconductors (TiO_2), electrodes absorb photons from the sunlight, the dye molecules become excited and inject electron in the TiO_2 semiconductor. Graphene oxide is a sing1e layer of carbon atom network and oxygen functional groups, such as epoxides, carboxylic acids, and alcohols, while reduced graphene oxide are single-layered sheets derived from the chemical reduction of graphene oxide (GO). These oxygen functional groups enable GO to exhibit good hydrophilicity, allowing it to disperse well in solvents, especially water. In improving DSSC, graphene has been explored by fusing the graphene material with titanium dioxide to form the photoanode. With this, increase in the efficiency of this solar cell may be achieved as, increase in the dye absorption can result in the increase in the absorption of photons [328]. Other reasons for enhanced performance may include improved porosity of the photoanode and improved charge collection facilitated by intimate contact between the highly conductive graphene materia1 and the TiO_2 [1, 329]

In the last two decades, renewed interests have been geared up for fabrication of rGO-TiO_2 binary semiconductor nano particles. Composite as a photo anode in dye sensitized solar cell rGO-TiO_2 or TiO_2-rGO is the molecu1ar formula for reduced graphene oxide-titanium (iv) oxide. It is a binary semiconduction material which is formed by blending rGO-TiO_2 semiconductor material resulting to a composite which is now termed rGO-TiO_2 [330, 331, 298]. [332] reported that rGO-TiO_2 is generated by stacking a layer of rGO onto mesoporous surface of TiO_2 either through chemica1 bath deposition or hydrothermal process.

Titanium (IV) Oxide – reduced graphene oxide (TiO_2 – rGO) is utilized as a photo anode in dye sensitized solar cell (DSSC) [333, 334]. This is due to its outstanding quality in improving photo energy absorption, ability to increase mobility rate of photo electron and enhance the transport of

photo generated electron [326, 335, 336, 337] in their work discovered that the improved performance of the DSSC is traced to result from the improvement of all the component of the cell. The photo anode of the DSSC comprise of a dye sensitizer layer of semiconductor decorated on a conducting substrate. An ideal photo anode should exhibit high surface area for dye loading, be highly transparent, possess a high electron mobility rate, contain a hydroxyl group or defect site for trapping the photo generated e1ectron-ho1e pair to be separated [338, 339].

However, TiO_2 is only active in the ultraviolet (UV) region of sunlight, which limits the light absorption of the bare TiO_2 crystal to only 3% of the total solar energy output. Hence, deve1oping its band gap into a state capable of permeating into the visible region and thereby enhancing its efficiency of photo catalyst reactions required a1tering the band gap via band gap engineering [340]. In other to improve TiO_2 performance for enhanced light absorption and reducing the electron hole recombination rate demands introduction on TiO_2 crystal structures a suitable high surface area material such as graphene oxide or its partly reduced type [341, 342, 343, 344].

Graphene and its partly reduced type called reduced graphene oxide (rGO) have attracted research interest and have emerged as a vehicle for photo catalytic application and have been regarded as a superior candidate due to their abundance, non-toxic nature, low cost and pronounced electronic properties and absorption ability of solar radiation in the visible region [345, 346]. Inclusively, rGO unique physical, chemical, optical and electric/electronic properties like fractional quantum hall effect at zero kelvin bipolar electric field effect couple with rapid conduction of charge carrier, alterable band gap and statistic feature have led to its recommendation as a way out to the draw back and constraint inherent in bare TiO_2 semiconductor material [347, 348, 349].The synergic integration of rGO on TiO_2 resu1ts in separation of photo generated charge carrier thereby extending the lifetime of the excited state in the system and allow TiO_2 based hetero junction photo catalyst make use of the visible region of the solar spectrum [298, 350].

Reported results gotten from absorption spectroscopy measurement revea1ed that transfer of photo excited electron from rGO occur faster than charges recombination. Also, the recombination of photo excited electron hole pair in the composite material is slower and suppressed than that in TiO2 alone [351, 352]. Integrating rGO on TiO_2 orchestrated the amazing

electronic, chemical, optical and conductivity properties on the TiO_2, mesoporous surface. Computational studies further showed that both the type and the concentration of the functional groups strongly affect the band gaps and the work function of the composite [353, 354].

Against this background, this study reports the synthesis of reduced grapheme oxide -TiO2 composite as a photo anode and its application in DSSC to increase the efficiency and performance of dye sensitized solar cell. Thus, to investigate the effect of rGO-TiO_2 on the sensitizer (dye) in view to determining the effect of grapheme (rGO) on the recombination of the injected electrons, and the effect of grapheme (rGO) on the light scattering of the photoanode (TiO_2 film) were achieved.

5.1 Results and Discussion

Table 5.1: Result of Hall Effect measurements for the fabricated TiO_2 –rGO nanocomposites

Optica1 Properties	**1 Cyc1e**	**2 Cyc1e**	**3 Cyc1e**	**4 Cyc1e**
Bu1k\ Concentration cm-3	-1.42 x 10^{11}	-2.71 x 10^{11}	-2.48 x 10^{11}	-2.16 x 10^{13}
Mobi1ity cm2/Vs	9.31 x 10^{2}	8.78 x 10^{2}	4.95 x 10^{2}	4.10 x 10^{3}
Sheet- Resistance Ω/□	2.78 x 10^{8}	1.31 x 10^{8}	2.83 x 10^{3}	3.35 x 10^{6}
Resistivity Ωcm	4.73 x 10^{8}	2.62 x 10^{4}	5.10 x 10^{3}	7.04 x 10^{5}
Conductivity 1/Ωcm	2.11 x 10-5	3.81 x 10^{-5}	1.96 x 10^{-4}	1.42 x 10^{-3}
A-C Cross Ha11 Coefficient cm3/C	2.40 x 10^{8}	2.54 x 10^{8}	-4.22 x 10^{7}	1.83 x 10^{6}
Magneto- Resistance Ω	1.62 x 10^{8}	2.39 x 10^{8}	3.44 x 10^{7}	6.69 x 10^{6}
Average Ha11 Coefficient cm3/C	-4.40 x 10^{7}	-2.30 x 10^{7}	-2.52 x 10^{7}	-2.89 x 10^{5}
B-D Cross Ha11 Coefficient cm3/C	-3.61 x 10^{8}	-3.00 x 10^{8}	-8.20 x 10^{6}	-2.41 x 10^{6}
Ratio of Vertica1/Horizonta1	6.29 x 10^{-1}	-3.59x 10^{-1}	5.75 x 10^{-2}	5.07 x10^{-1}
Sheet Concentration cm-3	-2.41 x 10^{7}	-5.42 x 10^{7}	-4.46 x 10^{7}	-4.54 x10^{9}

Hall effect measurement carried out on the produced film with varying film thickness showed than increase in film thickness increased the average hall coefficient as seen with cyc1e 4 (-2.885 x 105 cm3/C) in Table 5.1. The increased film thickness increased the hall coefficient and mobility with a decrease in carrier concentration. RGO has attracted application in DSSC because it possesses high electron mobility. Incorporation of rGO in TiO_2 film can form a

heterojunction at its interface and induce an internal electric field that separates the electron-hole pairs from the charge recombination. Research has it that rGO -TiO_2 gives better electron mobility leading to improved electron transport and dye absorption properties [355]. However, some researchers have reported incorporating a high fraction of the reduced graphene oxide is not a good choice for photoanode application as a result of reduced dye anchoring. This is because the dye sensitizer can anchor efficiently on the TiO_2 surface rather than the rGO sheets. According to the results in (Table 5.1) above, the presence of graphene increased the mobility, which is expected to increase the electron transfer and power conversion efficiency of the DSSC. Also, the results are shown to be positive if the number of positive charges are more than the negative charges. The negative sign in A-C Cross Hall Coefficient is an indication of a defect present in sample 3 (3 cycle), it is insignificant. The negative sign in the ratio of vertical and horizontal in sample 2 shows there is a shift in size and crystallinity of the sample. It is also insignificant

Profilometry study revealed grain development and dispersion with some spherical rod-like structure that was partially agglomerated. According to the findings, the film is smooth with minor layer surface roughness.

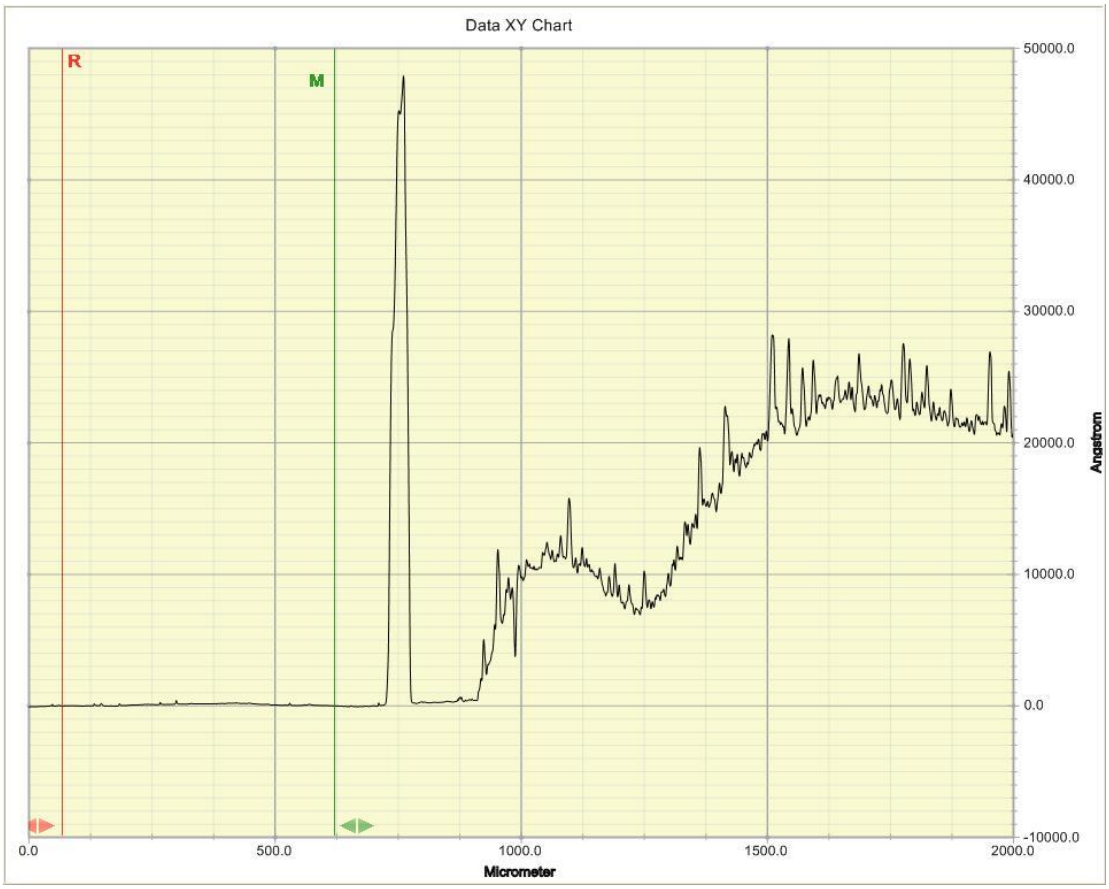

Figure 5.1: Profile graph for TiO_2 –rGO nanocomposites

UV−vis diffusive reflectance spectroscopy (DRS) is a powerful tool to investigate the light absorption phenomenon arising due to strong interactions between TiO_2 band and rGO nano sheets. The Diffuse Reflectance-Ultraviolet visible spectroscopy characterization of the reduced graphene showed highest absorbance value at 202.2nm. The UV–vis spectrum of the reduced graphene oxide shows a sing1e broad absorption band at 202.2 nm as displayed in Figure 5.2. The reflectance was 3.55 at 1086 nm, while the transmittance was 39%. The red shift is displayed with UV–vis spectra of the reduced graphene oxide is been attributed to $\pi \rightarrow \pi^*$ transition of the aromatic C–C bonds [356]. This shift in wavelength has been used to monitor the reduction reaction of graphene oxide (GO) to reduced graphene oxide.

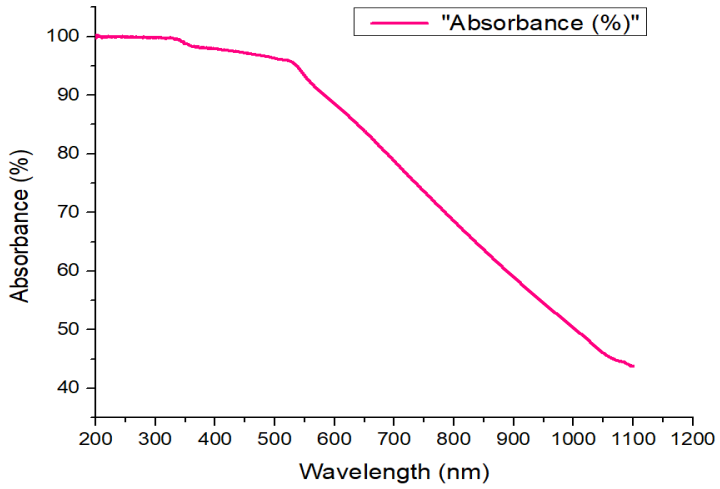

Figure 5.2: UV-Vis spectra showing Absorbance against Wavelength for TiO_2 –rGO

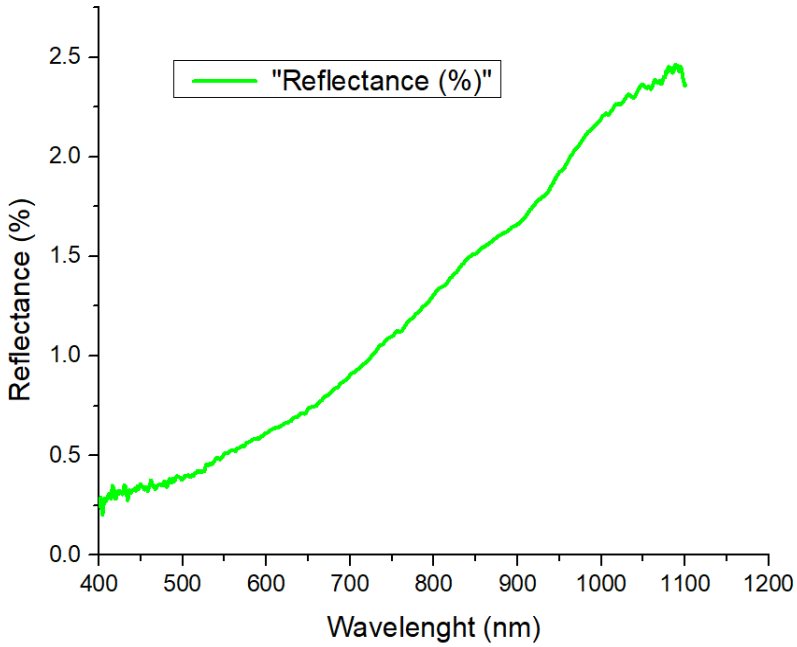

Figure 5.3: UV-VIS spectra showing Reflectance against Wavelength for TiO_2 –rGO

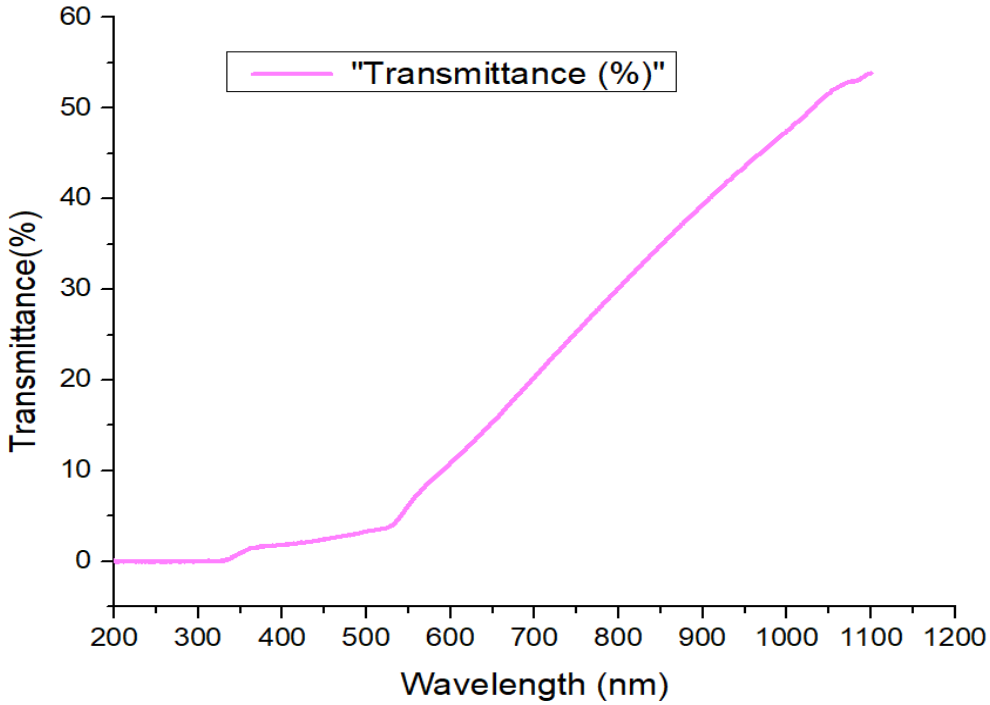

Figure 5.4: UV-Vis spectra showing Transmittance versus Wavelength for TiO_2 –rGO

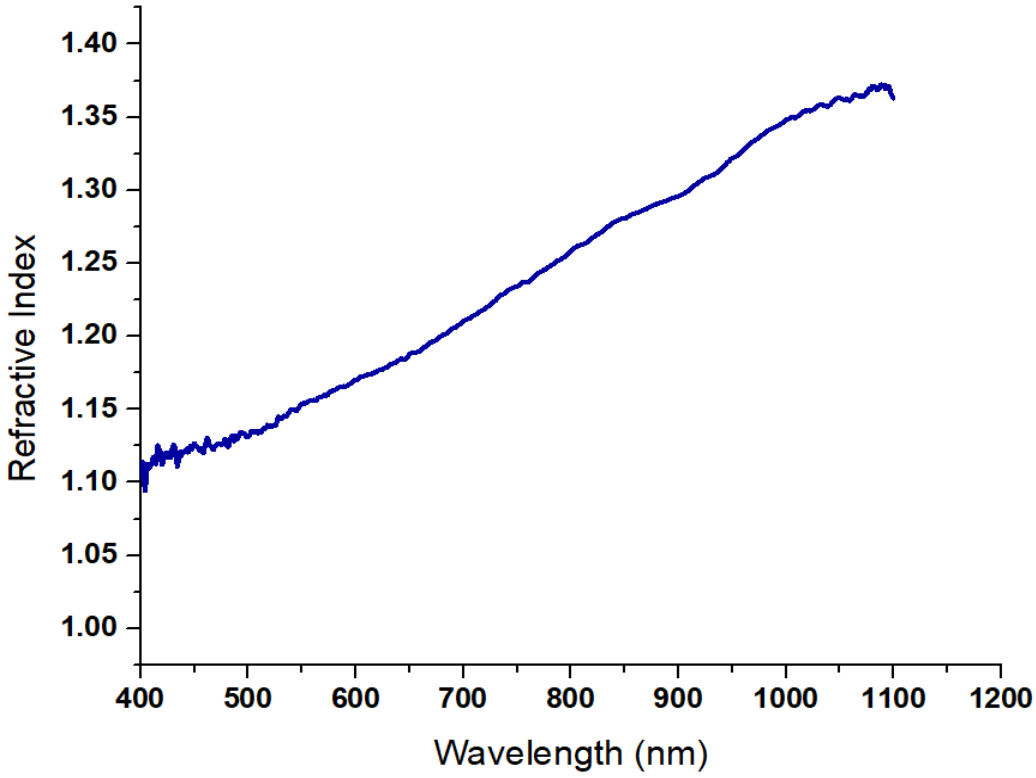

Figure 5.5: UV-Vis spectra showing Refractive index against Wavelength for TiO_2 –rGO

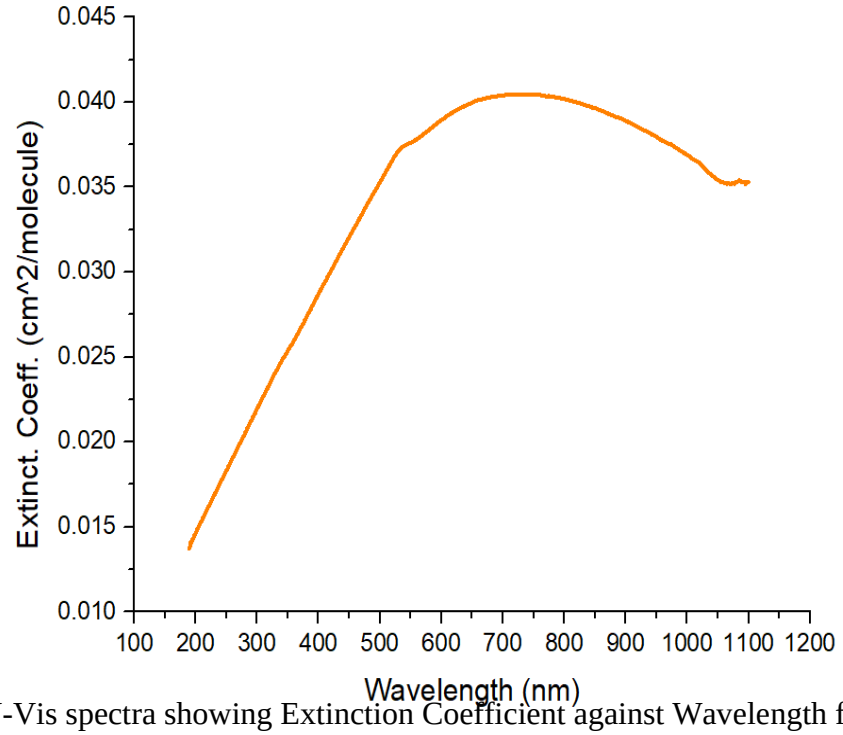

Figure 5.6: UV-Vis spectra showing Extinction Coefficient against Wavelength for TiO_2 –rGO

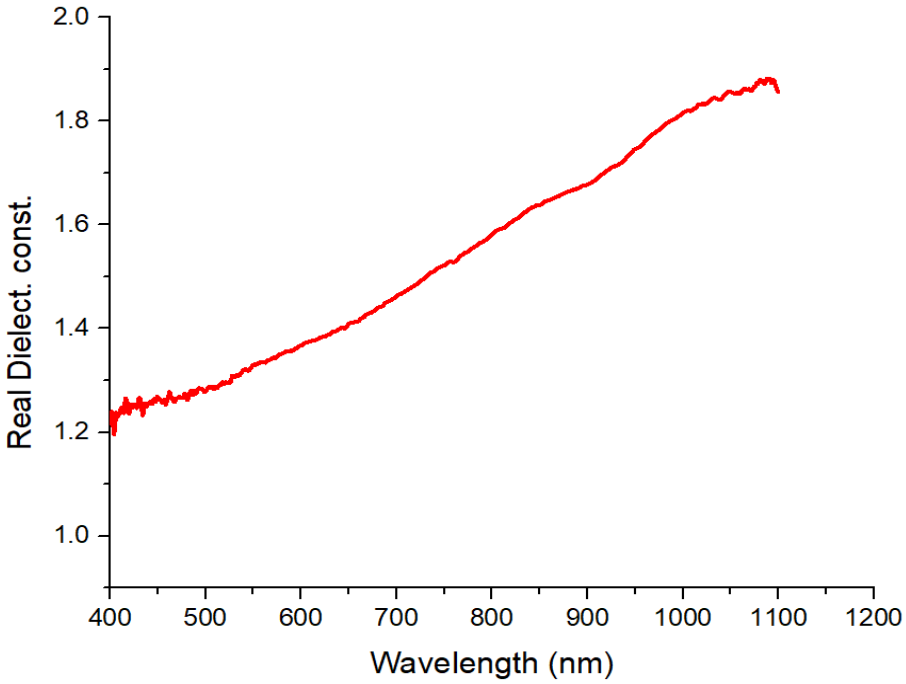

Figure 5.7: UV-Vis spectra showing Real Dielectric Constant against Wavelength for TiO_2 –rGO

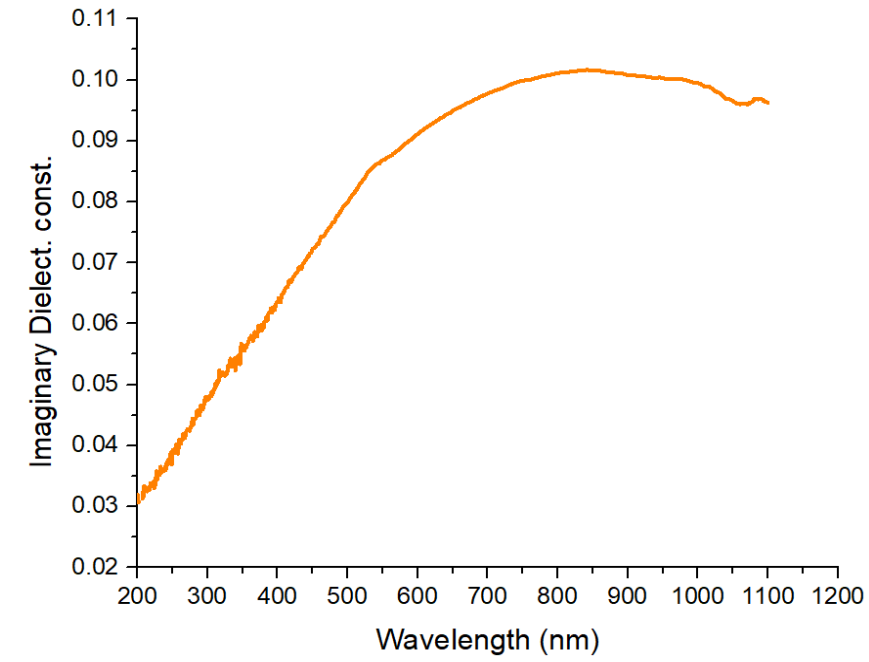

Figure 5.8: UV-Vis spectra showing Imaginary Dielectric Constant against Wavelength for TiO_2 –rGO

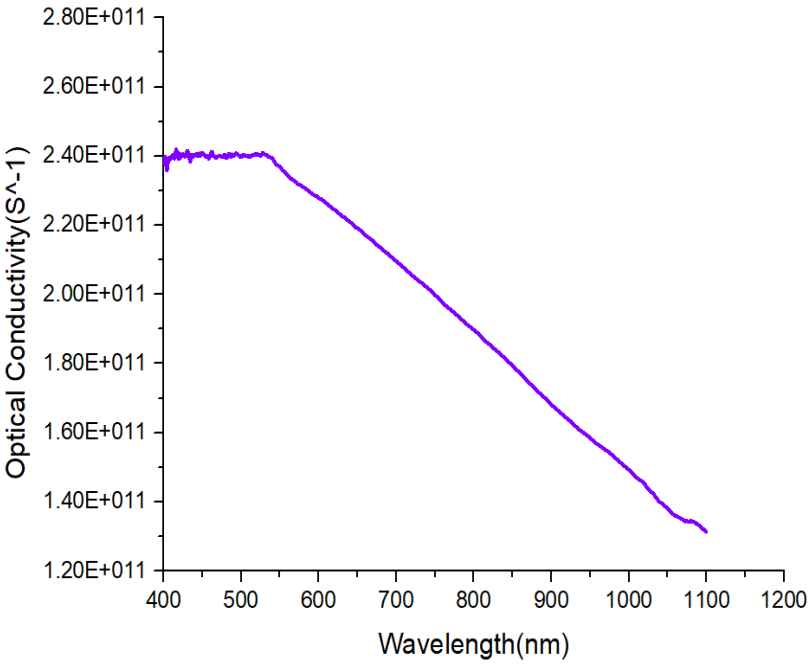

Figure 5.9: UV-Vis spectra showing Optical Conductivity against Wavelength for TiO_2 –rGO

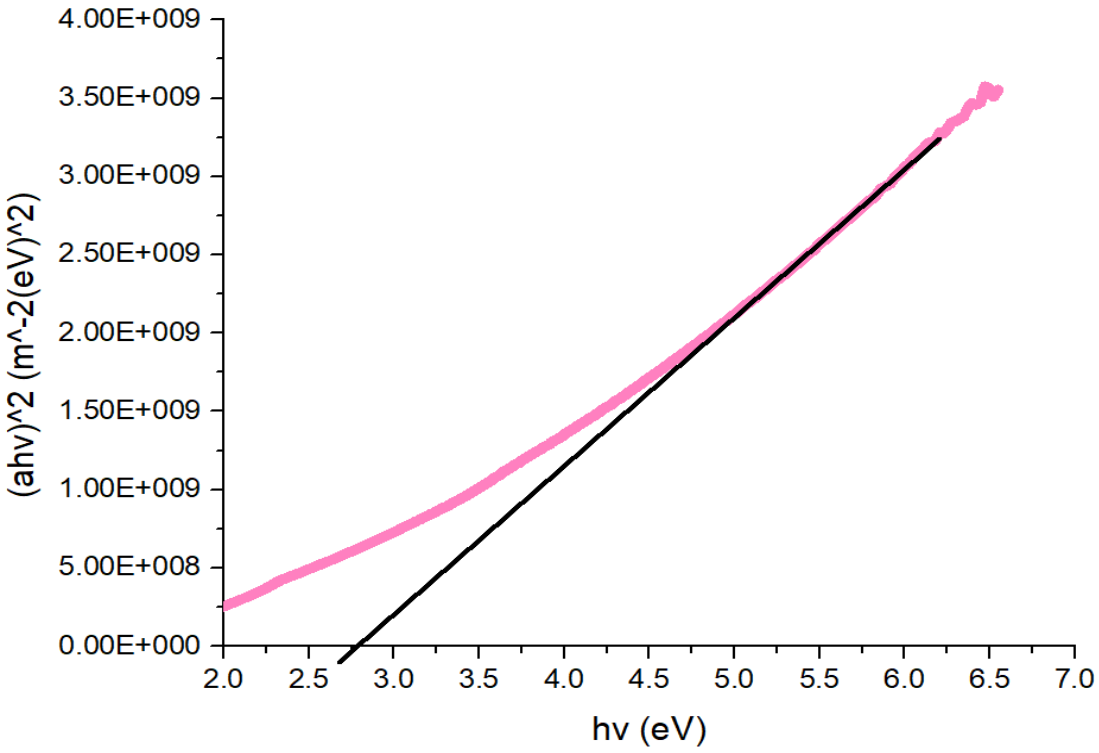

Figure 5.10: UV-Vis spectra showing **$(\alpha h\nu)^2$ Against Photon Energy ($h\nu$)** for TiO_2 – rGO

From figure 5.2, within the UV – region, absorbance is very high. At 200 nm, absorbance is 99.7 % up to 330 nm which reduces to 95.95 % at 400 nm. In the visible region, absorbance reduced from 97.95 % at 400 nm to 95.80 % at 525 nm and then to 68.40 % at 800 nm. At Near Infrared (NIR), the absorbances from 68.40 % at 800 nm to 44 % at 1100 nm. Generally, there was very high absorbance in the UV – region and to around 525 nm in the Vis – region before decreasing sharply to 44 % in the NIR – region. Due to the high absorbance of the material in the UV – region, it can be applied as absorbing layer in solar cell application.

From figure 5.3, no reflectance was observed within the UV – region. General increase was observed, though, very low, with reflectance of 0.27 % at 400 nm to 1.31 % at 800 nm in the visible region. In the NIR, the reflectance further from 1.31 % at 800 nm to 2.46 % at 1090 nm. With this material exhibiting high absorbance, low transmittance and very low reflectance in the UV – Vis regions, such material can be very useful as absorbing layers in solar cell applications and UV sensors.

From figure 5.4, no reflectance was observed within the UV- region. General increase was observed, thou, very low, with Reflectance of 0.27% at 400nm to 1.31% at 800nm in the visible

region .in the NIR, the reflectance further from 1.31 % at 800 nm to 2.46 % at 1090 nm. With this material exhibiting high absorbance, low transmittance and very low reflectance in the UV – Vis regions, such material can be very useful as absorbing layers in solar cell applications and UV sensors.

From figure 5.5 The refractive index of the material increased steadily within the visible region from around 1.12 at 400 nm to 1.22 at 800 nm. In the NIR. The increment continued from 1.22 at 800 nm to 1.37 around 1090 nm. On the whole, there was a gradual increase in the refractive index of the material.

From figure 5.6, it can be seen that the Extinction Coefficient increased sharply at about 200 nm wavelength to about 500 nm Wavelength before gradually climaxing at around 700 nm wavelength. From this point, at a value of about 0.040, it decreases steadily in the visible region into the NIR region to a value of about 0.034 around 1090 nm Wavelength.

From figure 5.7 the Real Dielectric Constant of the thin film increased from 1.22 at 400 nm to 1.52 at 800 nm in the visible region. In the NIR region, it further increased from 1.52 at 800 nm to around 1.84 at 1080 nm Wavelength.

From figure 5.8, the value of Imaginary dielectric constant increased from 0.03 at 200 nm wavelength to 0.055 at 400 nm in the UV region. It increased further from 0.055 at 400 nm to around 0.103 at 800 nm in the visible region before decreasing to 0.096 in the Near Infra- Red region.

From figure 5.9, it can be observed from the graph that from Wavelength of 400nm to 550nm the optical conductivity was constant with value at2.40E+011. At this point, it decreases steadily through the remaining part of visible Wavelength into Near Infra-red region to below 1.40E+011 at 1100nm Wavelength.

From figure 5.10, the direct band gap energy was obtained by extrapolating the straight portion of the graphs to the axis of photon energy ($h\nu$) where $(\alpha h\nu)^2 = 0$. The Band gap is found to be 2.75. This wide Band gap exhibited by the thin film indicates that it is a good material for solar cell applications.

The UV-Vis optical absorption data shows that the value of band gap energy decreased from 3.6eV to 1.4eV with increase in quantity of dopant. This reduction might be attributed to electron or hole trappy at the donor and acceptor level in the TiO_2- – rGO band structure. The visible light absorption is facilitated or increased due to the reduced recombination of photogenerated charge carrier and high specific surface area.

The results obtained suggests that there is a strong interaction between the TiO_2 and the rGO which could result in improved visible light absorption and certainly boost the light harvesting performance when used in the dye sensitized solar cell [357]. The optical band gap energy studied showed that the band-gap values of the sample reduced significantly with the presence rGO content, enhancing the interaction between TiO_2 and rGO nano sheets. It was also reported by researchers that the bond formation between TiO2 and rGO via a Ti−O−C or O−Ti−C linkage is highly responsible for reduction of band-gap energy, inhibiting recombination. [358]. This result also confirms the successful formation of TiO_2 –rGO nanocomposites.

The characteristics of the Dye-sensitized solar cell fabricated with roselle dye which is an extract of hibiscus sabdariffa with and without graphene is shown in (Table 5.2 and 5.3) below. The simulation results for the cell parameters obtained for the DSSC with reduced graphene oxide were; open circuit vo1tage (0.53V), short circuit photocurrent (0.11mA/cm^2), fill factor (0.02) and photoelectric conversion efficiency (11.52 %); while the results obtained for the DSSC without reduced graphene oxide were; open circuit voltage (0.56V), short circuit photocurrent (0.63mA/cm2), fill factor (0.03) and photoelectric conversion efficiency (4.70 %). The performance of the dyed cell with reduced graphene oxide showed a higher power conversion efficiency compared to the cell without graphene. Thus, showed an impressive out-door photovoltaic behaviour.

Tab1e 5.2: Summarized I-V measurements for simulation of dye sensitized solar cell with and without reduced graphene oxide

Fabricated DSSC	**Voc (v)**	**Jsc mA/cm^2**	**Pmax (w)**	**FF**	**η (%)**
With rGO	0.5390	0.119	0.0018	0.0243	11.52
Without rGO	0.5690	0.064	0.0013	0.0318	4.70

Tab1e 5.3: Results of I-V measurements for stability test of reduced graphene oxide synthesized DSSC

Time (hrs)	**Voc (v)**	**Jsc mA/cm^2**	**Pmax (w)**	**FF**	**η (%)**
72	0.497	0.1265	0.0019	0.0274	11.90
144	0.498	0.1165	0.0019	0.0291	11.02
216	0.497	0.1092	0.0019	0.0315	10.30
288	0.497	0.1048	0.0019	0.0242	9.90
360	0.496	0.0962	0.0018	0.0318	8.60
422	0.498	0.0852	0.0016	0.0326	6.80
504	0.496	0.0795	0.0015	0.0339	5.90
576	0.498	0.0771	0.0015	0.0332	5.80
648	0.497	0.0651	0.0006	0.0129	1.92

The presence of the rGO layer of 0.15 wt.% in the TiO_2 layer led to a better power conversion efficiency because of the TiO_2-rGO sandwich structure, the efficiency of DSSCs was improved. The enhanced performance of DSSCs with the sandwich structure can be attributed to an increase in electron transport efficiency and in the absorption of light in the visib1e range. The resu1ts obtained suggest that the recombination rate of electron–hole charge carriers can be effectively inhibited as a result of the reduced graphene oxide (rGO) in the composite and also

increase the rate of electron transfer in the DSSC operation. The presence of rGO in the TiO_2 increased the e1ectron transport efficiency, and this resu1ted in increase in the DSSC performance. This study shows that the incorporation of reduced graphene oxide has the potential of enhancing the absorption because the presence of rGO can affects the optical properties of TiO_2-rGO, through a decrease in band gap energy and a decrease in charge carrier recombination compared to pure TiO_2, thus increasing light absorbance [350]. The size of TiO_2 was reduced by the introduction of rGO that is electron rich material/surface where the electron attraction between Ti4+ and the rGO surface resulted to reduction in the size of TiO_2 [359]. The addition of rGO greatly increase the porosity of the active area for the roselle dye attachment [359]. Similarly, the active surface area of TiO_2-rGO is larger than pure anatase TiO_2 to activate the photocatalysis response from illumination, and this correspond to [360]. This study also shown that the inclusion of reduced graphene oxide in the nano composite decreased/eliminated the problem of recombination by functioning as electron acceptors. The results obtained agreed with the report by [361, 362, 363, 364, 366]. This resulted in an improved performance of DSSC combined with reduced graphene oxide utilizing a natural dye. In summary, the composite DSSC had a Voc of 0.50 V, a fill factor (FF) of 0.02, and a computed efficiency of 11.52%, which was greater than standard DSSC. The result also was in agreement with reports by (370, 371)

The electrolyte degradation within the period of four weeks were investigated by I-V measurements using a solar simulator under A.M. 1.5 ($100mw/cm^2$). The results for the long-term stability test (S) carried out is shown in Figures 5.11-5.15. The value for the short circuit current gradually decreased by 39 % of its initial value of 0.13 mA/cm^2 after the first 24 days. The value for efficiency was stab1e for the first 12 days then gradually decreased to 24 % of its initial value under white light irradiation after the first 24 days. The results for the stability test under white light irradiation showed a stable power conversion efficiency for the first 12 days. This was followed by a slight decrease, which was about 93% of its initial value after the first 12 days. This shows that DSSC fabricated with graphene is stable under white light irradiation. However, the cell exhibited a poorer photovoltaic behavior on the fourth week. The poor photovoltaic performance of the roselle-dyed cell under out-door operation can be clearly observed in Figure 5.12.

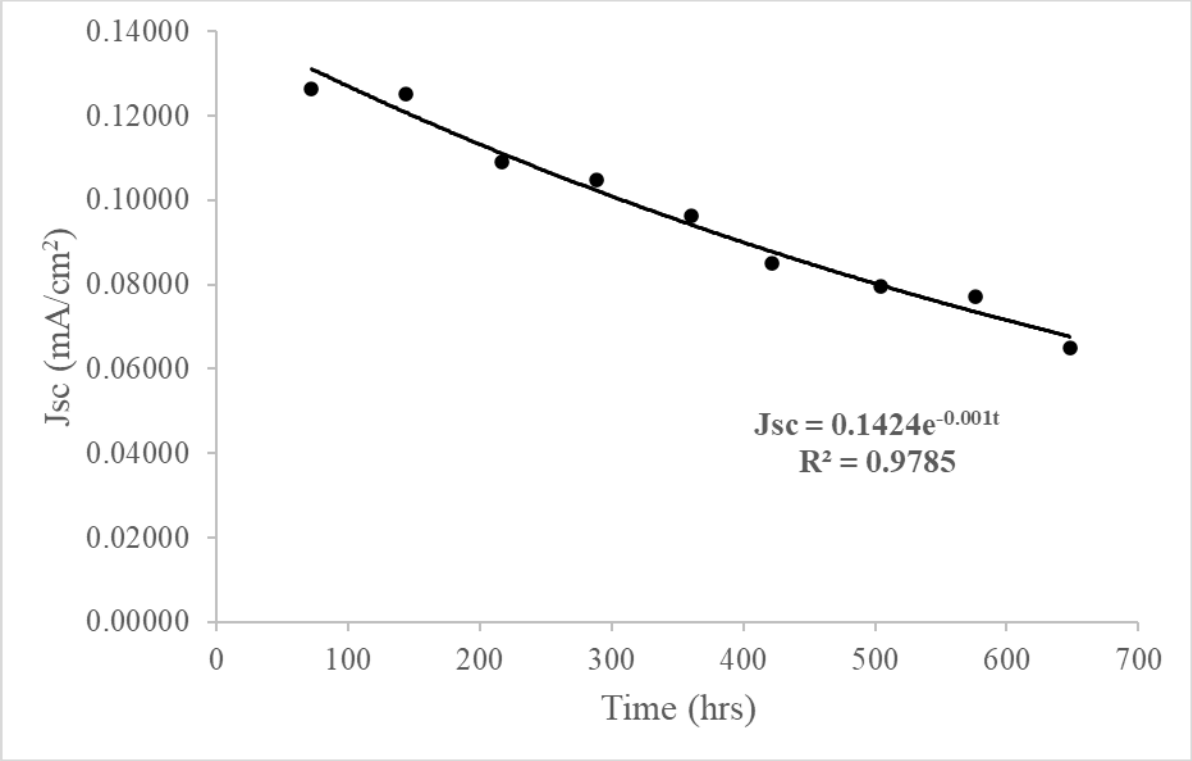

Figure 5.11: Graph of goodness of fit for Current density of DSSC Performance

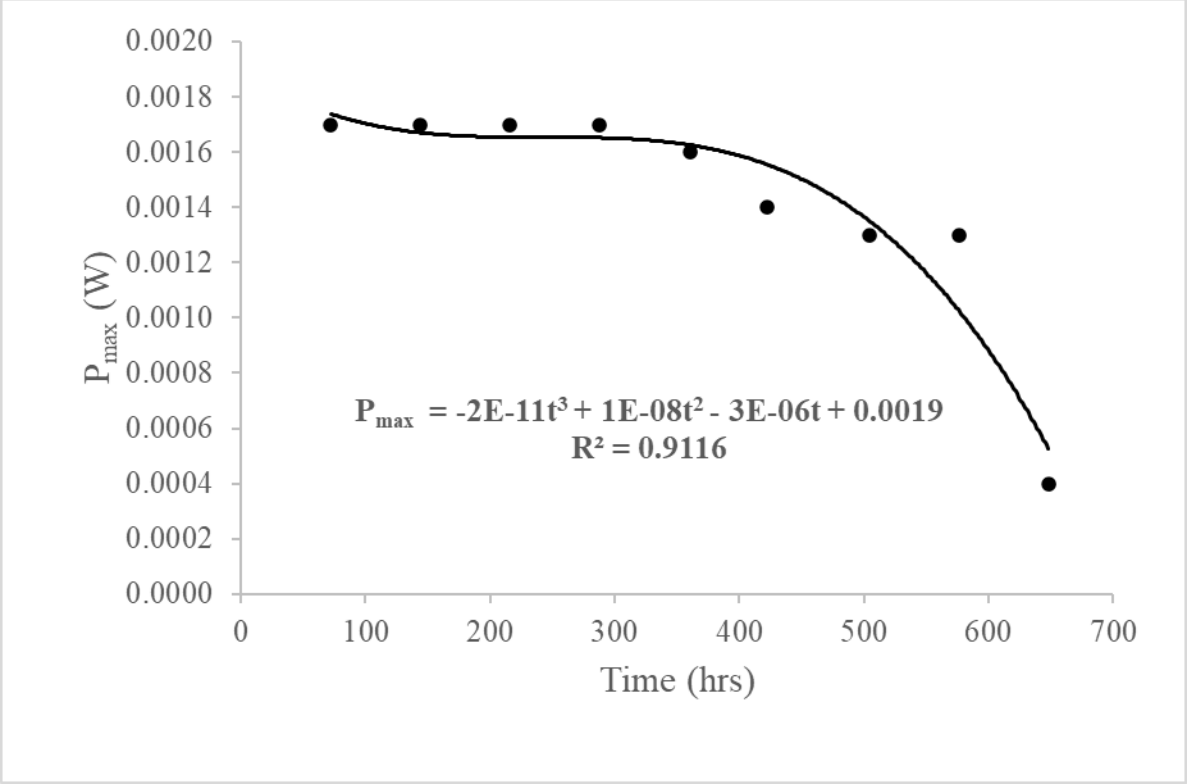

Figure 5.12: Graph of goodness of fit for Maximum Power (Pmax) output of DSSC

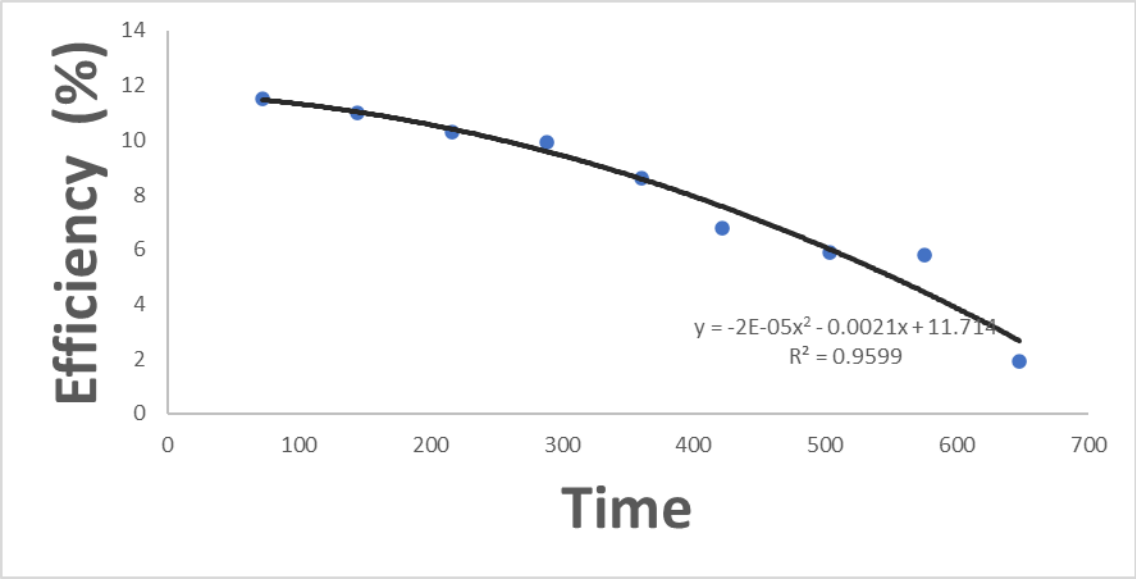

Figure 5.13: Graph of goodness of fit for Power conversion efficiency (PCE) of DSSC

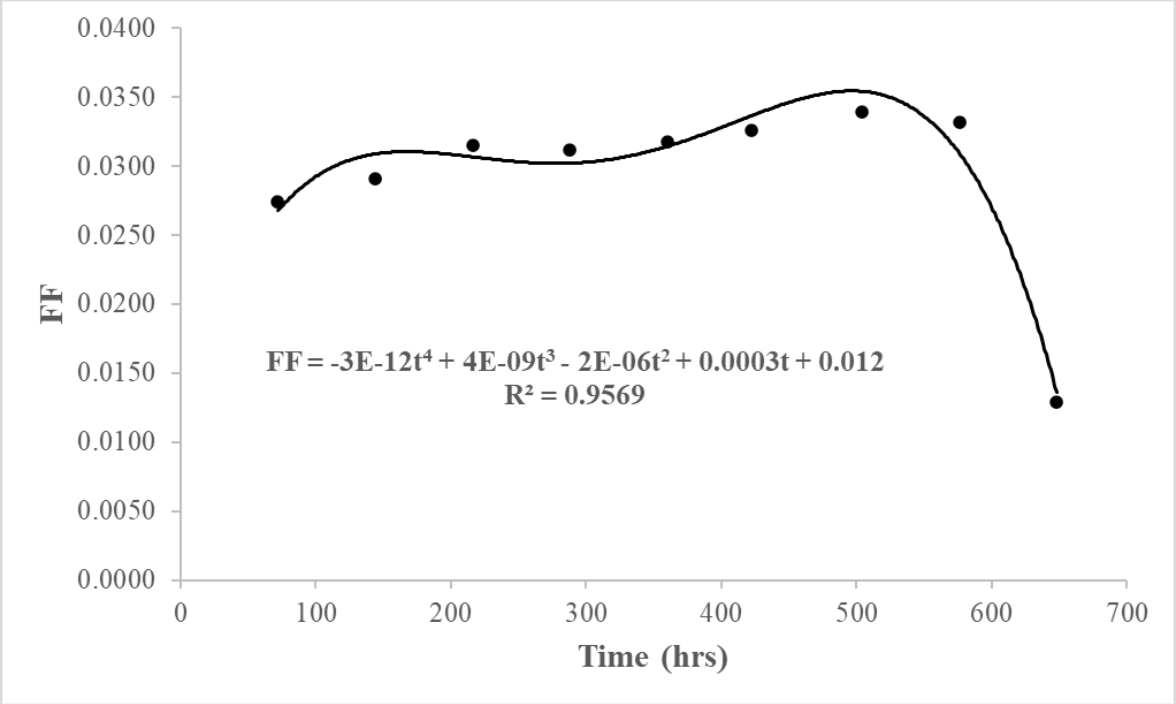

Figure 5.14: Graph of goodness of fit for Fill- Factor (FF) of DSSC

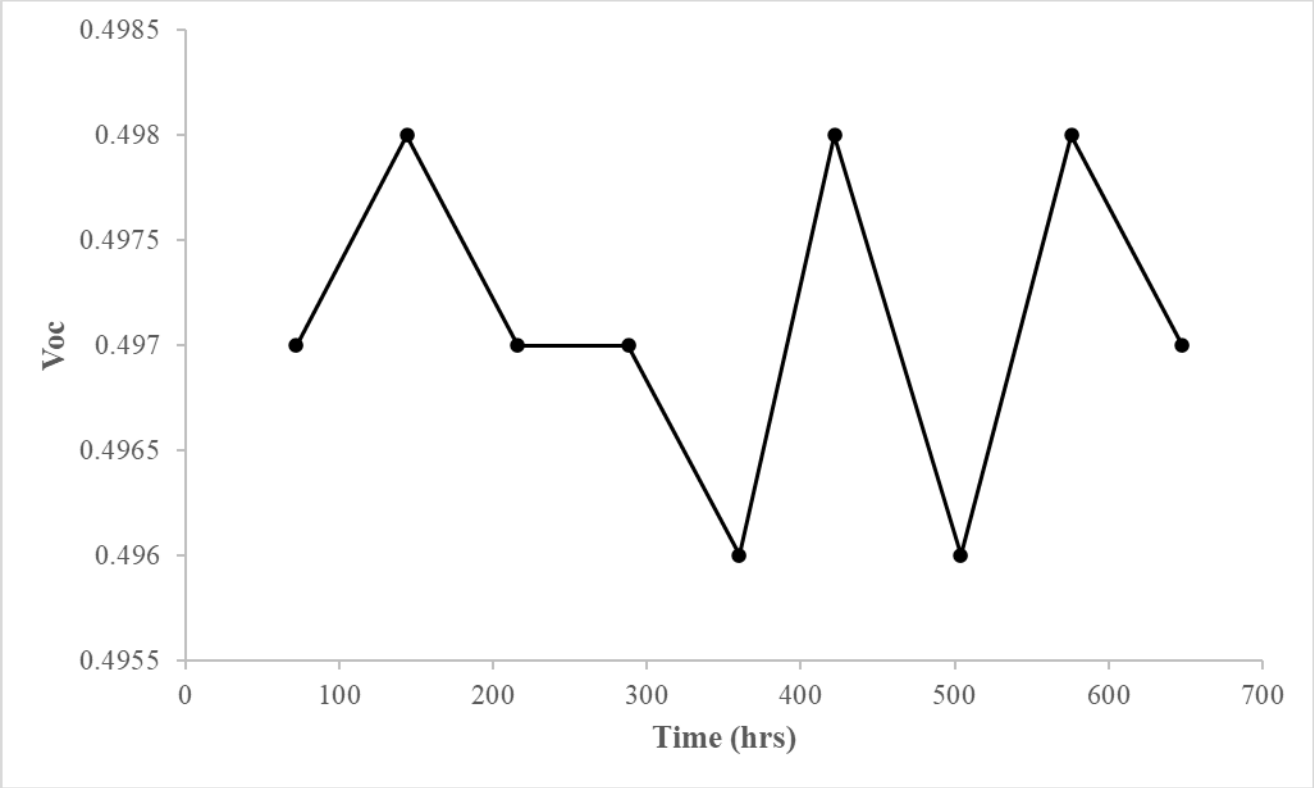

Figure 5.15: Graph of goodness of fit for open circuit voltage of DSSC.

From figure 5.15, the curve appears to be sinusoidal and hence Fourier Transformation was used to determine the voltage

$$V_{oc} = A_0 + A_1 \cos t + A_2 \sin t \qquad 5.1$$

The constants were determined using linear regression analysis;

$$V_{oc} = A_0 + A_1 \cos t + A_2 \sin t$$

$$V_{oc} \sin t = A_0 \sin t + A_1 \cos t \sin t + A_2 \sin^2 t$$

$$V_{oc} \cos t = A_0 \cos t + A_1 \cos^2 t + A_2 \cos t \sin t \qquad 5.2$$

$$\sum V_{oc} = nA_0 + A_1 \sum \cos t + A_2 \sum \sin t \qquad 5.3$$

$$\sum V_{oc} \sin t = A_0 \sum \sin t + A_1 \sum \cos t \sin t + A_2 \sum \sin^2 t$$

$$\sum V_{oc} \cos t = A_0 \sum \cos t + A_1 \sum \cos^2 t + A_2 \sum \cos t \sin t \qquad 5.4$$

Tab1e 5.4: show Voltage for stability test of DSSC after Fourier Transformation

Time (hrs)	V_{oc} (V)	$\cos t$	$\sin t$	$V_{oc} \times \sin t$	$V_{oc} \times \cos t$	$\cos t \times \sin t$	$\sin^2 t$	$\cos^2 t$
72	0.497	-0.967	0.254	0.126	-0.481	-0.246	0.064	0.936
144	0.498	0.871	-0.491	-0.245	0.434	-0.428	0.241	0.759
216	0.497	-0.718	0.696	0.346	-0.357	-0.500	0.484	0.516
288	0.497	0.518	-0.856	-0.425	0.257	-0.443	0.732	0.268
360	0.496	-0.284	0.959	0.476	-0.141	-0.272	0.920	0.080
422	0.498	0.518	0.856	0.426	0.258	0.443	0.732	0.268
504	0.496	0.224	0.975	0.483	0.111	0.218	0.950	0.050
576	0.498	-0.464	-0.886	-0.441	-0.231	0.411	0.785	0.215
648	0.497	0.673	0.739	0.367	0.335	0.498	0.546	0.454
Sum	4.474	0.371	2.246	1.114	0.185	-0.318	5.455	3.545

Substituting in the sum values in table 5.4 into equation 5.4 gives;

$$4.474 = 9A_0 + 0.371A_1 + 2.246A_2$$

$$1.114 = 2.246A_0 - 0.318A_1 + 5.455A_2$$

$$0.185 = 0.371A_0 + 3.545A_1 - 0.318A_2$$

Solving these equations with computer using matrix method yields;

$$A_0 = 49.992$$

$$A_1 = 0.768$$

$$A_2 = 1.001$$

Therefore, the model equation is;

$$\boldsymbol{V_{oc} = 49.992 + 0.768 \cos t + 1.001 \sin t}$$

$$R^2 = 0.999$$

$$V_{oc} = 49.992 + 0.768\cos t + 1.001\sin t$$

Where V_{oc} is the open circuit voltage and t is the time

From figures 5.11 to 5.14, the correlation coefficient or goodness of fit R^2 are 0.9786, 0.9116, 0.9599, and 0.9569 for $J_{sc,}$ $P_{max,}$ η, FF and 0.999 respectively. This shows that the higher the goodness of fit the higher the value of $J_{sc,}$ $P_{max,}$ η, FF and V_{oc}. which implies that the goodness of fit can be used to predict $J_{sc,}$ $P_{max,}$ η, FF and V_{oc} respectively. From figure 5.15 the curve appears to be sinusoidal and hence it was determined using Fourier Transformation. The equation for the voltage is V_{oc} = 49.992 + 0.768 cos t + 1.001 sin t. The correlation coefficient can be used to predict the $J_{sc,}$ $P_{max,}$ η, FF and V_{oc} parameters respectively.

From table 5.3, the efficiency of the cell reduced drastically during the fourth week of the experiment which may be due to gradual leakage of the electrolyte or less capacity to retain it. The results shows that there was a trend in the degradation. The degradation in efficiency and Jsc was in a decreasing trend after been stable for 12 days. This can be attributed to low amount of electron flows. Also, it can be attributed to electron recombination by the tri-iodide ions in the TiO_2/dye interface where it degrades the photovoltaic performance of the cell. Thus, the presence of the rGO facilitates the photogenerated electrons in the conduction band of the TiO_2 to flow into the external circuit of the DSSC where it acts as an e1ectron conducting path that suppress recombination and increases the Jsc values as deduced in the graph above (figure 5.11)

Research has shown that roselle dye seems to be unstable in their lifetime due to the degradation and low electron injection after 336 hours. [365] in his research reported that natural dye demonstrated lower power conversion efficiencies than dyes like ruthenium-based dye due to dye degradation. Also, [367] mentioned that weak binding energy of natural dyes with TiO_2 film and low charge transfer absorption in the visible light region can degrade their photovo1taic performance.

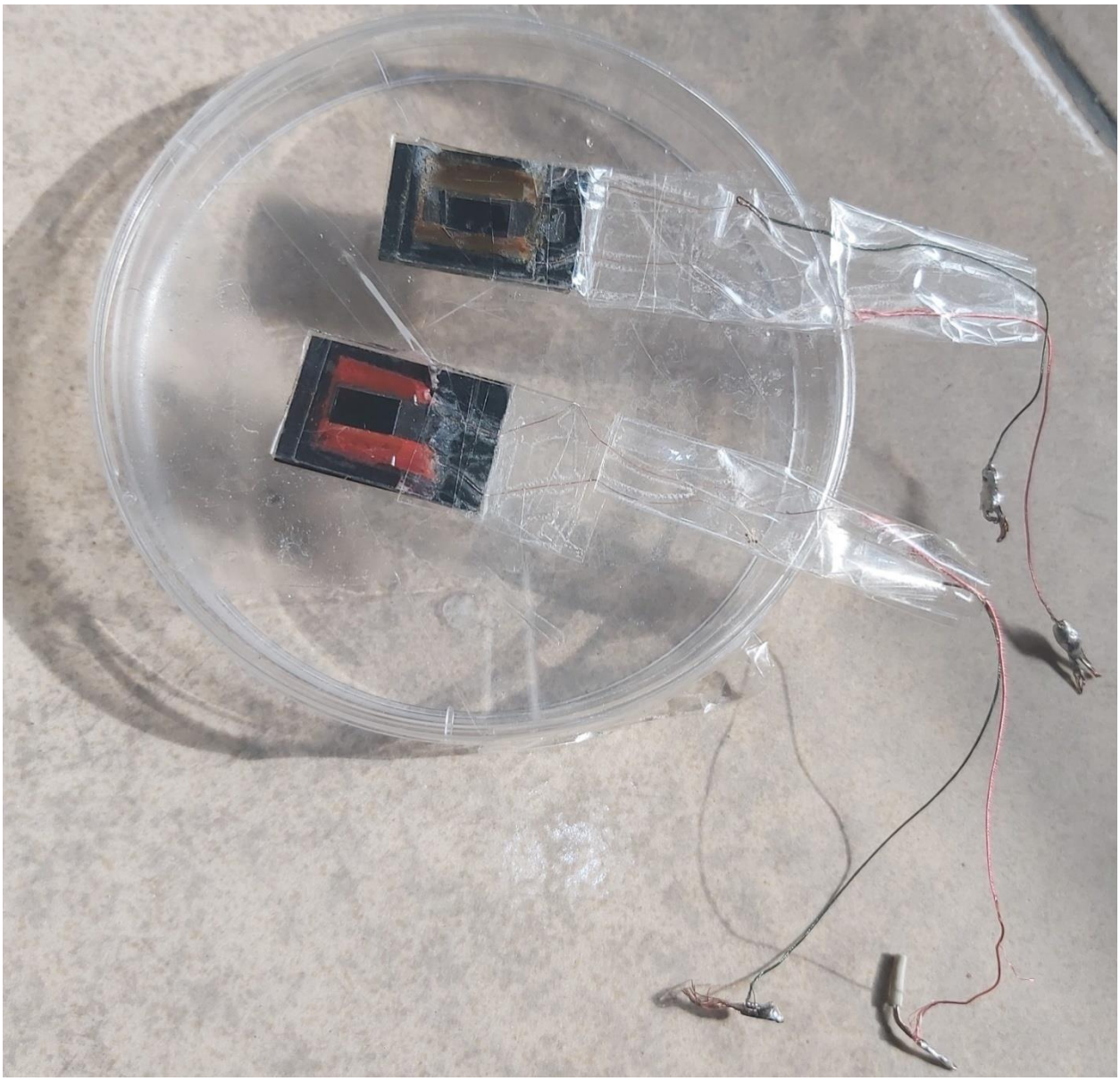

Figure 5.16: Fabricated DSSC- Dye-Sensitized So1ar Cell

5.2 Concluding Remarks

Titanium dioxide–reduced graphene oxide was synthesized successfully by a spin Coating method. The effect of TiO_2 -rGO on the sensitizer (dye) with a view to determine the effect of reduced graphene oxide (rGO) on the recombination of the injected electrons was investigated. The graphene in the composite material can effectively inhibit the recombination of

photogenerated electrons and holes, increase the contact area with dye molecules, improves the photocatalytic performance of the material, in line with [334].

I-V measurements utilizing a solar simulator under A.M. 1.5 (100mW/cm^2) were used to study the effect of electrolyte degradation over a four-week period. The rGO – TiO_2 incorporated dye sensitized solar cell demonstrated increased performance. These are evident in the simulation findings for the DSSC with rGO – TiO_2, which produced an open circuit voltage of 0.53V, a short circuit photocurrent of 0.12 mA/cm^2, and an enhanced photoelectric conversion efficiency of 11.52 %. The improved performance of DSSCs with rGO may be ascribed to an increase in electron transport efficiency and visible light absorption [247, 368].

When rGO is used, its performance improves due to increased light absorption, a wider range of absorption wavelengths, faster electron transport efficiency, and suppression of charge recombination. The power conversion efficiency (PCE) of DSSCs demonstrates that DSSCs constructed using reduced graphene oxide increased cell performance and demonstrated good outdoor stability. Thus, by adding rGO and natural dye into the cell, the efficiency of DSSCs increased. This is more environmentally friendly than traditional silicon-based cells,

CHAPTER SIX: GENERAL CONC1USIONS AND RECOMMENDATIONS

6.0 Conclusion

The synthesis of f1uorine-doped tin oxide (FTO) by Aerosol Assisted Chemica1Vapour Deposition (AACVD) using isopropanol as precursor due to its environmental friendliness was achieved and the application of Hummer's method (Tour's method) for the synthesis of the rGO was possible and effectively incorporated for which DSSC with a rGO -TiO_2 based photoanode was fabricated successfully. Based on this research, comparing the absorbance and transmittance of fluorine-doped tin oxide (F: SnO_2) at 4%, 8%, and 12% with regard to wavelengths (ג) at 230 nm and 1100 nm; It shows that at 12% (F: SnO_2), the lowest absorbance yields better transmittance, increasing the cell's efficiency by 11.52%. A DSSC cell with FTO thin films as a counter electrode and rGO-TiO2 as a photoanode and catalyst are made and characterized as part of the work. Cell efficiency served as the basis for evaluating cell performance. As a result, the study's aim has been accomplished. F:SnO_2 shows high carrier mobility and a more positive Conduction Band (CB) edge than TiO_2. The high carrier mobility leads to faster charge transport (CT) to TCO, thereby eliminating recombination. The wide bandgap (2.75) of ~3.6 eV does not allow the formation of oxidative holes in the SnO_2 CB in the presence of high-energy. Hence, it diminishes the dye degradation to ~1.4 eV and improves device stability.

Screen printing and spin coating were used to introduce rGO into the photoanode of DSSCs, which is a straight forward approach. The presence of rGO increased light absorption and absorption across a wide range of wavelengths. The numerous drops were divided into cycles, with cycle 4 being employed for this production. The graphene concentration in cycle four increased film thickness, which enhanced the hall coefficient and mobility with a drop-in carrier concentration. As a result, the DSSC's overall performance improved.

With reduced graphene oxide integration, the performance of the DSSC cell was improved with a photoelectric conversion efficiency of 11.52% (370) (371). The improved performance of DSSCs with rGO can be ascribed to an increase in electron transport efficiency and visib1e light absorption. When rGO was used, the performance improved due to increased light absorption, a wider range of absorption wavelengths, faster electron transport, and suppression of charge recombination. The study focused on the topic of recombination. The results indicate that the reduced graphene oxide (rGO) in the composite can effectively decrease the recombination rate

of electron–hole charge carriers while simultaneously increasing the rate of electron transfer in the DSSC operation.

The power conversion efficiency (PCE) of DSSCs demonstrates that DSSCs constructed using rGO -TiO_2 increased cell performance and demonstrated good outdoor stability. Thus, by integrating graphene and a natural dye (Roselle) inside the cell, the efficiency of the DSSCs can be increased. In general, the primary stability of DSSC has been a major issue; however, the incorporation of rGO into the DSSC component has enhanced the DSSC's efficiency and stability. The presence of reduced graphene oxide also resulted in increased light absorption and a broad spectrum of absorption wavelengths. It increased connectedness while decreasing recombination. Thus, rGO -TiO_2/TiO_2 – rGO was incorporated into DSSCs and improved its efficiency successfully, and has been revealed in this study as a good material for solar cell applications.

6.1 Suggestion for further work or recommendation

It will be interesting to explore the stability of DSSC when graphene is mixed with synthetic dye and compare its performance in terms of DSSC efficiency enhancement. It should be proved that the addition of graphene into a synthetic dye combination improves cell efficiency. More research can be done to determine the performance of DSSC modules when they are scaled up.

Further research can consider also, Improving the performance of dye-sensitized based carbon-nanotube ZnO_2 solar cell for power generation; fabrication of high-performance electrodes with polyelectrolytes in DSSCS for power generation.

Researchers should consider how to narrow the bandgap of the active material more by forming a heterojunction with the doping of another material.

References

1. Ikpesu Jasper E., Iyuke, Sunny E. Daramola, Michael; Okewale, A. Oyetunde (2020). Synthesis of improved dye-sensitized solar cell for renewable energy power generation. Solar Energy, 206, 918–934
2. International Energy Agency. (2012). *Key World Energy Statistics 2012.* Paris, France: International Energy Agency
3. Bagher Askari Mohammad, Mirazaei Mahmoud Abadi, Vahid Mirhabidi Mohsen(2015). Types of Solar Cells and Application. American Journal of Optics and Photonics. Vol. 3, No. 5, pp. 94-113
4. Bhagwat S., Dani R., Goswami P. and Kerawalla M. A. K. (2017). Recent advances in optimization of photoanodes and counter electrodes of dye-sensitized solar cells. *Current Science*, *113*(2), 228-235.

4a. Brian E. Hardin, Henry J. Snaith & Michael D. McGehee (2012). The renaissance of dye – sensitized solar cells, nature photonics 6, 162 -169.

5. Jayawardena, K.D.G.I.; Rozanski, L.J.; Mills, C.A.; Beliatis, M.J.; Nismy, N.A.; Silva, S.R.P. (2013). 'Inorganics-in-Organics': Recent developments and outlook for 4G polymer solar cells. Nanoscale, 5, 8411–8427.
6. Zhang, C., Zhang, J., Ma, X., & Feng, Q. (2021). *Semiconductor Photovoltaic Cells.* doi:10.1007/978-981-15-9480-9
7. Sujit, B., Plawan, K. J., Nirmalya, B.(2022). Unusual enhancement in efficiency of DSSCs upon modifying photoanodes with reduced graphene oxide. https://pubs.rsc.org/en/journals/journal/ra
8. Karan, S., Subhrajit, K., Pramod, K. S., Bhaskar, B.,(2019). Utilizing reduced graphene oxide for achieving better efficient dye sensitized solar cells, Journal of Alloys and Compounds, Volume 788, 2019, Pages 672-676,https://doi.org/10.1016/j.jallcom.2019.02.287.
9. Yen, M.Y; Teng, C.C; Hsiao, M.C et al. (2011) Platinum nano particles/graphene composite catalyst as a novel composite counter electrode for high performance dye sensitized solar cells. Journal of material chemistry, 21 (34) 12880-12888.

10. *Balasingam, S. K., & Jun, Y. (2015). Recent Progress on Reduced Graphene Oxide-Based Counter Electrodes for Cost-Effective Dye-Sensitized Solar Cells. Israel Journal of Chemistry, 55(9), 955–965. doi:10.1002/ijch.201400213*

11. Manal A. Awad, Awatif A. Hindi, Khalid M.O. Ortashi, Meznah M. Alanazi, Albandari W. Alrowaily, Taghreed Bahlool, Fatma Aouaini (2023). Enhanced efficiency of flexible organic polymer solar cells by incorporation of titanium dioxide nanoparticles

12. Zhijun Ning, Ying Fu, He Tian. Improvement of dye-sensitized solar cells: What we know and what we need to know (2010) Energy & Environmental Science

13. Chen Jiazang, Li Bo, Zheng Jianfeng, et al, (2012). Role of Carbon Nanotubes in Dye-sensitized TiO_2-Based Solar cells. *Journal of Physical Chemistry* C,116(28), pp. 14848-14856.

14. F. Liu, L. Zhou, W. Liu, Z. Zhou, Q. Yue, W. Zheng, R. Sun, W. Liu, S. Xu, H. Fan, L. F eng (2021). Organic Solar Cells with 18% Efficiency Enabled by an Alloy Acceptor: A Two-in-One Strategy, Adv. Mater., 2100830.

15. Batmunkh, M., Dadkhah, M., Shearer, C. J., Biggs, M. J., & Shapter, J. G. (2016). Incorporation of graphene into SnO2 photoanodes for dye-sensitized solar cells. *Applied Surface Science, 387*, 690-697.

16. Low, F. W., and Lai, C. W. (2018). Renewable and Sustainable Energy Reviews. Recent developments of graphene-TiO_2 composite nanomaterials as efficientphotoelectrodes in dye-sensitized solar cells: A review, 82(1), 103-125.

17. F. Yang, Y. Huang, Y. Li, Y. Li (2021). Large-area flexible organic solar cells. npj Flexible Electronics, 5 (1) (2021), pp. 1-12

18. K. Xu (2019). Silicon MOS optoelectronic micro-nano structure based on reverse-biased PN junction Physica status solidi (a), 216 (7), p. 1800868

19. Z. Wang, Y. Han, L. Yan, C. Gong, J. Kang, H. Zhang, X. Sun, L. Zhang, J. Lin, Q. Luo, C.Q. Ma (2021). High Power Conversion Efficiency of 13.61% for 1 cm2 Flexible Polymer Solar Cells Based on Patternable and Mass-Producible Gravure-Printed Silver Nanowire Electrodes Adv. Funct. Mater., 31 (4), p. 2007276

20. J.E. Ikpesu et al., (2021): Aerosol-assisted chemical vapour deposition synthesis of fluorine-doped tin oxide (FTO) for dye-sensitized solar cells (DSSCs): Effect of doping with fluorine, IOP Conf. Ser.: Mater. Sci. Eng. 1107 012117, doi:10.1088/1757-899X/1107/1/012117

21. Nguyen H. H. (2020). Graphene-Based Material for Fabrication of Electrodes in Dye-Sensitized Solar Cells. 10.5772/intechopen. 93637.

22. Błaszczyk, A., Joachimiak-Lechman, K., Sady, S., Tański, T., Szindler, M., & Drygała, A. (2021). *Environmental performance of dye-sensitized solar cells based on natural dyes. Solar Energy, 215, 346–355.* doi:10.1016/j.solener.2020.12.040

23. Calogero, G., Barichello, J., Citro, I., Mariani, P., Vesce, L., Bartolotta, A., Di Carlo, A., Di Marco, G., 2018. Photoelectrochemical and spectrophotometric studies on dyesensitized solar cells (DSCs) and stable modules (DSCMs) based on natural apocarotenoids pigments. Dyes Pigm. 155, 75–83. https://doi.org/10.1016/j. dyepig.2018.03.021.

24. Wathon, M.H., Beaumont, N., Benohoud, M., Blackburn, R.S., Rayner, C.M., 2019. Extraction of anthocyanins from Aronia melanocarpa skin waste as a sustainable source of natural colorants. Color. Technol. 135, 5–16. https://doi.org/10.1111/ cote.12385.

25. Silva, C., Santos, A., Salazar, R., Lamilla, C., Pavez, B., Meza, P., Hunter, R., Barrientos, L., 2019. Evaluation of dye sensitized solar cells based on a pigment obtained from Antarctic Streptomyces fildesensis. Sol. Energy 181, 379–385. https://doi.org/10.1016/j.solener.2019.01.035. Tabacchi, G., Fabbiani, M., Mino, L., Martra, G., Fois, E., 201

26. Green M.A. (2001). "Third Generation Photovoltaics: Ultra-High Conversion Efficiency at Low Cost", Progress in Photovoltaics 9, 123

27. Xiaoru, G., Ganhua, L. Junhong C. (2015). Graphene-Based Materials for Photoanodes in Dye-Sensitized Solar Cells Front. Energy Res., 14 December 2015 Sec. Nanotechnology for Energy Applications Volume 3 - 2015 | https://doi.org/10.3389/fenrg.2015.00050.

28. Varsha Yadav, Chandra Mohan Singh Negi, D. Kishore Kumar, Saral Kumar Gupta (2021). Fabrication of eco-friendly, low-cost dye sensitized solar cells using harda fruit-based natural dye, Optical Materials Volume 122, Part B, 111800

29. Wang, W.Y.; Klots, A.; Yang, Y.M.; Li, W.; Kravchenko, I.I.; Briggs, D.P.; Bolotin, K.I.; Valentine, J. (2015). Enhanced absorption in two-dimensional materials via Fano-resonant photonic crystals. Appl. Phys. Lett. 106, 181104.

30. Michael Grätzel. Review Dye-sensitized solar cells (2003) Elsevier Journal of Photochemistry and Photobiology C: Photochemistry Reviews 4: 145–153

31. Khamwannah, J. (2015). *Design and Fabrication of Efficient Electrodes for Dye Sensitized Solar Cells.* UC San Diego: Electronic Theses and Dissertations.

32 Rasmeet Singh, Sajid Ullah, Nikita Rao, Mandeep Singh, Indrajit Patra, Daniel Amoako Darko, C. Prince Jebedass Issac, Keyvan Esmaeilzadeh-Salestani, Rahul Kanaoujiya, and V. Vijayan (2022). Synthesis of Three-Dimensional Reduced-Graphene Oxide from Graphene Oxide, Nanomaterials for Sustainable Development: the UN 2030 goals, J. of Nanomaterials, Volume 2022, Article ID 8731429, https://doi.org/10.1155/2022/8731429

32. R. Singh, "Advancements in energy storage through graphene," in *Advances in Materials Processing and Manufacturing Applications. iCADMA 2020*, A. Patnaik, E. Kozeschnik, and V. Kukshal, Eds., Lecture Notes in Mechanical Engineering, pp. 165–173, Springer, Singapore, 2021.

33. Z. Sun, S. Fang, and Y. Hu, "3D graphene materials: from understanding to design and synthesis control," *Chemical Reviews*, vol. 120, no. 18, pp. 10336–10453, 2020.

34. Du, X., Skachko, I., Barker, A., & Andrei, E. Y. (2008). Approaching ballistic transport in suspended graphene. *Nature nanotechnology*, *3*, 491-495

35. Nair, R. R., Blake, P., Grigorenko, A. N., Novoselov, K. S., Booth, T. J., Stauber, T., . . . Geim, A. K. (2008). Fine Structure Constant Defines Visual Transparency of Graphene. *Science, 320*(5881), 1308 - 1308.

36. Du, J., Lai, X., Yang, N., Zhai, J., Kisailus, D., Su, F., . . . Jiang, L. (2010). Hierarchically Ordered Macro−Mesoporous TiO2−Graphene Composite Films: Improved Mass Transfer, Reduced Charge Recombination, and Their Enhanced Photocatalytic Activities. *ACS nano, 5*, 590-596..

37. Munkhbayar Batmunkh, C.J. Shearer, Mark Biggs, J.G. Shapter (2016) Solution processed graphene structures for perovskite solar cells, Journal of Materials Chemistry A, 4(7), pp. 2605-2616.

38. Rho, W. -Y., Song, D. H., Lee, S. H., & Jun, B. -H. (2017). Enhanced Efficiency in Dye-Sensitized Solar Cells by Electron Transport and Light Scattering onFreestanding TiO_2 Nanotube Arrays. *Nanomaterials, 7*(345), 1-11.

39. M.A.K.L. Dissanayake, J.M.K.W. Kumari, G.K.R. Senadeera, Hafeez Anwar (2021). Low cost, platinum free counter electrode with reduced graphene oxide and polyaniline

embedded SnO_2 for efficient dye sensitized solar cells, Solar Energy Volume 230, Pages 151-165, https://doi.org/10.1016/j.solener.2021.10.022

40. Bonaccorso F., Lombardo A., Hasan T., Sun Z., Colombo L., Ferrari A.C., (2012). Production and processing of graphene and 2d crystals; Materials Today 15(12) (2012), 564-589.
41. Y. Di *et al. (2018).* Nitrogen and sulfur dual-doped chitin-derived carbon/graphene composites as effective metal-free electrocatalysts for dye sensitized solar cells, Appl. Surf. Sci.
42. Brian O'regan and Michael Gratze. (1991). A low-cost, high-efficiency solar cell basedon dye-sensitized colloidal tio 2 films.
43. Thakur, A., Ghosh, D., Devi, P., Kim, K.-H., & Kumar, P. (2020). Current Progress and Challenges in Photoelectrode Materials for the Production of Hydrogen. Chemical Engineering Journal, 125415. doi:10.1016/j.cej.2020.125415
44. Nazeeruddin. M. K, Kay A, Rodicio I, Humphry Baker R, Mille E, List P, Vlachopoulos N and Gratzel M, (1993). Journal of the American Chemical Society vol. 115, no 14, p 6382.
45. T. Yang, J. Xue, H. Tan, A. Xie, S. Li, W. Yan, Y. Shen (2018). Highly ordered ZnO/ZnFe 2 O 4 inverse opals with binder-free heterojunction interfaces for high-performance photoelectrochemical water splitting, Journal of Materials Chemistry A
46. D.D.A. de Fátima Palhares, L.G.M. Vieira, J.J.R. Damasceno, Hydrogen production by a low-cost electrolyzer developed through the combination of alkaline water electrolysis and solar energy use, Int. J. Hydrogen Energy 43, 4265–4275.
47. A. Mishra, A. Mehta, S. Basu, N.P. Shetti, K.R. Reddy, T.M. Aminabhavi (2019). Graphitic carbon nitride (g–C3N4)–based metal-free photocatalysts for water splitting: a review, Carbon
48. W. Wang, M. Xu, X. Xu, W. Zhou, Z. Shao (2019). Perovskite oxide-based electrodes for high-performance photoelectrochemical water splitting: a review, Angew. Chem. Int. Ed.
49. Vázquez-Ortega, F., Lagunes, I., & Trigos, Á. (2020). Cosmetic dyes as potential photosensitizers of singlet oxygen generation. Dyes and Pigments, 108248. doi:10.1016/j.dyepig.2020.108248

50. Miles D. (2015). *Anodized ZnO Nanostructures for Next-Generation Photovoltaics.* University of Bath: University of Bath.

51. P. Koli, U. Sharma (2021). Use pigments present in the crude aqueous extract of the spinach for simultaneous solar power and storage at natural sun intensity Advanced Energy and Sustainability Research, 2 (11), p. 2100079

53. Md. Akhtaruzzaman, A. K. Mahmud Hassan (2022). Comprehensive Guide on Organic and Inorganic Solar Cells, Book, 195 -244 (Dye-sensitized solar cells**)**

52. Hagfeldt, A., Cappel, U. B., Boschloo, G., Sun, L., Kloo, L., Pettersson, H., & Gibson, E. A. (2018). Dye-Sensitized Photoelectrochemical Cells. McEvoy's Handbook of Photovoltaics, 503–565. doi:10.1016/b978-0-12-809921-6.00014-8

53. Lau, K. K. S., & Soroush, M. (2019). Overview of Dye-Sensitized Solar Cells. Dye-Sensitized Solar Cells, 1–49. doi:10.1016/b978-0-12-814541-8.00001-x

54. Hara K, Horiguchi T, Kinoshita T, Sayama K, and Arakawa H. (2001). Influence of electrolytes on the photovoltaic performance of organic dye-sensitized nanocrystalline tio 2 solar cells. *Solar Energy Materials and Solar Cells, 70*(2), 151–161.

55. Wu, J., Lan, Z., Lin, J., Huang, M., Huang, Y., Fan, L. Wei, Y. (2017). Counter electrodes in dye-sensitized solar cells. Chemical Society Reviews, 46(19), 5975–6023. doi:10.1039/c6cs00752j

56. Wu, J., Lan, Z., Lin, J., Huang, M., Huang, Y., Fan, L., Wei, Y. (2017). *Counter electrodes in dye-sensitized solar cells. Chemical Society Reviews, 46(19), 5975–6023.* doi:10.1039/c6cs00752j

57. REN21.2016, Renewables 2016 Global Status Report, REN21 Secretariat, Paris, 2016

58. Muhammad L. M. N. (2017). *Fabrication and Characterization of Nano Structrued Fluorine Doped Tin Oxide Thin Film for DSSC by Hydrothermal Method.* Malaysia: Universiti Tun Hussein Onn.

59. Khalil Ebrahim Jasim (2011). Dye Sensitized Solar Cells - Working Principles, Challenges and Opportunities Department of Physics, University of Bahrain Kingdom of Bahrain, www.intechopen.com

60. Askari Bagher Mohammad, Mirazaei Mahmoud Abadi, Vahid Mirhabidi Mohsen(2015). Types of Solar Cells and Application. American Journal of Optics and Photonics. Vol. 3, No. 5, pp. 94-113

61. Archer, M. D. and Nozik, A. J. (2008). Nanostructured and Photoelectrochemical Systems for Solar Photon Conversion; Imperial College Press: London, Vol. 3.

62. Ahmad D., Choi W.J, Seo Y.I, Sehun Seo, Sanghan Lee, Tuson Park, Mosqueira J., Genda Gu and Yong Seung Kwon (2017). Effect of proton irradiation on the fluctuationinduced magnetoconductivity of FeSe1−x Tex thin films, New J. Phys.19

63. van de Lagemaat, J., Frank, A. J. (2000). Effect of the Surface-State Distribution on Electron Transport in Dye-Sensitized TiO2 Solar Cells: Nonlinear Electron-Transport Kinetics. *The Journal of Physical Chemistry B, 104*(18), 4292-4294.

64. Soedergren S., Hagfeldt A., Olsson J., Lindquist S.E. (1994). Theoretical Models for the Action Spectrum and the Current-Voltage Characteristics of Microporous Semiconductor Films in Photoelectrochemical Cells. *The Journal of Physical Chemistry, 98*(21), 5552-5556.

65. Sulaeman, U., and Abdullah, A. Z. (2017). The way forward for the modification of dye-sensitized solar cell towards better power conversion efficiency. *Renewable and Sustainable Energy Reviews, 74*, 438–452.

66. Fisher A. C., Peter L. M., Ponomarev E. A., Walker A. B., Wijayantha K. G. U. (2000). Intensity Dependence of the Back Reaction and Transport of Electrons in Dye-Sensitized Nanocrystalline TiO2 Solar Cells. *The Journal of Physical Chemistry B, 104*(5), 949-958.

67. Bisquert J., Vikhrenko V. S. (2004). Interpretation of the Time Constants Measured by Kinetic Techniques in Nanostructured Semiconductor Electrodes and Dye-Sensitized Solar Cells. *The Journal of Physical Chemistry B, 108*(7), 2313-2322.

68. Bisquert J. Cahen D., Hodes G., Rühle S., Zaban A. (2004). Physical Chemical Principles of Photovoltaic Conversion with Nanoparticulate, Mesoporous Dye-Sensitized SolarCells. *The Journal of Physical Chemistry B, 108*(24), 8106-8118.

69. *Vallejo L., W. A., Quinones S., C. A., & Hernandez S., J. A. (2011). The Chemistry and Physics of Dye-Sensitized Solar Cells. Solar Cells - Dye-Sensitized Devices. doi:10.5772/20609*

70. Peter L. M.,Wijayantha K. G. U. (2000). Electron transport and back reaction in dye sensitized nanocrystalline photovoltaic cells. *Electrochimica Acta, 45*(28), 4543-4551
71. Frank A. J., Kopidakis N. and van de Lagemaat J. (2004). Electrons in nanostructured TiO_2 solar cells: transport, recombination and photovoltaic properties. *Coordination Chem. Rev., 248,* 1165–1179.
72. Hafeez Anwar (2013). Precious Metal-free Dye-sensitized Solar Cells, Doctor of Philosophy thesis, Dalhousie University Halifax, Nova Scotia
73. Gratzel M., Klug D. R., Durrant J. R. (2008). Dye-Sensitized Mesoscopic Solar Cells. (M. D. Nozik, Ed.) *Nanostructured and Photoelectrochemical Systems For Solar Photon Conversion, 3,* 503-536.
74. Cahen D. Hodes G. Gratzel M. GuillemolesJ. F. Riess I. (2000). Nature of photovoltaic action in dye-sensitized solar cells. *J. Phys. Chem. B, 104*(9), 2053-2059.
75. Haque S. A., Tachibana Y., Willis R. L., Moser J. E., Gratzel M., Klug D. R., Durrant J. R. (2000). Parameters influencing charge recombination kinetics in dye-sensitized nanocrystalline titanium dioxide films. *J. Phys. Chem. B, 104*(3), 538-547.
76. Kuciauskas D., Freund M. S., Gray H. B., Winkler J. R., Lewis N. S. (2000). Electron Transfer Dynamics in Nanocrystalline Titanium Dioxide Solar Cells Sensitized with Ruthenium or Osmium Polypyridyl Complexes. *The Journal of Physical Chemistry B, 105*(2), 392-403.
77. D D Pratiwi, F Nurosyid, Kusumandari, A Supriyanto and R Suryana [2017]. Performance improvement of dye-sensitized solar cells (DSSC) by using dyes mixture from chlorophyll and anthocyanin, IOP Conf. Series: Journal of Physics: Conf. Series 909, 012025
78. Maurya I C, Srivastava P, and Bahadur L (2016). Optical. Materials. 52 150-156
79. Bhogaita M, Shukla A D, and Nalini R P (2016). Solar. Energy. 137 212-224
80. Lenzmann, F.O.; Kroon, J.M. (2007). Recent Advances in Dye-Sensitized Solar Cells. Advances in Opto Electronics. 1-10
81. Eran Stark, Tibor Koos, and György Buzsáki (2012). Diode probes for spatiotemporal optical control of multiple neurons in freely moving animals, Journal of NeuroPhysilogy, https://doi.org/10.1152/jn.00153.2012
82. Kay A. and Gratzel M. (1996). Low cost photovoltaic modules based on dye sensitized nanocrystalline titanium dioxide and carbon powder. *Sol Energ Mat Sol C, 44*(1), 99-117.

83. Kang S.H, Kang M., Choi S. Kim J. Kim H. (2008). Improved Charge Transport in Dye-Sensitized Solar Cells Employing Viscous Non-Volatile Electrolytes. *Electrochem Commun, 10,* 1326-1329.

84. Mali, S. S., Patil, J. V., & Hong, C. K. (2019). *Nanorod-based dye sensitized solar cells. Nanomaterials for Solar Cell Applications, 349–374.* doi:10.1016/b978-0-12-813337-8.00010-2

85. Shahzad, N., Shah, Z., Shahzad, M. I., Ahmad, K. A., & Pugliese, D. (2019). Effect of seed layer on the performance of ZnO nanorods-based photoanodes for dye-sensitized solar cells. Materials Research Express. doi:10.1088/2053-1591/ab3a61

86. Long, R.; English, N. J.; Prezhdo, O. V. J.(2012) Am. Chem. Soc, 134, 14238

87. Jang H.-S.; Yun, J.-M.; Kim, D.-Y.; Park, D.-W.; Na, S.-I.; Kim, S.-S. (2015). Electrochim. Acta 2012, 81, 301

88. Boschloo G., Hagfeldt A. (2009). Characteristics of the Iodide/Triiodide Redox Mediatorin Dye-Sensitized Solar Cells. *Acc. Chem. Res, 42*, 1819-1826.

89. Zhang, R., Cao, Y., Li, P., Zang, X., Sun, P., Wang, K., . . . Zhu, H. (2014). Three-dimensional porous graphene spongesassembled with the combination of surfactant and freeze-drying. *Nano Research, 7*(10), 1477-1487.

90. Ginley D., Hosono H., Paine D. C. (2010). Handbook of Transparent Conductors; Springer Science and Business Media.

91. Granqvist C. G. (2007). Transparent Conductors as Solar Energy Materials: A Panoramic Review. *Sol.Energy Mater. Sol. Cells*, *91*(17), 529–1598

92. Longo C. and De Paoli. (2003.). M-A. Dye-Sensitized Solar Cells: a Successful Combination of Materials. *J. Braz. Chem. Soc., 14*, 889-901.

93. Sasha. A., Mohd Hanif, Lau, Mohamad W. K., Wan Zaki F., W. S., and Ahmad, M. K. (2015). Preparation of Nanostructured Fluorine Doped Tin Oxide (FTO) by Hydrothermal Method. Applied Mechanics and Materials, 773-774, 632–636.

94. Suhaimi, S., et al., (2015) *Materials for Enhanced Dye-sensitized Solar Cell Performance: Electrochemical Application.* Int. J. Electrochem. Sci, 2015. 10, 2859-2871.

95. Huang, G., Lu, C.-H., & Yang, H.-H. (2019). Magnetic Nanomaterials for Magnetic Bioanalysis. Novel Nanomaterials for Biomedical, Environmental and Energy Applications, 89–109. doi:10.1016/b978-0-12-814497-8.00003-5

96. Liu, Bin; Aydil, Eray S. (2009). *Growth of Oriented Single-Crystalline Rutile TiO ₂ Nanorods on Transparent Conducting Substrates for Dye-Sensitized Solar Cells. Journal of the American Chemical Society, 131(11), 3985–3990.* doi:10.1021/ja8078972

97. Yang, N., Zhai, J., Wang, D., Chen, Y., & Jiang, L. (2010). Two-Dimensional Graphene Bridges Enhanced Photoinduced Charge Transport in Dye-Sensitized Solar Cells. *ACS Nano, 4*(2), 887–894

98. Jubault, M., Pulpytel, J., Cachet, H., Boufendi, L., and Arefi-Khonsari, F. (2007). Deposition of SnO2:F Thin Films on Polycarbonate Substrates by PECVD for Antifouling Properties. Plasma Processes and Polymers, 4(S1), S330–S335.

99. Wang, J. T.; Shi, X. L.; Liu, W. W.; Zhong, X. H.; Wang, J. N.; Pyrah, L.; Sanderson, K. D.; Ramsey, P. M.; Hirata, M.; Tsuri, K. (2015). Influence of Preferred Orientation on the Electrical Conductivity of Fluorine-Doped Tin Oxide Films. *Sci. Rep, 6*, 3679–3687.

100. Najafi N. and Rozati S.M. (2017). Structural and Electrical Properties of SnO2:F Thin Films Prepared by Chemical Vapor Deposition Method, Acta Physica Polonica A, 131(2), 222- 225

101. Banyamin Z.Y., Kelly P.J., West G., Boardman J. (2014). Electrical and optical properties of fluorine doped tin oxide thin films prepared by magnetron sputtering. *Coatings*, *4*, 732-746.

102. Zhu B.L., Liua F., Li K., Lv K., Wu J., Gan Z.H., Liu J., Zeng D.W., Xie C.S. (2017). Sputtering deposition of transparent conductive F-doped SnO_2 (FTO) thin films in hydrogen-containing atmosphere. *Ceramics International, 43*, 10288–10298.

103. Maruyama T., Akagi H. (1996). Fluorine-doped tin dioxide thin films prepared by radio-frequency magnetron sputtering. *J. Electrochem. Soc, 143*, 283–287.

104. Liao B.H., Kuo C.C., Chen P.J., Lee C.C. (2011). Fluorine-doped tin oxide films grown by pulsed direct current magnetron sputtering with an Sn target. *Appl. Opt, 50*, 106-110.

105. Liao B.H., Chan S.H., Lee C.C., Kuo C.C., Chen S.H., Chiang D. (2014). FTO films deposited in transition and oxide modes by magnetron sputtering using tin metal target. *Appl. Opt, 53*, 148–153.
106. Jager T., Bissig B., Dobeli M., Tiwari A.N., Romanyuk Y.E. (2014). Thin films of SnO2:F by reactive magnetron sputtering with rapid thermal post-annealing. *Thin Solid*
107. Cox S.F.J., Davis E.A., Cottrell S.P., King P.J.C., Lord J.S., Gil J.M., Alberto H.V., Vilao, R.C., Duarte J.P., De Campos N.A., Weidinge A., Lichti L., Irvine S.J.C. (2001). Experimental confirmation of the predicted shallow donor hydrogen state in zinc oxide. *Phys. Rev. Lett, 86*, 2601–2604.
108. Lavrov E.V., Borrnet F., WeberA. (2005). Photoconductivity and infrared absorption study of hydrogen-related shallow donors in ZnO. *Phys. Rev. B, 72*, 085212.
109. Van de Walle C.G. (2012). Hydrogen as a cause of doping in ZnO. *Phys. Rev. Lett, 85*, 1012-1015.
110. De Moure-Flores F., Guillen-Cervantes A., Nieto-Zepeda K.E., QuinonesGalvan J.G., Hernandez-Hernandez A., de la M., Olvera L., Melendez-Lira M. (2013). SnO2:F thin films deposited by RF magnetron sputtering: effect of the SnF2 amount in the target on the physical properties. *Rev. Mex. Fis, 59*, 335–338.
111. Ziad Y. Banyamin, Peter J. Kelly, Glen West and Jeffery Boardman. (2014). Electrical and Optical Properties of Fluorine Doped Tin Oxide Thin Films Prepared by Magnetron Sputtering. *Coatings, 4*, 732-746.
112. Mcmaster H.A (1947), U. S. Patent No 2,429,420
113. J. M. Mochel (1947). U. S. Patent No 2,564,706
114. Aouaj, M. A.; Diaz, R.; Belayachi, A.; Rueda, F.; Abd-Lefdil, M. (2009). Comparative Study of ITO and FTO Thin Films Grown by Spray Pyrolysis. Mater. *Res. Bull, 44*(7), 1458–1461.Bagher A. M., Mirzaei M. A., Mohsen M. (2015). Types of Solar Cells and Application. *American Journal of Optics and Photonics, 3*(5), 94-113.
115. Napi Mohd M.L., Nayan N., Ahmad M.K., Fazlee F.I.M., Hamed N.K.A., Khalid N.S. (2016). Fabrication of Flourine Doped Tin Oxide with Different Volume. *Sains Malaysiana, 45*(8), 1207–1211.

116. Murakami, K., K. Nakajima, and S. Kaneko, (2007). Initial growth of SnO2 thin filmon the glass substrate deposited by the spray pyrolysis technique. Thin Solid Films, 515(24): 8632-8636.

117. Liyanage, D., (2013) Ethylene Glycol Assisted Synthesis of Fluorine DopedTin Oxide Nanorods Using Improved Spray Pyrolysis Deposition Method. Applied Physics Express, 6(8): p. 085501

118. Hussein, I. A., Mehmood, U., and Al-Ahmed, S., (2016). "Enhancing Power Conversion Efficiency of Dye-Sensitized Solar Cell Using TiO2-MWCNT Composite Photoanodes".

119. Aoki, H., and Dresselhaus, M. S. (2014). Preface. In H. Aoki, & M. S. Dresselhaus, *Physics of Graphene* (pp. v -vi). Cham, Switzerland: Springer.

120. Tahir, A. A., Ullah, H., Sudhagar, P., Teridi, M. A., Devadoss, A., & Sundaram, S. (2016). The Application of Graphene and ItsDerivatives to Energy Conversion,Storage, and Environmental andBiosensing Devices. *The Chemical Record,, 16*(3), 1591–1634.

121. Zhen, Z., and Zhu, H. (2018). Structure and Properties of Graphene. In H. Zhu, Z. Xu, D. Xie, & Y. Fang, *Graphene: Fabrication, Characterizations, Properties and Applications* (pp. 1-12). London, United Kingdom: Academic Press.

122. Chae, S., Jang, S., Choi, W. J., Kim, Y. S., Chang, H., Lee, T. I., & Lee, J. -O. (2017). Lattice Transparency of Graphene. *Nano Letters, 17*(3), 1711-1718.

123. Britnell, L., Ribeiro, R. M., Eckmann, A., Jalil, R., Belle, B. D., Mishchenko, A., . Novoselov, K. S. (2013). Strong Light-Matter Interactions in Heterostructures of Atomically Thin Films. *Science, 340*(6138), 1311-1314.

124. Wu, Jihuai; Lan, Zhang; Lin, Jianming; Huang, Miaoliang; Huang, Yunfang; Fan, Leqing; Luo, Genggeng; Lin, Yu; Xie, Yimin; Wei, Yuelin (2017). *Counter electrodes in dye-sensitized solar cells. Chem. Soc. Rev., (), 10.1039.C6CS00752J–* . doi:10.1039/C6CS00752J

125. Oshima, C., and Nagashima, A. J. (1997). Ultra-thin epitaxial films of graphite and hexagonal boron nitride on solid surfaces. *Journal of Physics: Condensed Matter, 9*(1), 1 -20.

126. Schmiedova, Veronika; Pospisil, Jan; Kovalenko, Alexander; Ashcheulov, Petr; Fekete, Ladislav; Cubon, Tomas; Kotrusz, Peter; Zmeskal, Oldrich; Weiter, Martin

(2017). *Physical Properties Investigation of Reduced Graphene Oxide Thin Films Prepared by Material Inkjet Printing. Journal of Nanomaterials, 2017(), 1–8.* doi:10.1155/2017/3501903

127. Gupta, Mukund; Makda, Shahab; Senthil, Ramalingam (2018). The latest trends in synthesis of dye-sensitized solar cells. IOP Conference Series: Materials Science and Engineering, 402(), 012176–. doi:10.1088/1757-899X/402/1/012176

128. Boehm, H. P., Clauss, A., Fischer, G. O., & Hofmann, U. (1962). The adsorption behavior of very thin carbon films. *Journal of Inorganic and General Chemistry B, 17*, 150-153.

129. Novoselov, K. S., Geim, A. K., Morozov, S. V., Jiang, D., Zhang, Y., Dubonos, S. V., . . . Firsov, A. A. (2004). Electric field effect inatomically thin carbon films. *Science, 306*(5696), 666-669.

130. Bhuyan, Sajibul Alam, Uddin, Nizam, Islam, Maksudul, Alam, Ferdaushi, Hossain, Sayed, (2016). Graphene a two dimensional material for sp2 hybridization of…Nano. letters 6 (2), 65–83.

131. Li, J., Li, J., Li, L., Yu, M., Ma, H., & Zhang, B. (2014). Flexible graphene fibers prepared by chemical reductioninducedself-assembly, J. Mater. Chem. A 2 (18) (2014) 6359. *Journal of Material Chemistry A, 2*(18), 6359-6362. doi:10.1039/C4TA00431K

132. Zhang, Y., Li, H., Kuo, L., Dong, P., & Yan, F. (2015). Recent Applications of Graphene in Dye-Sensitized Solar Cells. *Current Opinion in Colloid and Interface Science, 20*(5-6), 406-415. doi:10.1016/j.cocis.2015.11.002

133. Zhang, R., and Zhu, H. (2018). Potential Applications and Perspectives. In H. Zhu, Z. Xu, D. Xie, & Y. Fang, *Graphene: Fabrication, Characterizations, Properties and Applications* (pp. 233-249). London, United Kingdom: Academic Press.

134. Huilei, Zhao, Liu, Lianjun, Andino, Jean M, Li, Ying, (2012). Photocatalytic co2 reduction with h2o on tio2 nanocrystals: Comparison of anatase, rutile, and brookite polymorphs and exploration of surface chemistry. ACS Catal. 2 (8), 1817–1828.

135. Zhang, W., Yuan, C., Guo, J., Qiu, L., & Yan, F. (2014). Supramolecular ionic liquid gels forquasi-solid-state dye-sensitized solar cells. *ACS applied materials and interfaces, 6*, 8723-8728.

136. Xu, Y., Shi, G., and Duan, X. (2015). Selfassembled three-dimensional graphene macrostructures: synthesis and applications insupercapacitors. *Accounts of Chemical Research, 48,* 1666–1675.

137. Seok-Soon Kim, Yoon-Chae Nah, Yong-Young Noh, Jang Jo, and Dong-Yu Kim. (2006). Electrodeposited pt for cost-efficient and flexible dye-sensitized solar cells. *Electrochimica Acta*, 51(18):3814–3819.

138. Xu, Z., Sun, H., Zhao, X., and Gao, C. (2013). Ultrastrong fibers assembled from giant graphene oxide sheets. *Advanced Materials, 25*(2), 188-193.

139. Xiang, C., Young, C. C., Wang, X., Yan, Z., Hwang, C., Cerioti, G., . . . Tour, J. M. (2013). Large flake graphene oxide fiberswith unconventional 100% knot efficiency and highly aligned small flake graphene oxide fibers. *Advanced Materials, 25*(23), 4592-4597.

140. Luo, Y., Yuan, B., Yu, Q., & Feng, Y. (2012). Substrateless graphene fiber: a sorbent for solid-phase microextraction. *Journal of Chromatography A, 1268,* 9-15.

141. Li, S., Qiu, L., Shi, C., Chen, X., & Yan, F. (2014). Water-Resistant, Solid-State, Dye-Sensitized SolarCells Based on Hydrophobic Organic Ionic Plastic Crystal Electrolytes. *Advanced Materials, 26,* 1266-1271.

142. Li, X., Zhao, T., Wang, K., Yang, Y., Wei, J., Kang, F., . . . Zhu, H. (2011). Directly Drawing Self-Assembled, Porous, and Monolithic Graphene Fiber from Chemica l Vapor Deposition Grown Graphene Film and Its Electrochemical Properties. *Langmuir, 27*(19), 12164-12171. doi:10.1021/la202380g

143. Zou, J., and Kim, F. (2012). Self-Assembly of Two-Dimensional Nanosheets Induced by Interfacial Polyionic Complexation. *ACS Nano, 6*(12), 10606-10613. doi:10.1021/nn303608g

144. Li, J., Ye, S., Li, T., Li, X., Yang, X., & Ding, S. (2015). Preparation of graphene nanoribbons (GNRs) as an electroniccomponent with the multi-walled carbon nanotubes (MWCNTs). *Procedia Engineering, 10,* 492 – 498.

145. Li, X., Zhang, X., Hua, J., & Tian, H. (2017). Molecular engineering of organic sensitizers with o, p-dialkoxyphenyl-based bulky donors for highly efficient dye-sensitized solar cells. *Molecular Systems Design and Engineering, 2*(2), 98–122.

146. Kim Seok-Soon, Yoon-Chae Nah, Yong-Young Noh, Jang Jo, and Dong-Yu Kim. (2006). Electrodeposited pt for cost-efficient and flexible dye-sensitized solar cells. *Electrochimica Acta, 51*(18), 3814–3819.

147. Kim, K.S.; Kang, Y.S.; Lee, J.H.; Shin, Y.J.; Park, N.G.; Ryu, K.S. & Chang, S.H. (2006). Photovoltaic properties of nano-particulate and nanorod array ZnO electrodes for dye-sensitized solar cell. Bull Korean Chem. Soc, Vol. 27, pp. 295-298

148. Chen, Y.S.; Lee, J.; Tsai, S.; Ting, C. (2007). Manufacture of Dye-Sensitized Solar Cells and their I-V Curve Measurements. Proceedings of ICAM 2007, Taipei, Taiwan, November 26-28.

149. Li, D., and Kaner, R. B. (2008). Graphene-based composite materials. *Science, 320*(5880), 1170-1171. doi:10.1126/science.1158180

150. Ponomarenko T, Abdala AA, Schedin F, Kaltnelson MI, Yang R, Novoselov KS, Geim AK.(2008). Chaotic Dirac billiard in graphene quantum dots, Science. 320,356-358.

151. Zhang, L., & Shi, G. (2011). Preparation of highly conductive graphene hydrogels for fabricating supercapacitorswith high rate capability. *The Journal of Physical Chemistry C, 115*(34), 17206-17212.

152. Liu, X., Cui, J., Sun, J., & Zhang, X. (2014). 3D graphene aerogel-supported SnO2 nanoparticles for efficient detectionof NO2. *RCS Advances, 4*(43), 22601-22605.

153. Sui, Z., Zhang, X., Lei, Y., & Luo, Y. (2011). Easy and green synthesis of reduced graphite oxide-based hydrogels. *Carbon, 49*(13), 4314-4321.

154. Chen, T., Qiu, L. B., Cai, Z. B., Gong, F., Yang, Z. B., Wang, Z. S., & Peng, H. S. (2012). Intertwined aligned carbon nanotube fiber based dyesensitizedsolar cells. *Nano Letters, 12*(5), 2568–2572.

155. Yu, Q., Lian, J., Siriponglert, S., Li, H., Chen, Y. P., & Pei, S. (2008). Graphene segregated on Ni surfaces and transferredto insulators. *Applied Physics Letters, 93*, 113103.

156. Tang, B., Hu, G., Gao, H., & Shi, Z. (2013). Three-dimensional graphene network assisted high performance dyesensitized solar cells. *Journal of Power Sources, 234*, 60-68.

157. Nonjabulo P.D. Ngidi, Edigar Muchuweni, Vincent O. Nyamori (2021).

Dual heteroatom-doped reduced graphene oxide and its application in dye-sensitized solar cells, Optical Materials, Volume 122, Part B, 111689

158. X. Chen *et al. (2019).* Insights into nitrogen and boron-co-doped graphene toward high-performance peroxymonosulfate activation: maneuverable N-B bonding configurations and oxidation pathways, Appl. Catal. B Environ.
159. Ni, Z. H., Wang, H. M., Kasim, J., Fan, H. M., Yu, T., Wu, Y. H., . . . Shen, Z. X. (2007). Graphene thickness determition using reflection and contrast spectroscopy. *Nano Letters, 7*(9), 2758-2763.
160. Zheng, ,. Q., and Kim, J. -K. (2015). *Graphene for Transparent Conductors: Synthesis, Properties, and Applications.* New York: Springer. Synthesis, Structure and Properties of Graphene and Graphene Oxide; pp. 29–94.
161. Wang, X., Zhi, L., and Müllen, K. (2008). Transparent, conductive graphene electrodes for dye-sensitized solar cells. Nano Lett. 8, 323–327. doi:10.1021/ nl072838r
162. Bonaccorso F., Sun Z., Hasan T., and Ferrari A.C. (2010) Nature photonics
163. Punkct, C, Pope, M. A, Lui , J, Lin Y, Askay, I.A. (2010). Electroanalysis 2010. 22, 2834.
164. Joseph D. Roy-Mattew and Ilhan.A Askay. (2014). Graphene materials and their use in Dye Sensitized solar cells.Chem Reviews 2014, 114(12), 6323-6348.
165. Roy-Mayhew, Joseph D., Aksay, Ilham A., (2014). Graphene materials and their use in DyeSensitized Solar Cells. Chem. Rev. 114, 6323–6348.
166. Zhao, B.; Zhao, J.M.; Zhang, Z.M. (2015). Resonance enhanced absorption in a graphene monolayer using deep metal gratings. J. Opt. Soc. Am. B, 32, 1176–1185.
167. Lee, E., Ryu, J., and Jang, J. (2013). Fabrication of graphene quantum dots via size-selective precipitation and their application in upconversion-based DSSCs. Chem. Commun. (Camb) 49, 9995–9997
168. Huang, S.; Sun, H.; Huang, X.; Zhang, Q.; Li, D.; Luo, Y.; Meng, Q., (2012). Carbon nanotube counter electrode for high-efficient fibrous dye-sensitized solar cells. NanoscaleResearch Letters, 7 (1), 1-7.
169. Lee, K.M., Shih, K.L., Chiang, C.H. and Suryanarayanan, V. (2014) Fabrication of High Transmittance and Low Sheet Resistance Dual Ion Doped Tin Oxide Films and Their Application in Dye-Sensitized Solar Cells. Thin Solid Films, 570, 7-15
170. De, S; Coleman, J. N. (2010). Are There Fundamental Limitations onn the Sheet Resistance and Transmittance of Thin Graphene Film? ACS Nano, 4, 2713 -2720

171. Kavan , J. H. Yum and M Gratzel. (2011). Optically transmitted cathode for dye-sensitzed solar cells based on grapheme nano platelete. ACS Nano. 15(10), 165-172.
172. Zhu, G.; Xu, T.; Lv, T.; Pan, L.; Zhao, Q. (2011) Graphene-incorporated nanocrystalline TiO2 films for CdS quantum dot-sensitized solar cells. J. Electroanal. Chem. 650, 248.
173. Low, F.W., Lai, C.W., 2018. Renewable and Sustainable Energy Reviews. Recent developments of graphene-TiO2 composite nanomaterials as efficientphotoelectrodes in dye-sensitized solar cells. A review 82 (1), 103–125.
174. Yan X, B. Li, X Cui and L.S. Li. (2010).Large solution- processable grapheme quantum dots as light absorber for photovotalics. Nano Letters. 10 (5), 1869-1873.
175. Chen, Y., Chen, K., Bai, H., & Li, L. (2013). Electrochemically reduced graphene porous material as light absorber for light-driven thermoelectric generator. *Journal of Materials Chemistry, 22*(34), 17800-17804.
176. Joanni, E.; Savu, R.; de Sousa Goes, M.; Bueno, P. R.; de´ Freitas, J. N.; Nogueira, A. F.; Longo, E.; Varela, (2007). J. A. Scr. Mater, 57, 277.
177. Chappel, S.; Grinis, L.; Ofir, A.; Zaban, (2005). A. J. Phys. Chem. B, 109, 1643. (151)
178. Sun, Y., Sun, M., & Xie, D. (2018). Graphene Electronic Devices. In H. Zhu, Z. Xu, D. Xie, & Y. Fang, *Graphene: Fabrication, Characterizations,Properties and Applications* (pp. 103-155). London, United Kingdom: Academic Press.
179. W. Ahmad, A. Singh, K.K. Jaiswal, P. Gupta (2021). Synthesis of Photocatalytic TiO_2 Nanoparticles for Potential Application in Photochemical Degradation of Ornidazole, J. Inorg. Organomet. Polym Mater., 31 (2), pp. 614-623
180. Long, R.; English, N. J.; Prezhdo, O. V. J.(2012) Am. Chem. Soc, 134, 14238
181. Yang, N. (2017). *The Preparation of Nano Compositesand TheirApplications in SolarEnergy Conversion.* Verlag, Germany: Springer.
182. Zheng, H.; Neo, C. Y.; Mei, X.; Qiu, J.; Ouyang, J. (2012). J. Mater. Chem., 22, 14465.
183. Yum, J. H., Baranoff, E., Wenger, S., Nazeeruddin, M. K., & Gratzel, M. (2011). Panchromatic engineering for dye-sensitized solar cells. *Energy and Environmental Science, 4*(3), 842–857.
184. Fang, X.; Li, M.; Guo, K.; Zhu, Y.; Hu, Z.; Liu, X.; Chen, B.; Zhao, X. Improved properties of dye-sensitized solar cells by incorporation of graphene into the photoelectrodes. Electrochim. Acta 2012, 65, 174–178.

185. Mihalache, I., Radoi, A., Mihalia, M., Munteanu, C., Marin, A., Danila, M, (2015). Charge and energy transfer interplay in hybrid sensitized solar cells mediated by grapheme quantum dots. Electrochim 153, 306-315

186. Whelan, Patrick R.; Jessen, Bjarke S.; Wang, Ruizhi; Luo, Birong; Stoot, Adam C.; Mackenzie, David M.A.; Braeuninger-Weimer, Philipp; Jouvray, Alex; Prager, Lutz; Camilli, Luca; Hofmann, Stephan; Bøggild, Peter; Booth, Timothy J. (2017). *Raman spectral indicators of catalyst decoupling for transfer of CVD grown 2D materials. Carbon, 117(), 75–81.* doi:10.1016/j.carbon.2017.02.028.

187. C.T. Cherian, F. Giustiniano, I. Martin-Fernandez, H. Andersen, J. Balakrishnan, B. Özyilmaz, "Bubblefree" electrochemical delamination of CVD graphene films, Small. 11 (2015) 189–194. doi:10.1002/smll.201402024.

188. Zhang, Dongzhi; Sun, Yan'e; Li, Peng; Zhang, Yong (2016). *Facile Fabrication of MoS2-Modified SnO2 Hybrid Nanocomposite for Ultrasensitive Humidity Sensing. ACS Applied Materials & Interfaces, (), acsami.6b02206–*. doi:10.1021/acsami.6b02206

189. Wang, Pengfei; Jiang, Zhenxue; Ji, Wenming; Zhang, Chen; Yuan, Yuan; Chen, Lei; Yin, Lishi (2016). *Heterogeneity of intergranular, intraparticle and organic pores in Longmaxi shale in Sichuan Basin, South China: evidence from SEM digital images and fractal and multifractal geometries. Marine and Petroleum Geology, (), S0264817216300204–*. doi:10.1016/j.marpetgeo.2016.01.020

190. Wang, Zhong-Min; Wagner, Jeff; Ghosal, Sutapa; Bedi, Gagandeep; Wall, Stephen (2017). *SEM/EDS and optical microscopy analyses of microplastics in ocean trawl and fish guts. Science of The Total Environment, 603-604(), 616–626.* doi:10.1016/j.scitotenv.2017.06.047

191. Huayue Zhu; Ru Jiang; Ling Xiao; Yuhua Chang; Yujiang Guan; Xiaodong Li; Guangming Zeng (2009). *Photocatalytic decolorization and degradation of Congo Red on innovative crosslinked chitosan/nano-CdS composite catalyst under visible light irradiation. , 169(1-3), 933–940.*

192. Murakami, T. N.; Gratzel, M. (2008). Inorg. Chim. Acta, 361, 572

193. Desilvestro, H.; Boz, M.; Tulloch, S.; Tulloch, G (2010).In Dye Sensitized Solar Cells; Kalyanasundaram, K., Ed.; EPFL Press: Lausanne (189).

194. Hong, W.; Xu, Y.; Lu, G.; Li, C.; Shi, G. (2008).Electrochem. Commun. 10, 1555.

195. Choi, J.H., Kang, S.H., Oh, H.S., Yu, T.H. and Sohn, I.S. (2011) Design and Characterization of Ga-Doped Indium Tin Oxide Films for Pixel Electrode in Liquid Crystal Display. Thin Solid Films, 527, 141-146
196. Hsieh, C.-T.; Yang, B.-H.; Chen, Y.-F. (2012). Diamond Relat. Mater, 27−28, 68
197. Jang, H.-S., Yun, J.-M., Kim, D.-Y., Park, D.-W., Na, S.-I., Kim, S.-S., 2012. Electrochim. Acta 2012 (81), 301. Zheng, H., Neo, C.Y., Mei, X., Qiu, J., Ouyang, J., 2012. J. Mater. Chem. 22, 14465.
198. Zheng, H., Neo, C.Y., Mei, X., Qiu, J., Ouyang, J., 2012. J. Mater. Chem. 22, 14465.
199. Yang, N., 2017. The Preparation ofNano Compositesand TheirApplications in SolarEnergy Conversion. Springer, Verlag, Germany.
200. Lee, J.S.; Ahn, H.J.; Yoon, J.C.; Jang, J.H. (2012). Three dimensional nano foam of few layer graphene grown by CVD for DSSC. Physical chemistry chemical physics, 14(22) 7939-7943.
201. Gong, F.; Li, Z.; Wang, H.; Wang, Z.-S. (2012). J. Mater. Chem., 22, 17321
202. Shixin Wu, HuiqinZheng , Chin Yong Neo, and JianyongQuayang. (2013). Highly efficient iodide/triodide Dye sensitized solar cells with gel-coated reduce grapheme…. Applied materials & interface, 5 (14), 66657-6664
203. Roy-Mayhew, J. D.; Boschloo, G.; Hagfeldt, A.; Aksay, I. A. (2012). ACS Appl. Mater. Interfaces, 4, 2794.
204. *Wang, W. S., Wang, D. H., Qu, W.G., Lu, L. Q., Xu, A.W., (2012). Large ultrathin anatase TiO_2 nanosheets with exposed 001 facets on graphene for enhanced visible light photocatalytic activity, J. Phys. Chem. C 116 19893-19901.*
205. Afshana Afroj Bristi, S. M. Jahadun-Nobi, Md Nurul Abser, Md Mehadi Hassan. (2020). Performance Comparison of Cost Efficient Natural Dye Sensitized Solar Cell. American Journal of Electrical Power and Energy Systems. Vol. 9, No. 4, pp. 60-66. doi: 10.11648/j.epes.20200904.11
206. Simon, J., and Mosey, G.. Feasibility Study of Economics and Performance of Solar Photovoltaics at the VAG Mine Site in Eden and Lowell, Vermont. A Study Prepared in Partnership with the Environmental Protection Agency for the RE-Powering America's Land Initiative: Siting Renewable Energy on Potentially Contaminated Land and Mine Sites. United States: N. p., 2013. Web. doi:10.2172/1076623.

207. Fabian Schoden; Marius Dotter; Dörthe Knefelkamp; Tomasz Blachowicz; Eva Schwenzfeier Hellkamp (2021).. *Review of State of the Art Recycling Methods in the Context of Dye Sensitized Solar Cells . Energies, (), –.* doi:10.3390/en14133741

208. Baruch-Mordo, S.; Kiesecker, J.; Kennedy, C.M.; Oakleaf, J.R.; Opperman, J.J. Erratum (2019). From Paris to Practice: Sustainable Implementation of Renewable Energy Goals. Environ. Res. Lett. , 14, 024013

209. Charles, Rhys G.; Davies, Matthew L.; Douglas, Peter (2016). *[IEEE 2016 Electronics Goes Green 2016+ (EGG) - Berlin, Germany (2016.9.6-2016.9.9)] 2016 Electronics Goes Green 2016+ (EGG) - Third generation photovoltaics — Early intervention for circular economy and a sustainable future. , (), 1–8.* doi:10.1109/EGG.2016.7829820

210. Sarita Bose, Virendra Soni and K. R. Genwa (2015). Recent Advances and Future Prospects for Dye Sensitized Solar Cells: A Review, International Journal of Scientific and Research Publications, Volume 5, Issue 4, April 2015 1 ISSN 2250-3153

211. Hardin.B.E, H.J. Snaith, M.D. McGehee. The renaissance of dye-sensitized solar cells. Nature Photonics 6.3 (2012) 162-169.

212. Gratzel Michael (2005). Photovoltaic performance and long-term stability of dye-sensitized meosocopic solar cells, Published by Elsevier, C.R. Chimie 9 (2006), pp578-583

213. Gómez-Ortíz N.M., I.A. Vázquez-Maldonado, A.R. Pérez-Espadas, G.J. Mena-Rejón, J.A. Azamar-Barrios, G. Oskam, (2009). Dye-sensitized solar cells with natural dyes extracted from a chiote seeds. Sol. Energy Mater. Sol. Cells, 94: 40-44.

214. Law ChunHung, Shehan C Pathirana, Xaioe Li, Assaf Y Anderson, Piers RF Barnes, Andrea Listorti, Tarek H Ghaddar, et al. (2010). Water-based electrolytes for dye-sensitized solar cells. *Advanced Materials, 22*(40), 4505–4509.

215. Yang, M., Thompson, D., and Meyer, G. (2000). Dual Sensitization Pathways of TiO2 by Na2[Fe(bpy)(CN)4]. Inorg. Chem. Vol. 39, pp. 3738-3739.

216. Hao, S.; Wu, J.; Huang, Y. & Lin, J. (2006). Natural dyes as photosensitizers for dye-sensitized solar cell. Sol. Energy, Vol. 80, Issue 2, pp. 209-214.

217. Kumara, G.R.A., Kanebo, S., Okuya, M., Onwaona-Agyeman, B., Konno, A., and Tennakone, K. (2006) . Sol. Enrgy Mater. Sol. Cells, Vol. 90, pp.1220.

218. Polo, A.S., and Iha, N.Y. (2006). Blue sensitizers for solar cells: natural dyes from Calafate and Jaboticaba. Sol. Energy Mater. Sol. Cells, Vol. 90, pp.1936-1944.

219. Jasim, K. E. & Hassan, A.M. (2009). Nanocrystalline TiO2 based natural dye sensitised solar cells. Int. J. Nanomanufacturing, Vol. 4, Nos. 1/2/3/4, pp.242–247.

220. Jasim, K. E.; Al Dallal, S. & Hassan, A.M. (2011). Natural dye-sensitised photovoltaic cell based on nanoporous TiO2, Int. J. Nanoparticles,(in press 2011).

221. Kay. A and Gratzel M, (1993) Natural Pigment-Based Dye-Sensitized Solar Cells, J. Phys. Chem., 97 (23): 6272– 6277.

222. Chiba, Yasuo; Islam, Ashraful; Watanabe, Yuki; Komiya, Ryoichi; Koide, Naoki; Han, Liyuan (2006). *Dye-Sensitized Solar Cells with Conversion Efficiency of 11.1%. Japanese Journal of Applied Physics, 45(No. 25), L638–L640.* doi:10.1143/JJAP.45.L638

223. Jiang-Yang Shao, Dongmei Li, Jiangjian Shi, Chuang Ma, Yousheng Wang, Xiaomin Liu, Xianyuan Jiang, Mengmeng Hao, Luozheng Zhang, Chang Liu, Yiting Jiang, Zhenhan Wang, Yu-Wu Zhong, Shengzhong Frank Liu, Yaohua Mai, Yongsheng Liu, Yixin Zhao, Zhijun Ning, Lianzhou Wang, Baomin Xu, Lei Meng, Zuqiang Bian, Ziyi Ge, Xiaowei Zhan, Qingbo Meng (2023). Recent progress in perovskite solar cells: material science, *Science China Chemistry* volume 66, pages10–64

224. C. Liu, C. Xiao, C. Xie, W. Li (2021). Flexible organic solar cells: Materials, large-area fabrication techniques, and potential applications, Nano Energy, 89, Article 106399

225. Zhang, R., and Li, X. (2018). Multidimensional Assemblies of Graphene. In H. Zhu, Z. Xu, D. Xie, & Y. Fang, *Graphene: Fabrication, Characterizations, Properties and Applications* (pp. 27-72). London, United Kingdom: Academic Press.

226. Zhong-Sheng Wang, Hiroshi Kawauchi, Takeo Kashima, Hironori Arakawa. (2004) Review significant influence of TiO2 photo electrode morphology on the energy conversion efficiency of N719 dye-sensitized solar cell Elsevier.

227. Nonjabulo P.D. Ngidi, Edigar Muchuweni, Vincent O. Nyamori (2021). Dual heteroatom-doped reduced graphene oxide and its application in dye-sensitized solar cells, Optical Materials, Volume 122, Part B, 111689

228. S. A. Sapp, C. M. Elliott, C. Contado, S. Caramori and C. A. Bignozzi, J Am Chem Soc, 124 (37) (2002) 11215-11222.

229. Sujit, B., Plawan, K. J., Nirmalya, B.(2022). Unusual enhancement in efficiency of DSSCs upon modifying photoanodes with reduced graphene oxide. https://pubs.rsc.org/en/journals/journal/ra

230. Chen, K., Chen, L., Chen, Y., Bai, H., & Li, L. (2012). Three-dimensional porous graphene-based composite materials:electrochemical synthesis and application. *Journal of Materials Chemistry, 22*(39), 20968-20976.

231. Karan, S., Subhrajit, K., Pramod, K. S., Bhaskar, B.,(2019). Utilizing reduced graphene oxide for achieving better efficient dye sensitized solar cells, Journal of Alloys and Compounds, Volume 788, 2019, Pages 672-676,https://doi.org/10.1016/j.jallcom.2019.02.287.

232. Battumur, T. Sarfraj Mujawar, H. and Truong, T. Q. (2012). Graphene/Carbon Nanotubes composites as a counter counter electrode for dye sensitized solar cells. *Current Applied Physics,* 12 (1), pp49-pp53.

233. Yi-Chun Chiang, Wei-Yun Cheng and Shih-Yuan Lu (2012). Titania Aerogels as a Superior Mesoporous Structure for Photoanodes of Dye-Sensitized Solar Cells , Int. J. Electrochem. Sci., 7 6910 – 6919

234. Seok-Soon, Kim, Nah, Yoon-Chae, Noh, Yong-Young, Jo, Jang, Kim, Dong-Yu, 2006. Electrodeposited pt for cost-efficient and flexible dye-sensitized solar cells. Electrochim. Acta 51 (18), 3814–3819.

235. S.A. Hasan, J.A. Salman, S.S. Al-Jubori (2021). Biosynthesis and Characterization of TiO2 Nanoparticles by Lactococcus lactis ssp. lactis. Al-Mustansiriyah Journal of Science, 32 (4), pp. 21-25

236. Alagesan, W. and Hong-Wen. (2012). Effect of hydroxyl group attachment on dye sensitized solar cells. *Applied Surface Science,* Vol 258 (20), pp. 7833-7838.

237. Andualem A and Demiss S., (2018). Review on Dye-Sensitized Solar Cells (DSSCs), Edelweiss Appli Sci Tech 2: 145-150

238. Gong, Jiawei; Sumathy, K.; Qiao, Qiquan; Zhou, Zhengping (2017). *Review on dye-sensitized solar cells (DSSCs): Advanced techniques and research trends. Renewable and Sustainable Energy Reviews, 68(), 234–246.* doi:10.1016/j.rser.2016.09.097

239. F. De Rossi, T.M. Brown, T. Pontecorvo (92015). Flexible photovoltaics for light harvesting under LED lighting, In 2015 IEEE 15th International Conference on Environment and Electrical Engineering (EEEIC), IEEE (2015), pp. 2100-2103

240. Arakawa, H. (2007). Recent Advances in Research and development for Dye-sensitized solar Cells II. CMC Publishing.

241. Kimpa, I.M. (2016) Fabriction and Analysis of Dye Sensitized Solar Cells Using Natural Dyes Extracted from Pawpaw Leaf and Flame Tree Flower and the Synthetic Rutheniumn Dye. Master's Thesis, Usmanu Danfodiyo University, Sokoto.

242. Ahmed, M.H.M., Muraza, O., Galadima, A., Yoshioka, M., Yamani, Zain, H. and Yokoi, T. (2019) Choreographing Boron-Aluminum Acidity and Hierarchical Porosity in BEA Zeolite by in-Situ Hydrothermal Synthesis for a Highly Selective Methanol to Propylene Catalyst. Microporous and Mesoporous Materials, 273, 249-255. https://doi.org/10.1016/j.micromeso.2018.06.036

243. Hoseinnezhad, M. and Gharanjig, K. (2018) Synthesis and Application of an Organic Dye in Nanostructure Solar Cells Device. World Academy of Science, Engineering and Technology: International Journal of Chemical and Molecular Engineering, 12, 438-441.

244. Suriani, A.B.; Fatiatun, ; Mohamed, A.; Muqoyyanah, ; Hashim, N.; Rosmi, M.S.; Mamat, M.H.; Malek, M.F.; Salifairus, M.J.; Abdul Khalil, H.P.S. (2018). *Reduced Graphene Oxide/Platinum Hybrid Counter Electrode Assisted by Custom-Made Triple-tail Surfactant and Zinc Oxide/Titanium Dioxide Bilayer Nanocomposite Photoanode for Enhancement of DSSCs Photovoltaic Performance. Optik, (), S0030402618301694*–. doi:10.1016/j.ijleo.2018.02.013

245. Okoye Ikechukwu Francis, Alaekwe Ikenna (2021). Review of Dye-Sensitized Solar Cell (DSSCs) Development, Natural Science, Vol.13 No.12, 496-509.DOI: 10.4236/ns.2021.1312043

246. Khalil Abraham James (2014). Dye Sensitized Solar Cells – Working Principles, Challenges and Opportunities, Department of Physics, University of Bahrain, Kingdom of Bahrain, pp 171 = 195

247. M. Amrollahi-Sharifabadi, M. K. Koohi, E. Zayerzadeh, M. H. Hablolvarid, J. Hassan, and A. M. Seifalian (2018). "In vivo toxicological evaluation of graphene oxide nanoplatelets for clinical application," *International Journal of Nanomedicine*, vol. Volume 13, pp. 4757–4769,

248. H. R. H. Mohamed, M. Welson, A. E. Yaseen, and A. A. El-Ghor [2020] "Estimation of genomic instability and mutation induction by graphene oxide nanoparticles in mice liver and brain tissues," *Environmental Science and Pollution Research*, vol. 27, no. 1, pp. 264–278,.

249. N. Zahin, R. Anwar, D. Tewari et al. [2020] "Nanoparticles and its biomedical applications in health and diseases: special focus on drug delivery," *Environmental Science and Pollution Research*, vol. 27, no. 16, pp. 19151–19168.

250. Breyer, C. and A. Gerlach. (2011). Global Overview on Grid-Parity Event Dynamics, Proceedings of the 26th European Photovoltaic Solar Energy Conference, 5 – 9 September, Hamburg.C.

251. IEA International Statistics 2005 (http://www.iea-pvps.org/isr/index.htm)

252. Ezenwa, I.A. and Ekpunobi, A.J. (2010) Deposition and Characterization of Cds Thin Film by Chemical Bath Method. The Pacific Journal of Science and Technology, 11, 435-440.

253. International Energy Agency. (2012). *Key World Energy Statistics 2012*. Paris, France: International Energy Agency.

254. Zweibel K, (2004) "PV as a major source of global electricity", Conference at the University of Toledo (OH), 2/24/2004 (http://www.greenenergyohio.org/page.cfm?pageId=500).

255. Brabec, J.A. Hauch, P. Schilinsky, C. Waldauf,(2005). Production aspects of organic photovoltaics and their impact on the commercialization of devices. MRS Bulletin, 30, p. 50.

256. Green.A. Emery, K. King, D.L. Hishikawa, Y. Warta, W. (2006) *Solar cell efficiency tables (version 28)*.Prog. Photovoltaic. Res. Appl., 14(5), pp. 455 I

257. EIA, Independent Statistics and Analysis, U.S Energy Information Administration (2022), Solar Explained, Solar Ener gy and Environment, https://www.eia.gov/energyexplained/solar/solar-energy-and-the-environment.php

258. Huynh, W.U. Peng, X. Alivisatos, A.P. (1999). CdSe nanocrystal Rods/Poly(3-hexylthiophene) composite photovoltaic devices. *Adv. Mater*., 11(11), pp. 923 M

259. IRENA and Data from Japan's National Institute for Advanced Industrial Science and Technology (AIST, 2010)

260. Bony et al. (2010), Achieving Low-Cost Solar PV: Industry Workshop Recommendations for NearTerm Balance of System Cost Reductions. Rocky Mountain Institute, Co.

261. Mott MacDonald (2011), Costs of low-carbon generating technologies, Mott MacDonald, Bristol.

262. Xu , *Y, Bai, H, Lu, G, Li, G, Shi (*2008). Flexible graphene film via the filtration or water soluble non- covalent funtionalized graphene sheet, J.AM, Chem SOC. 130, 5856-5857

263. Daulay S, Madsuha A. F, Rosa E.S and YuwonaA.H (2019): Fabrication of Titanium Dioxide-reduced Graphene Oxide (TiO_2) nanocomposite as the photoanode on Dye Sensitized Solar Cell. 4th annual applied science and engineering conference. Journal of Physics. 1742-6596.

264. Hummers W. S and Offeman R.E(1958): Preparation of Graphene Oxide Journal of the American Chemical Society 80(6) 1339

265. Phiri J, Gane P and Maloney (2017). General overview of graphene; Production, properties and application in polymer composites Materials Science and Engineering : B. 2159 -28

266. Fang Xiaoming, Tingli Ma, Guo qing Guan, Morito Akiyama, Tetsya Kida and Eiichi Abe. (2004). Effect of the thickness of the pt film coated on a counter electro de on the p erformance of a dye-sensitized solar cell. *Journal of Electroanalytical Chemistry, 570*(2), 257–263.

267. Meyer, Jannik C.; Sundaram, Ravi S.; Chuvilin, Andrey; Kurasch, Simon; Burghard, Marko; Kern, Klaus; Kaiser, Ute; Gómez-Navarro, Cristina (2010). *Atomic Structure of Reduced Graphene Oxide. , 10(4), 1144–1148.* doi:10.1021/nl9031617

268. Agilent. (2014). IV and CV Characterizations of Solar / Photovoltaic Cells Using the B1500A. Application Note B1500A-14, (Cv). Retrieved from http://cp.literature.agilent.com / litweb/p df/5990-4428EN.pdf

269. Mikko Kokkonen;Parisa Talebi;Jin Zhou;Somayyeh Asgari;Sohail Ahmed Soomro;Farid Elsehrawy;Janne Halme;Shahzada Ahmad;Anders Hagfeldt;Syed Ghufran Hashmi; (2021). *Advanced research trends in dye-sensitized solar cells . Journal of Materials Chemistry A, (), –.* doi:10.1039/d1ta00690h

270. Y. Saygili, M. Stojanovic, N. Flores-D´ıaz, S. M. Zakeeruddin, N. Vlachopoulos, M. Gr¨atzel and A. Hagfeldt,(2019). Inorganics, 7, 30
271. S. C. Pradhan, A. Hagfeldt and S. Soman, J. Mater. Chem. A, 2018, 6, 22204–22214
272. Cheng, Pei; Zhan, Xiaowei (2016). *Stability of organic solar cells: challenges and strategies. Chem. Soc. Rev., (), 10.1039.C5CS00593K*–. doi:10.1039/C5CS00593K
273. S. Venkatesan, I.-P. Liu, W.-N. Hung, H. Teng and Y.-L. Lee, Chem. Eng. J., 2019, 367, 17–24
274. Chalkias, D.A.; Loizos, D.D.; Papanicolaou, G.C. (2020). *Evaluation and prediction of dye-sensitized solar cells stability under different accelerated ageing conditions. Solar Energy, 207(), 841–850.* doi:10.1016/j.solener.2020.06.115
275. Asghar, M.I., Zhang, J., Wang, H., Lund, P.D., 2017. Device stability of perovskite solar cells – a review. Renew. Sustain. Energy Rev. 77, 131–146.
276. Chalkias, D.A., Laios, A.I., Petala, A., Papanicolaou, G.C., 2018b. Evaluation of the limiting factors affecting large-sized, flexible, platinum-free dye-sensitized solar cells performance: a combined experimental and equivalent circuit analysis. J. Mater. Sci. Mater. Electron. 29, 9621–9634.
277. Khenkin, M.V., Katz, E.A., Abate, A., Bardizza, G., Berry, J.J., Brabec, C., Brunetti, F., Bulović, V., Burlingame, Q., Di Carlo, A., Cheacharoen, R., Cheng, Y.-B., Colsmann, A., Cros, S., Domanski, K., Dusza, M., Fell, C.J., Forrest, S.R., Galagan, Y., Di Girolamo, D., Grätzel, M., Hagfeldt, A., von Hauff, E., Hoppe, H., Kettle, J., Köbler, H., Leite, M.S., Liu, S.F., Loo, Y.-L., Luther, J.M., Ma, C.-Q., Madsen, M., Manceau, M., Matheron, M., McGehee, M., Meitzner, R., Nazeeruddin, M.K., Nogueira, A.F., Odabaşı, Ç., Osherov, A., Park, N.-G., Reese, M.O., De Rossi, F., Saliba, M., Schubert, U.S., Snaith, H.J., Stranks, S.D., Tress, W., Troshin, P.A., Turkovic, V., Veenstra, S., Visoly-Fisher, I., Walsh, A., Watson, T., Xie, H., Yıldırım, R., Zakeeruddin, S.M., Zhu, K., Lira-Cantu, M., (2020). Consensus statement for stability assessment and reporting for perovskite photovoltaics based on ISOS procedures. Nat. Energy 5, 35–49.
278. Kontaxis, L.C., Pavlou, C., Portan, D.V., Papanicolaou, G.C., 2018. Effect of saline absorption on the flexural stress relaxation behavior of epoxy/cotton composite materials for orthopedics applications. In: AIP Conference Proceedings. AIP Publishing, p. 030020.

279. Wu, Xu; Shao, Yan; Liu, Hang; Feng, Zili; Wang, Ye-Liang; Sun, Jia-Tao; Liu, Chen; Wang, Jia-Ou; Liu, Zhong-Liu; Zhu, Shi-Yu; Wang, Yu-Qi; Du, Shi-Xuan; Shi, You-Guo; Ibrahim, Kurash; Gao, Hong-Jun (2017). *Epitaxial Growth and Air-Stability of Monolayer Antimonene on PdTe ₂*. *Advanced Materials, 29(11), 1605407–*. doi:10.1002/adma.201605407.

280. Wu, J, Shi, G, Anderson, B et al 2015, 'Stability conditions and phase transition for Kalman filtering over Markovian channels', *Chinese Control Conference, CCC 2015*, ed. Zhao Q.Liu S., IEEE, Online, pp. 6721-6728.

281. Stefan Haid; Magdalena Marszalek; Amaresh Mishra; Mateusz Wielopolski; Joël Teuscher; Jacques-E. Moser; Robin Humphry-Baker; Shaik M. Zakeeruddin; Michael Grätzel; Peter Bäuerle (2012). *Significant Improvement of Dye-Sensitized Solar Cell Performance by Small Structural Modification in π-Conjugated Donor–Acceptor Dyes. , 22(6), 1291–1302.* doi:10.1002/adfm.201102519

282. Zhang S. (2017). Study of florine-doped tin oxide (FTO) thin fims for photovoltaics applications. Université Grenoble Alpes,.

283. Ginley D., Hosono H., Paine D. C. (2010). *Handbook of Transparent Conductors; Springer Science and Business Media.*

284. Longo C. and De Paoli. (2003.). M-A. Dye-Sensitized Solar Cells: a Successful Combination of Materials. *J. Braz. Chem. Soc., 14*, 889-901.

285. Yang, N., Zhai, J., Wang, D., Chen, Y., & Jiang, L. (2011). Two-Dimensional Graphene Bridges Enhanced Photoinduced Charge Transport in Dye-Sensitized Solar Cells. *ACS Nano, 4*(2), 887–894

286. Sujit, B., Plawan, K. J., Nirmalya, B.(2022). Unusual enhancement in efficiency of DSSCs upon modifying photoanodes with reduced graphene oxide. https://pubs.rsc.org/en/journals/journal/ra

287. Napi, Muhammad L. M.; Sultan, S. M.; Ismail, Razali; Ahmad, Mohd K.; Chai, G. M. T. (2019). *Optimization of a Hydrothermal Growth Process for Low Resistance 1D Fluorine-Doped Zinc Oxide Nanostructures. Journal of Nanomaterials, 2019(), 1–10.* doi:10.1155/2019/4574507

288. Nurdin, N.; Hatta, M.; Mashoreng, S.; Amri, K.; Pulubuhu, D.A.T.; Aris, A.; AS, M.A.; Komatsu, T. (2019). Remote Sensing of Population and Coral Destruction for Long Term on Small Islands. Preprints 2019, 2019110173 (doi: 10.20944/preprints201911.0173.v1).

289. Subalakshmi, K., and Senthilselvan, J. (2018). Effect of fluorine-doped TiO2 photoanode on electron transport, recombination dynamics and improved DSSC efficiency, Solar Energy, Volume 171, Pp.914-928.

290. Yu, S.; Freitas, J. N.; Nogueira, A. F.; Wang, Y.; Ahmad, S.; Wang, Z.-S (2016). DyeSensitized Solar Cells Employing Polymers. Prog. Polym. Sci. 2016, 59, 1–40.

291. Alejandra Chavarría-Castilloa , Patricia Amézaga-Madrida *, Oswaldo Esquivel-Pereyraa , Wilber Antúnez-Floresa , Pedro Pizá Ruiza , Mario Miki-Yoshidaa (2016). Synthesis and Microstructural Characterization of SnO2 :F Thin Films Deposited by AACVD Karen, Materials Research; 19(Suppl. 1): 97-102, DOI: http://dx.doi.org/10.1590/1980-5373-MR-2016-0350

292. Noh S. I., Han H.I, Riu D.(2012). Photovoltaic property dependence of dye-sensitized solar cells on sheet resistance of FTO substrate depositedvia spray pyrolysis, Ceram. Int. 38, 3735-3739.

293. Oluwaseun Adedokun, Victoria Mofoluke Odebunmi and Yekinni Kolawole Sanusi (2019). Effect of Annealing Temperature on Structural, Optical and Electrical Properties of Spin Coated Tin Oxide Thin Films for Solar Cells Application, Int. J. Thin. Fil. Sci. Tec. 8, No. 3, 157-162 (2019) 157 I

294. Oluwaseun Adedokun et al., (2019). Citrus fruit peels extracts as light harvesters for efficient ZnO-based dye-sensitized solar cells, J. Phys.: Conf. Ser. 1299 012010

295. Arifin, Zainal; Soeparman, Sudjito; Widhiyanuriyawan, Denny; Suyitno, Suyitno (2017). *Performance Enhancement of Dye-Sensitized Solar Cells Using a Natural Sensitizer. International Journal of Photoenergy, 2017(), 1–5.* doi:10.1155/2017/2704864

296. Waode Sukmawat Arsyad, Aricia Pristian, La Argusu and Rahman Itidayat (2019): rGO based photoanode in Dye Sensitized Solar Cells and its photovoltaic characteristics. IOP Conference series: Materials Science and Engineering 622: 012008

297. N. Sakai, T. Miyasaka, and T. N. Murakami, “Efficiency enhancement of ZnO-based dye-sensitized solar cells by low-temperature $TiCl_4$ treatment and dye

optimization," *Journal of Physical Chemistry C*, vol. 117, no. 21, pp. 10949–10956, 2013.

298. F. Bella *et al.(2018).* Patterning dye-sensitized solar cell photoanodes through polymeric approach: a perspective, Mater. Sci. Semicond. Process.
299. Susilawati, ; Doyan, A.; Muliyadi, L.; Hakim, S.; Taufik, M.; Nazarudin, (2019). *Characteristics and Optical Properties of Fluorine Doped SnO ₂ Thin Film Prepared by a Solâ€ "Gel Spin Coating. Journal of Physics: Conference Series, 1397(), 012003*–. doi:10.1088/1742-6596/1397/1/012003
300. Suyitno, A. Zainal, A. S. Ahmad, T. S. Argatya, and Ubaidillah, "Optimization parameters and synthesis of fluorine doped tin oxide for dye-sensitized solar cells," *Applied Mechanics and Materials*, vol. 575, pp. 689–695, 2014
301. Suyitno, A. Zainal, A. S. Ahmad, T. S. Argatya, and Ubaidillah, "Optimization parameters and synthesis of fluorine doped tin oxide for dye-sensitized solar cells," *Applied Mechanics and Materials*, vol. 575, pp. 689–695, 2014
302. Peter N, O. Gillospie and Natalia Martsinorich (2019): Origin of Charge Trapping in TiO_2/Reduced graphene oxide photocatalytic composite: Insight from theory. Applied materials and interfaces 11, 3190-31922

303. Gong, F.; Xu, X.; Zhou, G. (2013). Graphene as counter electrode for DSSC. Electrochim Acta, 66, 151.
304. Roy-Mayhew, J. D.; Bozym, D.J, Punct C and Askay I.A. (2010). Functionalized grapheme as catalytic counter electrode in DSSC. ACS Nano, 4 (10) 6203-6211.
305. Yun, S. et al. (2018). New-generation integrated devices based on dye-sensitized and perovskite solar cells. Energy Environ. Sci. 11, 476–526
306. Chindaprasirt, P. & Rattanasak, U. (2017). Characterization of the high-calcium fy ash geopolymer mortar with hot-weather curing systems for sustainable application. Adv. Powder Technol. 28, 2317–2324
307. Nwofe, P.A. (2015). Influence of Film Thickness on the Optical Properties of Antimony Sulphide Thin Films Grown by the Solution Growth Technique. Euro. J. Appl. Eng. Sci. Res., 2015, 4 (1):1-6
308. Zeng R, Mannaerts CM and Lievens C (2023), Assessment of UV-VIS spectra analysis methods for quantifying the absorption properties of chromophoric dissolved organic matter (CDOM). Front. Environ. Sci. 11:1152536. doi: 10.3389/fenvs.2023.1152536
309. Zhang Shawn Divitt, Qingbin Fan, Wenqi Zhu, Amit Agrawal, Yanqing Lu, Ting Xu, and Henri J. Lezec (2020). Low-loss metasurface optics down to the deep ultraviolet region, Science & Applications), 2047-7538, https://doi.org/10.1038/s41377-020-0287-y

310. Çiplak, Zafer; Yildiz, Nuray; Çalimli, Ayla (2015). *Investigation of Graphene/Ag Nanocomposites Synthesis Parameters for Two Different Synthesis Methods. Fullerenes, Nanotubes and Carbon Nanostructures, 23(4), 361–370.* doi:10.1080/1536383x.2014.894025

311. Mäntele, Werner; Deniz, Erhan (2016). *UV-VIS Absorption Spectroscopy: Lambert-Beer reloaded. Spectrochimica Acta Part A: Molecular and Biomolecular Spectroscopy, (), S1386142516305558–.* doi:10.1016/j.saa.2016.09.037

312. Kanta, Uea-aree; Thongpool, Voranuch; Sangkhun, Weradesh; Wongyao, Nutthapon; Wootthikanokkhan, Jatuphorn (2017). *Preparations, Characterizations, and a Comparative Study on Photovoltaic Performance of Two Different Types of Graphene/TiO ₂ Nanocomposites Photoelectrodes. Journal of Nanomaterials, 2017(), 1–13.* doi:10.1155/2017/2758294

313. Tapa, A. R. et al. Porous rGO/ZnSe/CoSe2 dispersed in PEDOT:PSS as an efcient counter electrode for dye-sensitized solar cells. Mater. Chem. Front. 5, 2702–2714 (2021).

314. Sadhukhan, Sourav; Ghosh, Tapas Kumar; Rana, Dipak; Roy, Indranil; Bhattacharyya, Amartya; Sarkar, Gunjan; Chakraborty, Mukut; Chattopadhyay, Dipankar (2016). Studies on synthesis of reduced graphene oxide (RGO) via green route and its electrical property. Materials Research Bulletin, 79(), 41–51. doi:10.1016/j.materresbull.2016.02.039

315. Das, Tapas K.; Banerjee, Seemita; Pandey, M.; Vishwanadh, B.; Kshirsagar, R.J.; Sudarsan, V. (2017). *Effect of surface functional groups on hydrogen adsorption properties of Pd dispersed reduced graphene oxide. International Journal of Hydrogen Energy, 42(12), 8032–8041.* doi:10.1016/j.ijhydene.2016.12.024

316. Ghosh, Ruma; Nayak, Arpan Kumar; Santra, Sumita; Pradhan, Debabrata; Guha, Prasanta Kumar (2015). *Enhanced ammonia sensing at room temperature with reduced graphene oxide/tin oxide hybrid films. RSC Adv., 5(62), 50165–50173.* doi:10.1039/C5RA06696D

317. F. Bella *et al. (2017).* Interfacial effects in solid−liquid electrolytes for improved stability and performance of dye-sensitized solar cells ACS Appl. Mater. Interfaces.

318. Bella, F.; Gerbaldi, C.; Barolo, C.; Grätzel, M. Aqueous dye-sensitized solar cells. Chem. Soc. Rev. 2015, 44, 3431–3473

319. Peter, I. John; Vignesh, G.; Vijaya, Subbiah; Anandan, Sambandam; Ramachandran, K.; Nithiananthi, P. (2019). *Enhancing the power conversion efficiency of SrTiO3/CdS/Bi2S3 quantum dot based solar cell using phosphor. Applied Surface Science, (), S0169433219321282–*. doi:10.1016/j.apsusc.2019.07.092

320. Comes R.B., P.V. Sushko, S.M. Heald, R.J. Colby, M.E. Bowden, and S.A. Chambers. 2014. "Band-Gap Reduction and Dopant Interaction in Epitaxial La,Cr Co-doped SrTiO3 Thin Films." *Chemistry of Materials* 26, no. 24:7073-7082. PNNL-SA-105536. doi:10.1021/cm503541u

321. Pagin, Peter (2014), 'Pragmatic enrichment as coherence raising'. *Philosophical Studies* 168: 59-100

322. Sushko P.V., and S.A. Chambers. 2020. "Extracting band edge profiles at semiconductor heterostructures from hard-x-ray core-level photoelectron spectra." *Scientific Reports* 10. PNNL-SA-145389. doi:10.1038/s41598-020-69658-9

323. Jie, Zhang ; Javed, Hafiz Muhammad Asif ; Khan, M. Ijaz ; Awais, Muhammad ; Sarfaraz, Muhammad ; Que, Wenxiu ; Mustafa, Muhammad Salman ; Khan, Sami Ullah ; Khan, M. Riaz ; Galal, Ahmed M. ; Elnaggar, Ashraf Y. ; Masod, Mohamed Bakry ; Naixin, Tao (2022). Designing of TiO_2-rGO nanocomposite-based photoanode to enhance the performance of dye-sensitized solar cells, The European Physical Journal Special Topics, Volume 231, Issue 15, p.2919-2926 10.1140/epjs/s11734-022-00546-1

324. Kakiage K, Aoyama Y, Yano T, Otsuka T, Kyomen T, Unnoc M & Hanaya M (2014). Chemical communication, Vol 50, No 48, P 6379.

325. Daulay, S; Madsuha, A F; Rosa, E S; Yuwono, A H (2019). *Fabrication of Titanium Dioxide-reduced Graphene Oxide (TiO ₂ /rGO) nanocomposites as the Photoanode in Dye Sensitized Solar Cells. Journal of Physics: Conference Series, 1402(), 055101–*. doi:10.1088/1742-6596/1402/5/055101

326. Soedergren S., Hagfeldt A., Olsson J., Lindquist S.E. (1994). Theoretical Models for the Action Spectrum and the Current-Voltage Characteristics of Microporous Semiconductor Films in Photoelectrochemical Cells. *The Journal of Physical Chemistry, 98*(21), 5552-5556.

327. J Phiri, P Gane and T C Maloney 2017 General overview of graphene: Production, properties and application in polymer composites Materials Science and Engineering: B. 215 9-28.

328. Xu, T., Zhang, L., Cheng, H., Zhu, Y., 2011. Significantly enhanced photocatalytic performance of ZnO via graphine hybridization and the mechanism study. Appl. Catal. B 101, 382-387

329. Foo Wah Low, and Chin Weil Lai, 2018. Recent developments of graphene -TiO_2 composite nanomaterials as efficient photoeletrodes in dye-esensitized solar cells: A review. Journal of Renewable and Sustainable Energy Reviews 82, 103 -125

330. Arsyad, Waode Sukmawati; Pristianti, Aricia; Agusu, La; Hidayat, Rahmat (2019). *rGO based photo-anode in dye-sensitized solar cells (DSSC) and its photovoltaic characteristics. IOP Conference Series: Materials Science and Engineering, 622(), 012008*–. doi:10.1088/1757-899X/622/1/012008

331. W Wang, Z Wang, J Liu, Z Luo, SL Suib, et al. (2017) Single-step One-pot Synthesis of TiO_2 Nanosheets Doped with Sulfur on Reduced Graphene Oxide with Enhanced Photocatalytic Activity. Sci Rep 7: 46610

332. X Zhang, G Yi, Z Zhang, J Yu, H Fan, et al. (2021) Magnetic graphene-based nanocomposites as highly efficient absorbents for Cr(VI) removal from wastewater. Environ Sci Pollut Res Int 28(12): 14671-14680.

333. Yu, L.; Xu, W.; Liu, H.; Bao, Y. (2022). Titanium Dioxide–Reduced Graphene Oxide Composites for Photocatalytic Degradation of Dyes in Water. J. Catalysts, 12, 1340. https://doi.org/10.3390/ catal12111340

334. Fukugaichi, S. Fixation of Titanium Dioxide Nanoparticles on Glass Fiber Cloths for Photocatalytic Degradation of Organic Dyes. ACS Omega 2019, 4, 15175–15180.

335. Nazeeruddin K., Kay A., Rodicio I., Humphry-Baker R., Muller E., Liska P., Vlachopoulos N., and Gratzel M. (1993). Conversion of light to electricity by cis-x2bis (2, 2'-bipyridyl-4, 4'-dicarboxylate) ruthenium (ii) charge-transfer sensitizers (x= cl-, br-, i-, cn-, and scn-) on nanocrystalline titanium dioxide electrodes. *Journal of the American Chemical Society, 115*(14), 6382–6390.

336. Peter N, O. Gillospie and Natalia Martsinorich (2019): Origin of Charge Trapping in TiO_2/Reduced graphene oxide photocatalytic composite: Insight from theory. Applied materials and interfaces 11, 3190-31922

337. Meysam. Tayebi, Morteza Kolaei, Ahmed Tayyebi, Zohreh Masoumi, Zeynab Belbasi and Byeony – Kyu Lee (2019): Reduced graphene oxide(rGO) on TiO_2 for an improved photoelectrochemical and photocatalytic activity. Journal of Solar Energy 190: 185-194.

338. Gaya, U. I., Abdullah, A. H. (2008). Heterogeneous photocatalytic degradation of organic contaminants over titanium dioxide: a review of fundamentals, progress and problems. J. Photochem. Photobiol., C 9, 1 – 12

339. Liu, Z., Liu, Z., Cui, T., Li, J., Zhang, J., Chen, T., et al., (2014). Photocatalyst of two-dimensional honeycomb-like ZnOnanowells on zeolite. Chem. Eng. J. 235, 257-263.

340. Byrappa K, Subramani A.K, Ananda S, Rai K.M.L, Sunitha M.H, Basavalingu B, et al., (2006): Impregnation of ZnO onto activated carbon under hydrothermal conditions and its photobatalytic properties. J. Mater. Sci 41, 1355-1362.

341. Ching, Y. C., Rahman, A., Ching, K. Y., Sukiman, N. L., and Cheng, H. C. (2015)"Preparation and characterization of polyvinyl alcohol-based composite reinforced with nanocellulose and nanosilica," BioResources 10(2), 3364-3377. DOI:10.15376/biores.10.1.1519-1527

342. Gregory S.H Thien, Fatin Saiha Omar, Nur IlySyuhada Ahmad Biya, Wee Siong Chiu, Hong Ngee Lim, Ramin Yousefi, Farid-Jamali Heini, and Nay Ming Huang (2014). Improved Synthesis of Reduced Graphene Oxide -Titanium Dioxide Composite with Highly Exposed {001} Facets and its Photoelectrochemical Response. International Journal of Photoenergy. 650583, 9.

343. William, G., Kamat, P.V., 2019. Graphene- semiconductor nanocomposites: excited-state interactions between ZnO nanoparticles and graphene oxide. Langmuir 25, 13869-13873.

344. Bai X., Wang L., Zong R., Lv Y., Sun Y. and Zhu Y., (2013). Performance enhancement of ZnO photocatalyst via synergic effect of surface oxygen defect and graphene hybridization. Langmuir 29, 3097 -3105.

345. Adelkhani, H., Tayebi, M., (2018). Improve corrosion resistance of zircaloy by copper-graphene nanocomposite coatings. Russ. J. appl. Chem. 91, 2052-2057

346. Choi W., Lahiri I., Seelaboyina R. and Kang Y. S., (2010). Synthesis of graphene and its applications: a review. Crit. Rev. Solid State Matter. Sci. 35

347. Tayebi, M., Lee, B.K., (2019). Recent advances in BiVO4 semiconductor materials for hydrogen production using photoelectrochemical water splitting. Renew. Sustain.

348. Yufam Zhang, Fan Fu, Feng Zhou, Xi Yang, DesuoZhany and YuyueChen(2020): Synergistic effect of rGO/TiO_2 nanosheets with exposed (0.01 facets for boosting visible light photocatalytic activities, applied surface science, 510 -145 451

349. Bell N.J, Ng Y.H, Dui A, Coster H, Smith S.C, and Amal R. (2011): understanding the enhancement in phoelectrochemical properties of photocatalytical prepared TiO_2 – rGO composite. J. Phys. Chem. 115, 6004 -6009

350. Morais A. Longo C, Araujo J.R, Barroso M, Durrant J. R, Nogueiru A.F, Wang D, Manivannan A, Bristow A.D and Wu N.Q (2016): Nano crystalline anatase TiO_2/reduced Graphene Oxide Composite films as photoanode for photochemical water splitting studies; The role of reduced Graphene Oxide. Phys. Chem. 18, 2608-2616

351. Kumer P.V, Bernardi M and Grossman J.C (2013): The impact of functionalization on the reduced Graphene Oxide. ACS nano 7, 1638-1645

352. Boukhvalov D. W and Katsnelson M.I, (2008): Modelling of Graphite Oxide. J. AM. Chem.Soc. 130, 10697- 10701

353. Rouhani1 S., Hosseinnezhad M., Nasiri S.3, GharanjigK. (2021). Investigation of the Effect of rGO/TiO2 on Photovoltaic Performance of DSSCs Devices.Prog. Color Colorants Coat. 15 (2022), 123-131.

354. Cahen D. Hodes G. Gratzel M. GuillemolesJ. F. Riess I. (2000). Nature of photovoltaic action in dye-sensitized solar cells. *J. Phys. Chem. B, 104*(9), 2053-2059.

355. Yang, Li; Kruse, Björn (2004). *Revised Kubelka–Munk theory I Theory and application. josaa/21/10/josaa-21-10-1933.pdf, 21(10), 1933–0.* doi:10.1364/JOSAA.21.001933

356. Sakthivel, S.; Kisch, H (2003). Daylight photocatalysis by carbon-modified titanium dioxide. *Angew. Chem., Int. Ed. , 42*, 4908

357. Samsudin, E.M.; Abd Hamid, S. B.; Juan, J. C.; Basirun. W.J.; Kandjani, A. E. (2015). Surface modification of mixed-phase hydrogenated TiO_2 and corresponding photocatalytic response. Appl. Surf. Sci., 359, 883 - 896

358. Siddick, Siti Zubaidah; Lai, Chin Wei; Juan, Joon Ching; Hamid, Sharifah Bee (2017). Reduced Graphene Oxide – Titania nanocomposite film for improving Dye – Sensitized Solar Cell (DSSCs) performance. Current Nanoscience, 13(5), 494 -500

359. Hara K., Arakawa H. (2003). Current status of dye-sensitized solar cells. Semiconductor photochemistry and photophysics. (S. S. V. Ramamurthy and Kirk, Ed.) 123-171.

360. Zhao F, Dong B, Gao R, Su G, Liu W, Shi L, Xia C, Cao L (2015) A three-dimensional graphene-TiO_2 nanotube nanocomposite with exceptional photocatalytic activity for dye degradation. App Surf Sci 351:303–308. https://doi.org/10.1016/j.apsusc.2015.05.121

361. Aawani E, Memarian N, Dizaji HR (2018) Synthesis and characterization of reduced graphene oxide–V_2O_5 nanocomposite for enhanced photocatalytic activity under different types of irradiation. J Phys Chem Solids 125:8–15. https://doi.org/10.1016/j.jpcs.2018.09.028

362. Pronay Makal and Debajyoti Das (2021). Reduced Graphene Oxide-Laminated One-Dimensional TiO_2–Bronze Nanowire Composite: An Efficient Photoanode Material for Dye-Sensitized Solar Cells, *ACS Omega* 2021, 6, 6, 4362–4373,

363. M Z Iqbal and A-U Rehman 2018 Recent progress in graphene incorporated solar cell devices Solar Energy 169 634-47.

364. Das, D.; Makal, P. Narrow band gap reduced TiO_2-B:Cu nanowire heterostructures for efficient visible light absorption, charge separation and photocatalytic degradation. *Appl. Surf. Sci.* **2020**, *506*, 144880, DOI: 10.1016/j.apsusc.2019.144880

365. Tekerek, S., Kudret, A. & Alver, Ü (2011). Dye-sensitized solar cells fabricated with black raspberry, black carrot and rosella juice. Indian J Phys 85, 1469–1476 (2011). https://doi.org/10.1007/s12648-011-0166-8

366. Mehmood, Umer; Malik, M. Irfan; Ul Haq Khan, Anwar; Hussein, Ibnelwaleed A.; Harrabi, Khalil; Al-Ahmed, Amir (2018). *Effect of outdoor temperature on the power-conversion efficiency of newly synthesized organic photosensitizer based dye-sensitized solar cells. Materials Letters, (), S0167577X18304191–*. doi:10.1016/j.matlet.2018.03.055

367. Tarko Fentaw Emiru and Delele-Worku Ayele (2017) Controlled Synthesis, Characterization of graphene oxide. A convenient method for Large Scale Production, Egypt Journal of Basic and Applied Sciences, Vol. 4, Issue, Pp 74-79.

368. Das, Papari; Deoghare, Ashish B.; Maity, Saikat Ranjan (2020). *A Novel Approach to Synthesize Reduced Graphene Oxide (RGO) at Low Thermal Conditions. Arabian Journal for Science and Engineering, (), –*. doi:10.1007/s13369-020-04956-y

369. Kocijan, M.; Curkovi´c, L.; ´ Gonçalves, G.; Podlogar, M. (2022). The Potential of rGO@TiO2 Photocatalyst for the Degradation of Organic Pollutants in Water. Sustainability, 14, 12703. https://doi.org/ 10.3390/su141912703

370. Efficiency of Dye sensitized solar cell cells by co-sensitizing novel thieno (3, 2-b) indole-Based organics dyes with a promising porphyrin sensitizer. Advanced Energy Materials, 10 (15). doi:10.1002/aenm.202000124

371. Leonardo, R; Higor, O; Arcano M; Sebastian, S; Ana L. (2023). Evaluation of solar conversion efficiency in DSSCs using natural dyes extracted from alpinoa purpurata and Alstroemeria flower petals as novel photosensitizers. Colorants 2023, 2 (4), 618-631. https://doi.org/10.3390/colorants 2040032.

APPENDIX

Quantity of materials used

i. 0.1 mol $SnCl_2$

50ml x 225.6 x 0.1/1000 =1,128g

ii. 0.4 mol acetyl acetonate

50ml x 100.16 x0.4/1000 =2.003g

iii. 0.1 mol Ammonium fluoride (NH_4F)

20 ml x 37.04 x 0.1/1000 = 0.074g

Amount of dopant used

i. 4% doppant

4/100 X 200 ml = 8 ml

(8 ml ammonium fluoride was added to 192 ml Tin acetyl acetonate)

Similarly the above calculation was repeated for 8%, and 12% respectively);

8/100 X 200 ml =16 ml, (16 ml ammonium fluoride was added to 184 ml Tin acetyl acetonate)

12/100 X 200 ml = 24 ml; (24 ml ammonium fluoride was added to 176 ml Tin acetyl acetonate)

Dispersion of GO

15mg of powder rGO was dispersed in 70% acetone and 30% of H_2O i.e. 11ml of acetone and H_2O.

$$Total\ volume\ of\ acetone\ and\ water = 11ml$$

$$Graphene = 15mg$$

$$\therefore\ the\ concentration\ of\ GO\ is\ 70\%\ acetone\ and\ 30\%\ of\ H_2O = \frac{15mg}{11ml}$$

1.4 mg/ml

Therefore, the concentration of rGO was 1.4 mg/ml (15mg of GO + 11ml of 70% acetone and 30% H_2O)

Calculation of efficiency

Applying equation $\eta = V_{oc} \times J_{sc} \times ff/P_{in} \times 100$

Where $ff = \frac{V_{oc} \times J_{sc} \times P_{max}}{V_{oc} \times J_{sc}} = P_{max} = 0.0018$

$V_{oc} = 0.5390$, $J_{sc} = 0.118739$, and $P_{in} = 1/1000$, $ff = 0.0018$

$$\eta = 0.5390 \times 0.118739 \times 0.0018 \times 100 \times 1000$$

$$= 11.52\ \%$$



A: Chemical Vapour Deposition (CVD)



B : Four-point probe for electrical characterization



C: UV-Vis spec for photo-response determination



D: Spin-coater for deposition of the blocking layer (BL)



E: Water Distiller



F: Furnace for annealing and sintering processes

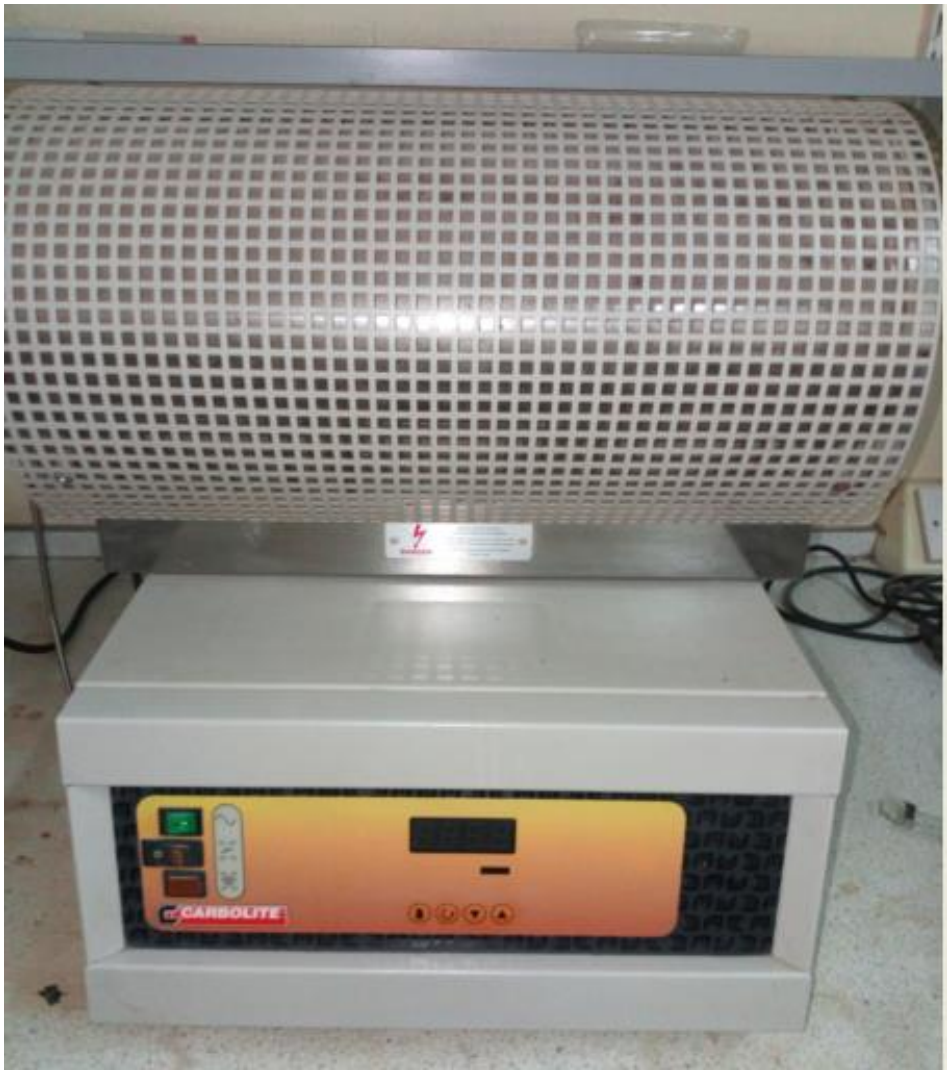

G: Tubular Furnace



H: Solar Simulator for the determination of cell efficiency (I-V characteristics)



I: AACVD – Aerosol Assisted Chemical Vapour Deposition



J: Screen Printing and Spin coating of TiO_2-rGO



K: Magnetic Stirrer hotplate – drying of TiO_2 – rGO nano composite



L: Piranha and slides (Cleaning of slides)

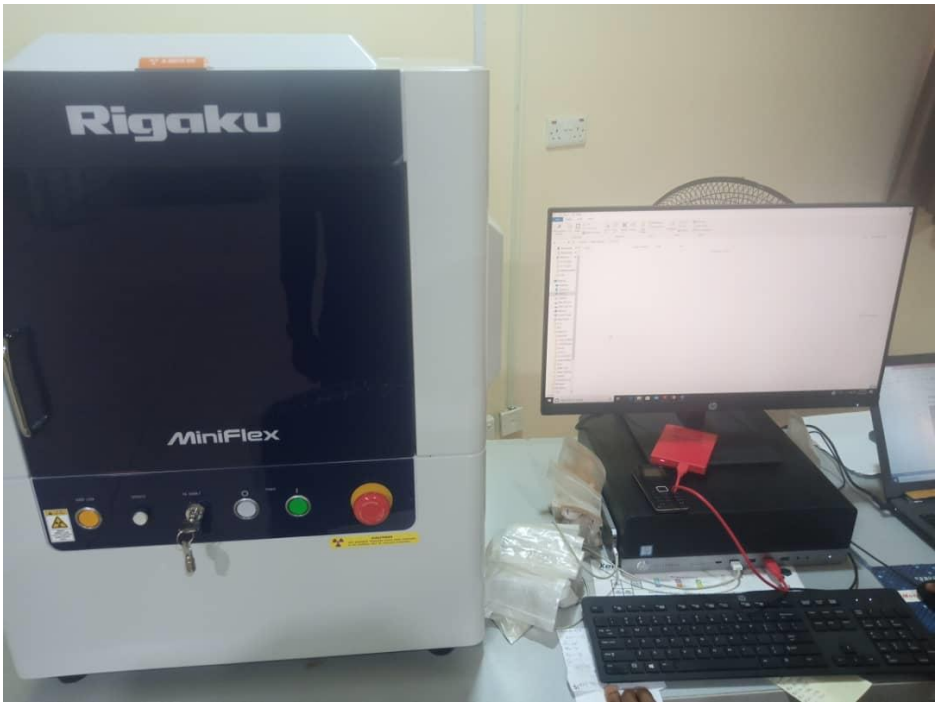

M: XRD Machine



N: SEM/EDX Machine

Journal of SE Copyright Permission to Use

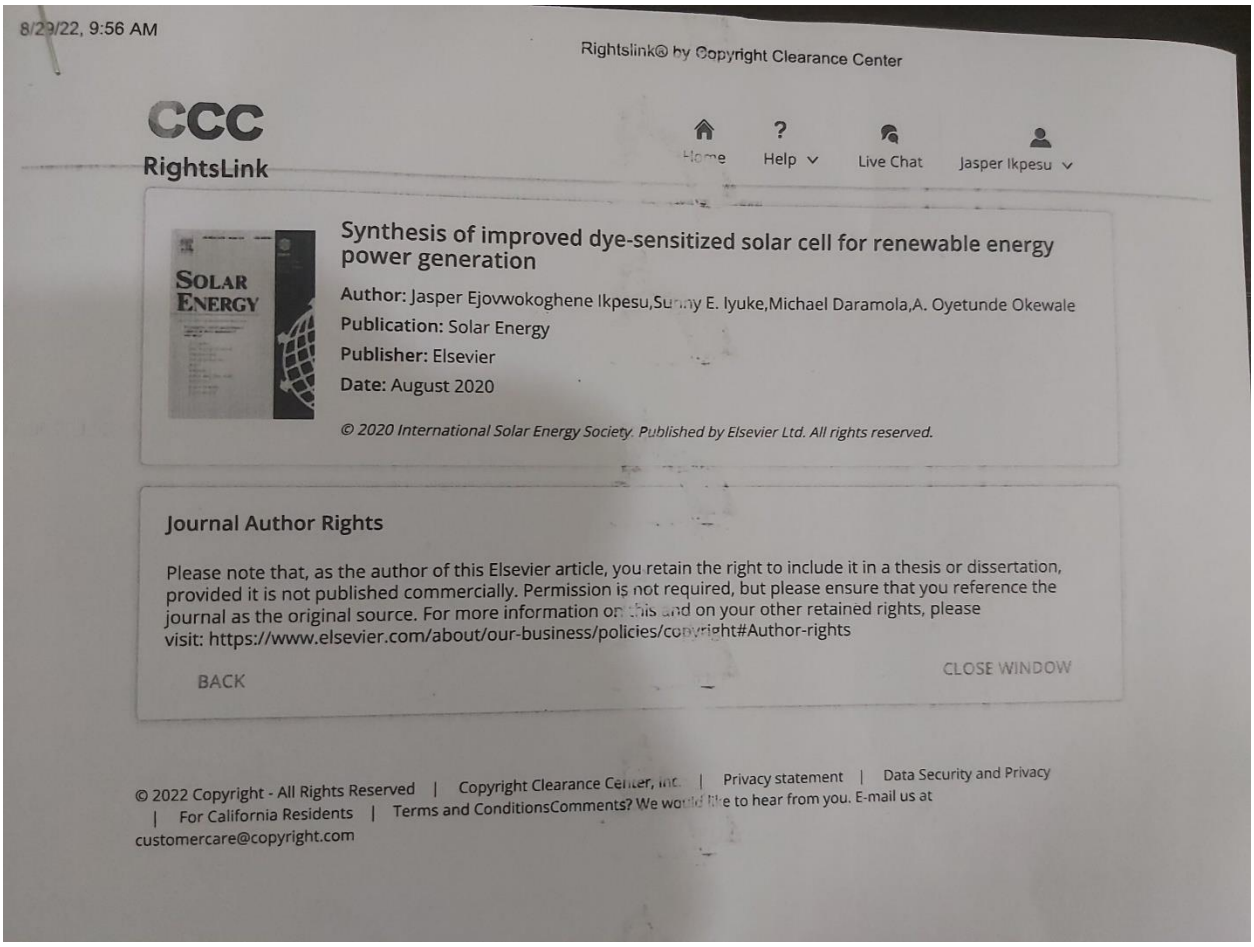

8/29/22, 9:56 AM Rightslink® by Copyright Clearance Center

CCC RightsLink

Home | Help | Live Chat | Jasper Ikpesu

Synthesis of improved dye-sensitized solar cell for renewable energy power generation

Author: Jasper Ejovwokoghene Ikpesu,Sunny E. Iyuke,Michael Daramola,A. Oyetunde Okewale

Publication: Solar Energy

Publisher: Elsevier

Date: August 2020

© 2020 International Solar Energy Society. Published by Elsevier Ltd. All rights reserved.

Journal Author Rights

Please note that, as the author of this Elsevier article, you retain the right to include it in a thesis or dissertation, provided it is not published commercially. Permission is not required, but please ensure that you reference the journal as the original source. For more information on this and on your other retained rights, please visit: https://www.elsevier.com/about/our-business/policies/copyright#Author-rights

BACK CLOSE WINDOW

© 2022 Copyright - All Rights Reserved | Copyright Clearance Center, Inc. | Privacy statement | Data Security and Privacy | For California Residents | Terms and ConditionsComments? We would like to hear from you. E-mail us at customercare@copyright.com

IOP Publishing Copyright Permission to Use

Permissions Fri, Sep 2, 5:30 AM

to me

Dear Jasper Ejovwokoghene Ikpesu,

Thank you for your request to reproduce content from IOP Conference Series: Materials Science and Engineering.

The content you have requested was published under a CC BY licence which permits reuse for any purposes, even commercial, provided the licence terms are adhered to.

Therefore, you may reuse the content without permission, so long as you reference it adequately and adhere to the terms of the CC BY licence.

Please note this does not apply to any content/Figure which is credited to another source in our publication or has been obtained from a third party, which is not available under a suitable open access licence. Express permission for such content/Figures must be obtained from the copyright owner.

Kind regards,

Sophie
Copyright & Permissions Team
Sophie Brittain - Rights & Permissions Assistant
Cameron Wood - Legal & Rights Adviser
Contact Details
E-mail: permissions@ioppublishing.org

For further information about copyright and how to request permission: https://publishingsupport.iopscience.iop.org/copyright-journals/
See also: https://publishingsupport.iopscience.iop.org/
Please see our Author Rights Policy https://publishingsupport.iopscience.iop.org/author-rights-policies/
Please note: We do not provide signed permission forms as a separate attachment. Please print this email and provide it to your publisher as proof of permission. **Please note**: Any statements made by IOP Publishing to the effect that authors do not need to get permission to use any content where IOP Publishing is not the publisher is not intended to constitute any sort of legal advice. Authors must make their own decisions as to the suitability of the content they are using and whether they require permission for it to be published within their article.

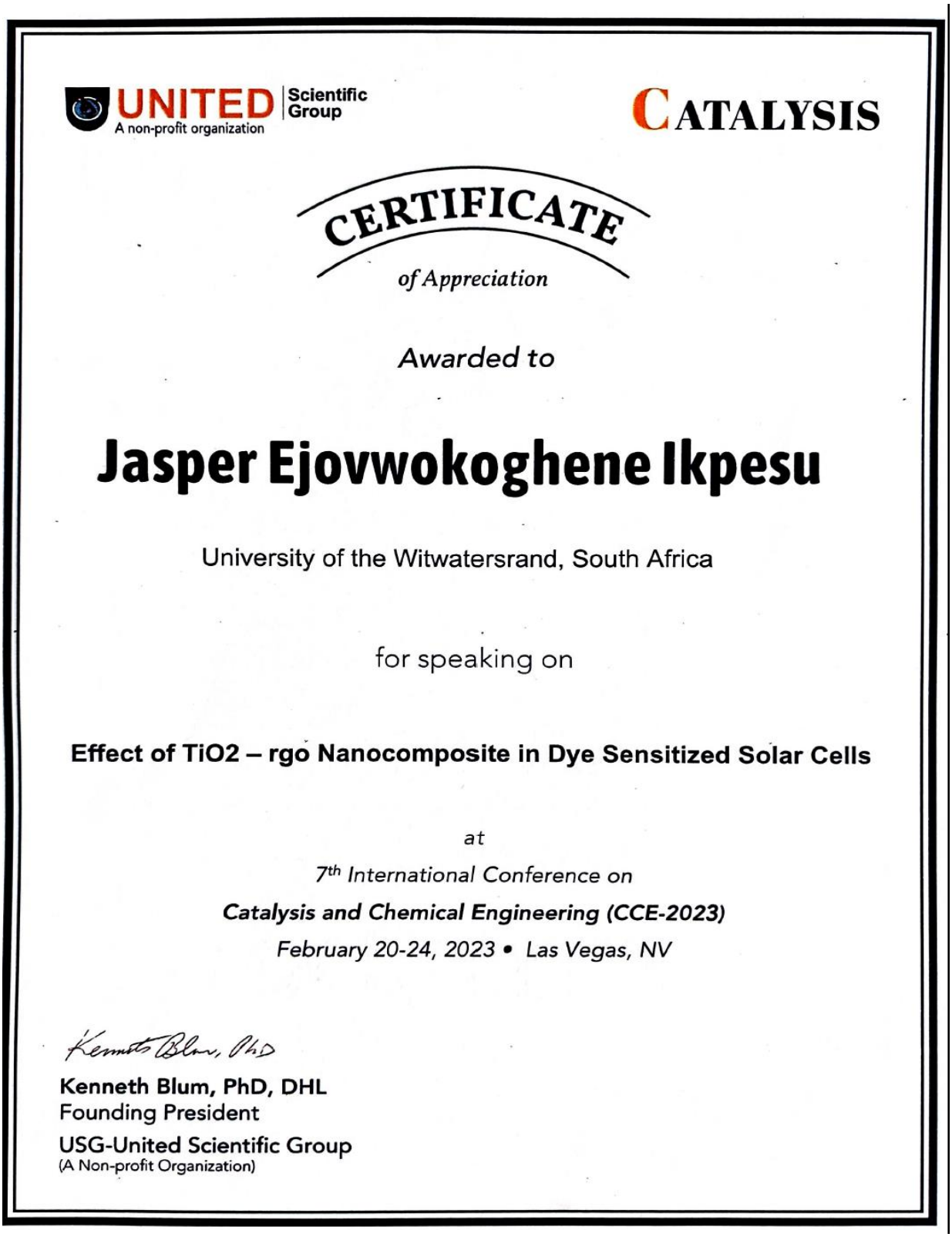

Certificate of conference paper presented